

Ocean Engineering & Oceanography 11

Srinivasan Chandrasekaran  
Gaurav Srivastava

# Design Aids of Offshore Structures Under Special Environmental Loads Including Fire Resistance

 Springer

# **Ocean Engineering & Oceanography**

Volume 11

## **Series editors**

Manhar R. Dhanak, Florida Atlantic University SeaTech, Dania Beach, USA  
Nikolas I. Xiros, New Orleans, USA

More information about this series at <http://www.springer.com/series/10524>

Srinivasan Chandrasekaran  
Gaurav Srivastava

# Design Aids of Offshore Structures Under Special Environmental Loads Including Fire Resistance

Srinivasan Chandrasekaran  
Department of Ocean Engineering  
Indian Institute of Technology Madras  
Chennai, Tamil Nadu  
India

Gaurav Srivastava  
Department of Civil Engineering  
Indian Institute of Technology Gandhinagar  
Gandhinagar, Gujarat  
India

ISSN 2194-6396 ISSN 2194-640X (electronic)  
Ocean Engineering & Oceanography  
ISBN 978-981-10-7607-7 ISBN 978-981-10-7608-4 (eBook)  
<https://doi.org/10.1007/978-981-10-7608-4>

Library of Congress Control Number: 2017960286

© Springer Nature Singapore Pte Ltd. 2018

This work is subject to copyright. All rights are reserved by the Publisher, whether the whole or part of the material is concerned, specifically the rights of translation, reprinting, reuse of illustrations, recitation, broadcasting, reproduction on microfilms or in any other physical way, and transmission or information storage and retrieval, electronic adaptation, computer software, or by similar or dissimilar methodology now known or hereafter developed.

The use of general descriptive names, registered names, trademarks, service marks, etc. in this publication does not imply, even in the absence of a specific statement, that such names are exempt from the relevant protective laws and regulations and therefore free for general use.

The publisher, the authors and the editors are safe to assume that the advice and information in this book are believed to be true and accurate at the date of publication. Neither the publisher nor the authors or the editors give a warranty, express or implied, with respect to the material contained herein or for any errors or omissions that may have been made. The publisher remains neutral with regard to jurisdictional claims in published maps and institutional affiliations.

Printed on acid-free paper

This Springer imprint is published by Springer Nature  
The registered company is Springer Nature Singapore Pte Ltd.  
The registered company address is: 152 Beach Road, #21-01/04 Gateway East, Singapore 189721, Singapore

# Preface

The book titled Design Aids of Offshore Structures under Special Environmental Loads including Fire Resistance is focused to address analysis and design of structural members in general and offshore structures, in particular. Offshore structures possess high novelty by their form-dominance, whose analysis and design are different from other conventional civil engineering structures. Primary objective of this text book is to encapsulate the important technical fundamentals of analysis and design under special loads.

This book covers a descriptive explanation on different types of offshore structures, with special focus to their structural action under the encountered environmental loads. Special loads namely ice loads, loads that arise from springing and ringing waves, blast loads and fire loads are presented in detail. As application of loads on members of offshore structures invoke unsymmetrical bending, concepts of advanced structural analyses are covered in detail and explained with more numerical examples. Analysis and design of crane hooks, for example, can be seen as a distinct contribution to this section.

Safety of offshore platforms against fire needs to be ascertained due to their strategic importance. In addition to the deliberations on fire-resistant design of structural members, principles of fire and explosion safety are also presented in detail. A descriptive chapter on analysis and design of members in fire presents fundamental properties of steel and concrete under elevated temperatures and their significance in design. Numerical examples of assessment of fire resistance of structural members will help understand the presented concepts.

Contents of this book are carefully derived based on the extensive literature reviewed with the focus to make it simple and presentable in a class-room mode of teaching. Valuable contributions made by other authors in this important domain of structural engineering are sincerely acknowledged. We continue to believe that a text book on Design aids of offshore structures is possible only with both the industrial and academic inputs. While authors agree that subject matter of the book is not self-contained but with some details missing, basic purpose is not to be complete but to provide a starting point for those who wish to learn this subject with a relative degree of convenience. We thank our teachers, friends and colleagues

who continue to teach us the fundamentals of analysis and design under special environmental loads and fire-resistance.

We sincerely acknowledge the administrative support extended by Centre of Continuing Education, Indian Institute of Technology Madras and Indian Institute of Technology Gandhinagar during the writing of this text book. We continue to acknowledge our families, who provided support and encouragement throughout writing this book.

Tamil Nadu, India  
Gujarat, India

Srinivasan Chandrasekaran  
Gaurav Srivastava

# Contents

<b>1</b>	<b>Introduction</b>	<b>1</b>
1.1	Novelty of Offshore Structures	1
1.2	Fixed Platforms	3
1.3	Compliant Platforms	5
1.3.1	Guyed Towers	6
1.3.2	Articulated Towers	7
1.3.3	Tension Leg Platform	8
1.4	Single Point Anchor Reservoir (SPAR)	11
1.5	Floating Platforms	13
1.5.1	Floating Production Storage and Offloading Platform (FPSO)	13
1.5.2	Semisubmersible	14
1.5.3	Jack-up Rigs	16
1.5.4	Drill Ships	17
1.6	New-Generation Offshore Platforms	17
1.7	Buoyant Leg Structures	18
1.8	Triceratops	19
1.9	Regasification Platforms	21
1.10	Environmental Loads and Complexities	22
1.11	Wave Loads	23
1.11.1	Wheeler's Modifications	25
1.11.2	Chakrabarti's Modifications	25
1.11.3	Pierson-Moskowitz (PM) Spectrum	26
1.11.4	Modified PM Spectrum	27
1.11.5	ISSC Spectrum (International Ship Structures Congress)	27
1.11.6	JONSWAP Spectrum (Joint North Sea Wave Project)	27
1.12	Wind Loads	28
1.12.1	Davenport Spectrum	31

1.12.2	Harris Spectrum . . . . .	32
1.12.3	Kaimal Spectrum . . . . .	32
1.12.4	API(2000) Spectrum . . . . .	32
1.13	Ice Loads . . . . .	33
1.14	Current Loads . . . . .	35
1.15	Analysis Under Seismic Loads . . . . .	36
1.16	Analysis Under Distinctly High Sea Waves . . . . .	38
1.16.1	Analytical Study . . . . .	39
1.17	Springing and Ringing Waves . . . . .	47
1.18	Blast Loads . . . . .	50
1.18.1	Protected Spaces . . . . .	51
1.18.2	Quantification of Blast Loads . . . . .	53
1.19	Fire Loads . . . . .	53
1.19.1	Types of Fire . . . . .	54
1.20	Research Study 1: Dynamic Analysis of Buoyant Leg Storage and Regasification Platforms (BLSRPs) . . . . .	55
1.21	Illustrated Examples . . . . .	59
1.22	Examples on Probability Distributions of Continuous Random Variables . . . . .	61
1.22.1	Normal Distribution . . . . .	61
1.22.2	Exponential Distribution . . . . .	63
1.22.3	Erlang Distribution . . . . .	64
1.22.4	Gamma Distribution . . . . .	65
1.22.5	Weibull Distribution . . . . .	66
1.22.6	Lognormal Distribution . . . . .	66
<b>2</b>	<b>Advanced Structural Analysis . . . . .</b>	<b>73</b>
2.1	Unsymmetrical Bending . . . . .	73
2.2	Example Problems on Unsymmetrical Bending . . . . .	78
2.3	Shear Center . . . . .	87
2.4	Example Problems on Shear Center . . . . .	90
2.5	Curved Beams . . . . .	100
2.5.1	Curved Beams with Small Initial Curvature . . . . .	101
2.5.2	Deflection of Curved Beam with Small Initial Curvature . . . . .	103
2.5.3	Curved Beam with Large Initial Curvature . . . . .	104
2.5.4	Circular Cross Section . . . . .	109
2.5.5	Rectangular Cross Section . . . . .	113
2.5.6	T Section . . . . .	114
2.5.7	I Section . . . . .	116
2.5.8	Triangular Cross Section . . . . .	117
2.5.9	Trapezoidal Cross Section . . . . .	119
2.6	Simplified Equations to Estimate Stresses . . . . .	120
2.7	Example Problems in Curved Beams . . . . .	121

- 2.8 Marine Risers . . . . . 126
  - 2.8.1 Low-Pressure Risers . . . . . 126
  - 2.8.2 High-Pressure Drilling Riser . . . . . 127
  - 2.8.3 Flexible Risers . . . . . 127
  - 2.8.4 Top Tensioned Risers (TTR). . . . . 127
- 2.9 Members Under Vortex-Induced Vibration (VIV) . . . . . 130
- 2.10 Research Case Study: Effect of Suppression System  
on VIV of Spar Cylinder. . . . . 131
- 3 Fire Safety in Offshore Structures . . . . . 159**
  - 3.1 Introduction . . . . . 159
  - 3.2 Fire and Explosion Characteristics . . . . . 161
  - 3.3 Best Practices in Fire Safety . . . . . 163
    - 3.3.1 Common Mistakes in Fire Accidents . . . . . 164
  - 3.4 Fire Risk . . . . . 164
  - 3.5 Classification of Fire . . . . . 165
    - 3.5.1 Pool Fire . . . . . 165
    - 3.5.2 Jet Fire . . . . . 165
    - 3.5.3 Fire Ball . . . . . 166
    - 3.5.4 Flash Fire . . . . . 167
    - 3.5.5 Minimum Ignition Energy . . . . . 167
  - 3.6 Fire Protection in Offshore Platforms . . . . . 167
    - 3.6.1 Complications in the Fire-Resistant Design . . . . . 169
    - 3.6.2 Firefighting Equipments . . . . . 170
  - 3.7 Objectives of Fire Safety . . . . . 170
  - 3.8 Fire Behavior and Development . . . . . 171
    - 3.8.1 Fire Behavior . . . . . 172
  - 3.9 Egress and Human Behavior . . . . . 174
  - 3.10 Fire Resistance . . . . . 174
  - 3.11 Detection and Fire Control . . . . . 174
    - 3.11.1 Active Control of Fire . . . . . 175
    - 3.11.2 Passive Control of Fire . . . . . 175
    - 3.11.3 Compartmentation . . . . . 176
  - 3.12 Fire Load . . . . . 176
  - 3.13 Combustion of Materials . . . . . 177
  - 3.14 Initiation of Fire . . . . . 178
  - 3.15 Open Fire . . . . . 178
  - 3.16 *t*-Squared Fire Model . . . . . 179
  - 3.17 Compartment Fire . . . . . 183
    - 3.17.1 Pre-flashover . . . . . 184
    - 3.17.2 Flashover . . . . . 184
    - 3.17.3 Post-flashover . . . . . 186
  - 3.18 Fire Resistance . . . . . 188

3.19	Equivalent Fire Severity . . . . .	190
3.19.1	Area Equivalence . . . . .	191
3.19.2	Maximum Temperature Equivalence . . . . .	191
3.19.3	Minimum Load Capacity Equivalence . . . . .	191
3.20	Fire Resistance Tests . . . . .	192
3.20.1	Furnace Parameters . . . . .	193
3.20.2	Test Specimens . . . . .	193
3.20.3	Fire-Resistance Ratings . . . . .	193
<b>4</b>	<b>Analysis and Design of Members in Fire . . . . .</b>	<b>201</b>
4.1	Material Properties at Elevated Temperatures . . . . .	201
4.2	Thermal Properties of Concrete . . . . .	202
4.2.1	Specific Heat . . . . .	202
4.2.2	Density . . . . .	202
4.2.3	Thermal Conductivity . . . . .	203
4.3	Thermal Properties of Steel . . . . .	204
4.3.1	Specific Heat and Density . . . . .	205
4.3.2	Thermal Conductivity . . . . .	206
4.3.3	Thermal Diffusivity . . . . .	206
4.4	Mechanical Properties . . . . .	207
4.4.1	Concrete . . . . .	207
4.4.2	Steel . . . . .	207
4.5	Constitutive Models for Concrete and Steel Under Fire . . . . .	209
4.5.1	Concrete . . . . .	209
4.5.2	Steel . . . . .	210
4.6	Design of Steel Members Exposed to Fire . . . . .	212
4.6.1	Temperature Assessment . . . . .	212
4.6.2	Eurocode Approach (EN 1993-1-2) . . . . .	214
4.6.3	Bare Steelwork . . . . .	215
4.6.4	Protected Steelwork . . . . .	215
4.7	Fire Rating Based on Temperature Criterion . . . . .	215
4.8	Strength Assessment . . . . .	216
4.8.1	Fire Rating Based on Strength Criterion . . . . .	216
4.9	Numerical Examples . . . . .	218
4.10	Design of Concrete Members Under Fire . . . . .	262
4.10.1	Temperature Analysis . . . . .	262
4.10.2	Wickstrom's Method . . . . .	263
4.10.3	Hertz's Method . . . . .	264
4.11	Strength Assessment of Concrete Members Under Fire . . . . .	265
4.11.1	500 °C Isotherm Method . . . . .	265
4.11.2	Zone Method (Method of Slices) . . . . .	268
4.12	Numerical Example for Concrete Members Under Fire . . . . .	268

- 4.13 Composite Structures Under Fire . . . . . 285
  - 4.13.1 Composite Beams . . . . . 285
  - 4.13.2 Critical Temperature-Based Approach . . . . . 286
- 4.14 Moment Capacity-Based Approach . . . . . 287
- 4.15 Numerical Example on Composite Section Under Fire . . . . . 289
- 4.16 Composite Columns . . . . . 291
- References** . . . . . 321

## About the Authors

**Srinivasan Chandrasekaran** is a faculty member in the Department of Ocean Engineering at IIT Madras, Chennai, India. He has 23 years of teaching, research, and industrial experience, in the course of which he has supervised many sponsored research projects and offshore consultancy assignments both in India and abroad. His current areas of research are the dynamic analysis and design of offshore platforms, development of geometric forms of compliant offshore structures for ultra-deepwater oil exploration and production, subsea engineering, rehabilitation and retrofitting of offshore platforms, structural health monitoring of ocean structures, seismic analysis and design of structures, and risk analyses and reliability studies for offshore and petroleum engineering plants.

He has also been a visiting fellow at the University of Naples Federico II, Italy, for a period of 2 years, during which he conducted research on the advanced nonlinear modeling and analysis of structures under different environment loads with experimental verifications. He has published 110 research papers in international journals and refereed conferences organized by professional societies around the world. He has also authored three textbooks that are highly popular among graduate students of civil and ocean engineering. He is a member of many national and international professional bodies and has delivered invited lectures and keynote addresses at various international conferences, workshops, and seminars organized in India and abroad.

**Gaurav Srivastava** is a faculty member in the Discipline of Civil Engineering at IIT Gandhinagar since 2013. His main area of research is design and analysis of structural systems and building façades subjected to fire. His research group has been involved in the development of efficient structural fire analysis algorithms for reinforced concrete and steel structures and experimental characterization of structural materials at high temperatures. He is also carrying out full-scale characterization of building façade systems subjected to fire in the unique façade testing facility that has been developed at IIT Gandhinagar. Other areas of his interest include computational mechanics and uncertainty quantification. Before joining IIT Gandhinagar, he worked in the Department of Mechanical and Aerospace

Engineering, University of Notre Dame, as a postdoctoral research associate toward simulation of combustion of solid rocket propellant. Prior to that, he completed his doctoral and master's degrees in Civil Engineering from the University of Minnesota and bachelor's degree in Civil Engineering from IIT (BHU), Varanasi.

# Chapter 1

## Introduction

**Abstract** Offshore structures are special in terms of its geometric configuration and functional requirements as well. In order to understand design philosophy and analysis methods, it is imperative to develop technical know-how about their salient features. Though about 15,000 platforms are constructed worldwide, each one of them is unique by one way or the other. Various construction projects successfully executed in construction, installation, and commissioning of offshore platforms are episodes to read and admire. Thanks to the developer's intelligence, designer's courage, and contractor's skills, we, as a scientific community, are fortunate to applaud our achievements and contributions to the world's economic growth. This chapter highlights uniqueness of offshore platforms and different types of special loads encountered by them. A detailed understanding about their structural behavior under a variety of environmental loads is targeted. This is achieved through discussions under various perspectives, making the reader to understand them easily while appreciating their novelty.

### 1.1 Novelty of Offshore Structures

Structures are generally designed to resist encountered loads under its strength capabilities (Chandrasekaran 2013a, b, c). Strength to resist applied loads essentially arises from two sources, namely: (i) material properties and (ii) structural form (geometric form). While reviewing the concepts of different structural forms that have been conceived to meet various functional requirements, one can notice a good trend emerging (Aktan et al. 1998a; Chandrasekaran 2015a, 2016a, 2017a). For example, designs of public buildings like airports and bridges are not similar to those of olden days. One can visualize a large span, unsupported structural form, developed and constructed in the recent past. It is therefore important to realize that function-based requirements dominate such design patterns. However, this view is reversed as far as offshore structures are concerned (Faltinsen 1998). For the same functional requirements such as drilling, production, storage, and transportation, different geometric forms of offshore structures are conceived (Adams and Baltrop

1991; Adrezin et al. 1996; Logan et al. 1996). This was necessary because sea states, water depth of installation, operational conditions, etc., are not similar between the platforms (Chandrasekaran and Yuvraj 2013; Muren et al. 1996). Hence, one can easily recognize that offshore structures are increasingly becoming form-dominant (Chandrasekaran and Madhuri 2015). This evolved new-generation offshore platforms in the recent past (Chandrasekaran and Sengur 2016; Chandrasekaran et al. 2013). To name a few, triceratops, buoyant leg structures (BLS), Buoyant Leg Storage and Regasification Platforms (BLSRPs) are salient examples of novel structural configurations (Halkyard et al. 1991; Robert et al. 1995; White et al. 2005).

Offshore structures are becoming more complicated due to the development of new structural forms to suit ultra-deep-water exploration and production requirements (Chandrasekaran et al. 2004, 2006, 2007a, b, c). In addition, platforms are also preferred as a multi-functional asset in terms of offshore power generation units. Main reason for such innovations is to reduce the response of these platforms under the action of environmental loads (Chandrasekaran and Madhuri 2012, 2013; Marco and Meyer 2008; Sadehi 1989, 2001, 2007). Emphasis is more toward operational safety than reliable design (Chandrasekaran and Madhavi 2014a, b, c). Unfortunately, environmental loads encountering offshore platforms have many uncertainties in estimating their magnitude and direction. Return period of the event makes them very complex (Kareem 1983; Kareem and Zhao 1994; Kareem and Dutton 1982). Further, offshore structures under special loads leave a complex behavior in their response (Chandrasekaran and Madhavi 2015a, b, c; Mangala and Haym 2006). Sound knowledge is therefore required to estimate such special loads and assess dynamic response under such special loads. Offshore structures are considered to be functionally unique due to the following reasons:

- (i) They need to remain functional and operable even on exceedance of their service life.
- (ii) Under the given variation of environmental loads and strength degradation due to corrosion, they require a periodic assessment or continuous health monitoring to plan for preventive maintenance.
- (iii) Frequent intervention of their function for repair and maintenance is not advisable.
- (iv) Platforms should remain functional even during repair and maintenance works.
- (v) No special code regulations are available to carry out repairs of offshore structures while under operation.

Design of offshore structures should be cost-effective, while the chosen structural form should be capable of transmitting encountered loads. Even the structural repair and maintenance works should be cost-effective and provide a long-term solution to the problem. However, repairs in offshore platforms are performed only on convective basis and not on preventive basis. Hence, the offshore structures are

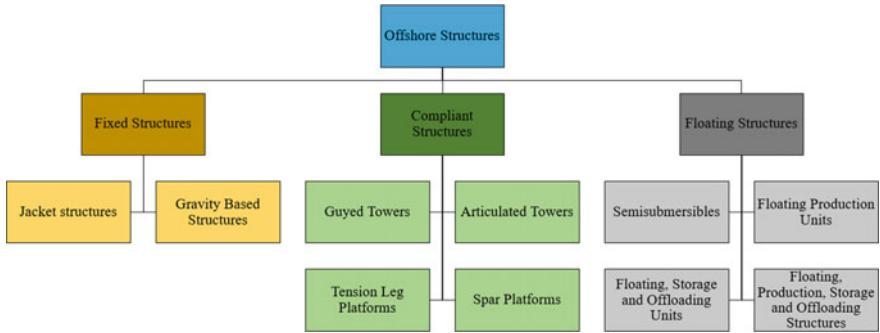


**Fig. 1.1** Classifications of offshore platforms

said to be unique and novel, by both design and their functional requirements. The important factors considered during their design are as follows:

- (i) Structural geometry should be simple and stable.
- (ii) Easy fabrication, installation, and decommissioning.
- (iii) Low CAPEX.
- (iv) Early start of production and high return on investment with uninterrupted production.

Under certain conditions, occurrence of an extremely rare event may lead to severe consequences, increasing the risk; this also makes offshore structures unique. Thus, uniqueness is contributed by innovative design, special functional requirements, technology-driven repair and maintenance approach, and the high risk factor associated with them. Figure 1.1 shows classifications of offshore platforms.

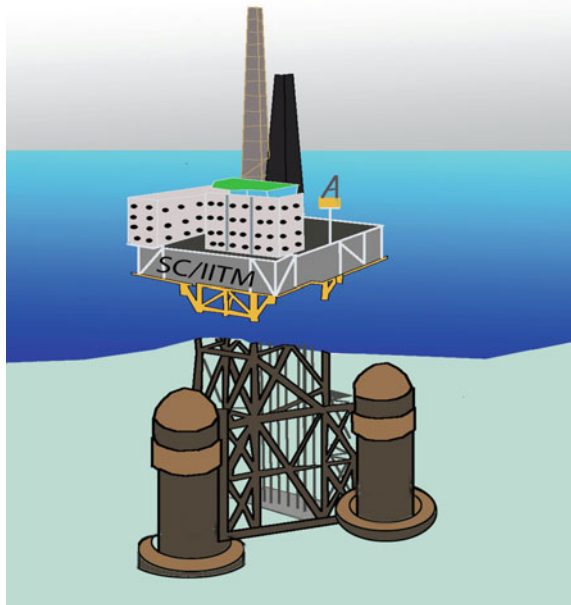
## 1.2 Fixed Platforms

These are the bottom-supported structures, which rest on pile foundation. Due to its fixity, it tends to attract more forces (BS 5950 1982). These structures withstand forces by the virtue of their strength (Freudenthal and Gaither 1969). They are generally stiff, and their natural period varies from 4 to 6 s (1–1.5 rad/s). Most commonly used material for construction is steel (and a few of them in concrete). Foremost advantage of fixed structures is that they are relatively insensitive to lateral loads. Fixed platforms are capable of supporting large magnitude of deck loads and support large exploration/production wells. These structures can be constructed in parts and transported. However, they also have few demerits:

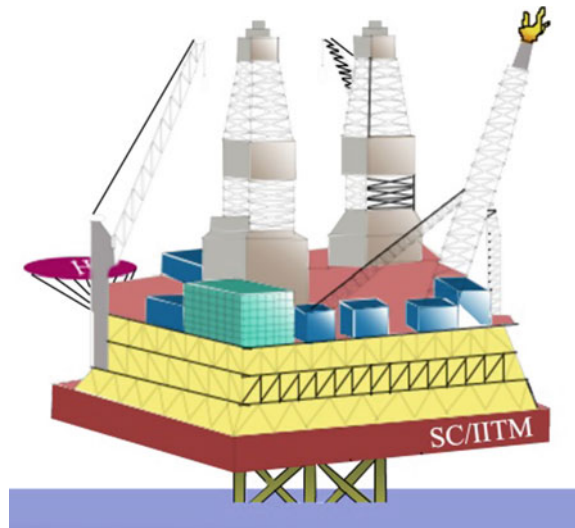
- (i) Installation is highly complex and is technically challenging.
- (ii) Cost increases with the increase in the water depth.
- (iii) It triggers brittle mode of failure.
- (iv) Rigid failure.
- (v) High initial cost.
- (vi) Unsuitable for cyclic loading and earthquake loads.
- (vii) Corrosion of steel reducing their service life.
- (viii) Delay in production and commissioning due to longer period of construction.

Figure 1.2 shows steel gravity platform, while Fig. 1.3 shows steel jacket platform. While both the platforms are fixed-type in nature, their force-resistance mechanics are different (Hove and Foss 1974; Hsu 1981; Issacson and Det 1982; James 1984, 2003; Moe and Verley 1980; Young et al. 1975). Commonness between them is that they are of large weight and hence stiff by their geometric design (Mayerhof 1976; Moan and Sigbjørnson 1977; Mogridge and Jamieson 1975).

**Fig. 1.2** Maureen Alpha:  
steel gravity base platform



**Fig. 1.3** Bullwinkle: steel jacket platform



### 1.3 Compliant Platforms

Compliance is the term related to flexibility. Relative degree of flexibility is felt necessary as fixed-type structures showed brittle-type failure modes (Gadagi and Benaroya 2006; Gasim et al. 2008). Considering the demerits possessed by fixed-type platforms as listed above, these structures are gradually replaced by compliant structures (Gerwick 1986; Mohammad 2013). Compliant structures are permitted to undergo large displacement in the form of rigid body motion, which is expected to counteract the encountered environmental loads (Ahmad 1996; Adrezin and Benaroya 1999; Chandrasekaran and Shihas 2016; Moharrami and Tootkaboni 2014). Compliant structures resist loads by virtue of their relative displacement but it is also imperative to ensure a good recentering capability by making them position restraint. It is very interesting to note that evolution of compliant structures follows the concept of ‘made flexible by their geometric form, not by introducing flexibility to their members.’ Major advantages of compliant structures include:

- (i) Flexible structural form, which will attract lesser forces.
- (ii) Forces are distributed by the relative displacement of the structural system.
- (iii) Better behavior under the cyclic loads.
- (iv) Easy installation.
- (v) Early start of production.
- (vi) High reusability.

Novelty of such platforms arises by designing them as positively buoyant, which means that buoyancy force exceeds their colossal weight. Positive buoyancy tends the platform to float, enabling easy installation, towing, decommissioning, etc., but needs to be position-restrained to make them operable. Usually, they are

position-restrained by wires or cables; even large diameter pipes are also used and term as tethers or tendons. Compliancy is desired in the horizontal plane whereas stiffness in the vertical plane. Hence, a hybrid concept of design concept is followed in the geometric development of complaint platforms.

### 1.3.1 Guyed Towers

Figure 1.4 shows schematic view of a guyed tower. Guyed tower acts like an inverted pendulum; rotation of the tower about the hinged joint at the bottom enables the tower to counteract the wave loads by introducing the desired compliancy. Guyed tower rests on spud-can arrangement, which acts like an inverted cone enabling the platform to rotate about the hinge. Platform is also position-restrained with catenary mooring lines, provided circumferentially. Point where the mooring is connected to the tower is called fair lead, and the point of connection between the mooring and the seabed is called touchdown point. At the touchdown point, additional clump weights are provided to hold down the mooring line against lifting. Merits of the platform include lower cost, good stability, high reusability, and recentering capabilities (Hitchings et al. 1976; Herbich 1991). Demerits are high maintenance cost, suitability to small exploration/production fields, and complex mooring system.

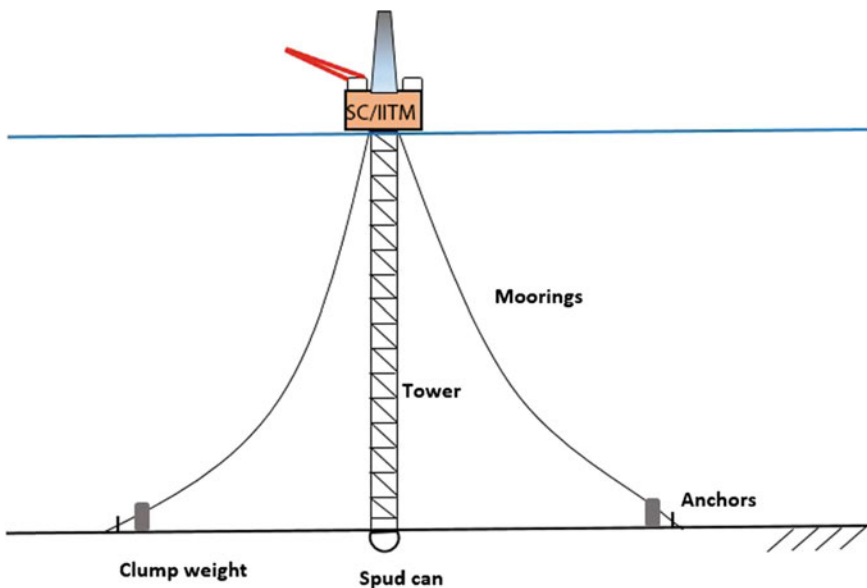


Fig. 1.4 Guyed tower: schematic view showing main components

### 1.3.2 Articulated Towers

Figure 1.5 shows articulated tower, whose deck is supported by a tower; tower rests on the seabed by an articulation called ‘universal joint.’ This is similar to that of a hinged joint as seen in guyed tower with ability to rotate 360°. Hence, rotational compliancy offered by universal joint is relatively higher, enabling more resistance to the tower (Chandrasekaran et al. 2010a, b; Hans et al. 1991; Helvacioğlu and Incecik 2004; Sellers and Niedzwecki 1992). As seen in the figure, tower is provided with a buoyancy chamber at its top and a ballast chamber at the bottom. While the idea is to maintain positive buoyancy for more stability, buoyancy chamber enables restoration of the platform to its original position and also contributes to reduction in overall colossal weight. Articulation allows rotational degrees of freedom and restrains the translational degrees of freedom and makes recentering of the tower more gentle unlike in case of guyed tower. This shows an improved operational safety and convenience.

One of the demerits of the design concept shall be deliberate induction of the failure point at the articulation; this joint is also susceptible to fatigue failure. Restoring moment in articulated towers is given by:

$$\text{Resisting moment} = \{[(B\rho - M_B)gl_B] - [M_Dgl_D]\}\theta \tag{1.1}$$

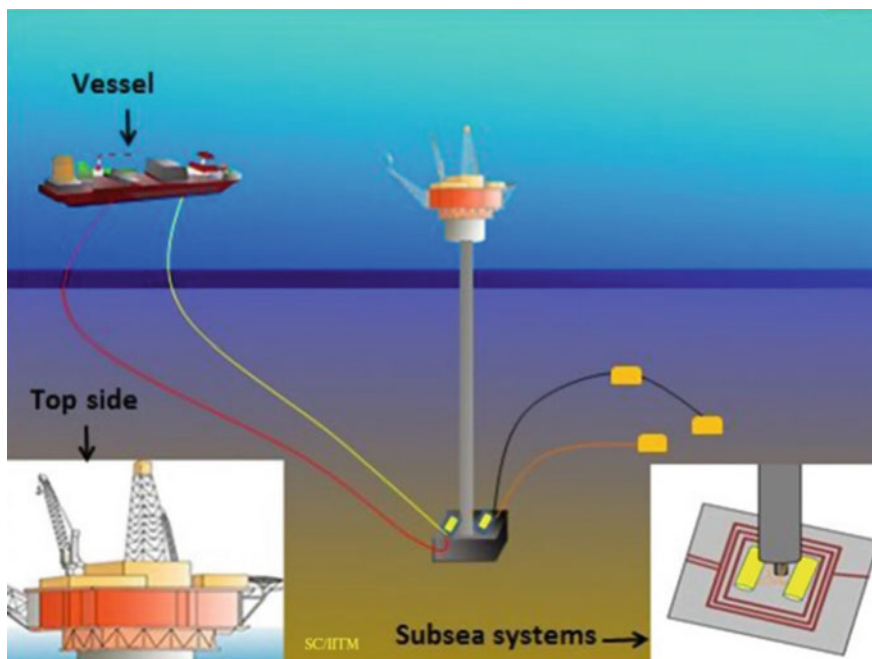


Fig. 1.5 Articulated tower

where  $B$  is buoyancy provided by the buoyancy tank,  $l_D$  is the distance of CG of the deck from the articulated joint,  $l_B$  is the distance of center of buoyancy from the articulated joint,  $\theta$  is the degree of freedom of rotation of the joint,  $M_B$  is mass of the buoyancy tank, and  $M_D$  is mass of the deck. Moment of inertia for rotation about the articulation is given by:

$$I = M_D l_D^2 + (M_B M_{BH}) l_B^2 \quad (1.2)$$

where  $M_{BH}$  is the hydrodynamic mass (or added mass) of the buoyancy tank. Angular frequency in pitch degree of freedom is given by:

$$(\omega_n)_{\text{pitch}} = \sqrt{\frac{g[(B\rho - M_B)l_B - (M_D l_D)]}{M_D l_D^2 + (M_B M_{BH}) l_B^2}} \quad (1.3)$$

### 1.3.3 Tension Leg Platform

Figure 1.6 shows a Tension Leg Platform (TLP). As seen in the conceptual figure, deck of TLP is supported by pontoons and columns, which in turn are connected to the seabed by taut-mooring system. Columns and pontoons are tubular members, which ensure large displacement volume for smaller weight (Chandrasekaran et al. 2006, 2013, 2015a, b; Hsien and Juang 2012). This is advantageous during transportation of the platforms as it causes high-displaced volume (API-RP 2T 1997; Chandrasekaran 2007; Chandrasekaran and Jain 2002a, b; Hsien and Wang 2000; Hsien et al. 1999). Excess buoyancy, implicitly induced in the geometric design, is counteracted by large initial pretension in tethers (Chuel et al. 2007; Inyeol and Jose 1996; Minoos and Joel 1991); tethers have a large axial stiffness to sustain this pretension magnitude (Arnott et al. 1997; James et al. 2002). Unlike articulated towers, TLPs do not have universal joints and thus fatigue failure of the joint is avoided (Demirbilek 1990; Jefferys and Patel 1982; Haritos 1985; Ney Riotman et al. 1992; Niedzwecki and Huston 1992). Platform is commissioned by ballasting the platform at site, which is relatively easier and less expensive as it does not involve expensive crane and other construction equipments (Clauss et al. 1992; Class and Birk 1996; Kim et al. 2007; Kobayashi 1987; Nobuyoshi 1976). TLPs are flexible in horizontal plane and rigid in vertical plane (Chandrasekaran et al. 2013; Kurian et al. 2008; Low 2009). Surge, sway, and yaw degrees of freedom are highly flexible, making it more compliant in horizontal plane (Emil Simiu and Stefan 1984; Ertas and Lee 1989; Mekha et al. 1996; Nordgren 1987). Stiffness is ensured in vertical plane with low heave period (Mercier 1982; Oriol et al. 1991). Further motion in vertical plane is also restrained by large initial pretension and hydrodynamic damping offered by water body (Chandrasekaran and Abhishek 2010; DNV 1982; DNV-RP-F205 2010; Peter 1990, 1995). Typical time periods in all six

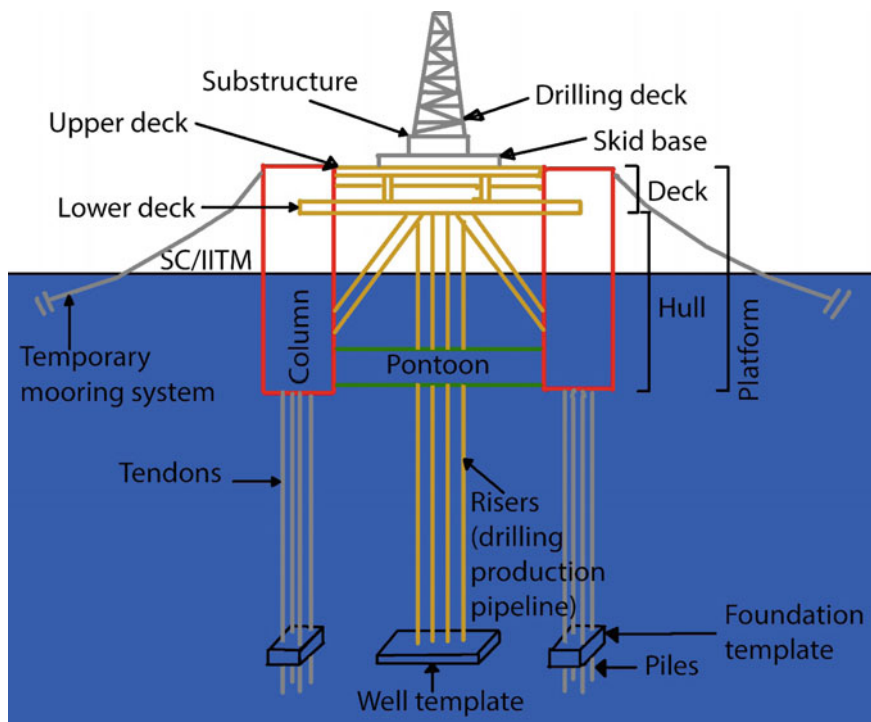


**Fig. 1.6** Tension leg platform (TLP)

degrees of freedom are: surge and sway (90–110 s); heave, roll, and pitch (2–5 s); and yaw (60–90 s) (DOE-OE 1985; Donely and Spanos 1991).

Novelty of the platform lies in the development of both stiff and flexible degrees of freedom in a single structure; this is termed as a hybrid design concept (Chen et al. 2006; Natvig 1996; Spanos and Agarwal 1984; Stansberg et al. 2004). TLPs are also referred to as hybrid structures, as the platform is restrained in vertical plane but compliant in horizontal plane. One of the major difficulties in the hybrid design concept is the clear band separation of frequencies (Tabeshpur et al. 2006; Tan and Boom 1981; Thiagarajan and Troesch 1998). This makes the platform sensitive to both wind and waves as the former is a low-frequency phenomenon and latter is a high frequency. This shall sometimes induce undesirable transfer of response to the hull from pontoons/columns (Vannucci 1996).

Under the wave action, platform moves laterally. This horizontal displacement of the platform is called offset, which will also result in a proportional vertical displacement, known as set-down (William et al. 1984, 2011). When the platform displaces from its original position, change in the pretension in the tendons occurs (Chaudhary and Dover 1985; Chen et al. 2006). While vertical component of the change in pretension adds to the weight of the structure and increases stability, horizontal component will resist the action of wave loads (Arvid and Torgeir 2013;

Yan 2009; Yoneya and Yoshida 1982). Merits of the platform are reusability, stability, low cost with the increase in water depth, deepwater capability, and easy installation (Yoshida et al. 1984; Younis et al. 2001). Demerits are high initial cost and fatigue failure of tethers under dynamic tether tension variation (Zeng et al. 2007). Figure 1.7 shows Heidrun TLP, installed in Gulf of Mexico (GoM).

Commonly used material for the tethers is steel hollow tubes, and they are filled with air at atmospheric pressure to reduce their weight in water. Diameter to thickness ratio of tethers varies from 20 to 30; tendons with stepped cross section, having large diameter at the top, are also used. This is done to withstand axial stresses and external water pressure of high magnitude. One of the recent applications of tendon material is carbon fiber composites, whose specific gravity is about 1.59. In addition to their fatigue resistance, they also possess reserve capacity to withstand static loads. While TLP concept looks simple, complexities arise in design of their components. A few of the special problems associated with tethers are as follows:

- (i) Fatigue caused by the dynamic tether tension variation.
- (ii) High amplitude of initial pre-tension so that no slackening occurs.
- (iii) Requirement of high axial strength capacity in tension to avoid tether pullout.

Stiffness of the tethers is given by:

$$k_n = \frac{(nA_t)E}{l_t} \quad (1.4)$$

**Fig. 1.7** Heidrun TLP



where  $A_t$  is area of tendon;  $n$  is number of tendons;  $E$  is modulus of elasticity of steel; and  $l_t$  is length of the tendon. Heave oscillation period of TLP is given by:

$$(T_n)_{\text{heave}} = 2\pi \sqrt{\frac{M_{\text{heave}} l_t}{n A_t E}} \quad (1.5)$$

Under the wave action, when TLP displaces in surge degree of freedom, restoring force in surge degree of freedom to ensure recentering is given by:

$$f_r(x) = n_t T_t x / l_t \quad (1.6)$$

where  $T_t$  is the initial pretension in each tendon;  $n_t$  is the number of tendons;  $n_t T_t$  is the total initial pretension; and  $x$  is the surge displacement. Horizontal restoring force, including the weight of the tendon, is given by:

$$f_r(x) = \left( n_t T_t - \frac{w l_t}{2} \right) \frac{x}{l_t} \quad (1.7)$$

Surge oscillation period is given by:

$$T_{\text{surge}} = 2\pi \sqrt{\frac{M_{\text{surge}} l_t}{n T_t}} \quad (1.8)$$

In yaw motion, restoring moment and the period are given by:

$$D_y(\theta) = R_y^2 n_t T_t \theta / l_t \quad (1.9a)$$

$$T_{\text{yaw}} = \frac{2\pi}{R_y} \sqrt{\frac{I_y l_t}{n_t T_t}} \quad (1.9b)$$

## 1.4 Single Point Anchor Reservoir (SPAR)

Spar platforms are deep-draft floating caissons (Glanville et al. 1991; Graff 1981; Ran et al. 1996; Zhang et al. 2007). It consists of a hollow cylinder, similar to that of a large buoy (Finn et al. 2003; Newman 1963; Faltinsen et al. 1995; Reddy and Arockiasamy 1991). Cylinders are provided with helical strakes to reduce vortex-induced vibrations (Chandrasekaran and Merin 2016; Montasir et al. 2008; Montasir and Kurian 2008). Figure 1.8 shows conceptual view of a Spar platform. Platform is designed to be flexible in surge degree of freedom with a period of about 100–120 s. It is also relatively flexible in pitch degree of freedom with a period of about 60 s. As discussed earlier, as compliancy offers load resistance capacity by virtue of its geometric form, Spar platforms are designed to remain compliant in

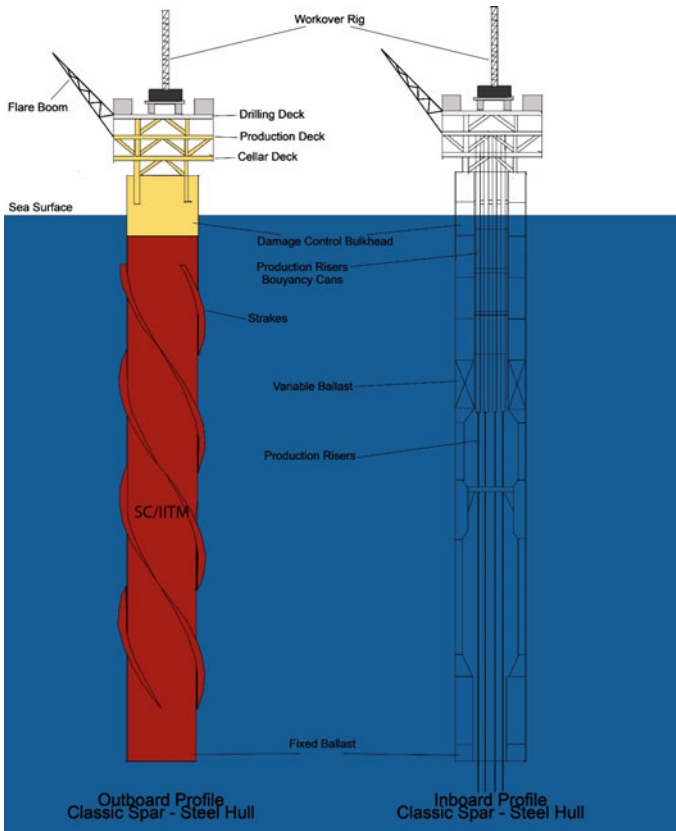


**Fig. 1.8** Conceptual view of Spar platform

surge and pitch degrees of freedom (Agarwal and Jain 2002; Koo et al. 2004; Niedzweki et al. 2000). However, to ensure safe and convenient operability, it is designed to remain stiff in heave degree of freedom with a period of about 25–40 s. One of the major differences between Spar and TLP is in their structural action (Leonard and Young 1985; Patel 1989; Patel and Lynch 1983; Patel and Park 1995). While TLP intends to resist lateral loads by initial pretensioned tendons, Spar platforms resist them by buoyancy characteristics (deep-draft concept). As resistance is not offered by mooring lines, they are not taut-moored but catenary moored only to ensure position-restrained under large displacements. In addition to their structural superiority, Spar platforms also have the following advantages:

- (i) Consists of free-floating structural system with lower response in heave and pitch degrees of freedom.
- (ii) Drilling risers are protected from the wave action, as they are provided inside the cylinders.

- (iii) Fabrication is simple and easy.
- (iv) Geometric form offers unconditional stability even when the mooring lines are disconnected (unlike in case of TLP, where it may cause instability).

Demerits of the platform are namely: (i) difficulty in installation; (ii) little storage capacity; (iii) no drilling facilities; and (iv) corrosion susceptibility of spar hull. Vertical displacement in heave degree of freedom will induce restoring force and is given by:

$$f_r(x) = \rho g R^2(x) \quad (1.10)$$

where  $\rho$  is the density of sea water;  $g$  is acceleration due to gravity; and  $R$  is radius of the cylindrical tank.

## 1.5 Floating Platforms

Floating platforms are used for exploratory drilling, which includes:

- (i) Jack-up rigs, which are suitable up to water depth of 90 m.
- (ii) Semisubmersibles, which are suitable up to water depth of 200 m.
- (iii) Drill ships, which are suitable up to water depth of 2000 m.

Floating platforms are most vulnerable for accidents, while they are transported (or even when towed) from one location to another (Chandrasekaran and Abhishek 2010; Paik and Thayamballi 2007; Witz et al. 1996). When they are afloat, they are more influenced by waves and wind.

### 1.5.1 Floating Production Storage and Offloading Platform (FPSO)

Floating, production, storage, and offloading platforms are the modified form of tankers or cargo vessels. Figure 1.9 shows schematic view of a typical FPSO platform. They are used for production and storage of hydrocarbons. In general, they are designed with a ship-shaped geometry. These platforms can be either permanently moored or disconnectable, turret moored to the seabed. Attractive features of FPSOs are as follows:

- (i) Disconnectable turret enhances movement of the platform to shielded area in case of severe storm.
- (ii) Lower turret moorings are located below the wave zone and hence not affected by the storm.
- (iii) Mooring systems and associated turret systems are small in size, making the design compact.

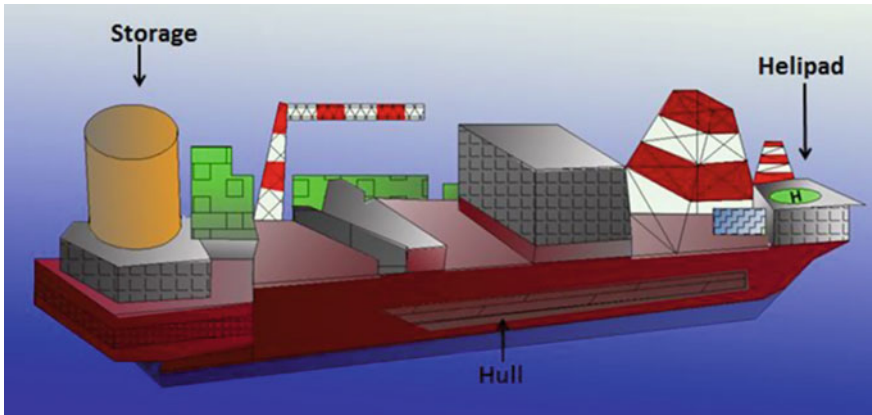


**Fig. 1.9** FPSO platform

Salient advantages of FPSO are low cost, high mobility, reduced load time, quick disconnecting ability, and little infrastructure. Disadvantages are small fields, low deck load capacity, and exposure of risers to wave action (Bai 2001).

### ***1.5.2 Semisubmersible***

These are one of the oldest types of offshore exploratory rigs, which are capable of operating in wet lands and swamps. Figure 1.10 shows a schematic view of a semisubmersible with a vertical riser storage. A semisubmersible rig floats on water surface when marched from one drilling site to another. On reaching the desired destination, a few compartments are flooded to submerge the lower part of the rig to seafloor. As the base of the rig is in contact with the ocean bottom, the effect of wind, waves, and currents is reduced (Kareem 1985; Alexnader 1985).

In these platforms, large vertical columns are connected to large pontoons; columns support the deck structure and the topside equipments. Generally, dynamic position systems (DPSs) are deployed to hold the semisubmersibles in position during production and drilling operations. Operating water depth of semisubmersibles varies from 90 to 1000 m. Salient advantages of semisubmersibles are mobility with high transit speeds (10 kn), minimum response to wave action, and large deck area. Disadvantages include high initial and operating costs, expensive to move large distances, limited dry-docking facilities and difficulties arise from mooring systems, land BOP stack, and riser in rough seas. By neglecting the influence of mooring lines, righting moment in roll motion is given by:

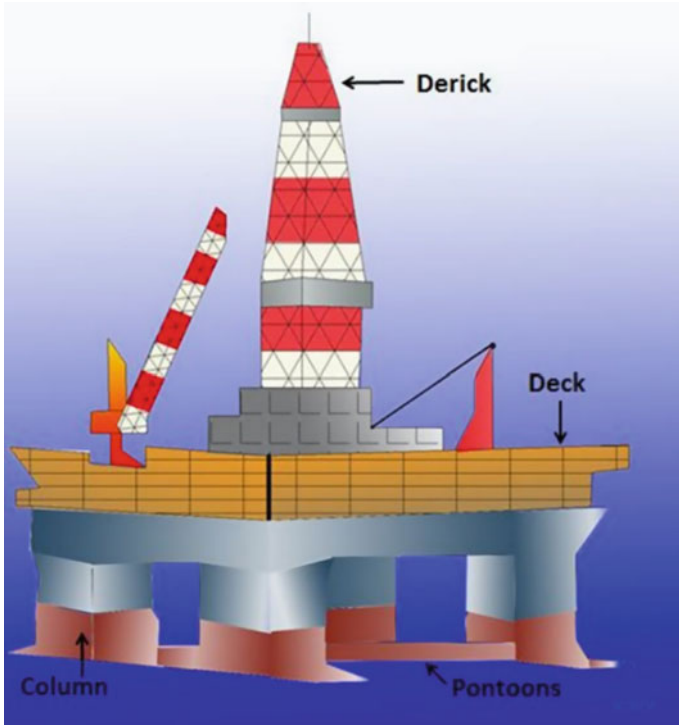


**Fig. 1.10** Semisubmersible with vertical riser storage

$$M_r = -\rho g V \overline{GM}_r \theta_r \quad (1.11)$$

where  $\overline{GM}_r$  is the metacentric height of the platform for roll. Similarly, for pitch degree of freedom, the following equation is valid:

$$M_p = -\rho g V \overline{GM}_p \theta_p \quad (1.12)$$

Roll and pitch periods of the platform are given by:

$$T_r = 2\pi \sqrt{\frac{I_v}{\rho g V \overline{GM}_r}} \cong 30 - 55 \text{ s} \quad (1.13a)$$

$$T_p = 2\pi \sqrt{\frac{I_p}{\rho g V \overline{GM}_p}} \cong 20 - 40 \text{ s} \quad (1.13b)$$

### 1.5.3 Jack-up Rigs

These structures are similar to barge with movable legs and are modified form of seagoing vessels. Figure 1.11 shows a schematic view of Jack-up rigs, indicating vital parts. They are mobile as their hulls have the requisite floating characteristics to enable towing from one site to another. When the legs are projecting upward, rig can be easily towed from one location to another. Jacking system provides an effective method to quickly lower or raise the hull. These structures attract lesser forces as the legs are transparent to waves; legs are fabricated with trusses. While the Jack-up is being towed to the site for exploratory drilling, legs will be projecting upward from the deck. On installation, legs will be pushed inside the seabed and the deck will be lifted up, hence the name ‘Jack-up rigs.’ Legs rest on the seabed with a spud-can foundation, similar to that of guyed towers (Hoeg and Tong 1977; Hoeg 1976). Components of Jack-up are namely: drilling derrick, draw works, drill floor, drill pipe, legs, living quarters, helipad, hull, spud-can, and moon pool. Failure may occur during sailing when the legs are completely above the hull. This is due to the overturning moment caused by the wind load on the projected legs. Failure may also occur at the joints of the truss legs due to bending. Rigs are capable of working even under harsh environments. Salient advantages are high mobility, stable when elevated, low cost, attracts less forces, easy fabrication, and decommissioning. Disadvantages are namely: unsuitable for all sea states, restricted to shallow depth

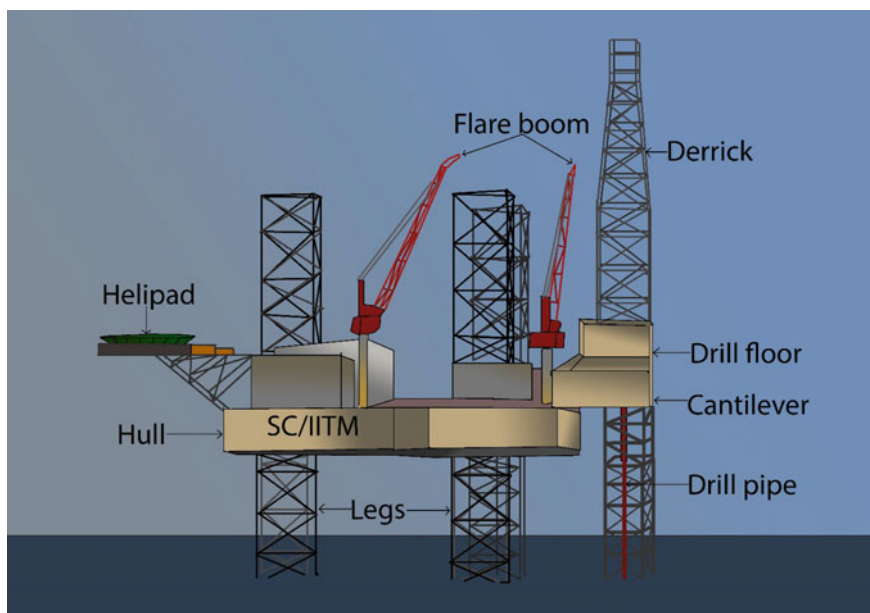


**Fig. 1.11** Jack-up platforms

of operation, initiates seabed scour leading to differential settlement, causing blowout due to soil liquefaction and not being suitable for areas with rocky stratum.

### ***1.5.4 Drill Ships***

Drill ships are designed to carry out drilling operations in deep-sea locations that are quite turbulent. A typical drill ship has the drilling platform and derrick located at the middle of its deck. They contain a moon pool, extending right through the ship down the hull. They use dynamic positioning system (DPS) for station-keeping. DPS comprises of electric motors on the underside of the ship hull and is capable of propelling the ship in any direction. Propeller motors are integrated with the computer system of the ship to maneuver in the desired path. It uses satellite-positioning technology, in conjunction with the sensors located on the drilling template to ensure that the ship is directly above the drill site at all the times during drilling operation. Advantages of the drill ships are namely: ship-shaped hull form enabling easy maneuvering, larger load-carrying capacity, and insensitivity to waves and wind even during longer periods of downtime.

## **1.6 New-Generation Offshore Platforms**

In compliant structures, major difficulty arises due to large displacement of deck in surge/sway/yaw degrees of freedom due to high flexibility in horizontal plane. It is also important to note that large displacements of the deck may cause inconvenience to crew on board and result in unsafeness under extreme sea states, in particular. Recent studies summarized conceptual development of new-generation offshore platforms by partially isolating the deck from its substructure. With such an innovative design, the following advantages are implicit, namely:

- Response of the substructure under wave loads will not influence the deck.
- Lateral loads on the deck under wind, causing high moments to the supporting structure, will be minimized.

Thus, deck response should remain local. On the other hand, it is also important to maintain sufficient level of stiffness in vertical plane to ensure safe operability. For example, large displacements in heave may result in significant tether tension variations, causing fatigue failure of tendons. It is also equally important to ensure gentle recentering under such isolated structural actions. Under the above considerations, many studies have hinted a possible set of structural forms capable of fulfilling these requirements, namely: (i) BLS; (ii) triceratops; and (iii) BLSRP (Chandrasekaran and Madhuri 2015; Chandrasekaran et al. 2007)

## 1.7 Buoyant Leg Structures

BLS are tethered spar platforms, where a group of cylinders are interconnected. Graham and Robert (1980) recent studies addressed the design of tethered buoyant platform production system highlighting the technical and economic advantages in rough sea state such as North Sea (Graham and Robert 1980; Shaver et al. 2001). Figure 1.12 shows schematic view of buoyant tower. Studies performed by researchers showed coupled in-place analysis of tension buoyant tower (TBT) using finite element software COPIPE under wind, current, and wave drift loads (Halkyard et al. 1991; Perryman et al. 1995). Based on the studies, it was concluded that the tethered buoyant platform is a cost-effective structure in comparison with that of conventional compliant offshore structures (Graham et al. 1980). Perryman et al. (1995) described the concept of tethered buoyant tower (TBT) for hydrocarbon reservoir operations capable of supporting up to 18 wells at water depth of 1800 ft. Tether tension variations of TBT are observed lesser than that of TLPs (Alexandros et al. 2008, 2009; Bar Avi 1999; Bar Avi and Benaroya 1996). Robert et al. (1995) suggested a cost-effective field development for buoyant leg structure, which is simple to fabricate, transport, and install. Recent studies highlighted several advantages on various aspects namely: i) Operational requirements;

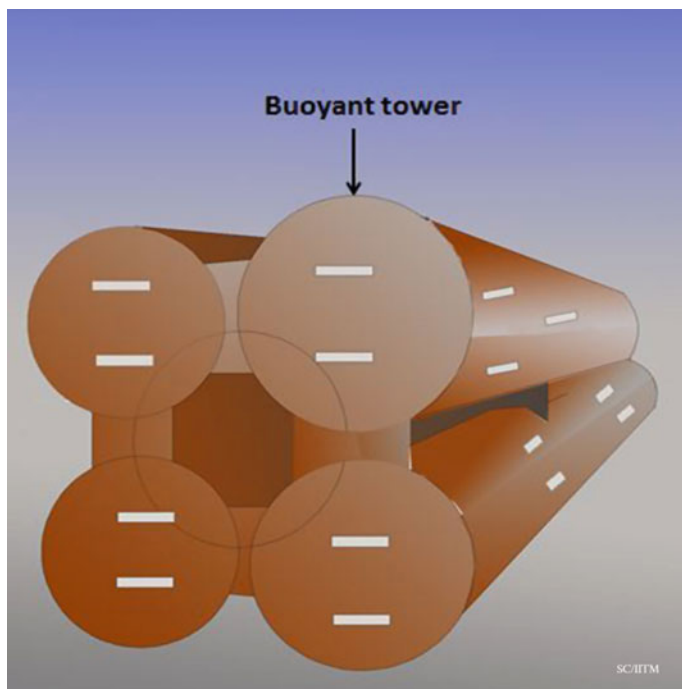


**Fig. 1.12** Buoyant tower in the fabrication yard

ii) in-service performance characteristics under critical sea states; iii) fabrication, transportation, and installation conveniences; and iv) cost savings in comparison to alternate concepts (Chandrasekaran et al. 2016). Under wave action, these structures show better performance in comparison with that of TLPs and Spar platforms. These structures are positively buoyant, which ensures high stability; further, they do not derive stability from tethers. One of the most essential features of BLS is deep draft and high stability, which makes the platform insensitive to the ultra-deep-waters (Buchner et al. 1999). Installation process of BLS is a combination of that of TLPs and spar platforms. Pretension in the support system is imposed by either ballasting or pull-down or a combination of both.

## 1.8 Triceratops

Triceratops is a new-generation offshore platform where ball joints isolate the deck from the buoyant legs, which support the deck (Capanoglu et al. 2002). Buoyant legs are in taut-moored to the seabed using tendons. Ball joints present between the deck and buoyant legs help isolate the deck from buoyant legs, making it less sensitive to encountered environmental loads. Offshore triceratops consists of a deck, which is supported by three buoyant legs. Figure 1.13 shows the conceptual view. Deck is connected to buoyant legs through ball joints that allow transfer of translation but restrain rotation between them. Under the encountered environmental loads, deck experiences reduced translational and rotation motion in comparison with that of the buoyant legs. Ball joints provide rotational compliancy to buoyant legs, conforming to horizontal position of the deck even under rough weather conditions. Ball joints transfer translational motion from buoyant legs to the deck under the wave action and vice versa under the wind action. They do not transfer moment about any axis. Buoyant legs are free to move under the action of waves, and the rotation of the BLS will not be transferred to the deck. As the ball joints transfer heave degree of motion, this ensures a rigid body motion in vertical plane similar to that of compliant structures. But the differential heave of the buoyant legs will result in pitch motion of the deck. Triceratops is similar to that of a TLP as both are heave-restrained and taut-moored to seabed. This enables to complete dry-tree installations at the mating site.

Wave direction does not influence the response of the platform as all the buoyant legs of the platform are symmetrically placed. It is also found that the deck response is lower than the buoyant leg response even in surge, which ensures better and safe operability. Rotational response of the deck is insignificant ensuring better operability. Salient advantages of the platform include:

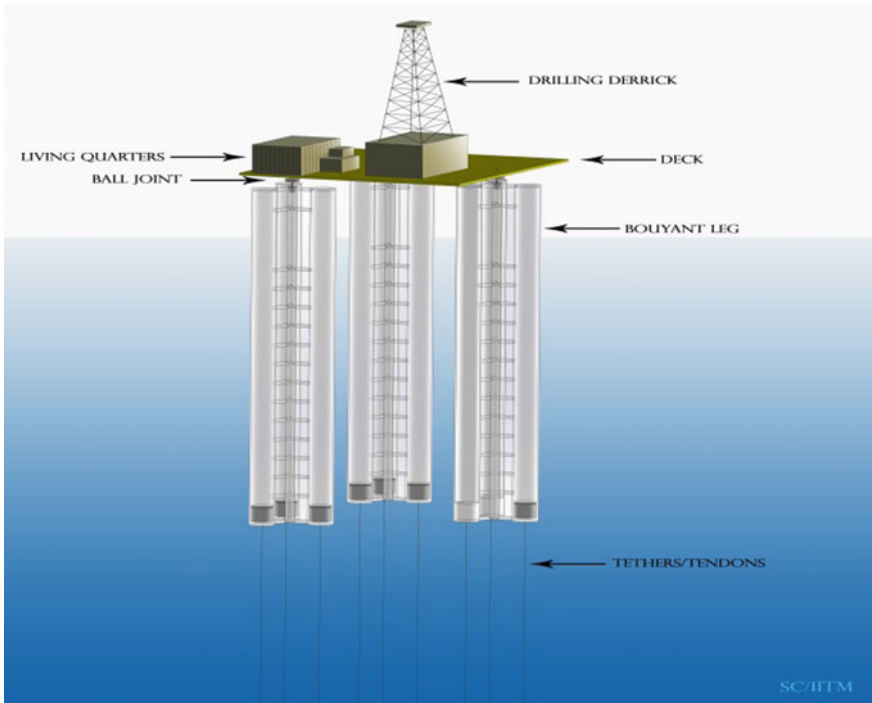


**Fig. 1.13** Conceptual view of triceratops

- Reduction of forces exerted on the platform deck due to presence of ball joints.
- Risers can be provided within the buoyant legs, and thus protecting them from the lateral loads.
- Structure is positively buoyant with a deep-draft caisson.
- Platform can float even after the failure of the tendons, which ensures safety of the platform under critical conditions.
- Easy and fast installation.
- Convenient decommissioning.
- Slow and steady recentering capability.
- Presence of ball joints for isolation of rotational degrees of freedom between the legs and the deck.

One of the major disadvantages of the platform is that the deep-draft caisson is susceptible to severe corrosion. Table 1.1 shows structural details of triceratops.

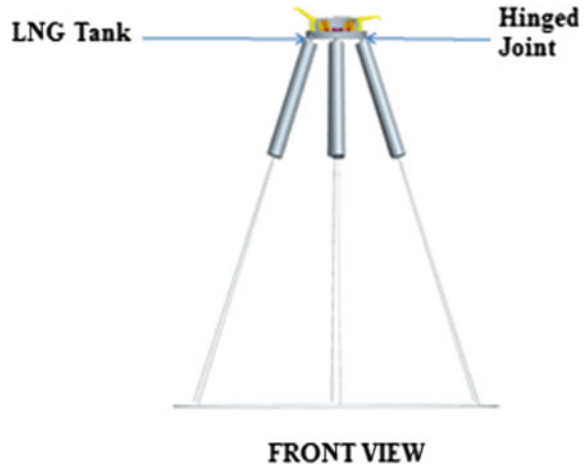
**Table 1.1** Structural details of triceratops

Description	Units	Triceratops
Water depth	m	600
Material		Steel
Unit weight	kg/m <sup>3</sup>	7850
C/C between buoyant legs	m	70
Diameter of each leg	m	17
Free board	m	22
Draft	m	74.7
Length of each leg	m	96.7
Tether length	m	525.3
Unit weight of surrounding fluid	kN/m <sup>3</sup>	10.25
Buoyancy	kN	521,600
Area of deck	m <sup>2</sup>	1732.41
Self weight + payload	kN	351,600
Radius of gyration about <i>x</i> -axis of BLS	m	33.31
Radius of gyration about <i>y</i> -axis of BLS	m	33.31
Radius of gyration about <i>x</i> -axis of BLS	m	5.02
Radius of gyration about <i>x</i> -axis of deck	m	24.9
Radius of gyration about <i>y</i> -axis of deck	m	24.9
Radius of gyration about <i>x</i> -axis of deck	m	24.6
Axial stiffness of the tether	kN/m	84,000
Diameter of tether	m	0.53
Area of tether	m <sup>2</sup>	0.22
Natural period in surge/sway	s	146
Natural period in heave	s	5.8
Natural period in roll	s	3.42
Natural period in pitch	s	2.81
Damping ratio in surge/sway	%	10.34
Damping ratio in heave	%	2.72
Damping ratio in roll/pitch	%	6.10

## 1.9 Regasification Platforms

When the crude oil is explored, it is either to be stored or to be transported to the shuttle tanker. Storage of oil is one of the major problems in compliant structures as it significantly affects the weight and buoyancy of such platforms. Usually, compliant platforms are not designed for high storage capacity; explored oil is transferred to shore either through pipe lines or shuttle tankers. While the former process is very expensive, latter involves a high risk of explosion and fire. To overcome such difficulties, innovative Floating Storage Regasification Units are developed in the recent past (Chandrasekaran and Lognath 2017). These platforms are one of the

**Fig. 1.14** Conceptual development of BLSRP: front view



effective alternatives for LNG terminals. While the main issue with LNG is its transportation, which is very hazardous, cost-effectiveness and sea state need to be accounted while transporting them by shuttle tankers. Regasification process needs a special attention in FSRUs, but it costs 50% lesser than that of the onshore production facility. But unfortunately, high degree of compliancy in horizontal plane does not suit LNG processing; thus, recent development of such platforms advocated a base-isolated deck. BLSRPs are conceived with a main objective of reducing the deck response. Figure 1.14 shows conceptual development of BLSRP.

In BLSRP, deck is supported by six buoyant legs, which are isolated by the presence of hinged joints. Similar to that of triceratops, buoyant legs are taut-moored to the seabed using tendons. A monolithic action between the deck and legs is ensured in translational degrees of freedom in the vertical plane but a complete isolation in rotational degrees of freedom. Platform shows rigid body motion in vertical plane and high compliancy in the horizontal plane. Prima facie studies carried out on BLSRP showed that the deck response is significantly lesser than that of buoyant legs in compliant degrees of freedom but without compromising on the recentering capability. As the rotational responses of the deck are also minimized, there is no danger of tether pullout. Figure 1.15 shows the geometric model of BLSRP.

## 1.10 Environmental Loads and Complexities

Environmental loads can be classified broadly as follows: (i) on the basis of physical phenomenon causing them and (ii) level of uncertainties exists in estimating them (Chandrasekaran and Roy 2006). Being time-variant, even their microscale variation affects structural response directly (Chandrasekaran and

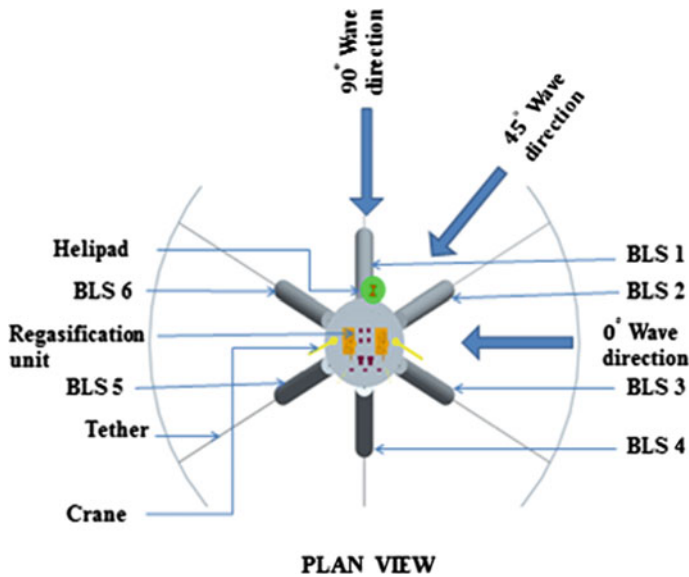
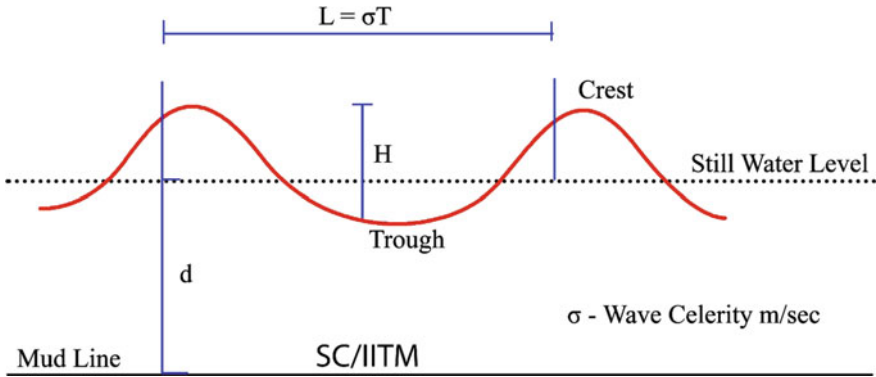


Fig. 1.15 Geometric model of BLSRP

Madhavi 2015; Chandrasekaran and Parameswara 2011). Macroscale variations include average wind velocity over a specific period of time, tidal current, significant wave height, peak period of the spectrum, and peak ground acceleration of the earthquake motion (Chandrasekaran and Gaurav 2008; Chandrasekaran and Paneerselvam 2009). Microscale variations are so rapid and give rise to the dynamic effects on the platform. Due to the degree of uncertainties present in estimating these loads that encounter offshore platforms, strong idealizations are in prevalence (Chandrasekaran and Saha 2011; Chandrasekaran and Yuvraj 2013).

### 1.11 Wave Loads

Wind-generated sea surface waves can be represented by a finite combination of regular waves (Kenny et al. 1976; Kim and Zhou 1995). Wave forces are generated based on horizontal and vertical water particle velocities and accelerations (Bea et al. 1999; Kjeldsen and Myrhaug 1979; Ker and Lee 2002; Morison et al. 1950; Morison 1953; Robert and Robert 2000; Soding et al. 1990). Airy’s wave theory is quite popular, which assumes linearity between the kinematic quantities and wave height (Mei 1993, 1966; Mei et al. 1974). It assumes a sinusoidal form of wave with wave height ( $H$ ) and wave length ( $\lambda$ ). Figure 1.16 shows schematic view of wave parameters.



**Fig. 1.16** Wave parameters

Set of governing equations to estimate water particle kinematics are given below (Ursell et al. 1960). Airy's theory is valid only up to mean sea level (MSL), and the submergence effect with respect to the mean sea level is not accounted in water particle kinematics (Hogben and Standing 1976).

$$\begin{aligned}
 \eta(x, t) &= \frac{H}{2} \cos(kx - \omega t) \\
 k &= \frac{2\pi}{\lambda} \\
 \dot{u}(x, t) &= \frac{\omega H \cos h(ky)}{2 \sin h(kd)} \cos(kx - \omega t) \\
 \dot{v}(x, t) &= \frac{\omega H \sin h(ky)}{2 \sin h(kd)} \sin(kx - \omega t) \\
 \ddot{u}(x, t) &= \frac{\omega^2 H \cos h(ky)}{2 \sin h(kd)} \sin(kx - \omega t) \\
 \ddot{v}(x, t) &= -\frac{\omega^2 H \sin h(ky)}{2 \sin h(kd)} \cos(kx - \omega t)
 \end{aligned} \tag{1.14}$$

where,  $H$  is wave height,  $\omega$  is wave frequency,  $t$  is wave period,  $k$  is wave number,  $\dot{u}$  is horizontal water particle velocity,  $\dot{v}$  is vertical water particle velocity,  $\ddot{u}$  is horizontal water particle acceleration, and  $\ddot{v}$  is vertical water particle acceleration. The following stretching modifications are considered to account for such update:

### 1.11.1 Wheeler's Modifications

$$\begin{aligned}\dot{u}(x, t) &= \frac{\omega H \cos h\left(ky \left[\frac{d}{d+\eta}\right]\right)}{2 \sinh(kd)} \cos(kx - \omega t) \\ \ddot{u}(x, t) &= \frac{\omega^2 H \cos h\left(ky \left[\frac{d}{d+\eta}\right]\right)}{2 \sinh(kd)} \sin(kx - \omega t)\end{aligned}\quad (1.15)$$

### 1.11.2 Chakrabarti's Modifications

$$\begin{aligned}\dot{u}(x, t) &= \frac{\omega H \cos h(ky)}{2 \sinh(k(d+\eta))} \cos(kx - \omega t) \\ \ddot{u}(x, t) &= \frac{\omega^2 H \cos h(ky)}{2 \sinh(k(d+\eta))} \sin(kx - \omega t)\end{aligned}\quad (1.16)$$

Waves can be classified as deep water, shallow water, and intermediate water based on the relation between the water depth and wavelength.

- Deep water:  $d > \lambda/2$ , phase speed is independent of water depth.
- Intermediate water:  $\lambda/20 < d < \lambda/2$ , phase speed will be influenced by both water depth and period.
- Shallow water:  $d < \lambda/20$ , phase speed depends only on water depth.

In order to calculate the maximum wave force, phase angle at which maximum force will occur should be first calculated. Total force is given by:

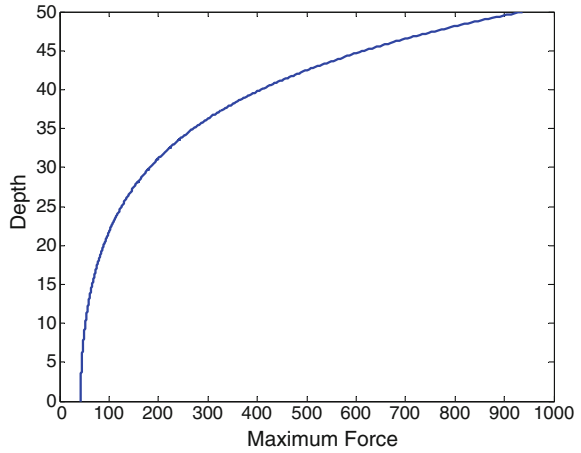
$$F_{\text{total}} = \frac{1}{2} \rho C_D D \left( \frac{\pi^2 H^2}{T^2} \right) \cdot \frac{\cos \theta [\cos \theta]}{T^2 h(kh)} \left[ \frac{\sinh(2kh)}{4k} + \frac{h}{2} \right] - C_m \rho \frac{\pi D^2}{4} \left( \frac{2\pi^2}{T^2} \right) \cdot \frac{H \sin \theta}{k}\quad (1.17)$$

To find the maximum force, the following equations hold good:

$$\frac{dF_T}{d\theta} = 0\quad (1.18)$$

$$\theta_{\text{max}} = \sin^{-1} \left[ -\frac{\pi D}{H} \cdot \frac{C_m}{C_D} \cdot \frac{2 \sin^2(kh)}{\sinh(2kh) + kh} \right]\quad (1.19)$$

**Fig. 1.17** Force variations with respect to water depth



Variation of the total force with respect to depth is shown in Fig. 1.17. Force variation also corresponds to the maximum phase angle.

Random wave is described by the following (Stokes 1880):

- (i) Short-term record length ( $T_S$ ), which indicates the duration of the system.
- (ii) Significant wave height ( $H_S$ ), which is the average wave height of the highest one-third wave in a short-term record.
- (iii) Root-mean-square of wave height ( $H_{rms}$ ), which gives the RMS value of individual wave height in a short-term record.
- (iv) Peak frequency ( $\omega_p$ ), which is the highest frequency of the system.
- (v) Significant wave frequency ( $\omega_s$ ), which is the average frequency corresponding to the significant wave height in a short-term record.
- (vi) Mean frequency ( $\bar{\omega}$ ), which gives the mean frequency of the individual wave in a short-term record.

Energy distribution of different frequencies in a sea state can be described by the wave spectrum (Liagre and Niedzwecki 2003). Spectrum is generally selected on the basis of the frequency characteristics of the wave environment (Madjid et al. 2011).

### 1.11.3 Pierson-Moskowitz (PM) Spectrum

It is a one parameter spectrum used for fully developed sea condition. It includes only the peak frequency and is given by:

$$S^+(\omega) = \frac{\alpha g^2}{\omega^5} \exp \left[ -1.25 \left( \frac{\omega}{\omega_0} \right)^{-4} \right] \quad (1.20)$$

where  $\alpha$  is Phillips constant  $\cong 0.0081$ .

#### ***1.11.4 Modified PM Spectrum***

This modified form of PM spectrum accounts for the wave height as well. It is used for describing the tropical storm waves generated by hurricanes. Governing equation is given by:

$$S^+(\omega) = \frac{5}{16} H_s \frac{\omega_0^4}{\omega^5} \exp \left[ -1.25 \left( \frac{\omega}{\omega_0} \right)^{-4} \right] \quad (1.21)$$

#### ***1.11.5 ISSC Spectrum (International Ship Structures Congress)***

This spectrum is a modified form of Bretschneider spectrum, used for fully developed sea condition. Governing equation of the sea state is given by:

$$S^+(\omega) = 0.1107 H_s \frac{\omega^{-4}}{\omega^5} \exp \left[ -0.4427 \left( \frac{\omega}{\bar{\omega}} \right)^{-4} \right] \quad (1.22)$$

$$\bar{\omega} = \frac{M_1}{M_0} \quad (1.23)$$

where,  $M_1$  and  $M_0$  are spectral moments.

#### ***1.11.6 JONSWAP Spectrum (Joint North Sea Wave Project)***

It is a modified form of PM spectrum recommended for reliability analysis. It is used for describing the winter storm waves in the North Sea. Governing equation of the sea state is given by:

$$S^+(\omega) = \frac{\bar{\alpha}g^2}{\omega^5} \exp \left[ -1.25 \left( \frac{\omega}{\omega_0} \right)^{-4} \right] \gamma^{a(\omega)} \quad (1.24)$$

where  $\gamma$  is the peakedness parameter

$$a(\omega) = \exp \left[ -\frac{(\omega - \omega_0)^2}{2\bar{\sigma}^2\omega_0^2} \right] \quad (1.25)$$

where  $\bar{\sigma}$  is spectral width parameter or shape parameter and is given by:

$$\bar{\sigma}_a = 0.07, \quad \omega \leq \omega_0 \quad (1.26)$$

$$\bar{\sigma}_b = 0.09, \quad \omega > \omega_0 \quad (1.27)$$

Modified Phillips constant is given by:

$$\bar{\alpha} = 3.25 \times 10^{-3} H_s^2 \omega_0^4 [1 - 0.287 \ln(\gamma)] \quad (1.28)$$

$$\gamma = 5 \text{ for } \frac{T_p}{\sqrt{H_s}} \leq 3.6 \quad (1.29)$$

$$= \exp \left[ 5.75 - 1.15 \frac{T_p}{\sqrt{H_s}} \right] \text{ for } \frac{T_p}{\sqrt{H_s}} > 3.6 \quad (1.30)$$

$$H_s = 4\sqrt{m_0} \quad (1.31)$$

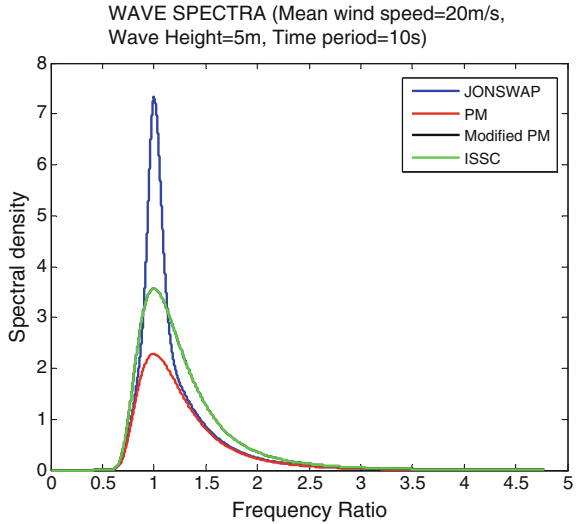
where  $\gamma$  varies from 1 to 7. Wave spectra plot for mean wind speed of 20 m/s, wave height 5 m, and period of 10 s is shown in Fig. 1.18. It is seen that the peak value of all the spectra lies on the same frequency. While highest energy peak is that of the JONSWAP spectrum, modified PM spectrum and ISSC spectrum have same spectral distribution (Subrata 1998, 2005).

## 1.12 Wind Loads

Most commonly used engineering approach in estimation of wind loads is based on the following assumptions (Davenport 1961; Dawson 1983):

- When stream of air flows with constant velocity ( $v$ ), it will generate force on the flat plate of area ( $A$ ).
- Plate will be placed orthogonal to the flow direction.
- Force imposed will be proportional to  $(Av^2)$ .

**Fig. 1.18** Comparison of wave spectra



- Proportionality constant is independent of area, which is verified by experimental studies.

Hence, wind force on a plate placed orthogonal to the wind flow direction can be determined by the net wind pressure and is given by:

$$p_w = \frac{1}{2} \rho_a C_w v^2 \tag{1.32}$$

where  $\rho_a$  is mass density of air ( $1.25 \text{ kg/m}^3$ ), which increases due to splash up to a height of 20–30 m, and  $C_w$  is wind pressure coefficient. Total wind-induced force on the plate is given by:

$$F_w = p_w A \tag{1.33}$$

If the plate is kept at an angle of inclination to that of the wind direction, then the projected area should be considered for calculating the wind pressure. Wind force has two components, namely: drag force and lift force. Wind forces in the directions parallel (drag force) and normal to the wind direction (lift force) are given by:

$$\begin{aligned} F_D &= \frac{1}{2} \rho C_D \bar{v}_z A \\ F_L &= \frac{1}{2} \rho C_L \bar{v}_z A \end{aligned} \tag{1.34}$$

Wind spectrum above water surface is given by 1/7th power law:

$$v_z = V_{10} \left[ \frac{z}{10} \right]^{\frac{1}{7}} \quad (1.35)$$

where  $v_z$  is the wind speed at elevation of  $z$  m above MSL,  $V_{10}$  is the wind speed at 10 m above MSL, and 10 m height, used in the above expression, is called the reference height. Power law is most widely used and found to be in good agreement with that of the actual field measurements. Wind has two components, namely: (i) mean wind component and (ii) fluctuating gust component. Gust component is generated by the turbulence in the flow field. It is shown that gust component is lesser than that of the mean wind component.

$$V(t) = \bar{v} + v(t) \quad (1.36)$$

where  $\bar{v}$  is the mean wind component and  $v(t)$  is the gust component.

Spatial dependence of the mean component is only along the height, while the gust component is homogenous in both space and time. Sustained wind speed is enhanced by the gust factor (=1.35–1.45) to account for the gust wind speed. Sustained wind speed is defined as one-minute average wind speed and is one of the important design parameters. In offshore platforms, a 100-year sustained wind velocity of 125 mph is used in the design. Wind is a dynamic process, and the following parameters are important in estimating the wind load:

- Length of the record, which may be either continuous or intermittent.
- Average time, which is the total time over which the record is averaged.
- Wind spectrum, which is an important input in the static analysis.
- Cross-spectrum, which is a measure of spatial distribution of wind speed.

Various complexities present in estimating wind loads arise from spatial distribution, gust component, duration of record, return period, etc. Equivalent static analysis is an alternative to address these issues, which uses aerodynamic admittance function (AAF) in estimating wind loads. Aerodynamic admittance function is used to find the equivalent total load on the members caused by wind. Reasons for using this function are namely:

- (i) To bypass the rigorous random process.
- (ii) This function can be measured experimentally using the wind tunnel experiments and hence can be easily quantified.

Considering wind as sum of mean component and gust component, the following statements hold good:

$$\begin{aligned}
 F_w(t) &= \frac{1}{2} \rho_a C_w v^2 A \\
 &= \frac{1}{2} \rho_a C_w A [\bar{v} + v(t)]^2 \\
 &= \frac{1}{2} \rho_a C_w A [\bar{v}^2 + (v(t))^2 + 2\bar{v}v(t)]
 \end{aligned} \tag{1.37}$$

by neglecting higher powers of gust component,

$$\cong \bar{F}_w + \rho_a C_w A \bar{v} v(t)$$

In the above equation, first term gives the steady mean drag force and the second term gives the fluctuating zero mean drag force.  $v(t)$  is handled as a random process, and for simplification, this can be modeled as a deterministic process. Considering wind as ergodic, power spectral density function of wind is given by:

$$S_F^+(\omega) = [\rho_a C_w A \bar{v}]^2 S_U^+(\omega) \tag{1.38}$$

By simplification,

$$S_F^+(\omega) = \frac{4[\bar{F}_w]^2}{[\bar{v}]^2} \left[ \chi \left\{ \frac{\omega \sqrt{A}}{2\pi \bar{v}} \right\} \right]^2 S_U^+(\omega) \tag{1.39}$$

The aerodynamic function varies as follows:

$$\begin{aligned}
 \text{for } \frac{\omega \sqrt{A}}{2\pi \bar{v}} \Rightarrow 0, \quad \chi \left\{ \frac{\omega \sqrt{A}}{2\pi \bar{v}} \right\} &\Rightarrow 1 \\
 \text{for } \frac{\omega \sqrt{A}}{2\pi \bar{v}} \Rightarrow \infty, \quad \chi \left\{ \frac{\omega \sqrt{A}}{2\pi \bar{v}} \right\} &\Rightarrow 0
 \end{aligned} \tag{1.40}$$

One of the main advantages of the function is that it simplifies the random process of wind load. In the following section, we shall discuss a few of commonly used wind spectra for offshore structure's analysis.

### 1.12.1 Davenport Spectrum

High-frequency content of wind data is focussed in this spectrum and is given by:

$$\frac{\omega S_u^+(\omega)}{\delta \bar{U}_p^2} = \frac{4\theta^2}{(1 + \theta^2)^{4/3}} \tag{1.41}$$

### 1.12.2 Harris Spectrum

Spatial correlation of mean wind velocity variation and the gust effects are considered in Harris spectrum and are given by:

$$\frac{\omega S_u^+(\omega)}{\delta \bar{U}_p^2} = \frac{4\theta}{(2 + \theta^2)^{5/6}} \quad (1.42)$$

Derivable variable ( $\theta$ ) is given by:

$$\theta = \frac{\omega L_u}{2\pi \bar{U}_{10}} = \frac{\delta L_u}{\bar{U}_{10}}, \quad 0 < \theta < \infty \quad (1.43)$$

where  $L_u$  is integral length scale (=1200 m for Davenport and 1800 m for Harris spectrum) and  $\delta$  is surface drag coefficient (=0.001 for offshore locations).

### 1.12.3 Kaimal Spectrum

$$\frac{\omega S_u^+(\omega)}{\sigma_u^2} = \frac{6.8\theta}{(1 + 10.2\theta)^{5/3}} \quad (1.44)$$

where  $\sigma_u^2$  is the variance of  $U(t)$  at reference height of 10 m. The derivable variable is given by:

$$\theta = \frac{\omega}{\omega_p} \quad (1.45)$$

where  $\omega_p$  is the peak frequency.

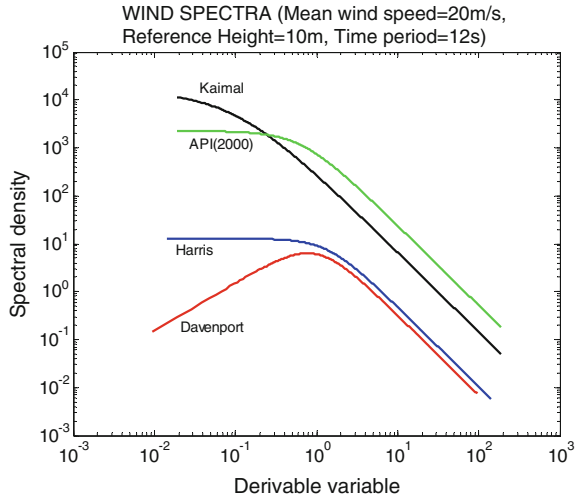
### 1.12.4 API(2000) Spectrum

$$\frac{\omega S_u^+(\omega)}{\sigma_u(z)^2} = \frac{(\omega/\omega_p)}{[1 + 1.5(\omega/\omega_p)]^{5/3}} \quad (1.46)$$

where  $\omega_p$  is peak frequency and  $\sigma_z^2$  is the variance of  $U(t)$ , which is not assumed as independent.

$$0.01 \leq \frac{\omega_p z}{\bar{U}(z)} \leq 0.1 \quad (1.47)$$

**Fig. 1.19** Wind spectra



$$\sigma_u(z) = \begin{cases} 0.15\bar{U}(z)\left(\frac{z}{Z_s}\right)^{0.125} & : Z \leq Z_s \\ 0.15\bar{U}(z)\left(\frac{z}{Z_s}\right)^{0.275} & : Z > Z_s \end{cases} \quad (1.48)$$

where  $Z_s$  is the thickness of the surface layer, which is usually taken as 20 m. Spectral density plot showing different wind spectra for mean wind speed of 20 m/s and time period 12 s at a reference height of 10 m is shown in Fig. 1.19.

### 1.13 Ice Loads

Ice loads are dominant in arctic region. Excitation caused by ice is modeled as sinusoidal pseudo-excitation. Response of the platform under ice loads is expressed using an appropriate transfer function. Prediction of ice loads is also associated with certain uncertainties. These are various ice conditions that exist, namely: (i) level ice; (ii) broken ice; (iii) ice ridges; and (iv) ice bergs. Ice loads may cause the following effects on the structure, namely: creep, cracking, buckling, spalling, and crushing. Ice loads exhibit high randomness in both space and time. Ice loads are classified as total load and local loads. The global/total loads affect overall motion and stability of the platform, while local load affects the structural member of the structure at local points. One of the main parameters that characterizes ice load is the frequency of interaction between the structure and ice. Codes handle ice loads as

extreme static loads. Ice loads depend upon the shape of the structure and formation shape of ice. Ice loads can cause less response on conical structures than that of the cylindrical structures. This may be attributed to the fact that a well-defined cone can change ice failure mode from crushing to bending. Ice spectrum on a narrow conical structure is given by:

$$S^+(f) = \frac{A \bar{F}_0^2 \bar{T}^{(-\delta)}}{f^\gamma} \exp \left[ -\frac{B}{\bar{T}^{(\alpha)} f^\beta} \right] \quad (1.49)$$

where  $A$  ( $=10$ ),  $B$  ( $=5.47$ ) are constants;  $\bar{F}_0$  is the force amplitude on the structure;  $\bar{T} = L_b/v$  is the period of ice;  $L_b$  is ice-breaking length, which is typically 4–10 times of thickness of ice;  $v$  is the velocity; and  $\alpha$ ,  $\beta$ ,  $\gamma$ ,  $\delta$  are constants whose values are typically 0.64, 0.64, 3.5, and 2.5, respectively. Force amplitude on the structure is given by:

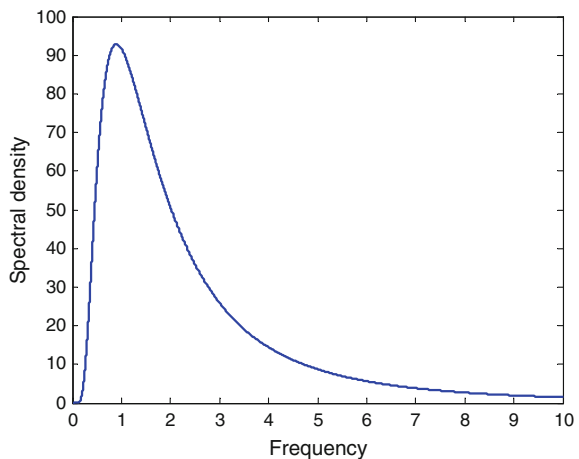
$$\bar{F}_0 = C \sigma_f h^2 \left( \frac{D}{L_c} \right)^{0.34} \quad (1.50)$$

where  $C$  is the constant (usually taken as 3.4);  $\sigma_f$  is bending strength of ice (0.7 MPa);  $h$  is the ice thickness;  $D$  is the diameter of the ice cone; and  $L_c$  is the characteristic length of ice, which is given by the following equation:

$$L_c = \left[ \frac{Eh^3}{12g\rho_w} \right]^{0.25} \quad (1.51)$$

where  $E$  is Young's modulus of ice ( $=0.5$  GPa) and  $\rho_w$  is density of water. Spectral density plot for Bohai Gulf region is shown in Fig. 1.20. Variables such as ice thickness, velocity of ice cap, and the diameter of the ice cone are chosen with respect to the Bohai Gulf region.

**Fig. 1.20** Ice spectrum for Bohai Gulf region



Ice-induced vibration may cause fatigue failure in the tubular joints, human discomfort, and flange loosening of pipes. Ice loads are normally measured by monitoring the acceleration of the deck, which is idealized as a stationary, Gaussian, and narrow banded process. It follows Rayleigh distribution, where the probability density function is given by:

$$p_a(a) = \frac{a}{\sigma_a^2} \exp\left(-\frac{a^2}{\sigma_a^2}\right) \quad (1.52)$$

where  $\sigma_a$  is given by:

$$\sigma_a^2 = \int_{-\infty}^{\infty} S_{\ddot{u}\ddot{u}}(f) df \quad (1.53)$$

where  $S_{\ddot{u}\ddot{u}}$  is the PSD of the deck acceleration response of ice load. If the ice velocity is divided into  $j$  groups and ice thickness is divided into  $i$  groups, the following statement holds good:

$$N = I \times J \quad (1.54)$$

Probability of occurrence of the  $k$ th ice case is given by:

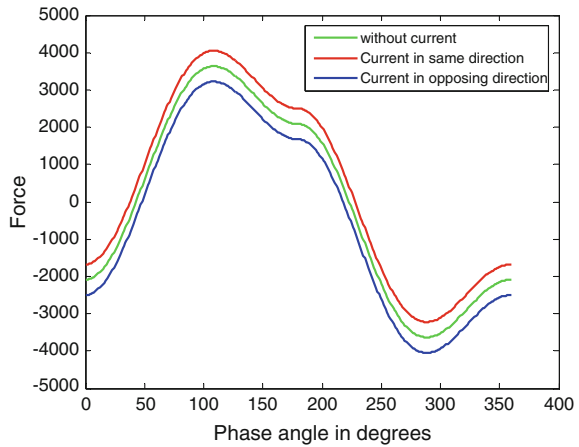
$$p_{ij} = \left[ \int_{k_i}^{k_{i+1}} p_h(h) dh \right] \left[ \int_{v_j}^{v_{j+1}} p_v(v) dv \right] \quad (1.55)$$

Ice loads on the platform can be studied in two ways, namely: (i) failure probability-based approach and (ii) expected loss-based approach. Former is more commonly practiced reliability assessment of offshore platforms (Moses 1976, 1977; Moses and Stevenson 1970).

## 1.14 Current Loads

When current is present in water, current velocity is added vectorially to the horizontal water particle velocity before computing the drag force. Current increases slowly with the increase in the depth. While opposing current will increase the force on the member, current on the same direction will decrease the force. Effect of current on the variation of total force with respect to phase angle is shown in Fig. 1.21. Effect of current on the total force is insignificant and is generally neglected. Presence of current is alternatively accounted by increasing the wave height to 10–15%, and all other effects are ignored.

**Fig. 1.21** Variation of total force due to current



## 1.15 Analysis Under Seismic Loads

Ground acceleration causes displacement and indirect load on the system. Earthquakes do not cause any direct force on the system but displace the system at the connection point, which induce forces (Venkataramana et al. 1993). Main component that governs earthquake loads is the ground acceleration, which is considered as:

- Zero mean, ergodic, and Gaussian process.
- Any system subjected to earthquake loads can be analyzed in time domain by a step-by-step algorithm.
- Actual earthquake record should be used, as far as possible.
- Process is assumed to be stationary for a time step of 20–50 s.
- Kanai-Tajimi power spectrum can be used for the analysis of offshore structures.

Once the spectrum of ground acceleration is known, wave radiation damping and inertia effects of the fluid structure interaction should be accounted (Ertas and Eskwaro-Osire 1991; Michel 1999). Offshore structures must be analyzed under the consideration of wave loads and seismic loads (Ertas and Lee 1989).

The following assumptions are made during the analysis of offshore structures under seismic loads (Chandrasekaran et al. 2008):

- (i) Seabed movement is horizontal.
- (ii) Earthquake does not cause movement of ocean surface appreciably.
- (iii) Second-order forces that can be developed in waves because of seabed movement is neglected.
- (iv) Additional wave forces that occur due to seabed movement are generally neglected (Boaghe et al. 1998).
- (v) Wind-generated wave forces are alone considered.

- (vi) If the structural member is slender, it does not produce waves of appreciable amplitude by their motion. Hence, radiation damping is neglected.

### ***Earthquake forces***

Consider motion of the supporting column member of an offshore structure in isolation. Let the seabed displace by  $u_g$  from its mean position. As a result, column deflects so that its actual displacement from the axis is considered as ' $u$ ' at any depth ' $z$ ', measured from the seabed.

Total displacement is given by:

$$u_t = u_g + u \quad (1.56)$$

The equation of motion is given by:

$$M\ddot{u}_t + C\dot{u} + ku = f(z, t) \quad (1.57)$$

where  $\ddot{u}_t$  accounts for the total acceleration caused by the earthquake and cylinder motion,  $ku$  is associated with the stiffness of the column member,  $C\dot{u}$  is the damping force, and  $F(z, t)$  is the usual Morison force for the moving structural member.

$$F(z, t) = C_m(\dot{v} - \ddot{u}_t) + C_A\dot{v} + C_D\sqrt{\frac{8}{\pi}}\sigma_r(v - \dot{u}_t) \quad (1.58)$$

where

$$C_m = \frac{\pi D^2}{4} C_m \rho \quad (1.59)$$

$$C_A = \rho A \quad (1.60)$$

Last term in the above equation approximated the drag linearization. ( $r$ ) refers to relative velocity between the structure and the fluid and is given by:

$$r = (v - \dot{u}_t) \quad (1.61)$$

$\sigma_r$  is taken to be equal to  $\sigma_v$ , as the first approximation. Rewriting the equation of motion:

$$M(\ddot{u} + \ddot{u}_g) + C\dot{u} + ku = C_M[\dot{v} - (\ddot{u} + \ddot{u}_g)] + C_A\dot{v} + C_D\sqrt{\frac{8}{\pi}}\sigma_r(v - \dot{u}_t) \quad (1.62)$$

Rearranging:

$$(M + C_M)\ddot{u} + \left( C + C_D \sqrt{\frac{8}{\pi}} \sigma_v \right) \dot{u} + ku = -(M + C_M)\ddot{u}_g - C_D \sqrt{\frac{8}{\pi}} \sigma_v \dot{u}_g + (C_M + C_A)\dot{v} + C_D \sqrt{\frac{8}{\pi}} \sigma_v v \quad (1.63)$$

Knowing the values of hydrodynamic coefficients, ground acceleration, and relative velocity, the above equation can be solved for the displacement  $\{u\}$  by standard iteration scheme. Iteration scheme is required as RHS and LHS of the equation are coupled.

TLPs are the hybrid platforms flexible in the horizontal plane and stiff in the vertical plane (Chandrasekaran et al. 2007a, b; Frank 1980). Displacement caused by the earthquake forces in the horizontal plane will have less consequence than that in the vertical plane (Chandrasekaran et al. 2008). Displacement in the vertical plane causes change in buoyancy, which may result in significant tether tension variations in tendons (Amr et al. 2013). In case of TLP, earthquake forces will affect the platform by the tether tension variation, unlike the fixed platforms having direct consequences (API RP WSD 2005). Studies showed that tether tension variation is about 12–15% of that of the initial value.

## 1.16 Analysis Under Distinctly High Sea Waves

Extreme waves are also known as freak waves, rough waves, monster waves, killer waves, and abnormal waves, as they are relatively large. These waves are a threat to large ships and platforms and challenge their survivability (Anagnostopoulos 1982; Bas and Tim 2007; Chakrabarti 1980; Chakrabarti and Tam 1975). Due to their transient nature, it is difficult to observe and also impose restraint in predicting them. Behavior of offshore platforms under distinctly high sea waves is vital (Chakrabarti et al. 1987). It is because earthquakes caused by seabed movement result in waves of large amplitude (seaquakes). In the analysis of the offshore platforms under distinctly high sea waves, the following difficulties will arise (Chakrabarti et al. 1976; Chakrabarti 1971, 1984, 1987, 1990):

- Sea surface elevation as an input is critical to evaluate.
- Shape of the wave should be steep.
- Wave should be asymmetric with respect to both vertical and horizontal axis.
- Shape of experimentally observed extreme waves is different significantly from that of the computed ones (Carl et al. 2002).
- No symmetric model is available to classify the asymmetric waves.
- Nonlinear kinematic wave theory should be used.

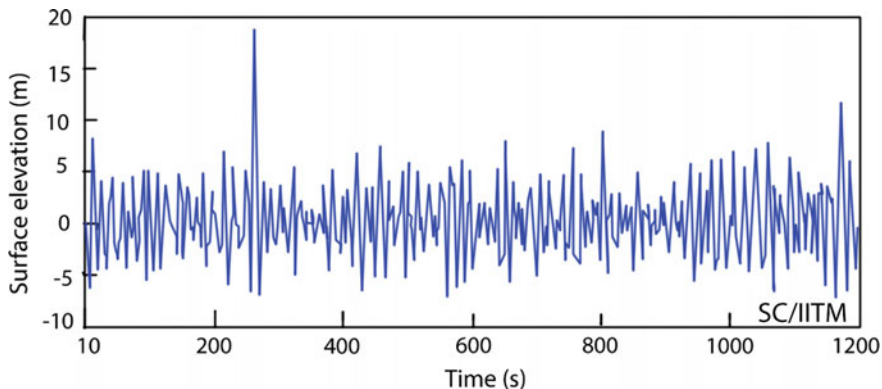


**Fig. 1.22** New Year Wave (Draupner wave)

Wave elevation is realized as the discrete sum of many sinusoidal functions, different angular frequencies, and random phase angles. Recent geographical changes in the sea state confirmed the presence of freak waves, which shall cause irreparable damages to offshore installations. Their scientific measurement is confirmed following the field observations of *Draupner wave* that occurred at the Draupner platform in the North Sea on January 1 1995 (Haver 2004); this wave is also named as New Year Wave due to the date of its occurrence. Time series of the waves is shown in Fig. 1.22.

These waves are formed due to the following reasons: (i) diffractive focusing; (ii) focusing by currents; (iii) modulation instability; (iv) wind waves; and (v) thermal expansion. Freak waves have higher potential of causing irreparable damage to offshore structures even though their probability of occurrence is very less. Researchers attempted to simulate the freak waves using linear and higher order wave theories and examined the response of offshore structures under these freak waves.

### 1.16.1 Analytical Study

An analytical study is carried out, where a combined wave model is used to simulate the sea surface elevation of freak waves and wave kinematics associated with the simulated waves. Simulated waves are compared with that of the recorded waves and thus validated by trial and error. An example TLP model is then investigated under the simulated waves; wave forces on pontoon and column members are computed using Morison equation (Burrows et al. 1992). Freak waves can excite TLPs at their natural frequencies and can result in the undesirable responses in stiff degree of freedom like heave (Chandrasekaran et al. 2011). Kriebel (2000) suggested a combined wave model to simulate the freak wave using

JONSWAP spectrum. Wave energy present in the spectrum is split at each frequency, which comprises of random waves ( $P_R$ ) and transient waves ( $P_T$ ) in the appropriate percentage, respectively. Sea surface elevation of the combination of random and transient wave is given by:

$$\eta(x, t) = \sum_{i=1}^N A_{Ri} \cos(k_i x - \omega_i t + \varepsilon_i) + \sum_{i=1}^N A_{Ti} \cos(k_i(x - x_0) - \omega_i(t - t_0)) \quad (1.64)$$

$$A_{Ri} = \sqrt{2P_R S(\omega) \Delta\omega} \quad (1.65a)$$

$$A_{Ti} = \sqrt{2P_T S(\omega) \Delta\omega} \quad (1.65b)$$

where  $A_i$  is the amplitude of wave components at  $i$ th frequency  $\omega_i$ ,  $k_i$  is the wave number,  $\varepsilon_i$  is the phase of the wave components which is a random number in the interval  $[0, 2\pi]$ ,  $N$  is the number of wave components, and  $x_0$  and  $t_0$  represent the focus point and time of the extreme transient wave, respectively.

Rayleigh statistics suggest that wave height ( $H$ ) greater than twice that of the significant wave height ( $H_s$ ) shall occur only once in about 3000 waves. In the transient wave approach, phases of the spectral wave components are selected so that waves converge into a narrow wave group. In the present example study, extreme waves are simulated by combining the above two methods of simulation; generated wave is shown in Fig. 1.23. This method is more efficient and realistic as the extreme transient wave is embedded into a random sea to produce a realistic extreme-wave sea state. This combination produced a realistic sea containing a large wave with wave height in comparison with its significant wave height ( $H = 2.14 H_s$ ) and hence satisfying the adopted definitions of freak waves.

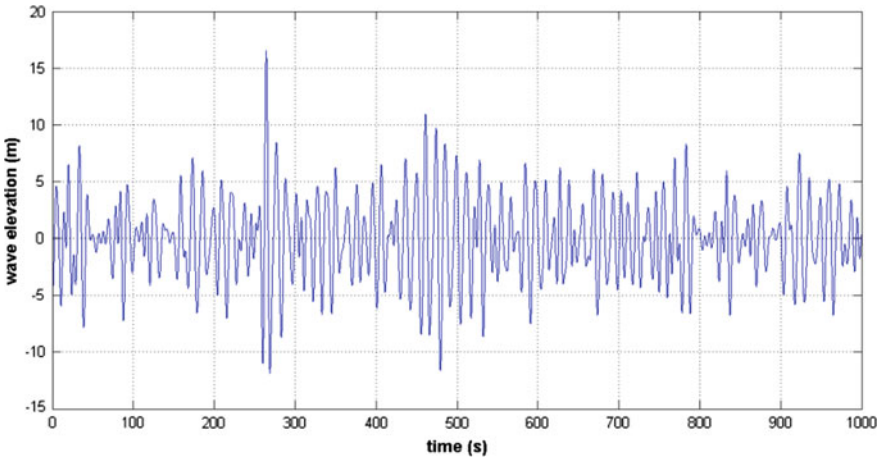


**Fig. 1.23** Sample wave records of extreme waves produced from both contrived and random process

The New Year freak wave is then simulated by embedding an extreme transient wave within a random sea, based on a partitioning of the total spectral wave energy with one part of the energy-going accounts for the underlying random waves while the remaining accounts for transient waves. Percentage of energy of random waves ( $P_R$ ) is taken as 80%, while that of the transient part ( $P_T$ ) is taken as 20%. The simulated wave is shown in Fig. 1.24.

The North Sea freak wave is also simulated by embedding an extreme transient wave within a random sea, based on a partitioning of the total spectral wave energy. By attempting several trails, characteristics of the simulated wave are made comparable with that of the recorded ones; random wave component is 78% and that of the transient component is 22%, which resulted in the simulation of the North Sea freak wave as shown in Fig. 1.25.

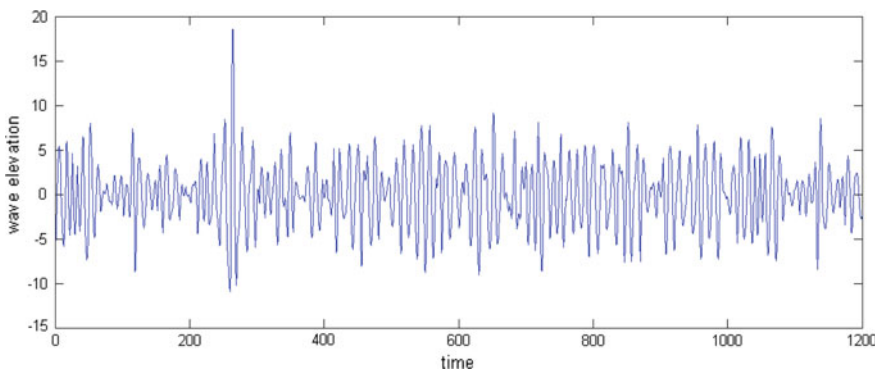


Fig. 1.24 Time series of simulated New Year extreme wave

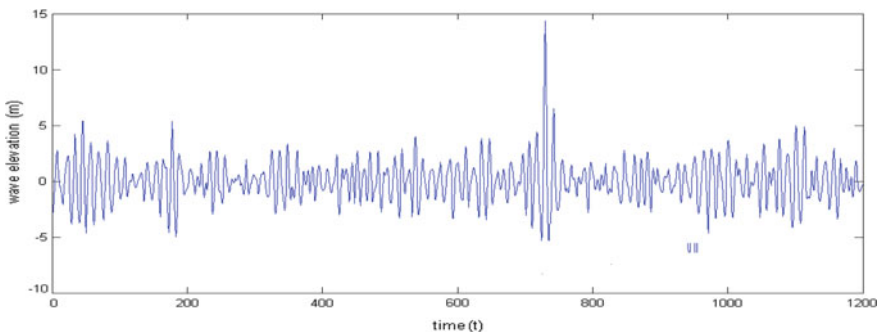


Fig. 1.25 Time series of simulated New Sea freak wave

### Hydrodynamic forces on TLP

Modified Morison's equation, accounting for relative motion between the platform and waves, is used to estimate hydrodynamic force per unit length on the members of TLP and is given by (Chandrasekaran and Jain 2004):

$$F(t) = \frac{\pi D_c^2}{4} \rho C_m \ddot{u} + \frac{1}{2} \rho C_d D_c (\dot{u} - \dot{x}) |\dot{u} - \dot{x}| \pm \frac{\pi D_c^2}{4} \rho (C_m - 1) \ddot{x} \quad (1.66)$$

where  $\dot{x}, \ddot{x}$  are horizontal structural velocity and acceleration,  $\dot{u}, \ddot{u}$  are horizontal water particle velocity and acceleration,  $\rho$  is mass density of seawater,  $C_d$  and  $C_m$  are hydrodynamic drag and inertia coefficients, and  $D_c$  is diameter of cylinder, respectively.

### Dynamic analysis of TLP

TLP model considered is square in plan as shown in Fig. 1.26 with four columns of diameter  $D_c$  and four horizontal cylindrical pontoons of diameter  $D$ . The structure is anchored to the seabed by taut-moored tethers that are attached to each corner of the platform. Properties of the TLP model are given in Table 1.2 (Fig. 1.27).

### Response of TLP under New Year Freak Wave

Dynamic response of TLP under the simulated waves is carried out in time domain; studies are carried out for TLP encountered with freak waves at different wave

Fig. 1.26 Plan of TLP model

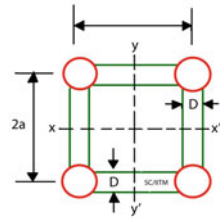


Table 1.2 Properties of TLP model

Description	Property
Weight (kN)	351,600
$F_B$ (kN)	521,600
$T_0$ (kN)	170,000
Tether length (m)	568
Water depth (m)	600
CG from keel (m)	28.44
$AE/I$ (kN/m)	84,000
Plan dimension (m)	70
$D_c$ (m)	17
$r_x, r_y, r_z$ (m)	35.10

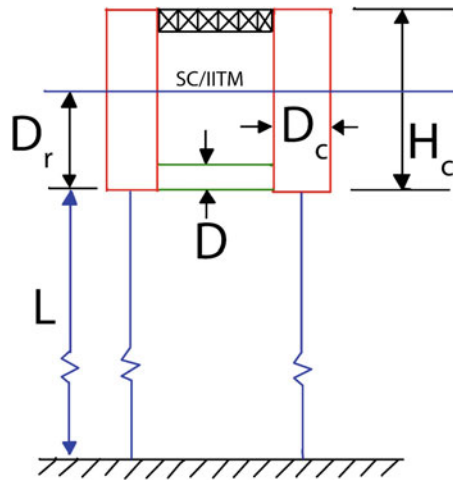


Fig. 1.27 Elevation of TLP model

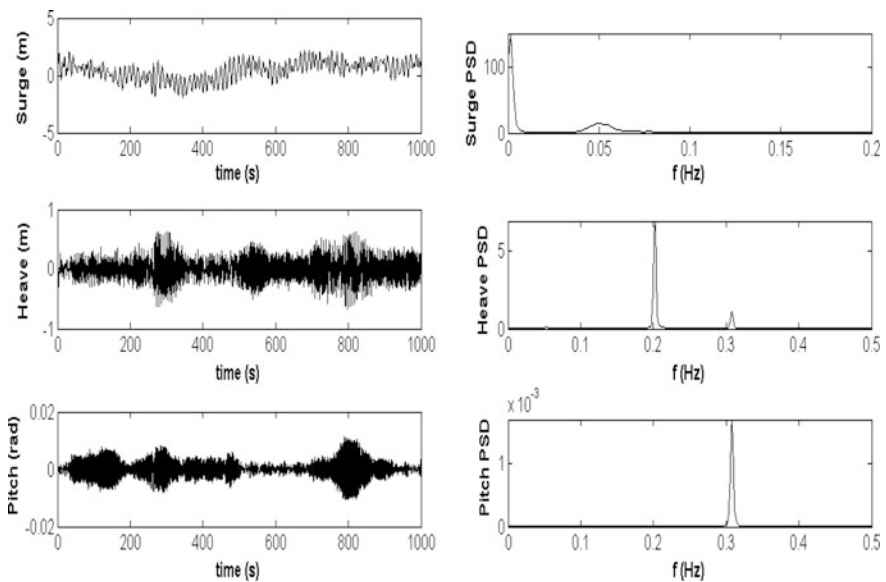


Fig. 1.28 Responses of TLP under New Year freak wave

approach angles. Figure 1.28 shows the responses of TLP in time domain and the corresponding power spectral density function (PSD) of time series data when excited by New Year Wave for waves acting along the surge direction.

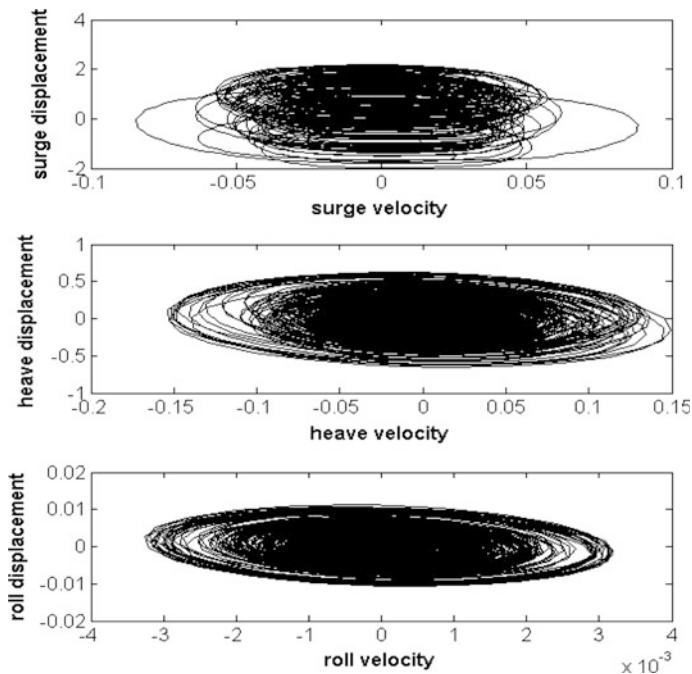
It is seen that the maximum response in surge degree of freedom is seen as 2.18 m, while that in heave and pitch degrees of freedom are found to be 0.62 m and 0.011 rad, respectively. Frequency plot of heave response shows its peak at 0.2 Hz, while that of the pitch response is seen close to 0.3 Hz. Due to symmetry, responses in sway, roll, and yaw degrees of freedom are zero for unidirectional waves acting along surge axis. Influence of different wave approach angles of New Year freak waves on the dynamic response of TLP is also investigated. Wave approach angles are varied from  $0^\circ$  to  $90^\circ$  in the interval of  $10^\circ$ , and the corresponding response of TLP in all active degrees of freedom is obtained. By comparing the surge response for all wave approach angles considered for the study, it is seen that the surge response decreases with increase in the wave approach angle from  $10^\circ$  to  $90^\circ$ . By comparing the plots of sway responses, it can be seen that the sway response increases with the increase in wave approach angle. This is due to the fact that the platform is symmetric about surge and sway axes, as a result of which such response behavior is observed. Table 1.3 gives the summary of the maximum response in all active degrees of freedom for different wave approach angles, varying from  $0^\circ$  to  $90^\circ$ . Maximum response of surge is 2.18 m at  $0^\circ$  while that of sway is  $90^\circ$ , while the maximum amplitude remains same.

Figure 1.29 shows the phase plots of the response in all active degrees of freedom, namely: surge, heave, and pitch degrees of freedom. As the formation of phase plots is elliptical, it is clear that the platform is stable under New Year freak waves for zero degree wave approach angle.

Phase plots of the response of TLP under New Year Wave are also plotted for all wave approach angles varying from  $10^\circ$  to  $90^\circ$  to examine the stability of the platform under varying wave directions. It is seen that the structure is stable under the encountered New Year freak waves, as the nature of the plots is only important to note the stability of the platform under the excited wave forces.

**Table 1.3** Maximum response of TLP for New Year freak wave

Wave approach angle ( $^\circ$ )	Surge (m)	Sway (m)	Heave (m)	Roll (rad)	Pitch (rad)
0	2.177	0	0.6223	0	0.0111
10	2.1721	1.2622	0.7548	0.0035	0.0117
20	2.1123	1.4788	0.9496	0.0065	0.0119
30	2.0366	1.6892	1.0132	0.0087	0.0115
40	1.9819	1.8866	1.025	0.0095	0.0099
45	1.9315	1.9315	1.0561	0.0097	0.0097
50	1.8864	1.9819	1.0533	0.0099	0.0095
60	1.6892	2.0366	1.0151	0.0115	0.0087
70	1.4788	2.1123	0.934	0.0119	0.0065
80	1.2622	2.1721	0.7285	0.0117	0.0035
90	0	2.177	0.6114	0.0111	0



**Fig. 1.29** Phase plots of response of TLP under New Year freak wave

***Response of TLP under North Sea Freak Wave***

TLP model is analyzed under the action of North Sea freak waves; wave approach angles are varied from 0° to 90° at intervals of 10°. Figure 1.30 shows the response of TLP in time domain and the corresponding power spectral density function (PSD) of the time series data when excited by North Sea freak wave acting along the surge direction. Maximum response in surge degree of freedom is found to be 1.38 m, while that in heave and pitch degrees of freedom are found to be 0.37 m and 0.0037 rad, respectively. The frequency plot of heave response shows its peak at 0.2 Hz, while that of the pitch response is seen close to 0.3 Hz.

Influence of different wave approach angles of New Year freak waves on the dynamic response of TLP is also investigated. Wave approach angles are varied from 0° to 90° in the interval of 10°, and the corresponding response of TLP in all active degrees of freedom is obtained. Table 1.4 gives the summary of the maximum response in all active degrees of freedom for different wave approach angles, varying from 0° to 90°. Maximum response of surge is 1.38 m at 0°, while that of sway is at 90° with the same amplitude.

Figure 1.31 shows the phase plot of the response in all active degrees of freedom, namely: surge, heave, and pitch degrees of freedom. As the formation of the plots is elliptical, it is clear that the platform is stable under North Sea freak waves for zero degree wave approach angle. Phase plots of the response of TLP under

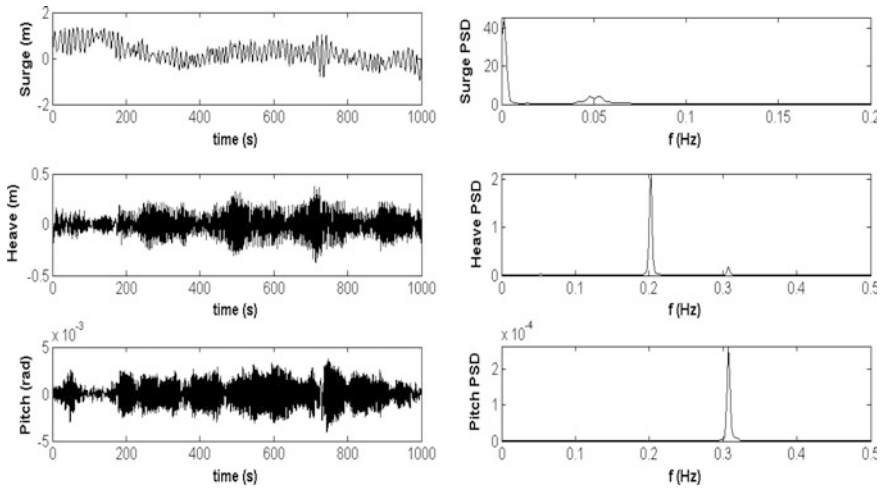


Fig. 1.30 Response of TLP under North Sea freak wave

Table 1.4 Maximum response of TLP for North Sea freak wave

Wave approach angle (°)	Surge (m)	Sway (m)	Heave (m)	Roll (rad)	Pitch (rad)
0	1.3772	0	0.3744	0	0.0037
10	1.3939	0.6392	0.412	0.0014	0.0047
20	1.3459	0.8864	0.4879	0.0025	0.0051
30	1.3015	1.0576	0.5488	0.0036	0.0047
40	1.2446	1.168	0.5749	0.004	0.0043
45	1.2106	1.2106	0.5901	0.004	0.004
50	1.168	1.2446	0.5792	0.0043	0.004
60	1.0576	1.3015	0.5468	0.0047	0.0036
70	0.8864	1.3459	0.4959	0.0051	0.0025
80	0.6392	1.3939	0.4108	0.0047	0.0014
90	0	1.3772	0.3746	0.0037	0

North Sea freak wave are also plotted for all wave approach angles varying from 10° to 90° to examine the stability of the platform under varying wave directions. It is seen that the structure is stable under the encountered North Sea freak waves, as the nature of the plots is only important to note the stability of the platform under the excited wave forces.

**Comparison of responses**

Responses of TLP under both the extreme waves are also compared. Figure 1.32 shows variation of maximum response under both New Year Wave and North Sea wave under different wave approach angles. By comparing the variations in the

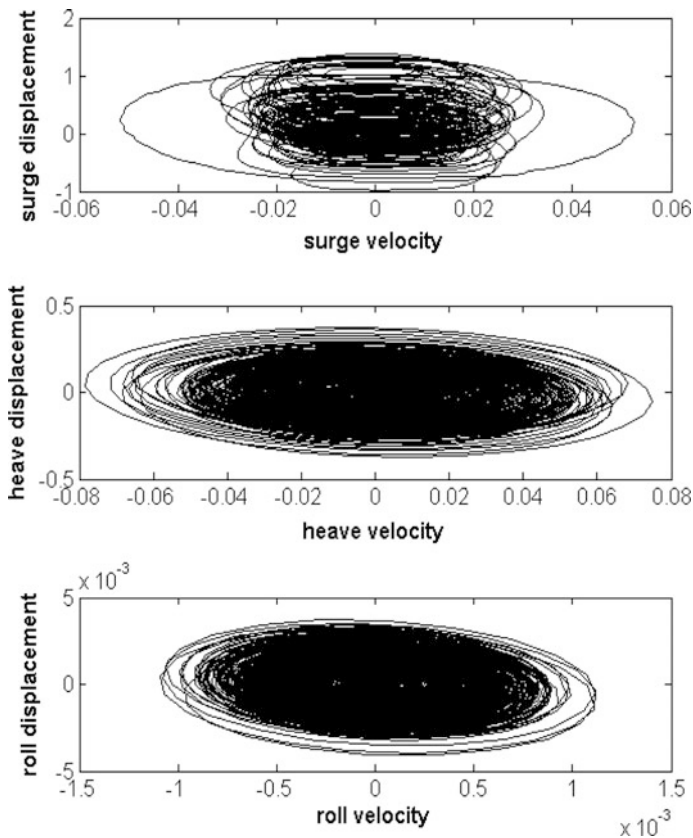


**Fig. 1.31** Phase plots of response of TLP for North Sea freak waves

maximum responses in surge and sway degrees of freedom, it is seen that maximum surge response is seen at  $0^\circ$  wave approach angle while that of the sway response at  $90^\circ$  under both the extreme waves.

### 1.17 Springing and Ringing Waves

High-frequency vibration of offshore platforms, which is referred as springing and ringing, challenged structural designers during commissioning of compliant offshore structures (Chandrasekaran et al. 2011; Chandrasekaran and Jamshed 2015a, b; Gurley et al. 1998; Peter et al. 2006). Significance of ringing and springing is accounted in the current design codes for designing tethers (Basim et al. 1996; Booton et al. 1987; Chandrasekaran et al. 2010). A study is carried out to investigate the ringing response of offshore triceratops under distinctly high sea waves

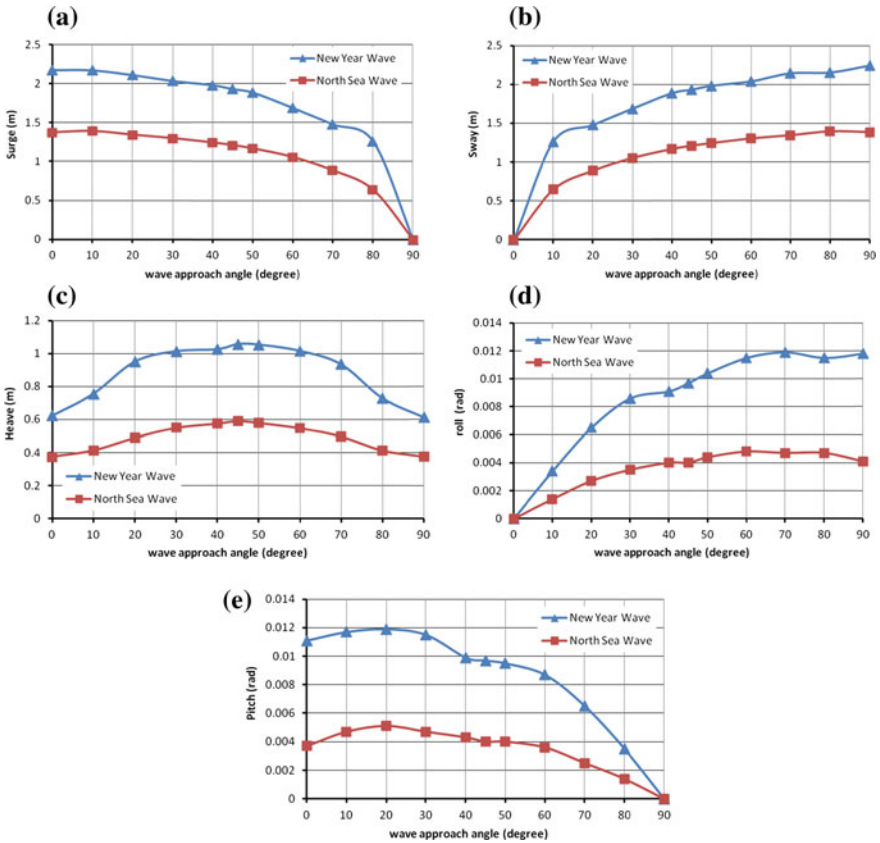


**Fig. 1.32** Variation of maximum response under North Sea wave and New Year wave: **a** surge, **b** sway, **c** heave, **d** roll, and **e** pitch

(Chandrasekaran et al. 2011). Ringing response is observed during the Heidrun TLP model tests (Kim et al. 1997a, b; Munkejord 1996; Murray and Mercier 1996). It is named after the similarity of time history with that of a church bell being struck (Jefferys and Rainey 1994). There is a fast buildup of amplified oscillations as the bell is being struck, which is followed by a slow decay as the bell transients to its tone; oscillations occur at the resonant frequency (Takezawa and Hirayama 1977; Marthinsen et al. 1992). Ringing is strong transient response of the structure observed in bending modes under severe loading conditions (Chandrasekaran et al. 2009; Davies et al. 1994). It is triggered by passage of a high steep wave in an irregular wave train (Kim et al. 1990, 1996, 1997b; Farnes et al. 1994). Ringing occurs due to the strong asymmetric waves that are generated in the transient wave mode. As data is short to interpret in statistical analysis of the response to random sea containing such strong asymmetric waves, Zou et al. (1996) developed a method to generate the same from JONSWAP spectrum by

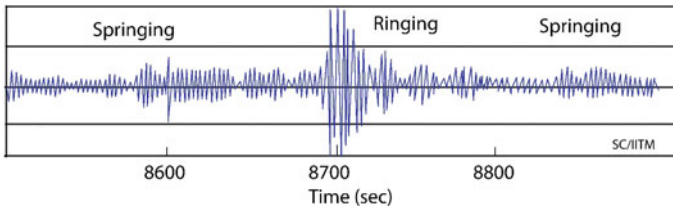


**Fig. 1.33** Springing and ringing waves

varying the parameters like significant wave height, wave period, and vertical asymmetric factor (Zou and Kim 1995; Tucker et al. 1984). Ringing phenomenon was evidently due to the strongly asymmetric transient waves. Offshore triceratops, when subjected to impact waves due to strong asymmetrical wave, shall result in the ringing, which is of larger interest to offshore structural engineers for designing tethers and fatigue life of the structure (Chandrasekaran et al. 2010). Figure 1.33 shows the schematic diagram of springing and ringing waves.

A ringing event involves excitation of transient structural deflections, closer to the natural frequency of the platform arising at third harmonic of the incident wave field (Kim et al. 1997a). In this study, numerical analysis is carried out to obtain the structural response. The structural properties of the triceratops are given in Table 1.5.

Figure 1.34 shows the numerical model of offshore triceratops. Representation of high sea state is in the form of JONSWAP spectrum. A filtered spectrum method with record length of 16 min is used to capture ringing response of tethers. Response analyses of triceratops under the chosen wave spectrum are carried out in time domain. As buoyant legs are not interconnected, studies are focused on one of the legs and the deck. Figure 1.35 shows the response amplitude operator of buoyant leg in surge, sway, heave, roll, pitch, and yaw degrees of freedom, respectively. Ringing response becomes bursting closer to 500 s, which is evident in surge, heave, and pitch responses of the buoyant leg for the unidirectional wave. This is attributed to the near-resonance response of the input wave, whose peak is at 490 s.

Response of deck and  $BLS_1$  is shown in Fig. 1.36. It is seen from the figure that pitch response of the deck is marginal in comparison with that of the buoyant leg under the impact load caused by ringing waves. Presence of ball joints restrained transfer of rotation from buoyant legs to the deck, which ensures good recentering capability even under extreme sea states (wave A with significant wave height of about 10 m).

**Table 1.5** Structural properties of triceratops

Description	Units	Triceratops
Water depth	m	600
Material		Steel
Unit weight	kg/m <sup>3</sup>	7850
C/C between buoyant legs	m	70
Diameter of each leg	m	17
Free board	m	22
Draft	m	74.7
Length of each leg	m	96.7
Tether length	m	525.3
Unit weight of surrounding fluid	kN/m <sup>3</sup>	10.25
Buoyancy	kN	521,600
Area of deck	m <sup>2</sup>	1732.41
Self weight + payload	kN	351,600
Radius of gyration about x-axis of BLS	m	33.31
Radius of gyration about y-axis of BLS	m	33.31
Radius of gyration about x-axis of BLS	m	5.02
Radius of gyration about x-axis of deck	m	24.9
Radius of gyration about y-axis of deck	m	24.9
Radius of gyration about x-axis of deck	m	24.6
Axial stiffness of the tether	kN/m	84,000
Diameter of tether	m	0.53
Area of tether	m <sup>2</sup>	0.22

## 1.18 Blast Loads

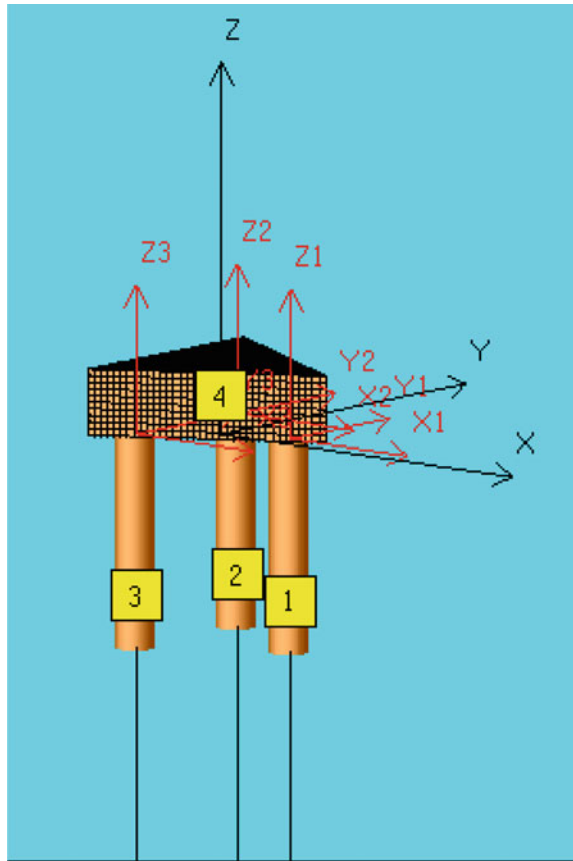
Explosion is a chemical process, which causes blast waves. Amplitude and duration of the peak over pressure vary from case to case, and it depends upon the following factors:

- (i) Distance of the object from the blast source.
- (ii) The type of explosive or flammable chemicals.

Blast waves are intensive and multi-directional and hence have the potential to cause damage from all directions. Peak over pressure ( $P_o$ ) decreases with the direction of wave propagation and distance of the location from blast source. As the blast waves propagate, they get reflected from the members encountered by them. Due to the formation of multiple wave fronts, waves cause more damage. Effective pressure applied on the face of the member is also increased due to successive reflections. The blast resistance is governed by the following factors:

- Energy absorption capacity of the construction material of the member.
- Dynamic response characteristics of the structural member itself.

**Fig. 1.34** Numerical model of offshore triceratops



In general, flexible members are less prone to severe damage under blast loads. Flexible members can absorb significant energy either by allowance to undergo large displacement by design or to avoid reflections due to their compliant nature. Steel and reinforced concrete members have significant energy absorption capacity and hence show ductile behavior. Potential points on the topside of an offshore platform could be the mass points with the epicenter of large machinery and equipment. During explosion, mass points will be targeted first.

### ***1.18.1 Protected Spaces***

Areas within the offshore platform which are intended to habitat platform occupants, vital machinery, and equipment such as control rooms, escape routes are termed as protected space. Protected space in an offshore platform should be carefully designed during the layout of the platform. Vital support systems should

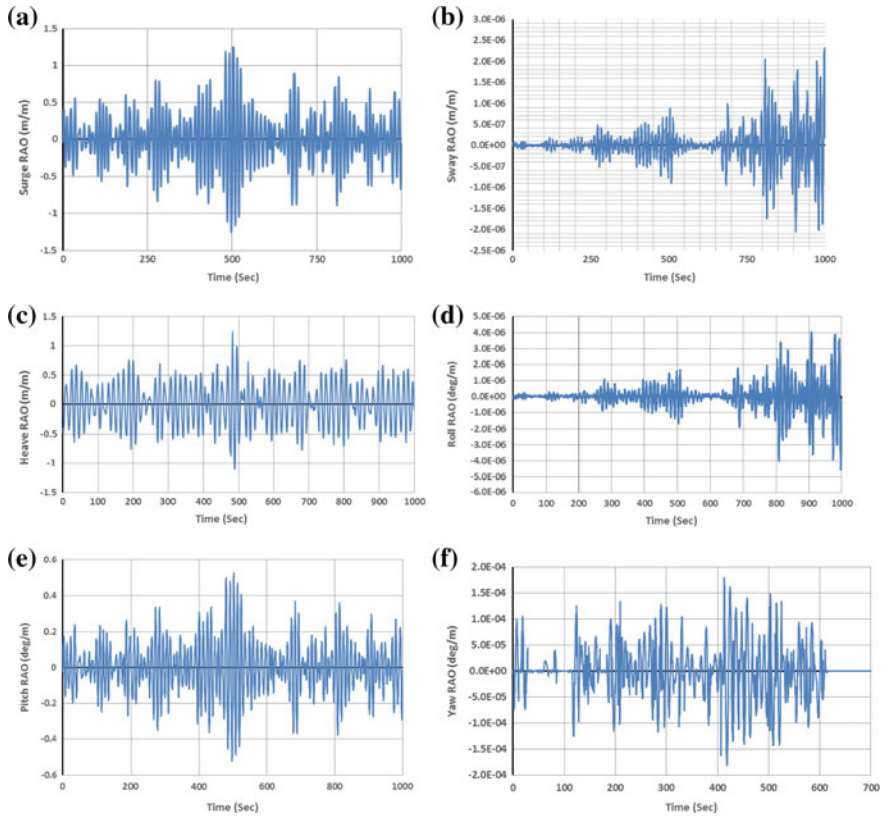


Fig. 1.35 Response of buoyant leg in a surge, b sway, c heave, d roll, e pitch, and f yaw motions

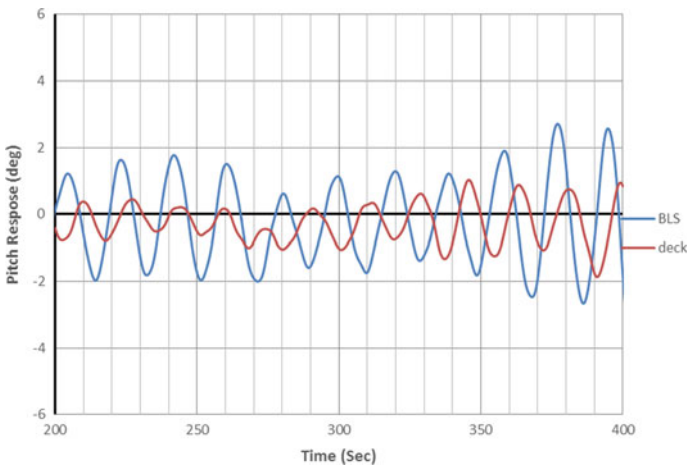


Fig. 1.36 Pitch response of deck and buoyant leg

be epicentered and located at far distance from these potential points. Protected space should be designed to remain blast-resistant. It should not become extensively hot, so that the heat load should be removed by artificial ventilation. Temperature, humidity, and ventilation should be controlled within the protected space. Special material with enhanced energy absorption capacity should be used for the construction.

### ***1.18.2 Quantification of Blast Loads***

Blast wave is the sudden release of energy into the atmosphere, which results in pressure buildup. Blast waves propagate outward in all directions from the source with the speed of either sonic or supersonic. Magnitude and shape depend on the nature of energy released from explosion and the distance of the explosion epicenter. Blast waves includes: (i) shock waves and (ii) pressure waves. Principal parameters of the blast wave are required to be defined to estimate the blast design load on an offshore platform. They are as follows:

- Peak side-on positive overpressure.
- Positive phase duration.
- Corresponding impulse.
- Peak side-on negative overpressure.
- Negative phase duration.
- Corresponding impulse.
- Peak-reflected pressure.
- Peak dynamic pressure.
- Shock front velocity.
- Blast wavelength.

## **1.19 Fire Loads**

Offshore facilities are essentially constructed to explore, produce, process, and store hydrocarbons (Mather 2000). They are large and expensive structures with unique geometry, and hence, the fire protection is very important in offshore structures (Chang 1999, 1997). Fire-resistant design of an offshore facility is complex as the topsides are laid out in a congested manner (Eurocode 3 2005; Kodur 2000, 2005; Kodur and Lee 1997; Melinek 1989). In addition, proximity of speed of fire of the blast waves from one unit to the adjacent is very high (Cheng et al. 2004; Purkiss 1984). Fire or explosion is a short-time phenomenon, and the intensity decays with the passage of time (BS 5950 2003; Majumdar and Marchertas 1997; Malhotra 1956, 1982, 1987). The propagation of the wave and the type of fire depend up on

the layout of the critical elements or members that need to be protected against fire. The potential risks in the offshore platforms include:

- Blowout.
- Riser and process leak.
- Fire and explosion.
- Vessel collision.
- Helicopter accidents.
- Dropped objects.

Level of risk is also higher due to the following reasons:

- (i) Facilities, equipment, and process design are unique, and hence, protection becomes mandatory (Twilt 1991).
- (ii) Retrofitting the damaged platform is very expensive.
- (iii) Offshore platforms operate in a remote and harsh environment.
- (iv) Offshore facilities do not have any auxiliary support of firefighting on demand.

### ***1.19.1 Types of Fire***

Fire is triggered when leakage or spill of flammable mixture occurs in the presence of potential ignition source. Fire can be classified as follows:

- (i) Pool fire.
- (ii) Jet fire.
- (iii) Fire ball.
- (iv) Flash fire.

The subclassification includes flares, fire on sea surface, and running liquid fire.

**Pool fire** is the turbulent diffusion fire, which burns above the pool of vaporizing hydrocarbon. The probability of occurrence of pool fire in offshore platform is very high due to continuous handling of hydrocarbons. It occurs from the rupture of pipelines (BoyunGuo et al. 2005).

**Jet fire** is the turbulent diffusion of the flame resulting from the combustion of fuel and release continuously. It has a significant momentum to propagate in a particular direction, especially in the downwind direction. It can affect the offshore installation, even located far away from the potential source of fire.

**Fire ball** is the rapid, turbulent combustion of fuel. Usually, it is in the form of rising and expanding a radiant ball of fire. When a fire ball attacks a vessel/tank containing pressure-liquefied gas, the pressure inside the vessel increases leading to the catastrophic failure of the vessel and loss of the complete inventory in the vessel. Under BLEVE release, explosion and thermal radiation hazard may occur.

**Flash fire** is the transient fire resulting from the ignition of the gas or vapor cloud. It initially forms a vapor cloud expanding radial and then the cloud explodes. It is more catastrophic and causes damage to large area. Fire ball can remain as a continuous flame either by sudden ignition or by delayed ignition.

## 1.20 Research Study 1: Dynamic Analysis of Buoyant Leg Storage and Regasification Platforms (BLSRPs)

In offshore structural engineering, BLSRP is one of the recent innovative structural forms that are archived to suit industrial requirements (Chandrasekaran et al. 2015; Chandrasekaran and Lognath 2015). Proposed platform consists of a deck, which is connected to six BLSs through the hinged joints, while BLS units are connected to the seabed using taut-mooring tethers. The conceived structural form is a hybrid concept, which restrains transfer of both rotational and translational responses from the BLS units to the deck and vice versa. The main advantage is the improved functionality in terms of increase in the storage and regasification capacity of liquefied natural gas (LNG).

### Experimental Investigations

Experimental investigations are carried out on a scaled model of BLSRP (1:150) under regular waves for two different wave approach angles. Free vibration tests are carried out on the scaled model to estimate the natural periods. While the deck and hinged joints are of stainless steel, BLS units are fabricated using PVC, which is ballasted with sand to achieve the required draft and pretension in tethers. Stainless steel wire ropes are used as tethers, which are pretensioned to the desired level. A mild steel base plate, placed at the flume bed, is used as the template to anchor the tethers at desired angles. Tethers are connected to each BLS unit and to the base plate of the flume bed with taut-mooring. Six rollers are attached to the circumference of the base plate for guiding the mooring lines during installation and commissioning. Experimental investigations are carried out under regular waves of 0.1 m wave height for 0° and 90° incident wave directions. Figure 1.37 shows the installed BLSRP in deepwater wave flume. Piezoelectric type accelerometers are used to measure the translational responses (i.e., surge, sway, and heave). Sensitivity of the accelerometers used in the present study is lesser than 5%. Output signal of 1 v corresponds to 9.81 m/s<sup>2</sup> acceleration, as calibrated; weight of the accelerometer is about 48 gm. Inclinometers are used to measure the rotational responses. A small spring-mass system moves in response to the change of position about a reference axis; this change in position is subsequently measured in terms of voltage. Input voltage for the device is 10 v, and range of measurement is ±80°. Output is in volts or in deg. based on the calibration constant. The calibration of inclinometer showed 1 V corresponding to 40° of rotation; weight of the

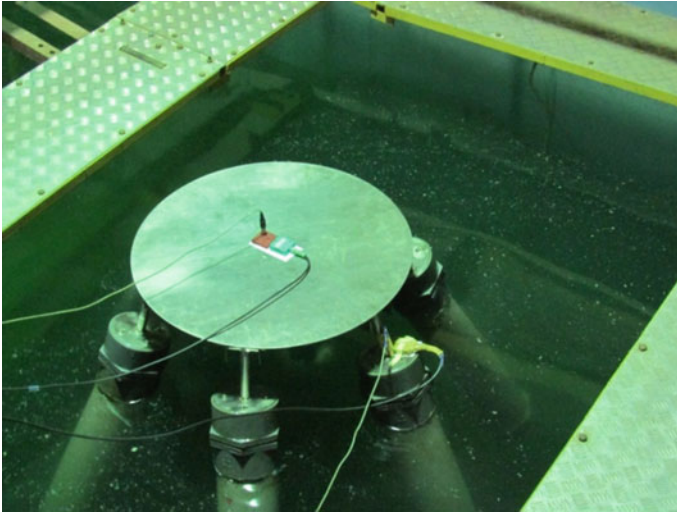


**Fig. 1.37** BLSRP in deepwater wave flume

inclinometer is about 50 gm. A set of accelerometers and inclinometers are placed both on the deck and on each BLS units to record the responses under wave loads.

### ***Response of BLSRP***

Figure 1.38 shows the response in translational degrees of freedom of the deck and each BLS units for  $90^\circ$  wave approach angle. Wave height is taken as 0.1 m, which corresponds to 15 m in the prototype. It is seen from the figures that the deck response is significantly lesser than that of any of the BLS unit, validating the use of the hinged joint. Differences in the responses of BLS units are mainly due to their asymmetry by position with respect to the wave direction. Geometric design of the BLS units, as attempted in the present study, also ensures a good recentering capability of the deck in all the translational degrees of freedom. It is important to note that hinged joints restrain the transfer of rotational motion from the BLS units to the deck and not the translational motion. Lesser heave response of deck in comparison with that of the BLS units ensures comfortable and safe operability. Hinged joints also serve as isolators, which control the deck motion even for a large BLS movement.

Figure shows the response in rotational degrees of freedom of the deck and each BLS units for  $90^\circ$  wave approach angle. It is interesting to note the presence of rotational responses in the deck despite the presence of hinged joint at each BLS units. The roll and pitch responses of the deck are due to the differential heave response that occurred from the dynamic tether tension variations. Based on the studies conducted, it is seen that the deck response is significantly lesser than that of any of the BLS units, validating the use of the hinged joint. Lesser heave response

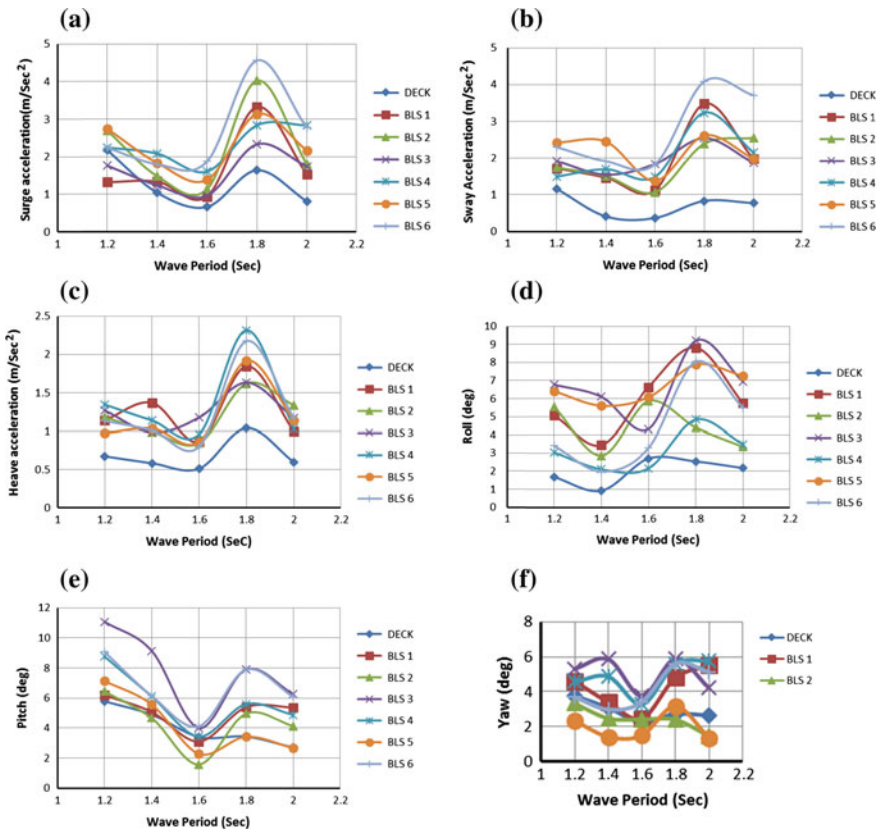


Fig. 1.38 Response of BLSRP in a surge, b sway, c heave, d roll, e pitch, and f yaw motions

of deck in comparison with that of the BLS units ensures comfortable and safe operability. Yaw response of the deck is mainly due to the time delay in the recentering capability of the BLS units under directional wave loads.

**Numerical studies**

Numerical analysis of the BLSRP is also carried out whose geometric properties are given in Table 1.6.

Numerical studies are carried out in ANSYS AQWA 14.5 software. PIPE288 tubular elements are used to model the buoyant legs, which is suitable for analyzing slender to moderately thick pipe structures. Diameter of the tubular members and their thickness are assigned in the design modeler, while deck of the platform is assigned by SOLID186 element. This element is a higher order 3-D, 20-noded solid element that exhibits quadratic displacement behavior and more suitable for tracing any in-plane deformations of the deck element under the considered loads. Mass

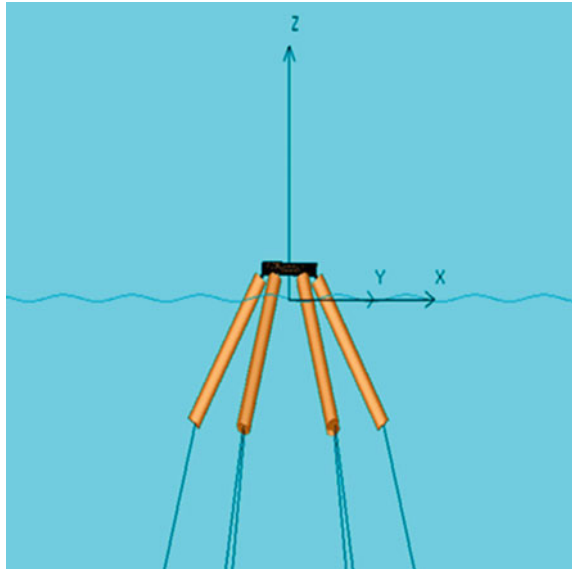
**Table 1.6** Geometric properties of BLSRP

Description	Prototype	Units
Water depth	600	m
Mass of the structure	400,000	ton
Utilities	10000	ton
Secondary deck plate	1250	ton
Stainless steel tank	1800	ton
LNG	25,000	ton
Main deck plate	2500	ton
BLS (6 no)	25,500	ton
Ballast	333,950	ton
Diameter of the BLS	22.5	m
Length of the BLS	200	m
Diameter of the deck	100	m
Draft	163.57	m
Metacentric height	15.18	m
Length of the tether	470.84	m
<i>Deck</i>		
$I_{XX}, I_{YY}$	2530725.5	ton-m <sup>2</sup>
$I_{ZZ}$	4,729,752	ton-m <sup>2</sup>
$r_{XX}, r_{YY}$	7.9	m
$r_{ZZ}$	10.8	m
<i>Single BLS</i>		
$I_{XX}, I_{YY}$	85,147,115	ton-m <sup>2</sup>
$I_{ZZ}$	1159825.3	ton-m <sup>2</sup>
$r_{XX}, r_{YY}$	37.7	m
$r_{ZZ}$	4.4	m
Tether diameter	0.05	m
Tether stiffness	875741	N/m
Height of the LNG tank	7	m
Modulus of tether	2.1E+11	N/m <sup>2</sup>

properties, center of gravity, moment of inertia, and radius of gyration of various elements like BLS units and the deck are assigned in AQWA design modeler, separately. Figure 1.39 shows the numerical model of BLSRP.

Figure 1.40 shows the response plots of all six degrees of freedom for all the six buoyant legs and the deck under 90° wave approach angle for 15 m wave height. It is seen that while all buoyant legs respond even under unidirectional waves at 90°, surge response of the deck is absent; only sway response is noticed. Under the imposed lateral load from waves, sway response of the deck is significantly lesser than that of a few of the buoyant legs. This ensures a better recentering capability of

**Fig. 1.39** Simulation of BLSRP in ANSYS AQWA



the platform. Hinged joint ensures monolithic action by transferring the translational displacements in heave motion. It can be seen that heave response of the deck is lesser than that of a few of the buoyant legs, ensuring safe and comfortable operability of BLSRP. Presence of hinged joints should have imposed restraints in transferring roll and pitch motion from BLS to that of the deck. But presence of pitch and roll responses of the deck essentially arises due to differential heave, as heave is transferred from BLS to the deck. It is evident from the study that rotational responses are not transferred from BLS to the deck; only translational responses are transferred. The yaw response of the deck is lesser than that of a few buoyant legs. This verifies the fact that the platform exhibits stiff behavior in yaw motion unlike other taut-moored platforms like TLPs.

## 1.21 Illustrated Examples

1. A spar buoy has a cylindrical tank of diameter 29 m and height of 137 m. It is commissioned at a water depth of 140 m with a draft of 107 m. The vertical displacement of the platform is  $66 \times 10^3$  tons and computes the corresponding hull oscillation time period of the system.

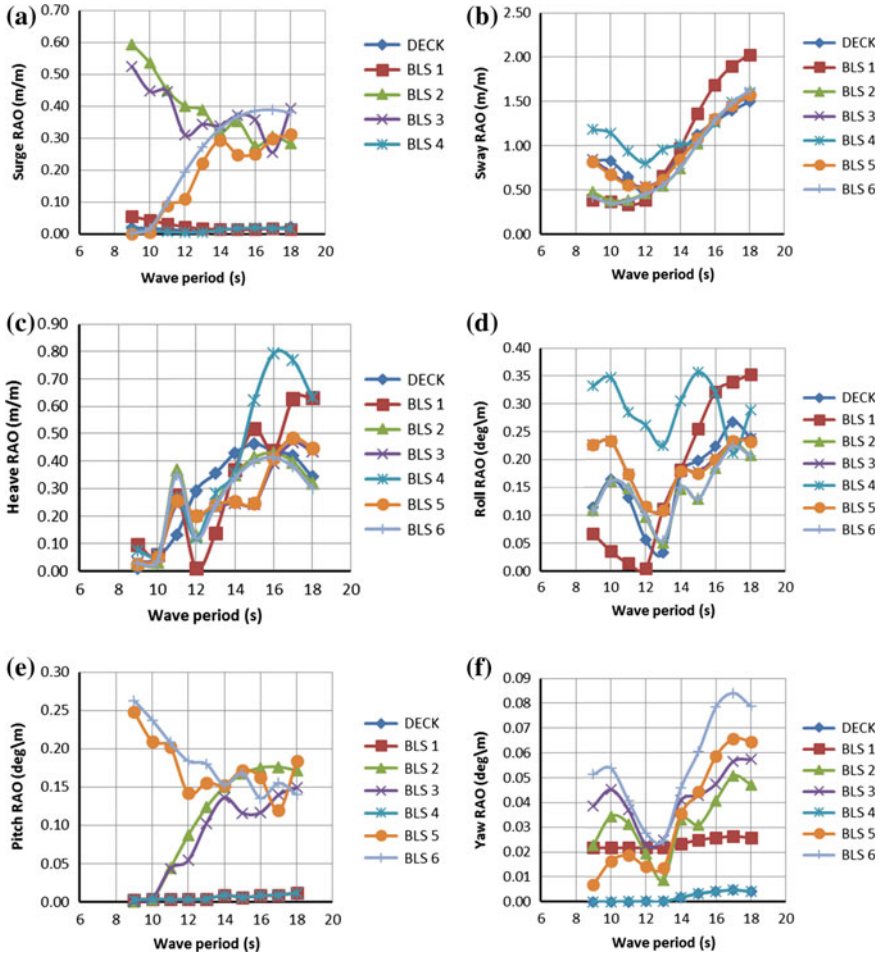


Fig. 1.40 Response of BLSRP in **a** surge, **b** sway, **c** heave, **d** roll, **e** pitch, and **f** yaw motions

The restoring force per unit displacement is given by:

$$f_r(x) = \rho g R^2(x)$$

$$f_r(x) = 1025 \times 9.81 \times 14.5^2 \times 1$$

$$= 6.64 \times 10^6 \text{ N/m}$$

Stiffness,  $k = 6.64 \times 10^6 \text{ N/m}$

Mass in the heave degree of freedom is given by:

$$m = 66 \times 10^3 \text{ tons} = 6.6 \times 10^7 \text{ kg.}$$

The heave natural period is

$$\omega_n = \sqrt{k/m} = 20.78 \text{ s}$$

2. Find the surge oscillation period of a TLP with mass of  $2 \times 10^7$  kg, total initial pretension  $10^7$  N, and length of 200 m.

The surge oscillation period is given by:

$$\begin{aligned} T_{\text{surge}} &= 2\pi \sqrt{\frac{M_{\text{surge}} l_t}{n T_t}} \\ &= 2\pi \sqrt{\frac{2 \times 10^7 \times 200}{10^7}} \\ &= 125.67 \text{ s} \end{aligned}$$

## 1.22 Examples on Probability Distributions of Continuous Random Variables

### 1.22.1 Normal Distribution

A random variable  $\{x\}$  with probability density function given as below

$$f(x) = \frac{1}{\sqrt{2\pi}\sigma} e^{-\frac{(x-\mu)^2}{2\sigma^2}}$$

is a normal random variable with parameters  $\mu$ , where  $-\infty < \mu < \infty$  and  $\sigma > 0$ .

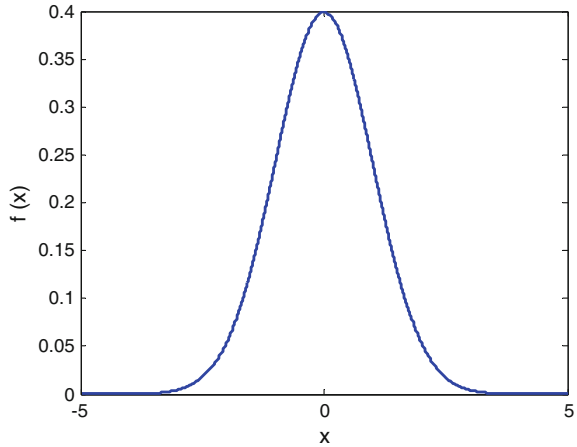
A normal random variable with  $\mu = 0$  and  $\sigma^2 = 1$  is called a standard normal random variable, and it is denoted as  $Z$ .

Cumulative distribution function of a standard normal random variable is denoted as:

$$\Phi(z) = P(Z \leq z)$$

If  $\{x\}$  is the normal random variable with  $E(x) = \mu$  and  $V(x) = \sigma^2$ , the random variable  $\{z\}$

**Fig. 1.41** Standard normal distribution curve



$$Z = \frac{X - \mu}{\sigma}$$

is a normal random variable with  $E(Z) = 0$  and  $V(Z) = 1$ . Figure 1.41 shows standard normal distribution curve.

**Example 2** Yield strength of the steel in an offshore platform is supposed to follow the normal distribution, with mean 500 Mpa and standard deviation 50 Mpa.

- (i) What is the probability that the yield strength will exceed 540 Mpa?
- (ii) What is the probability that the yield strength will lie between 490 and 510 Mpa?
- (iii) What is the probability that the yield strength is less than 400 Mpa?
- (iv) What is the yield strength of the steel for which the probability is below 0.99?

(Use standard normal distribution tables)

**Solution**

- (i) Since

$$Z = \frac{X - \mu}{\sigma}$$

$$\begin{aligned} P(X > 540) &= P\left(\frac{X - 500}{50} > \frac{540 - 500}{50}\right) \\ &= P(Z > 0.8) \\ &= 1 - P(Z \leq 0.8) \end{aligned}$$

Form the normal distribution table,

$$\begin{aligned} P(Z > 0.8) &= 1 - 0.7881 \\ &= 0.2119 \end{aligned}$$

$$\begin{aligned} \text{(ii)} \quad P(490 < X < 510) &= P\left(\frac{490 - 500}{50} < Z < \frac{510 - 500}{50}\right) \\ &= P(-0.2 < Z < 0.2) \\ &= P(Z \leq 0.2) - P(Z \leq -0.2) \\ &= 0.5793 - 0.4207 \text{ (from the table)} \\ &= 0.1586 \end{aligned}$$

$$\begin{aligned} \text{(iii)} \quad P(X < 400) &= P\left(Z < \frac{400 - 500}{50}\right) \\ &= P(Z < -2) \\ &= 0.0228 \text{ (from the table)} \end{aligned}$$

$$\begin{aligned} \text{(iv)} \quad P(X < x) &= P\left(\frac{X - 500}{50} < \frac{x - 500}{50}\right) \\ &= P\left(Z < \frac{x - 500}{50}\right) \\ &= 0.99 \end{aligned}$$

From the table,  $P(Z < 2.33) = 0.990097$

Thus,  $\frac{x-500}{50} = 2.33$

$x = 616.5$  Mpa.

### 1.22.2 Exponential Distribution

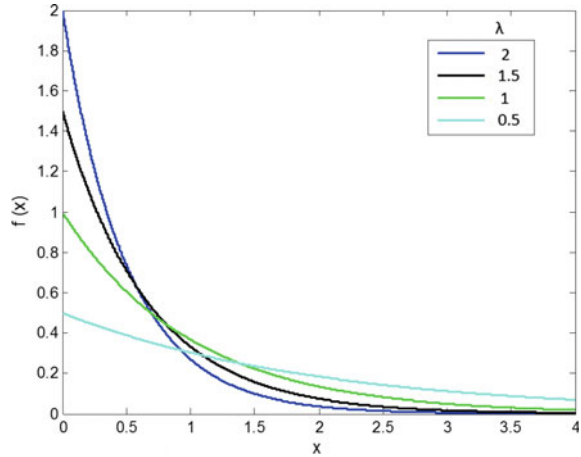
If the random variable has an exponential distribution with the parameter  $\lambda$ , then the probability density function of  $X$  is given by:

$$f(x) = \lambda e^{-\lambda x} \text{ for } 0 \leq x \leq \infty$$

Here,  $\mu = E(X) = \frac{1}{\lambda}$  and  $\sigma^2 = V(X) = \frac{1}{\lambda^2}$

Figure 1.42 shows the plot of exponential distribution.

**Fig. 1.42** Exponential distribution for different values of  $\lambda$



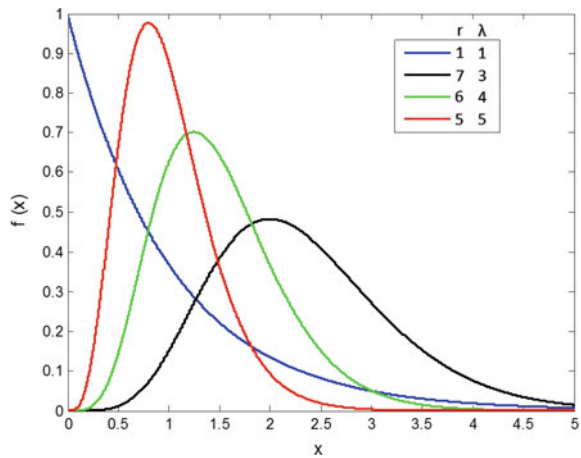
### 1.22.3 Erlang Distribution

Random variable  $\{x\}$  that equals the interval  $r$  counts occurs in a Poisson process with mean  $\lambda > 0$  that has an Erlang random variable with parameters  $\lambda$  and  $r$ . The probability density function of  $X$  is given by:

$$f(x) = \frac{\lambda^r x^{r-1} e^{-\lambda x}}{(r-1)!}, \quad \text{for } x > 0 \text{ and } r = 1, 2, \dots$$

Figure 1.43 shows the plot of Erlang distribution.

**Fig. 1.43** Erlang distribution for different values of  $\lambda$  and  $r$



### 1.22.4 Gamma Distribution

The gamma function is given by:

$$\Gamma(r) = \int_0^{\infty} x^{r-1} e^{-x} dx, \quad \text{for } r > 0$$

The random variable  $X$  with probability density function is

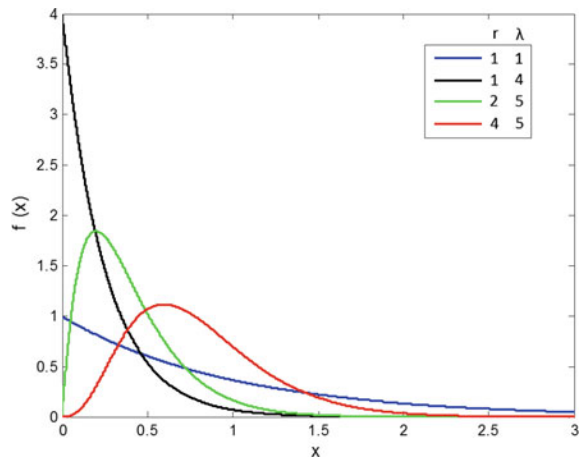
$$f(x) = \frac{\lambda^r x^{r-1} e^{-\lambda x}}{\Gamma(r)}, \quad \text{for } x > 0$$

If  $\{x\}$  is a gamma random variable with parameters  $\lambda$  and  $r$ , then the following relation holds good:

$$\mu = E(X) = \frac{r}{\lambda} \quad \text{and} \quad \sigma^2 = \frac{r}{\lambda^2}$$

Figure 1.44 shows the plot of gamma distribution.

**Fig. 1.44** Gamma distribution for different values of  $\lambda$  and  $r$



### 1.22.5 Weibull Distribution

Random variable  $\{x\}$  with probability density function is given by:

$$f(x) = \frac{\delta}{\beta} \left(\frac{x}{\delta}\right)^{\beta-1} \exp\left[-\left(\frac{x}{\delta}\right)^\beta\right], \quad \text{for } x > 0$$

and is a Weibull function with scale parameter  $\delta > 0$  and the shape parameter  $\beta > 0$ . The cumulative distribution function of  $X$  is given by:

$$F(x) = 1 - e^{-\left(\frac{x}{\delta}\right)^\beta}$$

Figure 1.45 shows the Weibull distribution.

### 1.22.6 Lognormal Distribution

Let  $\{w\}$  have a normal distribution mean  $\theta$  and variance  $\omega^2$ ; then,  $X = \exp(W)$  is a lognormal random variable with the probability density function:

$$f(x) = \frac{1}{x\sigma\sqrt{2\pi}} \exp\left[-\frac{(\ln x - \theta)^2}{2\omega^2}\right]$$

**Fig. 1.45** Weibull distribution with different values of  $\delta$  and  $\beta$

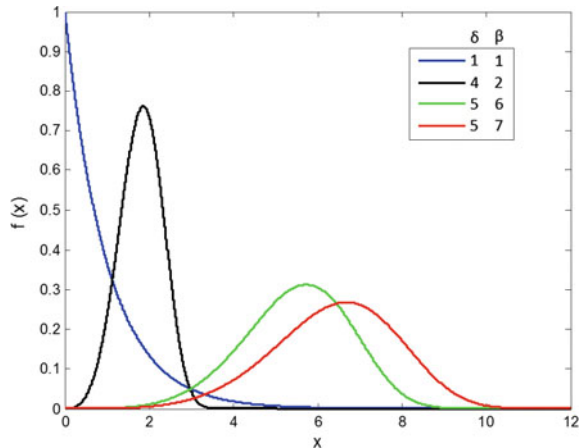
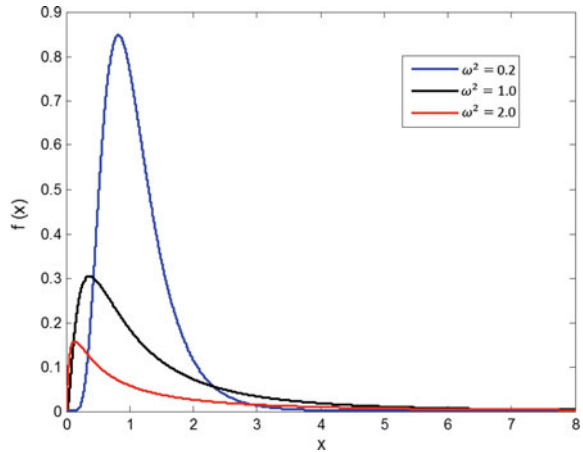


**Fig. 1.46** Lognormal distribution with  $\theta = 0$  and different values of  $\omega^2$



The mean and variance of  $X$  are given by:

$$E(X) = e^{\theta + \frac{\omega^2}{2}} \text{ and } V(X) = e^{2\theta + \omega^2} (e^{\omega^2} - 1)$$

Figure 1.46 shows the plot of lognormal distribution.

### *Tutorial 1: Novelty of offshore structures*

**Time: 60 min**

**Max marks: 20**

#### **Part A: Objective questions (10 marks)**

1. Strength degradation in offshore structural members take place due to \_\_\_\_\_ (corrosion)
2. Fixed type platforms withstand lateral loads by \_\_\_\_\_ and not by \_\_\_\_\_ (strength, relative displacement)
3. Brittle modes of failure are undesirable feature of \_\_\_\_\_ (stiff platforms)
4. Compliant offshore structures are flexible by \_\_\_\_\_ and not by \_\_\_\_\_ (geometric form, reduction in stiffness of members)
5. \_\_\_\_\_ are used to position-restrain compliant platforms (tendons/tethers/mooring lines)
6. Guyed tower acts like a \_\_\_\_\_ (inverted pendulum)
7. Capacity of the platform to reach its equilibrium position is called \_\_\_\_\_ (recentering capacity)
8. Articulated towers rely on \_\_\_\_\_ for recentering (buoyancy)

9. Tension leg platforms remain \_\_\_\_\_ in horizontal plane and rigid in \_\_\_\_\_ plane (flexible, vertical plane)
10. Tendons in TPLS are fabricated using Carbon fiber composites, whose specific gravity is \_\_\_\_\_ (1.57)

**Part B: Descriptive questions (10 marks)**

1. Why offshore structures need to adapt innovative geometric forms?  
Innovative structural form is required to make offshore structures, more adaptive to the encountered environmental loads. Main objective is to reduce the response under applied loads
2. List a few special issues that make functionality of offshore structures unique  
Should remain functional, even when they undergo repair although service life is exceeded, they are expected to serve frequent intervention, in terms of repair and rehabilitation is not preferred and not advisable  
No special/dedicated codal provisions exist to carry out repair on offshore structures.
3. List few factors considered during design of offshore structures  
Proposed structural geometry should be simple and stable  
Easy to fabricate, install and de-commissioning  
Low CAPEX  
Early state of production.
4. Discuss geometric form of compliant structures as evolved from fixed platforms  
Rigid systems, are replaced by flexible systems  
large deformation/displacements are enabled  
Design philosophy shifted from strength-based design to displacement-based design  
Flexibility introduced in the structural form features less attraction of forces encountered forces are not counteracted by strength but by large relative displacement.
5. Explain mechanics of Tension Leg Platform  
Buoyancy exceeds weight, by a large amount, which introduces flexibility to the structural form.  
Tendons are used to compensate for excessive buoyancy  
Vertical component of tether forces, in displaced position adds to the weight and improves stability in positioning while horizontal component resists lateral loads. This results in reduction in forces on structural members.

**Tutorial 2: Offshore structures****Time: 60 min****Max marks: 20****Part A: Objective questions (10 marks)**

1. Write the expression for righting moment of Articulated tower

$$[\{(B\rho) - M_B\}gl_B] - \{M_Dgl_s\}\theta$$

where  $B$  is buoyancy provided by buoyancy tank,  $\rho$  density of sea water,  $M_B$  mass of buoyancy tank,  $l_b$  distance of centre of buoyancy tank from the articulated joint,  $l_D$  length of deck (same as distance of cg of the deck from the articulated joint)

2. Write expression for righting moment of semi-submersible

$$M_r = -\rho g VGM_r \theta_r$$

3. What is snapping  
alternate slackening and tensioning
4. What is hybrid concept in compliant platform design?  
flexibility in horizontal plane and stiffness in vertical plane is called hybrid concept
5. In new generation platforms, deck response remain \_\_\_\_\_ (local or confined only to the super-structure)
6. Action of added mass offers gentle recentering due to \_\_\_\_\_ (variable submergence effect)
7. In Buoyant leg platforms, buoyant legs do not derive stability from \_\_\_\_\_ (tethers)
8. Pretension in tethers can be imposed by \_\_\_\_\_, \_\_\_\_\_ and \_\_\_\_\_ (ballasting, pull-down, both)
9. \_\_\_\_\_ in Triceratops restrain transfer of moments from the legs to deck (ball joints)
10. offshore triceratops has \_\_\_\_\_ degrees of freedom (Nine; 6 for BLS and 3 for deck)

**Part B: Descriptive questions (10 marks)**

1. List a few lacunas in compliant type offshore structures that intuted development of new-generation platforms  
Large hull displacement; quick restoration, causing damage to connecting risers; fatigue failure; snapping effect; and corrosion of deep-draft caissons (spar)
2. List difficulties in the hybrid design concept of offshore compliant platforms  
Clear band separation of frequencies make platform sensitive to both wave (high frequency phenomenon) and wind (low frequency phenomenon)

3. List one of the major deviations in the design concept of offshore platforms in the recent past  
Structural form, which resists loads by large displacement of rigid body motion is not preferred. Deck isolation from the support system is preferred
4. Highlight two vital parameters of offshore platforms, that make them insensitive to ultra-deep waters  
Deep-draft and high stability
5. While Articulated tower and Guyed tower are semi-compliant, what innovative idea, design of Articulated tower has, which replaced guyed wires  
Guyed wires offer position-restraint to the guyed tower, which also resulted in twisting moment in the guyed wires. Restoration of GT are very fast, which causes additional second order vibration around the tower. Additional loads on guy wires due to marine growth causes failure of structural action. In ATs, additional chambers namely: buoyant chamber, ballast chamber etc. are introduced. Position and size of these chambers are chosen such that recentering is gentle and invoked by variable buoyancy only. Thus, high axial tension, postulated in Guy wires, which resulted in fatigue failure was avoided.

### *Tutorial 3: Environmental loads and Special loads*

*Time: 60 min*

*Max marks: 20*

#### **Part A: Objective questions (10 marks)**

1. Offshore platforms with large compliancy need to be designed with \_\_\_\_\_ (good recentering capability)
2. How are environmental loads classified? (based on physical phenomenon causing them and their uncertainty)
3. Linear wave theory assumes linearity between \_\_\_\_\_ and \_\_\_\_\_ (water particle kinematics and wave height)
4. \_\_\_\_\_ account for water particle kinematics up to actual level of submergence (stretching modifications)
5. What is an ergodic process?  
It is a special process, which has same mean square value as that of the unique mean square value of the single sample of the ensemble.
6. Random waves are described by \_\_\_\_\_ (energy density spectrum)
7. Average gust factor used in wind load analysis is \_\_\_\_\_ (1.35)–(1.43)
8. State two advantages of using Aerodynamic admittance function in wind load analysis (it simplifies the random process for wind load estimate, this function can be estimated with higher accuracy experimentally)
9. \_\_\_\_\_ spectrum is commonly used for wind load analysis of large offshore structures (Kaimal spectrum; Dyrbye and Hensen 1997)
10. \_\_\_\_\_ is used to assess characteristic value of environmental loads (Mean return period)

**Part B: Descriptive questions (10 marks)**

1. What makes offshore Tension Leg platforms unique?  
 This is a hybrid structure, where both stiff and flexible degrees of freedom are integrated  
 Excessive buoyancy makes in afloat, which ensures no failure of the platform even in case of tendon pull-out  
 Excessive buoyancy also ensures no capsizing of the platform, making it safe even in rough weather
2. List a few attractive features of floating offshore platforms  
 They possess minimum environmental hazard because crude oil processing can be suspended, system disconnected and moved to shielded area during severe storm  
 Since lower turret mooring are located below the wave zones, it is not affected by storm  
 Mooring system and turret system are compact  
 Low cost due to high mobility  
 Quick disconnecting ability in case of storm weather  
 Reduced lead time.
3. List design objectives of tendon of TLP  
 Fatigue damage, initiated by change in tether tension variation is to be checked  
 Initial pretension should be always +ve. It means that tethers cannot slack  
 Tendons are designed to resist axial stresses and external pressure from water waves.
4. Write a brief note on heave oscillation of a Spar buoy  
 Heave oscillations develop resisting force in vertical direction. Heave oscillations are produced by vertical displacement of the spar. Restoring force is mainly due to change in buoyancy effect. Mooring lines do not contribute to the restoring action of Spar.
5. What are micro and macro scale variations in environmental loads?  
 Macro-scale variations are those which do not affect the platform response directly (for example, average wind velocity, tidal current, PGA of earthquake motion etc.). Micro-scale variations are so rapid such that they make significant influence on the response behaviour of the platform. They give rise to dynamic effects.

***Tutorial 4: Special loads******Time: 60 min******Max marks: 20*****Part A: Objective questions (10 marks)**

1. \_\_\_\_\_ is the probability that extreme value event will be exceeded in any one year (inverse of return period)
2. What is the expression to compute probability of exceedance of design load at least once within lifetime of the structure  

$$P_n = \left\{ 1 - \left\{ 1 - \frac{1}{R} \right\}^n \right\}$$
 where  $R$  is return period and  $n$  is life time of the structure

3. What parameter characterizes ice loads?  
Frequency of interaction between the structure and ice
4. Codes handle ice loads as \_\_\_\_\_ (extreme static loads)
5. Ice force spectrum is based on field data namely: \_\_\_\_\_ and \_\_\_\_\_ (ice velocity and ice thickness)
6. Relationship between variance spectrum of response and variance spectrum of load is determined by \_\_\_\_\_ (Transfer function or impulse response function)
7. Stress and strain will have a phase lag in \_\_\_\_\_ materials (visco-elastic)
8. Earthquakes cause \_\_\_\_\_ and not \_\_\_\_\_ to the system (displacement; force)
9. \_\_\_\_\_ are caused by waves generated from large sea-bed movement (sea quakes)
10. What is the design criteria for fixed offshore platform? (to limit stresses in the members)

**Part B: Descriptive questions (10 marks)**

1. What is mean return period?  
It is the expected # of years between a given, seasonal maximum value to occur. For example, if the return period is 50 years, characteristics load is expected to occur only once in 50 years
2. How many ways, a return period of an event can be expressed?  
In terms of probability of exceedance within life time of the structure; in terms of time frame; and in terms of risk associated with the event
3. What are various ice conditions that exist in life time of an offshore platform?  
Level ice, broken ice, ice ridges and ice bergs. Ice loads can cause, irrespective of any form, creep, cracking, buckling spaling and crushing. Ice loads can even change modes of failure from cracking to crushing. Ice loads exhibit high randomness both in space and time. They are classified as total load (global ice load) and local load or pressure.
4. What is White noise approximation?
5. What are the factors that govern Dynamic Modulus of Elasticity?

# Chapter 2

## Advanced Structural Analysis

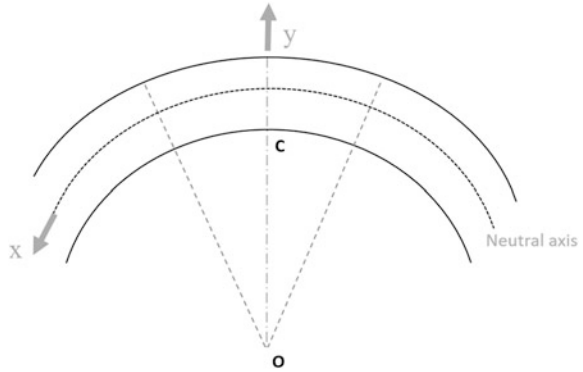
**Abstract** Analysis of offshore structures is offset from the conventional methods due to the advanced geometric forms that are conceived. As design of offshore compliant structures is no more strength based but displacement controlled, knowledge about advanced analysis methods is inevitable for a designer. Sections on unsymmetrical bending and shear center are presented in a detailed manner with an objective to serve as reference guide for the designers. Design of curved beams, which is generally discussed as a topic in advanced strength of material is also included in this chapter to make the knowledge base complete and competent. In order to understand design philosophy and analysis methods, many numerical examples following the equations that are derived from first principles are included. This chapter highlights various advanced analysis methods, which are applicable to offshore structural design in various stages. A detailed understanding of analysis tools with a precursor about special environmental loads will make this chapter interesting and self-explanatory.

### 2.1 Unsymmetrical Bending

While members are idealized as one dimensional, it is convenient to compute stresses in the cross section under the applied loads applied at the prefixed points. It is important to note that one of the major assumptions is that bending takes place parallel to the plane of the applied moment. Further, simple bending equation, which is used to estimate the bending stress assumes that neutral axis of the cross section, is normal to the plane of loading. Figure 2.1 shows the trace of the plane of applied moment. In Fig. 2.1,  $YY$  axis is the trace of the plane of the applied moment. Bending moment in the  $YY$  axis is said to be zero and mathematically,

$$\sum M_y = \int_A \sigma_x dA = 0 \tag{2.1}$$

**Fig. 2.1** Conceptual figure showing trace of applied moment



The statement  $\int zy dA = 0$  is true only when both  $ZZ$  and  $YY$  axes are the principal axes of inertia. For symmetrical bending, following conditions hold good:

- i. It is essential that the plane containing one of the principal axes of inertia, plane of applied moment, and the plane of deflection should coincide.
- ii. It is also obvious that the neutral axis will coincide with other principal axes of inertia.

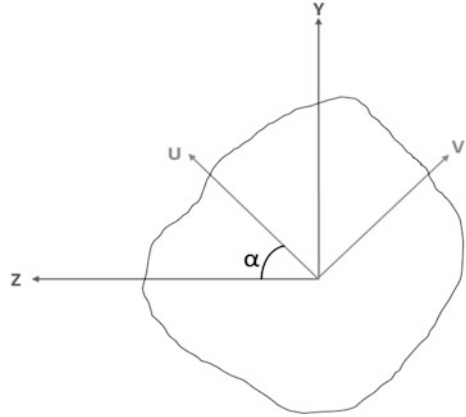
When trace of the plane of applied moment does not coincide with any of the principal axes of inertia, then this type of bending is called *unsymmetrical bending* or *non-uniplanar bending*. Under such conditions, neutral axis is no longer normal to the trace of the applied moment plane. Therefore, deflection curve will not be a plane anymore. One of the major consequences of unsymmetrical bending is that members that are symmetric about vertical axis (for example, thin-walled sections) will undergo twisting under transverse loads. It is important to note that thin-walled cross sections are common in offshore structures. Following are the conditions where unsymmetrical bending may occur:

- i. Section shall be symmetric but line of action of load is inclined to both the principal axes.
- ii. Section shall be asymmetric, and line of action of load is along any one of the centroidal axes.

In case of unsymmetrical bending, applied moment will cause bending about both the principal axes of inertia. Therefore, it is important to locate principal axes before computing stresses at any point in the cross section. If moment acts on the plane of symmetry, then the conventional simple bending equation can be used to calculate the stresses. In such cases, the following equation holds good:

$$\sigma_b = \frac{M}{I} y \quad (2.2)$$

**Fig. 2.2** Centroid and principal axes



But, if the load acts on other plane, it becomes asymmetric where one cannot use the conventional equation of flexure to obtain stresses at any point in the cross section. In such case, following procedure may be adopted to compute stresses at any point in the cross section:

**Step1: To transform the problem of unsymmetrical bending to uniplanar bending**

Consider a cross section of beam under the action of a bending moment  $M$ . Let  $\{ZZ, YY\}$  be coordinate axes passing through the centroid and  $\{UU, VV\}$  be the principal axes inclined at an angle  $\alpha$  to the  $ZZ$  axis, as shown in Fig. 2.2.

To locate the principal axes of inertia, the following equations hold good:

$$u = z \cos \alpha + y \sin \alpha \tag{2.3a}$$

$$v = -z \sin \alpha + y \cos \alpha \tag{2.3b}$$

where angle is measured in the positive coordinate. To estimate the bending stresses, moment of inertia about  $UU$  and  $VV$  axes should be calculated. The following equations hold good:

$$I_u = \int_A v^2 dA \tag{2.4}$$

$$= \int_A (-z \sin \alpha + y \cos \alpha)^2 dA \tag{2.5}$$

$$= \int_A (z^2 \sin^2 \alpha + y^2 \cos^2 \alpha - 2z \sin \alpha \cos \alpha) dA \tag{2.6}$$

$$= \sin^2 \alpha \int_A z^2 dA + \cos^2 \alpha \int_A y^2 dA - \sin 2\alpha \int_A yz dA \quad (2.7)$$

$$= I_y \sin^2 \alpha + I_z \cos^2 \alpha - I_{yz} \sin 2\alpha \quad (2.8)$$

$$\cos 2\alpha = 1 - 2 \sin^2 \alpha \quad (2.9)$$

$$= 2 \cos^2 \alpha - 1 \quad (2.10)$$

Substituting in the above equation, we get:

$$I_u = \frac{I_y}{2}(1 - \cos 2\alpha) + \frac{I_z}{2}(1 + \cos 2\alpha) - I_{yz} \sin 2\alpha \quad (2.11)$$

$$= \frac{I_y + I_z}{2} + \frac{I_z - I_y}{2} \cos 2\alpha - I_{yz} \sin 2\alpha \quad (2.12)$$

$$I_u = \frac{I_y + I_z}{2} + \frac{I_z - I_y}{2} \cos 2\alpha - I_{yz} \sin 2\alpha \quad (2.13)$$

$$I_v = \int_A u^2 dA \quad (2.14)$$

$$= \int_A (z \cos \alpha + y \sin \alpha)^2 dA \quad (2.15)$$

$$= \int_A (z^2 \cos^2 \alpha + y^2 \sin^2 \alpha + 2zy \sin \alpha \cos \alpha) dA \quad (2.16)$$

$$I_v = \cos^2 \alpha \int_A z^2 dA + \sin^2 \alpha \int_A y^2 dA + \sin 2\alpha \int_A zy dA \quad (2.17)$$

$$= \cos^2 \alpha I_z + \sin^2 \alpha I_y + I_{zy} \sin 2\alpha \quad (2.18)$$

$$= (1 + \cos 2\alpha) \frac{I_y}{2} + \frac{1 - \cos 2\alpha I_z}{2} + I_{zy} \sin 2\alpha \quad (2.19)$$

$$I_v = \frac{I_z - I_y}{2} - \frac{I_z - I_y}{2} \cos 2\alpha + I_{zy} \sin 2\alpha \quad (2.20)$$

$$I_u + I_v = I_z + I_y \quad (2.21)$$

$$I_{uv} = \int_A (uv) \, dA \quad (2.22)$$

$$= \int_A (z \cos \alpha + y \sin \alpha)(-z \sin \alpha + \cos \alpha) \, dA \quad (2.23)$$

$$= \int_A (-z^2 \sin \alpha \cos \alpha - yz \sin^2 \alpha - yz \cos^2 \alpha - y^2 \sin \alpha \cos \alpha) \, dA \quad (2.24)$$

$$\int_A z^2 \, dA = I_y \quad (2.25)$$

$$\int_A yz^2 \, dA = I_z \quad (2.26)$$

$$\int_A yz \, dA = I_{yz} \quad (2.27)$$

Using the above relationship, we get:

$$I_{uv} = -I_y \sin \alpha \cos \alpha + I_z \sin \alpha \cos \alpha + I_{yz}(\cos^2 \alpha - \sin^2 \alpha) \quad (2.28)$$

$$I_{uv} = \frac{I_z + I_y}{2} \sin 2\alpha + I_{yz} \cos 2\alpha \quad (2.29)$$

For both  $\{U, V\}$  being the principle axes of inertia, the following relationship holds good:

$$I_{uv} = 0 \quad (2.30)$$

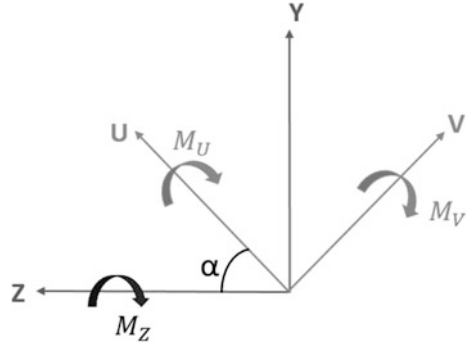
$$I_{uv} = \frac{I_z + I_y \sin 2\alpha}{2} + I_{yz} \cos 2\alpha = 0 \quad (2.31)$$

$$\tan(2\alpha) = -\frac{2I_{yz}}{I_z - I_y} \quad (2.32)$$

**Step 2: To determine the bending stress at any point in the cross section**

Figure 2.3 shows moments about the principal axes. Moments about the principal axes are given by the following relationships:

**Fig. 2.3** Direction of moments about principal axes



$$M_u = M_z \cos \alpha \quad (2.33)$$

$$M_v = M_z \sin \alpha \quad (2.34)$$

Stress at any point  $p(u, v)$  is then given by the following relationships:

$$\frac{M_u}{I_v}(v) - \text{compressive stress} \quad (2.35)$$

$$\frac{M_u}{I_v}(u) - \text{tensile stress} \quad (2.36)$$

Consider the stress equation as follows:

$$\sigma_p = \frac{M_u}{I_u}v + \frac{M_v}{I_u}u \quad (2.37)$$

$$= - \left[ \frac{M_u}{I_u}v + \frac{M_v}{I_u}u \right] \quad (2.38)$$

Negative sign in the above equation indicates compressive stress. As the quadrant of the stress decides the nature of resultant bending stress, signs of both  $\{u, v\}$  should be accounted for properly while determining the resultant stress. It is also important to note that maximum stress will occur at a point, which is at a greatest distance from the neutral axis.

## 2.2 Example Problems on Unsymmetrical Bending

**Example 1** Locate the principal axes of inertia of the section shown in Fig. 2.4. Note that all dimensions are in mm.

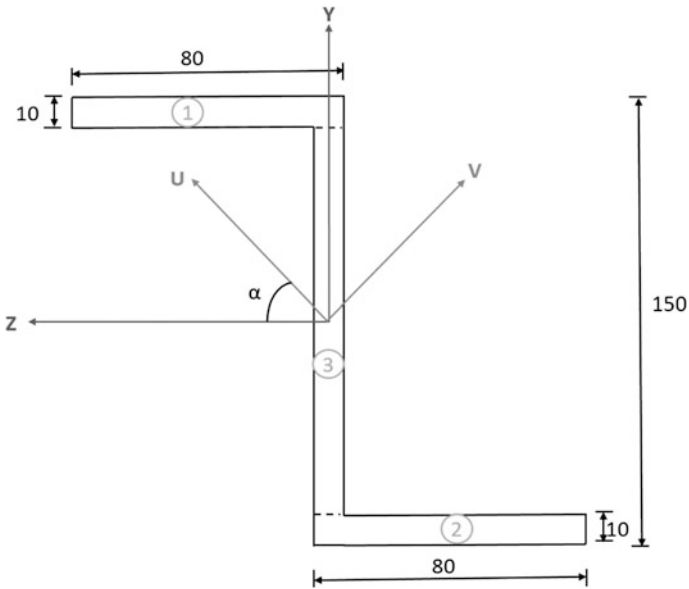


Fig. 2.4 Example problem-1

(i) *Calculation of  $I_Z$ ,  $I_Y$ , and  $I_{ZY}$ :*

$$I_Z = 2 \left\{ \frac{80 \times 10^3}{12} + (80 \times 10 \times 70^2) \right\} + \frac{10 \times 130^3}{12} = 9.684 \times 10^6 \text{ mm}^4$$

$$I_Y = 2 \left\{ \left( \frac{10 \times 80^3}{12} \right) + (80 \times 10 \times 35^2) + \left( \frac{130 \times 10^3}{12} \right) \right\} = 2.824 \times 10^6 \text{ mm}^4$$

$$I_{ZY} = \int (zy) \, dA = [(80 \times 10)(35 \times 70)] + [(80 \times 10)(-35)(-70)] + \text{zero}$$

$$= 3.92 \times 10^6 \text{ mm}^4$$

(ii) *To locate principal axes (u, v):*

$$\tan(2\alpha) = -\frac{2I_{YZ}}{I_Z - I_Y} = -\frac{2 \times 3.92 \times 10^6}{(9.684 - 2.824) \times 10^6} = -1.143$$

$$\alpha = 62.64^\circ$$

Since,  $u$  and  $v$  are the principal axes,  $I_{UV} = \text{zero}$ .

$$I_U = \frac{I_Y + I_Z}{2} + \frac{I_Z - I_Y}{2} (\cos(2\alpha)) - I_{YZ} \sin(2\alpha) = 1.054 \times 10^6 \text{ mm}^4$$

$$I_V = (I_Z + I_Y) - I_U = 11.454 \times 10^6 \text{ mm}^4$$

**Example 2** Find the stresses on the cantilever beam shown in Fig. 2.5.

(i) *Calculation of  $I_z$ ,  $I_y$ , and  $I_{zy}$ :*

$$\bar{y} = \frac{\sum ay}{\sum a}$$

$$\bar{y} = \frac{(30 \times 5 \times 2.5) + (45 \times 5 \times (22.5 + 5))}{(30 \times 5) + (45 \times 5)} = 17.5 \text{ mm}$$

$$\bar{z} = \frac{\sum az}{\sum a}$$

$$\bar{z} = \frac{(30 \times 5 \times 15) + (45 \times 5 \times 2.5)}{(30 \times 5) + (45 \times 5)} = 7.5 \text{ mm}$$

$$I_y = \frac{5 \times 30^3}{12} + 30 \times 5 \times (15 - 7.5)^2 + \frac{45 \times 5^3}{12} + 45 \times 5 \times (7.5 - 2.5)^2$$

$$= 2.579 \times 10^4 \text{ mm}^4$$

$$I_z = \frac{30 \times 5^3}{12} + 30 \times 5 \times (17.5 - 2.5)^2 + \frac{5 \times 45^3}{12} + 45 \times 5 \times (27.5 - 17.5)^2$$

$$= 9.453 \times 10^4 \text{ mm}^4$$

$$I_{yz} = (30 \times 5)(15 - 7.5)(17.5 - 2.5) + (45 \times 5)(-(7.5 - 2.5))(- (27.5 - 17.5))$$

$$= 2.813 \times 10^4 \text{ mm}^4$$

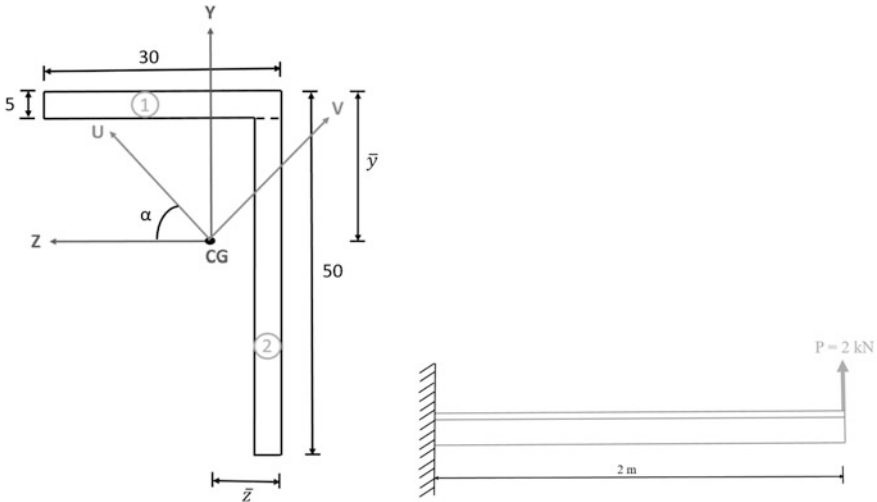


**Fig. 2.5** Example problem-2

(ii) **To locate principal axes ( $u,v$ ):**

$$\tan(2\alpha) = -\frac{2I_{YZ}}{I_Z - I_Y} = -\frac{2 \times 2.813 \times 10^4}{(9.453 - 2.579) \times 10^4} = -0.818$$

$$\alpha = 70.36^\circ$$

Since,  $u$  and  $v$  are the principal axes,  $I_{UV} = \text{zero}$ .

$$I_U = \frac{I_Y + I_Z}{2} + \frac{I_Z - I_Y}{2} \cos(2\alpha) - I_{YZ} \sin(2\alpha) = 1.575 \times 10^4 \text{ mm}^4$$

$$I_V = (I_Z + I_Y) - I_U = 10.457 \times 10^4 \text{ mm}^4$$

(iii) **To find the stresses:**

Moment about  $Z$ -axis = load  $\times$  perpendicular distance =  $2 \times 2 = 4 \text{ kNm}$   
(Fig. 2.6).

$$M_U = M_Z \cos \alpha = 1.344 \text{ kNm}$$

$$M_V = -M_Z \sin \alpha = -3.767 \text{ kNm}$$

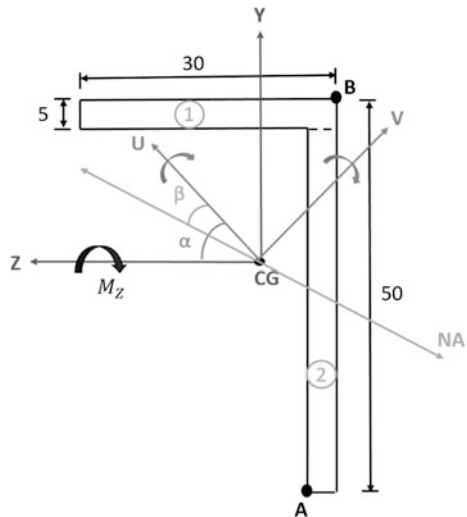
$$\sigma_x = -\left(\frac{M_U}{I_U} v - \frac{M_V}{I_V} u\right)$$

Substituting  $\sigma_x = \text{zero}$  for the neutral axis.

$$\frac{v}{u} = -0.422 = \tan \beta$$

where  $\beta$  is the inclination between the neutral axis and  $U$ .

**Fig. 2.6** Location of stress points



$$\beta = -22.88^\circ$$

In cantilever beam with the point load acting upwards at the free end, the top fibres in the cross section will be under compression and the bottom fibres will be under tension. In the given cross section, point A will be under compression; point B will be under tension. Using the classical equations for flexure, unsymmetrical bending problem is converted to uniplanar bending.

**For point A:**

$$u_A = z \cos \alpha + y \sin \alpha = (-7.5) \cos (70.36) + (17.5) \sin (70.36) = 13.96 \text{ mm}$$

$$v_A = -z \sin \alpha + y \cos \alpha = (-7.5) \sin (70.36) + (17.5) \cos (70.36) = 12.95 \text{ mm}$$

$$\sigma_A = -\left(\frac{M_U}{I_U} v_A - \frac{M_V}{I_V} u_A\right) = -1608.66 \text{ N/mm}^2 \text{ (compression)}$$

**Similarly for point B:**

$$u_B = z \cos \alpha + y \sin \alpha = -(2.5) \cos (70.36) + (-(50 - 17.5)) \sin(70.36)$$

$$= -31.45 \text{ mm}$$

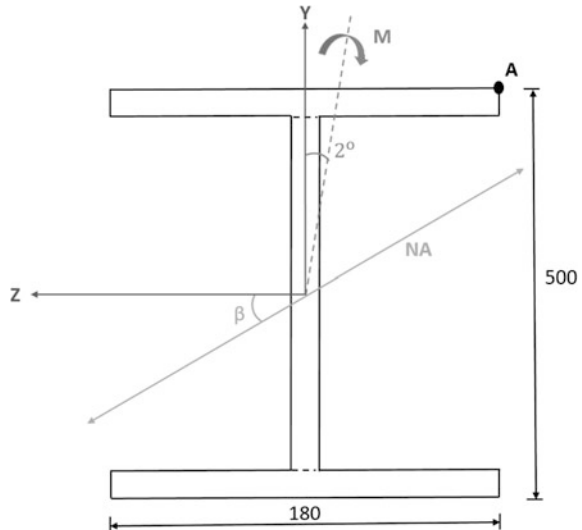
$$v_B = -z \sin \alpha + y \cos \alpha = (-2.5) \sin (70.36) + (-(50 - 17.5)) \cos (70.36)$$

$$= -8.57 \text{ mm}$$

$$\sigma_B = -\left(\frac{M_U}{I_U} v_B - \frac{M_V}{I_V} u_B\right) = 1864.72 \text{ N/mm}^2 \text{ (tension)}$$

**Example 3** An ISMB 500 @ 86.9 kN/m shown in Fig. 2.7 is used as a supporting member of an offshore deck. This section is subjected to a moment on a plane,

**Fig. 2.7** Example problem-3



making an angle  $2^\circ$  inclination to the vertical plane of symmetry. Locate the neutral axis and determine the stresses and compare the stresses with symmetric bending.

(i) **Properties of the section:**

$$I_Z = 45218.3 \times 10^4 \text{ mm}^4$$

$$I_Y = 1369.8 \times 10^4 \text{ mm}^4$$

Since Z- and Y-planes are the axes of symmetry,  $I_{ZY} = \text{zero}$ .

(ii) **To find the stresses:**

$$M_U = M_Z \cos \alpha = M \cos 2^\circ$$

$$M_V = -M_Z \sin \alpha = -M \sin 2^\circ$$

$$\sigma_X = -\left(\frac{M_U}{I_U} v - \frac{M_V}{I_V} u\right)$$

$$\begin{aligned} \sigma_A &= -\left(\frac{M_U}{I_U} v_A - \frac{M_V}{I_V} u_A\right) \\ &= -\frac{(M \cos 2^\circ)}{45218.3 \times 10^4} (250) + \frac{(-M \sin 2^\circ)}{1369.8 \times 10^4} (-90) = 0.32M \times 10^{11} \text{ N/mm}^2 \end{aligned}$$

The stress value when no inclined load acts is given by

$$\sigma'_A = \frac{M}{I} y = -0.55M \times 10^{11} \text{ N/mm}^2$$

$$\text{Percentage increase in moment} = \frac{0.55 - 0.32}{0.55} \times 100 = 41.8\%$$

To locate the neutral axis, substitute  $\sigma_X = \text{zero}$ ,

$$\frac{v}{u} = -1.153 = \tan \beta$$

where  $\beta$  is the inclination between the neutral axis and U.

$$\beta = -49.06^\circ$$

**Example 4** Find the stresses on the cantilever beam of I section shown in Fig. 2.8. Load acts at angle of  $10^\circ$  from the vertical axis (Fig. 2.9).

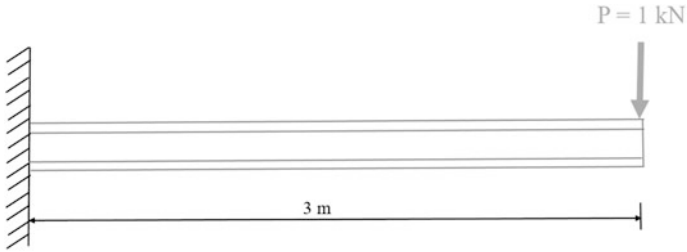


Fig. 2.8 Example problem-4

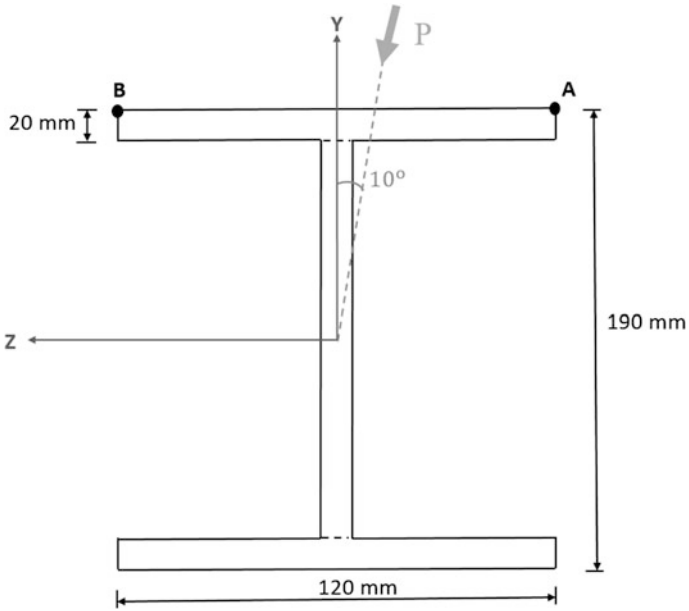


Fig. 2.9 Cross section details

(i) *Calculation of  $I_z$ ,  $I_y$ , and  $I_{zy}$ :*

$$\bar{y} = \frac{\sum ay}{\sum a} = 95 \text{ mm}$$

$$\bar{z} = \frac{\sum az}{\sum a} = 60 \text{ mm}$$

$$I_y = \frac{2 \times 20 \times 120^3}{12} + \frac{150 \times 20^3}{12}$$

$$= 0.586 \times 10^7 \text{ mm}^4$$

$$I_Z = 2 \left[ \frac{120 \times 20^3}{12} + 120 \times 20 \times (85)^2 \right] + \frac{20 \times 150^3}{12}$$

$$= 4.046 \times 10^7 \text{ mm}^4$$

(ii) *To locate principal axes ( $u$ ,  $v$ ):*

Since I section is symmetrical,  $ZZ$  and  $YY$  axes are the principal axes  $UU$  and  $VV$ , respectively.

$$I_U = 0.586 \times 10^7 \text{ mm}^4$$

$$I_V = 4.046 \times 10^7 \text{ mm}^4$$

(iii) *To find the stresses:*

Moment about  $Z$ -axis = load  $\times$  perpendicular distance =  $1 \times 3 = -3$  kNm.

$$M_U = M_Z \cos \alpha = -2.954 \text{ kNm}$$

$$M_V = -M_Z \sin \alpha = 0.521 \text{ kNm}$$

$$\sigma_X = - \left( \frac{M_U}{I_U} v - \frac{M_V}{I_V} u \right)$$

For point  $A$ ,

$$u_A = -60 \text{ mm}$$

$$v_A = +95 \text{ mm}$$

$$\sigma_A = - \left( \frac{M_U}{I_U} v_A - \frac{M_V}{I_V} u_A \right) = 1.602 \text{ N/mm}^2 \text{ (tension)}$$

Similarly for point  $B$ ,

$$u_B = 60 \text{ mm}$$

$$v_B = 95 \text{ mm}$$

$$\sigma_B = - \left( \frac{M_U}{I_U} v_B - \frac{M_V}{I_V} u_B \right) = 12.28 \text{ N/mm}^2 \text{ (tension)}$$

**Example 5** Find the stresses on the cantilever beam shown in Figs. 2.10 and 2.11.

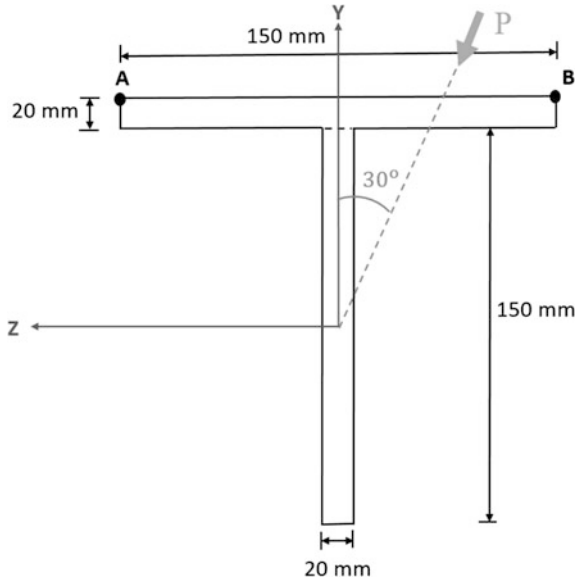


Fig. 2.10 Example problem-5

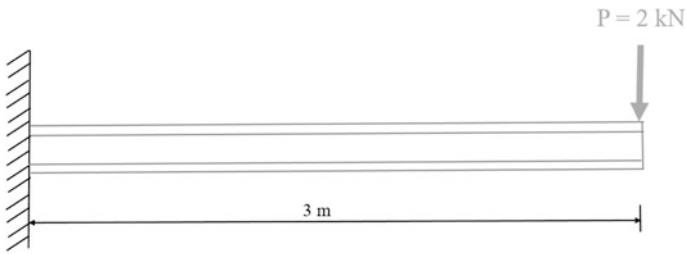


Fig. 2.11 Loading diagram for example problem-5

(i) *Calculation of  $I_z$ ,  $I_y$ , and  $I_{zy}$ :*

$$\bar{y} = \frac{\sum ay}{\sum a} = 52.5 \text{ mm}$$

$$\bar{z} = \frac{\sum az}{\sum a} = 75 \text{ mm}$$

$$I_y = \frac{20 \times 150^3}{12} + \frac{150 \times 20^3}{12}$$

$$= 5.725 \times 10^6 \text{ mm}^4$$

$$I_Z = \frac{150 \times 20^3}{12} + 150 \times 20 \times (42.5)^2 + \frac{20 \times 150^3}{12} + 20 \times 150 \times 42.5^2$$

$$= 16.562 \times 10^6 \text{ mm}^4$$

(ii) *To locate principal axes (u, v):*

Since I section is symmetrical, ZZ and YY axes are the principal axes UU and VV, respectively.

$$I_U = 5.725 \times 10^6 \text{ mm}^4$$

$$I_V = 16.562 \times 10^6 \text{ mm}^4$$

(iii) *To find the stresses:*

Moment about Z-axis = load  $\times$  perpendicular distance =  $2 \times 3 = -6$  kNm.

$$M_U = M_Z \cos \alpha = -5.196 \text{ kNm}$$

$$M_V = -M_Z \sin \alpha = 3 \text{ kNm}$$

$$\sigma_x = -\left(\frac{M_U}{I_U}v - \frac{M_V}{I_V}u\right)$$

For point A,

$$u_A = 75 \text{ mm}$$

$$v_A = 52.5 \text{ mm}$$

$$\sigma_A = -\left(\frac{M_U}{I_U}v_A - \frac{M_V}{I_V}u_A\right) = 61.234 \text{ N/mm}^2 \text{ (tension)}$$

Similarly for point B,

$$u_B = 60 \text{ mm}$$

$$v_B = 95 \text{ mm}$$

$$\sigma_B = -\left(\frac{M_U}{I_U}v_B - \frac{M_V}{I_V}u_B\right) = 34.065 \text{ N/mm}^2 \text{ (tension)}$$

## 2.3 Shear Center

Let us consider a resultant force,  $F_1$  generated due to the load  $V$  acting at a particular distance apart from the center of gravity of an I section as shown in Fig. 2.12. Due to symmetry, there is no net force along the Z-axis and the section

**Fig. 2.12** Resultant force acting on I section

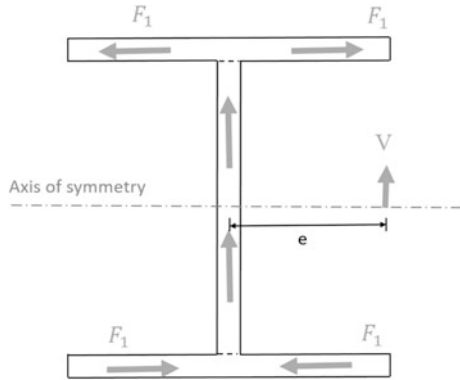
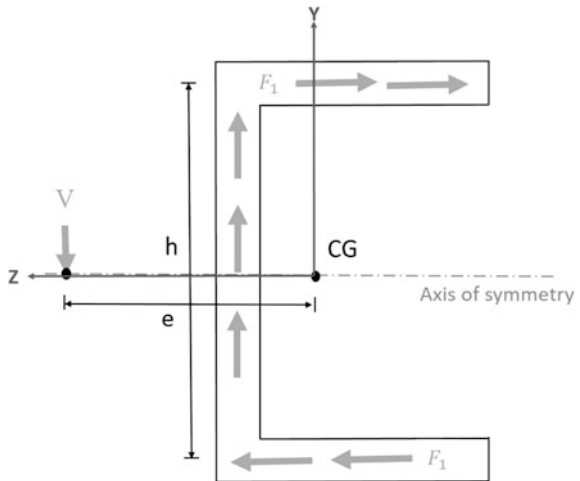


**Fig. 2.13** Resultant force acting in channel section



will not rotate. Now, let us consider a channel section with the resultant force  $F$ , as shown in Fig. 2.13. The vertical force is taken care by the resultant force in the Web, but the resultant shear force in the flanges will tend to form a couple. This will make the section to rotate about the point in the cross section. The point of rotation will not always coincide with the center of gravity due to asymmetry, and this point is referred to as *shear center*.

In order to avoid the twisting of the cross section, the line of action of the load should pass through the shear center. Shear center is also known as ‘center of twist’. Thus, shear center is defined as the intersection of the plane of loading and the bending axis. It is also denoted as the point of intersection of the longitudinal axis of the member with the line of action of the transverse load. At shear center, the applied force is balanced by sum of shear force contributions from different members. This is obtained by summing the shear stresses over the section. In case of offshore structures, members are usually thin and asymmetric. Further, cross

sections are generally weak in torsion and strong in bending. This will lead to the following special problems, namely:

- i. Member will have a premature failure due to twisting before it fails in bending.
- ii. Plasticization of the members resulting in severe extent of damage.

With reference to Fig. 2.13, let  $\{e\}$  be the distance of shear center from center of gravity. Moment developed on the cross section is given by:

$$M_Z = \left( F_Z \times \frac{h}{2} \right) \times 2 = F_Z h \tag{2.39}$$

This moment causes twisting in the cross section of the member. Now, if force  $\{P\}$  is applied at a distance from the center of gravity, moment developed due to the applied external load will counteract the generated twisting moment, which is given by:

$$Pe_Z = F_Z h \tag{2.40}$$

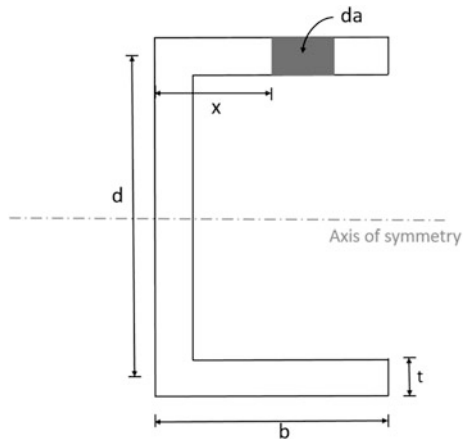
Principle involved in locating the shear center is that “load acting on the beam must lie in a plane having the resultant shear force on each section (component) of the beam”. Resultant shear force is calculated from the shearing stresses produced in the beam when it is loaded to avoid twisting at its ends. Hence, the following conditions apply:

- In case of sections with two axes of symmetry, shear center coincides with that of the centroid of the cross section.
- In case of sections with one axis of symmetry, shear center does not coincide with the centroid, but lies on the axis of symmetry.

**Shear stress calculation:**

Consider cross section, as shown in Fig. 2.14.

**Fig. 2.14** Cross section to calculate shear center



In order to find the shear stress in the flange, consider a strip of cross sectional area 'da' at a distance 'x' as shown in Fig. 2.14.

$$H = \int_x^b \frac{M}{I} y da \quad (2.41)$$

$$H + dH = \int_x^b \left( \frac{M + dM}{I} \right) y da \quad (2.42)$$

The unbalanced force, dH is determined as given below:

$$dH = \int_x^b \left( \frac{M + dM}{I} \right) y da - \int_x^b \frac{M}{I} y da \quad (2.43)$$

$$dH = \frac{dM}{I} \int_x^b y da \quad (2.44)$$

Since shear stress must oppose the unbalanced force, the following equation holds good:

$$\tau(t dz) = \frac{dM}{I} \int_x^b y da \quad (2.45)$$

$$\tau = \frac{dM}{dz} \frac{1}{It} \int_x^b y da = \frac{dM}{dz} \frac{1}{It} a\bar{y} = \frac{Va\bar{y}}{It} \quad (2.46)$$

Thus, the shear stress is given by:

$$\tau = \frac{Va\bar{y}}{It} \quad (2.47)$$

## 2.4 Example Problems on Shear Center

**Example 1** Locate the shear center 'C' for the section shown in Fig. 2.15.

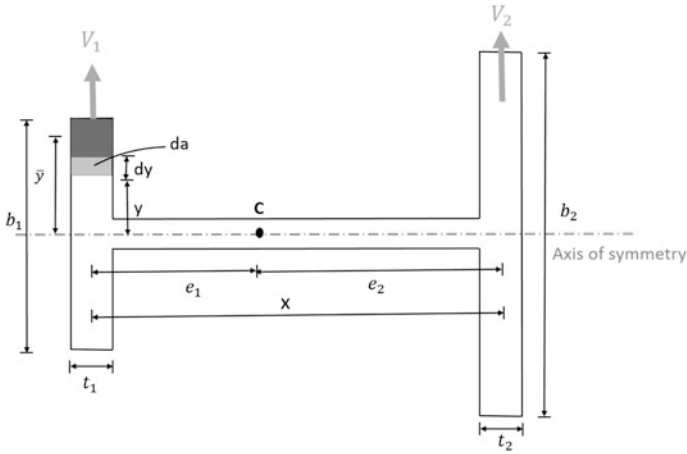


Fig. 2.15 Example problem-1 for shear center

The shear taken by the Web is neglected.

$$V = V_1 + V_2$$

Consider a strip of thickness ‘dy’ in the flange at a distance ‘y’ from the axis of symmetry. The area of the strip is taken as ‘da’.

$$da = dy(t_1)$$

The area of the section above the strip is given by:

$$A = \left(\frac{b_1}{2} - y\right)t_1$$

The centroid of the section above the strip is given by:

$$\begin{aligned} \bar{y} &= y + \frac{1}{2} \left(\frac{b_1}{2} - y\right) \\ &= y + \frac{b_1}{4} - \frac{y}{2} \\ &= \left(\frac{y}{2} + \frac{b_1}{4}\right) \end{aligned}$$

We know that  $\tau = \frac{VA\bar{y}}{I}$

$$\begin{aligned}
 \tau &= \frac{V}{It_1} \left( \frac{b_1}{2} - y \right) t_1 \left( \frac{y}{2} + \frac{b_1}{4} \right) \\
 &= \frac{V}{I} \left( \frac{b_1}{2} - y \right) \left( \frac{b_1}{2} + y \right) \frac{1}{2} \\
 &= \frac{V}{2I} \left[ \left( \frac{b_1}{2} \right)^2 - y^2 \right] \\
 V_1 &= \int_{-\frac{b_1}{2}}^{\frac{b_1}{2}} \tau \, da \\
 V_1 &= \int_{-\frac{b_1}{2}}^{\frac{b_1}{2}} \frac{V}{2I} \left[ \left( \frac{b_1}{2} \right)^2 - y^2 \right] dy t_1 \\
 &= \frac{Vt_1}{2I} \times 2 \times \int_0^{\frac{b_1}{2}} \left[ \left( \frac{b_1}{2} \right)^2 - y^2 \right] dy \\
 &= \frac{Vt_1}{2I} \left[ \frac{b_1^2}{4} y - \frac{y^3}{3} \right]_0^{\frac{b_1}{2}} \\
 &= \frac{Vt_1}{2I} \left[ \frac{b_1^3}{8} - \frac{b_1^3}{24} \right] \\
 &= \frac{V}{I} \left( \frac{t_1 b_1^3}{12} \right) \\
 &= \frac{V}{I} (I_1)
 \end{aligned}$$

Similarly,  $V_2 = \frac{V}{I} (I_2)$

where  $V = V_1 + V_2$

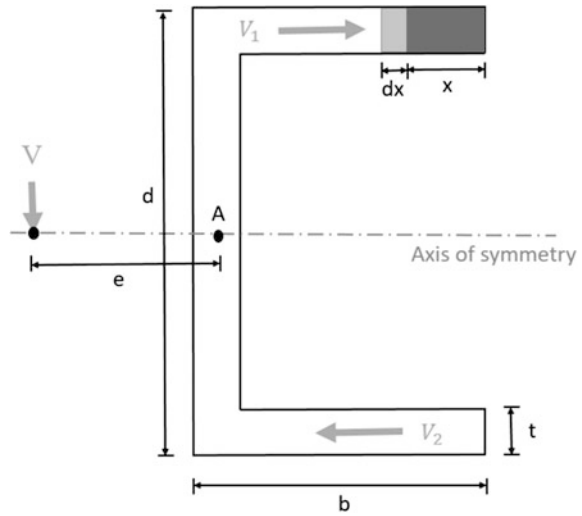
Moment of inertia of the whole section (I) can be computed from the first principles. Taking moment about point C, we get:

$$\begin{aligned}
 V_1 e_1 &= V_2 e_2 \\
 \frac{e_2}{e_1} &= \frac{I_2}{I_1}
 \end{aligned}$$

Calculate the value of  $e_1$  and  $e_2$  from the following equation:  $x = e_1 + e_2$

**Example 2** Locate the shear center for the channel section, shown in Fig. 2.16.

**Fig. 2.16** Example problem-2 on shear center



Consider a section of thickness ‘dx’ on the flange at a distance ‘x’ from the end. Following statement holds good:

$$V_1 = \int \tau da$$

$$V_1 = \int \frac{VA\bar{y}}{It} da$$

where  $A = tx$   
 $da = dx t$   
 $\bar{y} = d/2$

$$V_1 = \frac{V}{It} \int_0^b (tx)(dx t) \frac{d}{2}$$

$$= \left[ \frac{V t^2 d x^2}{It \cdot 2} \right]_0^b$$

$$= \frac{Vtb^2 d}{4I}$$

By symmetry,  $V_1 = V_2 = \frac{Vtb^2 d}{4I}$

Neglecting the shear taken by the Web and taking moment about the point A on the Web,

$$Ve = V_1 \frac{d}{2} + V_2 \frac{d}{2}$$

$$Ve = \frac{Vtb^2d}{4I} \times 2$$

$$e = \frac{tb^2d}{2I}$$

**Example 3** Locate the shear center for the section shown in Fig. 2.17.

By symmetry, following equations hold good:

$$V_1 = V_5$$

$$V_2 = V_4$$

(i) **To find  $V_1$ :**

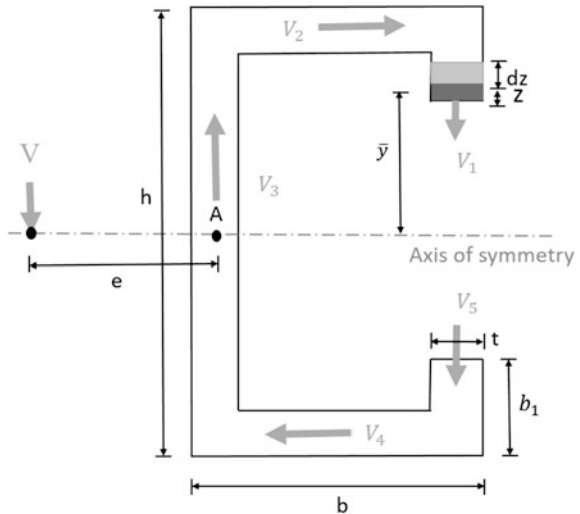
Consider a strip of thickness ‘dz’ on the lip portion, at a distance ‘z’ from the end. The area of the strip is ‘da’.

$$V_1 = \int \tau da$$

$$V_1 = \int \frac{VA\bar{y}}{It} da$$

where  $A = tz$   
 $da = dz t$   
 $\bar{y} = \frac{h}{2} - b_1 + \frac{z}{2}$

**Fig. 2.17** Example problem-3 on shear center



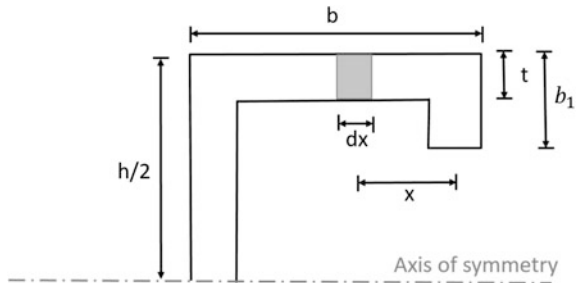
$$\begin{aligned}
 V_1 &= \int_0^{b_1} \frac{V}{It} (tz) \left( \frac{h}{2} - b_1 + \frac{z}{2} \right) dz \\
 &= \frac{Vt}{I} \left( \frac{h}{2} - b_1 + \frac{z}{2} \right) z dz \\
 &= \frac{Vt}{I} \left[ \frac{h}{2} \left( \frac{z^2}{2} \right) - b_1 \left( \frac{z^2}{2} \right) + \left( \frac{z^3}{6} \right) \right]_0^{b_1} \\
 &= \frac{Vt}{I} \left[ \frac{h}{2} \left( \frac{b_1^2}{2} \right) - \left( \frac{b_1^3}{2} \right) + \left( \frac{b_1^3}{6} \right) \right] \\
 &= \frac{Vt}{I} \left[ \frac{hb_1^2}{4} - \frac{b_1^3}{3} \right] \\
 &= \frac{Vtb_1^2}{I} \left( \frac{h}{4} - \frac{b_1}{3} \right)
 \end{aligned}$$

- (ii) **To find  $V_2$ :** Consider the partial section, shown in Fig. 2.18. Consider a strip of thickness ‘dx’ on the flange portion, at a distance ‘x’ from the lip portion. The area of the strip is ‘da’.

$$\begin{aligned}
 a\bar{y} &= \left\{ (b_1 t) \left( \frac{h}{2} - b_1 + \frac{b_1}{2} \right) \right\} + \int xt \frac{h}{2} \\
 &= \left( \frac{b_1 t h}{2} - b_1^2 t + \frac{b_1^2 t}{2} \right) + \int xt \frac{h}{2} \\
 (V_2)^* &= \int \frac{VA\bar{y}}{It} da
 \end{aligned}$$

where  $A = t x$   
 $da = dx t$   
 $\bar{y} = \frac{h}{2}$

Fig. 2.18 Partial section



$$\begin{aligned}
 (V_2)^* &= \int_0^b \frac{V}{It} (tx)(t \, dx) \left(\frac{h}{2}\right) \\
 &= \frac{Vth}{2I} \int_0^b x \, dx \\
 &= \frac{Vth}{2I} \frac{b^2}{2} \\
 &= \frac{Vthb^2}{4I} \\
 V_2 &= \frac{Vt}{I} \left[ b_1 \left(\frac{bh}{2}\right) - \frac{b_1^2 b}{2} + \frac{b^2 h}{4} \right]
 \end{aligned}$$

Taking moment about A,

$$\begin{aligned}
 Ve &= (V_1 + V_5)b + (V_2 + V_4)\frac{h}{2} \\
 Ve &= 2V_1 b + 2V_2 \frac{h}{2} \\
 e &= \frac{tb_1 h^2}{2I} b \left( 1 + \frac{b}{2b_1} - \frac{4}{3} \left(\frac{b_1}{b}\right) \right)
 \end{aligned}$$

**Example 4** Locate the shear center shown in Fig. 2.19.

Consider a strip of thickness 'dz' at a distance 'z' from the end.

$$\begin{aligned}
 V_1 &= \int \tau \, da \\
 V_1 &= \int \frac{VA\bar{y}}{It} \, da
 \end{aligned}$$

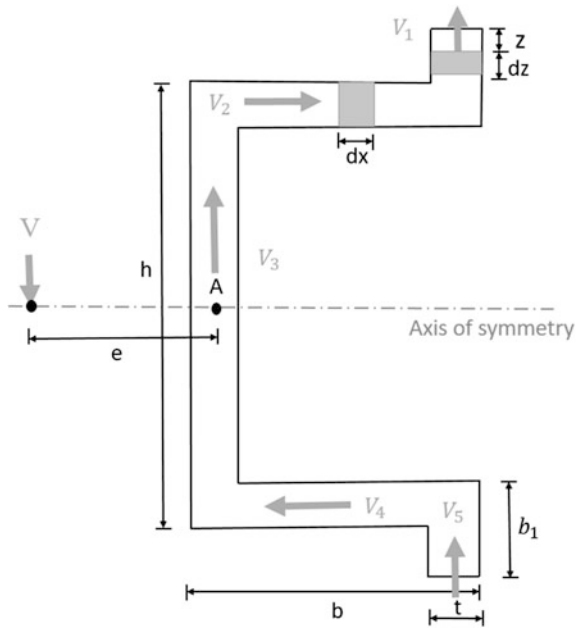
where  $A = t z$

$da = dz t$

$\bar{y} = \frac{h}{2} + b_1 - \frac{z}{2}$

$$\begin{aligned}
 V_1 &= \int_0^{b_1} \frac{V}{It} (tz)(t \, dz) \left(\frac{h}{2} + b_1 - \frac{z}{2}\right) \\
 &= \frac{Vt}{I} \left[ \frac{h}{2} \left(\frac{b_1^2}{2}\right) + \left(\frac{b_1^3}{2}\right) - \left(\frac{b_1^3}{3}\right) \right] \\
 &= \frac{Vt}{I} \left[ \frac{hb_1^2}{4} + \frac{b_1^3}{3} \right] \\
 &= \frac{Vtb_1^2}{I} \left(\frac{h}{4} + \frac{b_1}{3}\right)
 \end{aligned}$$

**Fig. 2.19** Example problem-4 on shear center



Moment of inertia of the section is given by:

$$I = \frac{th^3}{12} + \left[ \frac{tb_1^3}{12} + tb_1 \left( \frac{h}{2} + \frac{b_1}{2} \right)^2 \right] + \left( \frac{bt^3}{12} + \frac{bth^2}{4} \right)^2$$

(ii) **To find  $V_2$ :**

Consider a strip of thickness 'dx' on the flange portion, at a distance 'x'.

$$a\bar{y} = (b_1t) \left( \frac{h}{2} + \frac{b_1}{2} \right) + tx \left( \frac{h}{2} \right)$$

$$da = (t dx)$$

$$\begin{aligned} V_2 &= \frac{V}{It} \int_0^b t \left( \frac{b_1h}{2} + \frac{b_1^2}{2} + \frac{xh}{2} \right) t dx \\ &= \frac{Vt}{I} \left( \frac{b_1hb}{2} + \frac{b_1^2b}{2} + \frac{hb^2}{4} \right) \end{aligned}$$

Taking moment about A,

$$(V_2 + V_4) \frac{h}{2} - (V_1 + V_5)b = Ve$$

The value of 'e' can be calculated from the above expression.

**Example 5** Locate the shear center for the curved section shown in Fig. 2.20.

$$\tau = \frac{V}{It} \int_{\beta}^{\theta} y \, dA$$

where  $y = R \cos \theta$

$$dA = R t \, d\theta$$

$$\begin{aligned} \tau &= \frac{V}{It} \int_{\beta}^{\theta} (R \cos \theta) R (t \, d\theta) \\ &= \frac{VR^2}{I} (\sin \theta - \sin \beta) \end{aligned}$$

Elemental shear force,  $dv = \tau \, da$

$$dv = \frac{VR^3 t}{I} (\sin \theta - \sin \beta) \, d\theta$$

Moment of inertia about the center,  $dM = \frac{VR^4 t}{I} (\sin \theta - \sin \beta) \, d\theta$

Total moment

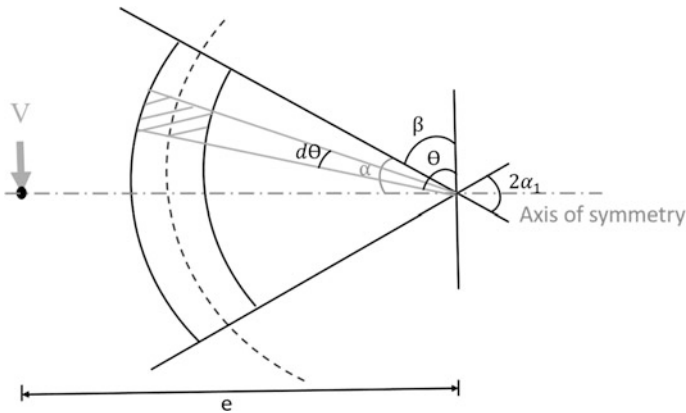


**Fig. 2.20** Example problem-5 on shear center

$$M = 2 \int_{\beta}^{\pi/2} \frac{VR^4t}{I} (\sin \theta - \sin \beta) d\theta = 2 \frac{VR^4t}{I} [(-\cos \theta - \sin \beta)]_{\beta}^{\pi/2}$$

Since,  $(\frac{\pi}{2} - \beta) = \alpha$

$$M = \frac{2VR^4t}{I} \left[ -\cos \frac{\pi}{2} + \cos \beta - \frac{\pi}{2} \sin \beta + \beta \sin \beta \right]$$

Substituting  $\beta = \frac{\pi}{2} - \alpha$

$$M = \frac{2VR^4t}{I} [\sin \alpha - \alpha \cos \alpha]$$

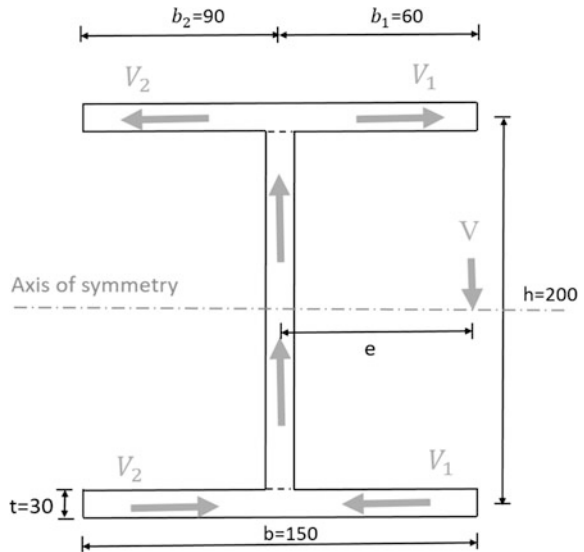
Equating the moment, we get:

$$Ve = \frac{2VR^4t}{I} [\sin \alpha - \alpha \cos \alpha]$$

$$e = \frac{2R^4t}{I} [\sin \alpha - \alpha \cos \alpha]$$

**Example 6** Determine the location of the shear center for an I section shown in Fig. 2.21. Consider the following dimensions: flange: 150 × 30 mm; Web: 20 × 200 mm.

**Fig. 2.21** Example problem-6 for shear center



Consider a section of thickness 'dx' on the flange at a distance 'x' from the end.

$$V_1 = \int \tau da$$

$$V_1 = \int \frac{VA\bar{y}}{It} da$$

where  $A = t x$   
 $da = dx t$   
 $\bar{y} = h/2$

$$V_1 = \frac{V}{It} \int_0^{b_1} (tx)(dx t) \frac{h}{2}$$

$$= \left[ \frac{V t^2 h x^2}{It \cdot 2} \right]_0^{b_1}$$

$$= \frac{V t b_1^2 h}{4I} = 0.0546 V$$

By symmetry,

$$V_2 = \frac{V t b_2^2 h}{4I} = 0.123 V$$

$$I = 9.886 \times 10^7 \text{ mm}^4$$

Taking moments about the center of the Web,

$$V e + V_1(h) - V_2(h) = 0$$

$$e = 13.66 \text{ mm}$$

## 2.5 Curved Beams

Curved beams are classified based on the initial curvature, as follows:

- i. Beams with small initial curvature whose ratio of the initial radius of curvature and the depth of the section is greater than 10.
- ii. Beams with large initial curvature in which ratio of the initial radius of curvature and the depth of the section is less than or equal to 10.

### 2.5.1 Curved Beams with Small Initial Curvature

Let us consider a curved beam with small initial curvature, as shown in Fig. 2.22.

Let the following be defined:

$d\phi'$  be the angle subtended after deformation.

$R$  be the initial radius of curvature.

$d\phi$  be the angle subtended at the center of curvature by the portion 'abcd'.

$R'$  be the radius of curvature after moment  $M$  is applied.

If  $R' < R$ , then the applied moment will tend to close the curvature. Let us consider a fibre  $PQ$  at a distance  $y$  from the neutral axis. Then, following conditions hold good:

Original length of the fibre =  $(R + y) d\phi$ .

Length of the fibre after application of the moment =  $(R' + y) d\phi'$ .

Change in length of the fibre =  $(R' + y) d\phi' - (R + y) d\phi$ .

$$\text{Strain, } \epsilon = \frac{(R' + y)d\phi' - (R + y)d\phi}{(R + y)d\phi}$$

As the length of the fibre at neutral axis remains unchanged, following relationship holds good:

$$ds = R d\phi = R' d\phi'$$

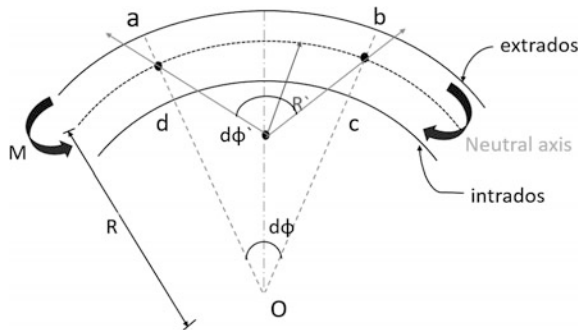
Substituting the above equation in the strain equation, we get:

$$\epsilon = \frac{y(d\phi' - d\phi)}{(R + y)d\phi} \tag{2.48}$$

In the above equation,  $y$  may be neglected, since  $y \ll R$ .

Hence, the following relationship holds good:

**Fig. 2.22** Curve beam with small initial curvature



$$\varepsilon = \frac{y(d\varphi' - d\varphi)}{R d\varphi} \quad (2.49)$$

On simplification, we get:

$$\varepsilon = \frac{y d\varphi'}{R d\varphi} - \frac{y d\varphi}{R d\varphi} = y \left( \frac{d\varphi'}{ds} - \frac{d\varphi}{ds} \right) \quad (2.50)$$

$$\varepsilon = y \left( \frac{1}{R'} - \frac{1}{R} \right) \quad (2.51)$$

Substituting  $\varepsilon = \frac{\sigma}{E}$ ,

$$y \left( \frac{1}{R'} - \frac{1}{R} \right) = \frac{\sigma}{E} \quad (2.52)$$

$$\frac{\sigma}{y} = E \left( \frac{1}{R'} - \frac{1}{R} \right) \quad (2.53)$$

Following assumptions are made in deriving the equation:

- i. Every cross section of the curved beam remains plane and perpendicular to the centroidal axis, before and after the application of external moment.
- ii. To satisfy the above condition, it is to be agreed that the net force acting on any cross section of the curved beam should be zero. If the net force is not equal to zero, then it may result in warping.

Mathematically,

$$\int_A \sigma dA = 0 \quad (2.54)$$

$$\int E y \left( \frac{1}{R'} - \frac{1}{R} \right) dA = 0 \quad (2.55)$$

$$E \left( \frac{1}{R'} - \frac{1}{R} \right) \int y dA = 0 \quad (2.56)$$

Since,  $E \left( \frac{1}{R'} - \frac{1}{R} \right) \neq 0$ ,  $\int y dA = 0$  implies that the geometric axis of the curved beam should coincide with the neutral axis of the curved beam. As the curved beam is in equilibrium condition under the applied moment, it can be stated that:

$$\int \sigma y dA = M \quad (2.57)$$

Substituting for  $\sigma$  in the above equation, we get:

$$E \left( \frac{1}{R'} - \frac{1}{R} \right) \int y^2 dA = M \quad (2.58)$$

Since  $\int y^2 dA = I$ ,

$$E \left( \frac{1}{R'} - \frac{1}{R} \right) I = M \quad (2.59)$$

Thus,

$$\frac{M}{I} = \frac{\sigma}{y} = E \left( \frac{1}{R'} - \frac{1}{R} \right) \quad (2.60)$$

### 2.5.2 Deflection of Curved Beam with Small Initial Curvature

For deriving the deflection of the curved beam, Castigliano's theorem is used. Strain energy of the curved beam is given by:

$$U = \int \frac{1}{2} M \Delta d\phi' \quad (2.61)$$

where  $d\phi'$  is the change in the angle produced by the moment  $M$  at the center of curvature.

Following equation holds good:

$$\frac{M}{I} = E \left( \frac{1}{R'} - \frac{1}{R} \right) \quad (2.62)$$

Multiplying  $ds$  on both the sides of the equation, we get:

$$\frac{M}{I} ds = E \left( \frac{1}{R'} - \frac{1}{R} \right) ds \quad (2.63)$$

Since the length of the fibre remains unchanged, the following relationship holds good:

$$ds = R d\varphi = R' d\varphi' \quad (2.64)$$

$$\frac{M}{I} ds = E(d\varphi - d\varphi') ds \quad (2.65)$$

$$\frac{M}{EI} ds = \Delta d\varphi \quad (2.66)$$

Thus, the strain of the curved beam is given by:

$$U = \int \frac{1}{2} \frac{M^2 ds}{EI} \quad (2.67)$$

By partially differentiating  $U$  with respect to  $p$ , we get:

$$\Delta = \frac{\partial U}{\partial p} = \int \frac{M}{EI} \frac{\partial M}{\partial p} ds \quad (2.68)$$

Similarly, the angular rotation may be obtained by partially differentiating  $U$  with respect to the angular momentum  $M_O$ ,

$$\theta = \frac{\partial U}{\partial M_O} = \int \frac{M}{EI} \frac{\partial M}{\partial M_O} ds \quad (2.69)$$

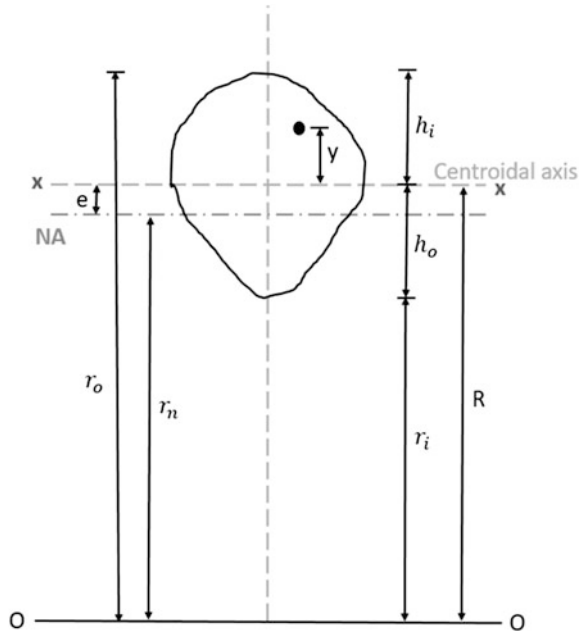
### 2.5.3 Curved Beam with Large Initial Curvature

Consider a strip in the cross section of the curved beam, as shown in Fig. 2.23. Concave side is called intrados, and the convex side is called extrados. Following points are valid:

- i. Stress variation is non-linear across the cross section; it is hyperbolic.
- ii. Experimental studies showed that stress on the concave side is large than that of the convex side.
- iii. Neutral axis will shift toward the center of curvature.
- iv. Neutral axis will not pass through the centroid of the cross section, since  $\sigma_{\text{concave side}} \neq \sigma_{\text{convex side}}$

Let us consider a curved beam with radius,  $R$ . Let it be subjected to a moment,  $M$ , which tends to decrease the radius of curvature. Cross section details are shown in the above figure. It causes tension in the extrados compression in the intrados. Consider an element  $ABDC$ , subtending an angle ( $d\varphi$ ) at the center. Under the applied moment,  $M$ , this element deforms to  $AB D'C'$  for curvature. It is assumed that  $AB$  is fixed and only plane  $CD$  rotates, and thus, the face  $\overline{CD}$  rotates to  $C'D'$  subtending an angle  $\Delta d\varphi$ .

**Fig. 2.23** Cross section of curved beam



Initial length of the fibre ( $\overline{PQ}$ ), which is located at distance ( $y$ ), from the centroidal axis is given by:

$$(R + y) d\phi \tag{2.70}$$

Change in length of the fibre on application of the moment,  $M$ , is given by:

$$(y + e)\Delta d\phi \tag{2.71}$$

where  $e$  is the distance of the neutral axis measured from the centroidal axis. Moment,  $M$ , is applied in such manner that neutral axis is shifted toward the center of curvature. The following relationship holds good:

$$\text{Strain, } \epsilon = \frac{(y + e)\Delta d\phi}{(R + y)d\phi} \tag{2.72}$$

Assuming that the longitudinal fibers do not undergo any deformation, stress is given by:

$$\sigma = E \left( \frac{y + e}{R + y} \right) \tag{2.73}$$

It is seen that stress distribution is non-linear and hyperbolic. Basic assumption made is that every section located normal to the centroid axis remains plane and perpendicular, before and after application of moment  $M$ . Hence, following relationship holds good:

$$\text{Total compressive force} = \text{total tensile force}$$

Since the average stress on the concave side is more than the convex side, the neutral axis will shift toward the center of curvature. By equating the sum of internal forces to zero at the cross section, we get

$$\int_A \sigma dA = 0 \quad (2.74)$$

Substituting the expression for stress, we get:

$$\int_A E \frac{A d\phi}{d\phi} \left( \frac{y+e}{y+R} \right) dA = 0 \quad (2.75)$$

$$E \frac{\Delta d\phi}{d\phi} \int_A \left( \frac{y+e}{y+R} \right) dA = 0 \quad (2.76)$$

Since,  $E \frac{\Delta d\phi}{d\phi} \neq 0$  and it is a constant, we get:

$$\int_A \left( \frac{y+e}{y+R} \right) dA = 0 \quad (2.77)$$

$$\int_A \left( \frac{y}{R+y} \right) dA + e \int_A \left( \frac{1}{y+R} \right) dA = 0 \quad (2.78)$$

We know that the first integral term,  $\int_A \frac{y}{R+y} dA = mA$ , where  $m$  is a constant depending on the geometry of the  $X$  section. The quantity  $(mA)$  is termed as modified area of the cross section which is modified due to the application of moment,  $M$ . The second integral term is given by:

$$e \int_A \frac{1}{(R+y)} dA = e \int \frac{R+y-y}{R} \cdot \frac{1}{(R+y)} dA \quad (2.79)$$

$$= \frac{e}{R} \int_A \frac{R+y}{R+y} dA - \int_A \frac{y dA}{R+y} = \frac{eA}{R} - \frac{e}{R} (mA) \quad (2.80)$$

$$mA + \frac{eA}{R} - \frac{emA}{R} = 0 \quad (2.81)$$

$$m + \frac{e}{R} - \frac{em}{R} = 0 \quad (2.82)$$

$$m = e \left( \frac{m}{R} - \frac{1}{R} \right) \quad (2.83)$$

$$m = \frac{e}{R} (m - 1) \quad (2.84)$$

$$e = \left( \frac{m}{m - 1} \right) R \quad (2.85)$$

where  $m$  is the geometry property of the section. It is to be noted that the applied moment in the cross section should be equal to that of the resisting moment. Hence, the following condition is valid:

$$\int_A (\sigma dA)y = M \quad (2.86)$$

Substitution for stress,  $\int_A \frac{y^2 + ye}{R + y} dA$  is to be evaluated.

$$\int_A \frac{y^2 dA}{R + y} + e \int_A \frac{y}{y + R} dA = \int_A \left( y - \frac{Ry}{R + y} \right) dA + e \int_A \frac{y}{y + R} dA \quad (2.87)$$

We know that

$$\int_A y dA = 0 \quad (2.88)$$

Hence,

$$\int_A \left( \frac{y^2 + ye}{R + y} \right) dA = -R \int_A \left( \frac{y}{R + y} \right) dA + e \int_A \frac{y dA}{R + y} \quad (2.89)$$

$$= -R(mA) + emA = -mA(R - e) \quad (2.90)$$

$$-E \left( \frac{\Delta d\varphi}{d\varphi} \right) = \frac{M}{mA(R - e)} \quad (2.91)$$

Since,  $m = \frac{e}{R-e}$

$$E \frac{\Delta d\varphi}{d\varphi} = \frac{M}{Ae} \quad (2.92)$$

On simplification, we get:

$$e = \frac{M}{Ae} \left( \frac{y+e}{R+y} \right) \quad (2.93)$$

It is also known that

$$\sigma = \frac{M}{(m-1)R} \quad (2.94)$$

$$\sigma = \frac{M}{AR} \frac{(m-1)}{m} \left[ \frac{y + \left(\frac{m}{m-1}\right)R}{R+y} \right] \quad (2.95)$$

$$= \frac{m}{AR} \frac{(m-1)}{m} \left[ \frac{(m-1)y + mR}{(m-1)(R+y)} \right] \quad (2.96)$$

$$\sigma = \frac{M}{ARm} \left[ \frac{m(y+R) - y}{y+R} \right] \quad (2.97)$$

$$\sigma = \frac{M}{AR} \left[ 1 - \frac{1}{m} \left( \frac{y}{R+y} \right) \right] \quad (2.98)$$

The above equation named as *Winkler–Bach equation* where  $\sigma$  is the tensile/compressive stress at distance  $y$  from the centroidal axis (not from the NA);  $M$  is the applied moment (causing decrease in curvature);  $A$  area of cross section;  $m$  is the section properties (geometry/shape of the cross section); and  $R$  is the radius of curvature of the unstressed curved beam.

**Sign convention:**

( $y$ ) is considered as negative when measured toward the concave side and positive when measured toward the convex side. Similarly, negative stress indicates compressive and positive stress indicates tensile stress. In the plastic design, to enable maximum load capacity, designers use sections with large shape factors. Hence, the following relationship holds good:

$$\sigma = \frac{M}{Ae} \left[ \left( \frac{y+e}{y+R} \right) \right] \quad (2.99)$$

where  $e$  is the offset of neutral axis from the center of gravity measured toward the center of curvature. Specific stress equations for intrados and extrados are to be used to find the maximum stress in the extreme fibers. They are given as follows:

$$\sigma_{\text{intrados}} = \frac{M}{Ae} \left[ \frac{-h_i + e}{R - h_i} \right] = -\frac{M}{Ae} \left[ \frac{h_i + e}{r_i} \right] \quad (2.100)$$

$$\sigma_{\text{extrados}} = \frac{M}{Ae} \left[ \frac{h_o + e}{R + h_o} \right] = \frac{M}{Ae} \left[ \frac{(e + h_o)}{r_o} \right] \quad (2.101)$$

From the above equations, it is clear that stress is a function of the parameter ( $m$ ). We already know that:

$$mA = \int_A \frac{y}{R + y} dA \quad (2.102)$$

### 2.5.4 Circular Cross Section

Consider a strip of area,  $dA$  on a circular cross section of radius,  $r$  with a thickness of the elemental strip is  $dy$ . Please refer to Fig. 2.24 for details.

$$dA = 2(r \cos \theta) dy \quad (2.103)$$

$$y = r \sin \theta \quad (2.104)$$

$$dy = r \cos \theta d\theta \quad (2.105)$$

$$dA = (2r \cos \theta) r \cos \theta d\theta \quad (2.106)$$

$$dA = 2r^2 \cos^2 \theta d\theta \quad (2.107)$$

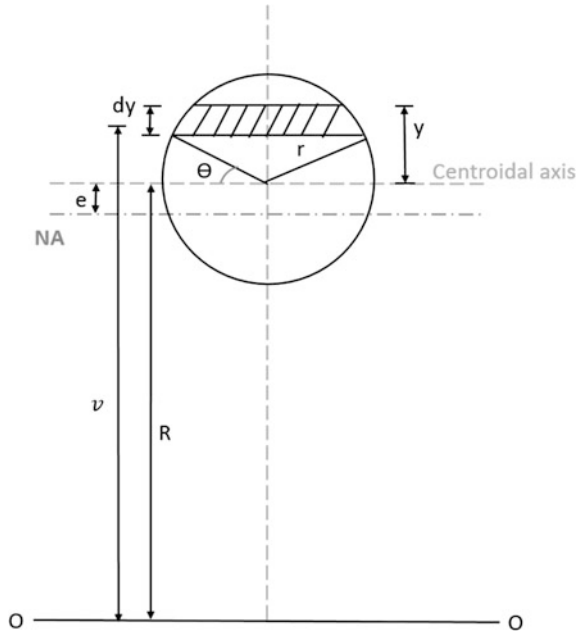
$$mA = \int_A \frac{y}{R + y} dA \quad (2.108)$$

$$= \int_A \frac{y - R}{y} dA \quad (2.109)$$

$$mA = \int_A dA - R \int \frac{dA}{y} \quad (2.110)$$

$$I_z = \int \frac{dA}{y} = \int \frac{2r^2 \cos^2 \theta d\theta}{r \sin \theta} = \int \frac{2r^2 \cos^2 \theta d\theta}{R + y} = \int \frac{2r^2 \cos^2 \theta d\theta}{R + r \sin \theta} \quad (2.111)$$

**Fig. 2.24** Details of circular cross section



$$\int \frac{dA}{v} = \int_{-\pi/2}^{\pi/2} \frac{2r^2 \cos^2 \theta d\theta}{R + r \sin \theta} \quad (2.112)$$

Let

$$k = \frac{R}{r}, \quad (2.113)$$

$$\int_A \frac{dA}{v} = \frac{2r^2}{r} \int_{-\pi/2}^{\pi/2} \frac{\cos^2 \theta}{k + \sin \theta} d\theta \quad (2.114)$$

$$= 2r \int_{-\pi/2}^{\pi/2} \frac{\cos^2 \theta}{k + \sin \theta} d\theta \quad (2.115)$$

$$= 2r \int_{-\pi/2}^{\pi/2} \frac{(1 - \sin^2 \theta)}{k + \sin \theta} d\theta \quad (2.116)$$

$$\int_A \frac{dA}{v} = 2r \int_{-\pi/2}^{\pi/2} \left[ (K - \sin \theta) + \left( \frac{1 - k^2}{k + \sin \theta} \right) \right] d\theta \quad (2.117)$$

$$= 2r \int_{-\pi/2}^{\pi/2} (K - \sin \theta) d\theta - 2r \int_{-\pi/2}^{\pi/2} \left( \frac{1 - k^2}{k + \sin \theta} \right) d\theta \quad (2.118)$$

For calculating  $I_1$ :

$$\int_{-\pi/2}^{\pi/2} (K - \sin \theta) d\theta = (K\theta + \cos \theta)_{-\pi/2}^{\pi/2} \quad (2.119)$$

$$\begin{aligned} &= k(\pi/2 - (\pi/2)) + 0 \\ &= k\pi \end{aligned} \quad (2.120)$$

$$I_1 = 2rk\pi$$

Similarly,

$$I_2 = \int_{-\pi/2}^{\pi/2} \left( \frac{1 - k^2}{k + \sin \theta} \right) d\theta \quad (2.121)$$

$$= (k^2 - 1) \int_{-\pi/2}^{\pi/2} \frac{d\theta}{k + \sin \theta} \quad (2.122)$$

$$\int_{-\pi/2}^{\pi/2} \frac{d\theta}{k + \sin \theta} \equiv \int_{-\pi/2}^{\pi/2} \frac{dx}{a + \sin x} \quad (2.123)$$

where  $a = k$ ,  $b = 1$ ,  $x = \theta$

$$= \frac{2}{\sqrt{a^2 - b^2}} \left[ \tan^{-1} \left( \frac{a \tan\left(\frac{x}{2}\right) + b}{\sqrt{a^2 - b^2}} \right) \right]_{\pi/2}^{\pi/2} \quad (2.124)$$

$$= \frac{2}{\sqrt{k^2 - 1}} \left[ \tan^{-1} \left( \frac{k \tan\left(\frac{\theta}{2}\right) + 1}{\sqrt{k^2 - 1}} \right) \right]_{\pi/2}^{\pi/2} \quad (2.125)$$

$$= \frac{2}{\sqrt{k^2 - 1}} \left[ \tan^{-1} \left( \frac{k+1}{\sqrt{k^2 - 1}} \right) - \tan^{-1} \left( \frac{-k+1}{\sqrt{k^2 - 1}} \right) \right] \quad (2.126)$$

$$= \frac{2}{\sqrt{k^2 - 1}} \left( \frac{\pi}{2} \right) \quad (2.127)$$

$$\int_A \frac{dA}{v} = 2\pi rk - 2r(k^2 - 1) \frac{\pi}{\sqrt{k^2 - 1}} \quad (2.128)$$

$$= 2\pi r \left( k - \sqrt{k^2 - 1} \right) \quad (2.129)$$

$$= 2\pi r \left( \frac{R}{r} - \sqrt{\frac{R^2}{r^2} - 1} \right) \quad (2.130)$$

$$= 2\pi r \left[ \frac{R}{r} - \sqrt{\frac{R^2 - r^2}{r^2}} \right] \quad (2.131)$$

$$\int \frac{dA}{v} = 2\pi \left[ R - \sqrt{R^2 - r^2} \right] \quad (2.132)$$

$$mA = \int dA - R \int \frac{dA}{v} \quad (2.133)$$

$$mA = \pi r^2 - R(2\pi) \left[ R - \sqrt{R^2 - r^2} \right] \quad (2.134)$$

$$m = \frac{\pi r^2}{A} - \frac{R(2\pi)}{\pi r^2} \left[ R - \sqrt{R^2 - r^2} \right] \quad (2.135)$$

$$= 1 - 2 \left( \frac{R}{r} \right) \left[ R - \sqrt{R^2 - r^2} \right] \quad (2.136)$$

$$m = 1 - 2 \left( \frac{R}{r} \right)^2 + 2 \left( \frac{R}{r} \right) \sqrt{\left( \frac{R}{r} \right)^2 - 1} \quad (2.137)$$

To find eccentricity of neutral axis with respect to  $CG$  axis:

$$mA = \int_A dA = R \int_A \frac{dA}{v} \quad (2.138)$$

$$mA = A - R \int_A \frac{dA}{v} \quad (2.139)$$

$$m = 1 - \frac{R}{A} \int_A \frac{dA}{v} \quad (2.140)$$

$$e = \left( \frac{m}{m-1} \right) R \quad (2.141)$$

$$e = \left( \frac{1 - \frac{R}{A} \int_A \frac{dA}{v}}{1 - \frac{R}{A} \int_A \frac{dA}{v}} \right) R \quad (2.142)$$

$$e = R - \frac{A}{\int \frac{dA}{v}} \quad (2.143)$$

$$\int \frac{dA}{v} = 2\pi \left( R - \sqrt{R^2 - r^2} \right) \quad (2.144)$$

$$e = R - \frac{\pi r^2}{2\pi \left( R - \sqrt{R^2 - r^2} \right)} \quad (2.145)$$

$$e = R - \frac{r^2}{2 \left[ R - \sqrt{R^2 - r^2} \right]} \quad (2.146)$$

### 2.5.5 Rectangular Cross Section

Consider a rectangular section of breadth,  $b$ , and height,  $h$ , as shown in the Fig. 2.25. Take an elemental strip on the section of thickness  $dy$  at a distance  $y$  from the centroidal axis.

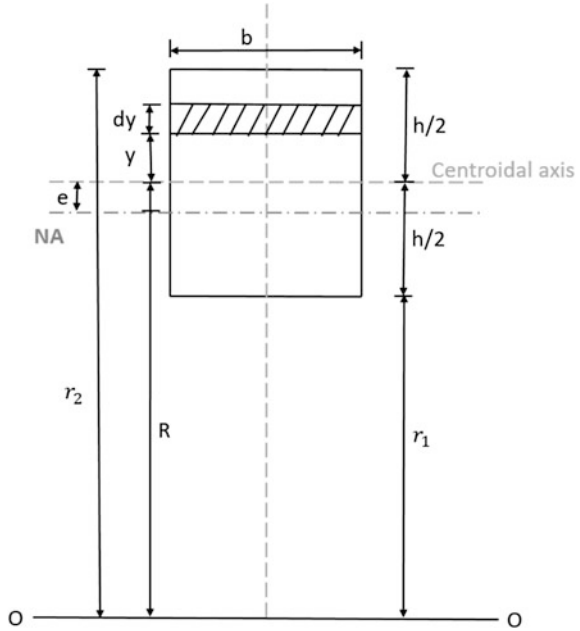
The area of the elemental strip is given by:

$$dA = b \, dy \quad (2.147)$$

$$mA = \int \frac{y}{(R+y)} dA \quad (2.148)$$

$$= \int \frac{v-R}{v} dA \quad (2.149)$$

**Fig. 2.25** Details of rectangular cross section



$$m A = \int_{r_1}^{r_2} dA - R \int_{r_1}^{r_2} \frac{dA}{v} \tag{2.150}$$

$$= A = R b \ln \left( \frac{r_2}{r_1} \right) \tag{2.151}$$

$$m = 1 - \frac{R}{A} b \ln \left( \frac{r_2}{r_1} \right) \tag{2.152}$$

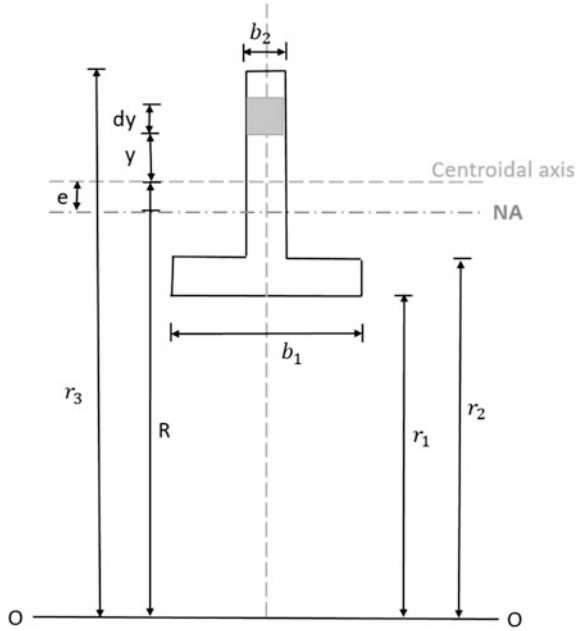
$$= 1 - \frac{R b}{A} \ln \left[ \frac{\left( R + \frac{h}{2} \right)}{\left( R - \frac{h}{2} \right)} \right] \tag{2.153}$$

### 2.5.6 T Section

Consider an elemental strip on the T section as shown in Fig. 2.26.

$$m A = \int \frac{y}{R + y} dA \tag{2.154}$$

Fig. 2.26 T-section



$$= \int_A \frac{v+R}{v} dA \tag{2.155}$$

$$= \int_A dA - R \int_A \frac{1}{v} dA \tag{2.156}$$

$$= k - R \left[ b_1 \int_{r_1}^{r_2} \frac{dv}{v} \right] - R \left[ b_2 \int_{r_1}^{r_3} \frac{dv}{v} \right] \tag{2.157}$$

$$= A - Rb_1 \ln\left(\frac{r_2}{r_1}\right) - Rb_2 \ln\left(\frac{r_3}{r_1}\right) \tag{2.158}$$

$$m = 1 - \frac{R}{A} \left[ Rb_1 \ln\left(\frac{r_2}{r_1}\right) - Rb_2 \ln\left(\frac{r_3}{r_1}\right) \right] \tag{2.159}$$

We also know that

$$e = \left(\frac{m}{m-1}\right)R \tag{2.160}$$

$$e = R \left\{ \frac{1 - \frac{R}{A} \left[ Rb_1 \ln\left(\frac{r_2}{r_1}\right) - Rb_2 \ln\left(\frac{r_3}{r_1}\right) \right]}{1 - \frac{R}{A} \left[ Rb_1 \ln\left(\frac{r_2}{r_1}\right) - Rb_2 \ln\left(\frac{r_3}{r_1}\right) \right] - 1} \right\} \tag{2.161}$$

$$= R \left\{ 1 - \frac{1}{\frac{R}{A} \left[ Rb_1 \ln\left(\frac{r_2}{r_1}\right) - Rb_2 \ln\left(\frac{r_3}{r_1}\right) \right]} \right\} \tag{2.162}$$

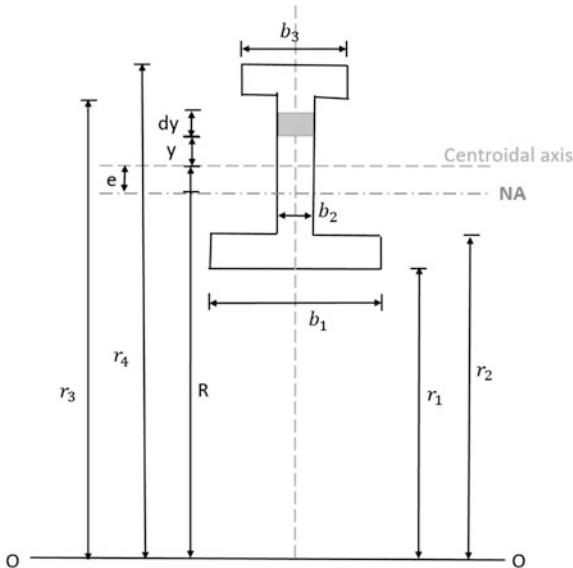
$$e = R - \frac{A}{b_1 \ln\left(\frac{r_2}{r_1}\right) - b_2 \ln\left(\frac{r_3}{r_1}\right)} \tag{2.163}$$

### 2.5.7 I Section

Consider an I section as shown in Fig. 2.27.

$$mA = \int_A \frac{y}{R + y} dA \tag{2.164}$$

Fig. 2.27 I section details



$$= \int_A \frac{v - R}{v} dA \quad (2.165)$$

$$mA = \int_A dA - R \int \frac{dA}{v} \quad (2.166)$$

$$= A - R \left[ \int_{r_1}^{r_2} \frac{b_1 dv}{v} + \int_{r_2}^{r_3} \frac{b_2 dv}{v} + \int_3^{r_4} \frac{b_3 dv}{v} + \right] \quad (2.167)$$

$$mA = A - R \left\{ b_1 \ln \left( \frac{r_2}{r_1} \right) + b_2 \ln \left( \frac{r_3}{r_2} \right) + b_3 \ln \left( \frac{r_4}{r_3} \right) \right\} \quad (2.168)$$

$$m = 1 - \frac{R}{A} \left[ b_1 \ln \left( \frac{r_2}{r_1} \right) + b_2 \ln \left( \frac{r_3}{r_2} \right) + b_3 \ln \left( \frac{r_4}{r_3} \right) \right] \quad (2.169)$$

The general expression for a section which is a combination of rectangles is given by:

$$e = R - \frac{A}{\sum_1^n b_n \ln \left( \frac{r_{n+1}}{r_n} \right)} \quad (2.170)$$

### 2.5.8 Triangular Cross Section

Consider an elemental strip of thickness  $dy$  on a triangular cross section as shown in Fig. 2.28. To calculate width of this elemental strip ( $x$ ), following equation holds good:

$$(r_2 - r_1) - \frac{b_1}{2} \quad (2.171)$$

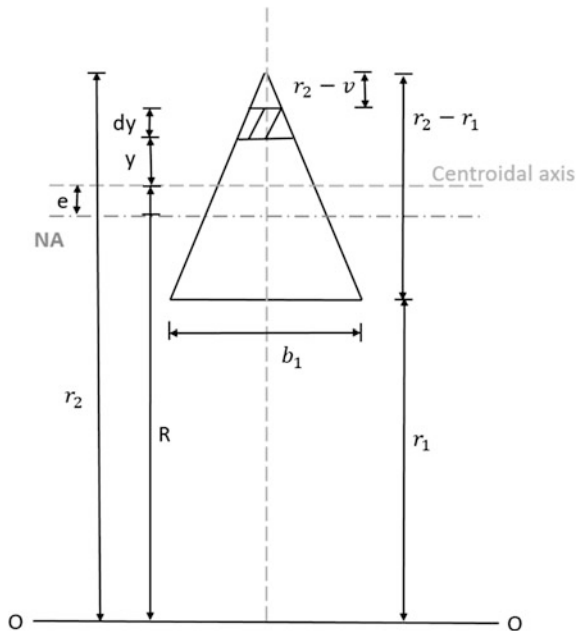
$$r_2 - v - \frac{x}{2} \quad (2.172)$$

$$\frac{x}{2}(r_2 - r_1) = \frac{b_1}{2}(r_2 - v) \quad (2.173)$$

$$x = b_1 \left( \frac{r_2 - v}{r_2 - r_1} \right) \quad (2.174)$$

$$mA = \int dA - R \int \frac{dA}{v} \quad (2.175)$$

**Fig. 2.28** Triangular cross section



$$= A - R \int_{r_1}^{r_2} b_1 \left( \frac{r_2 - v}{r_2 - r_1} \right) \frac{dv}{v} \quad (2.176)$$

$$= A - \frac{Rb_1}{r_2 - r_1} \int_{r_2}^{r_1} (r_2 - v) \frac{dv}{v} \quad (2.177)$$

$$= A - \frac{Rb_1}{r_2 - r_1} \left\{ \int_{r_2}^{r_1} r_2 \ln \left( \frac{r_2}{r_1} \right) - \int_{r_2}^{r_1} dv \right\} \quad (2.178)$$

$$= A - \frac{Rb_1}{r_2 - r_1} \left\{ r_2 \ln \left( \frac{r_2}{r_1} \right) - (r_2 - r_1) \right\} \quad (2.179)$$

$$m = 1 - \frac{R}{A} \left\{ \frac{r_2 b_1}{(r_2 - r_1)} \ln \left( \frac{r_2}{r_1} - b_1 \right) \right\} \quad (2.180)$$

$$e = R - \frac{A}{\left[ \frac{r_2 b_1}{(r_2 - r_1)} \ln \left( \frac{r_2}{r_1} - b_1 \right) \right]} \quad (2.181)$$

### 2.5.9 Trapezoidal Cross Section

Consider an elemental strip of thickness  $dy$  on a trapezoidal cross section as shown in Fig. 2.29. To calculate width of this elemental strip,  $x$  following relationship holds good:

$$(b_1 - b_2) - (r_2 - r_1) \tag{2.182}$$

$$x^* - (r_2 - v) \tag{2.183}$$

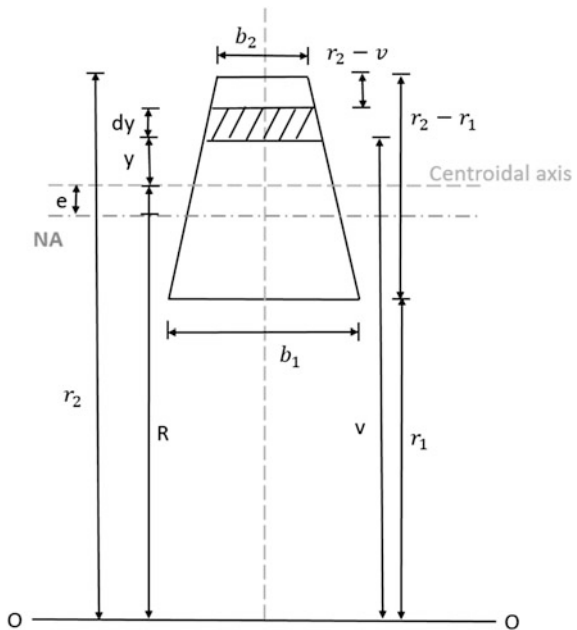
$$x^*(r_2 - r_1) = (r_2 - v)(b_1 - b_2) \tag{2.184}$$

$$x = (b_1 - b_2) \frac{(r_2 - v)}{(r_2 - r_1)} + b_2 \tag{2.185}$$

$$mA = \int dA - R \int \frac{dA}{v} \tag{2.186}$$

$$= A - R \int_{r_1}^{r_2} \left\{ b_2 \frac{(b_1 - b_2)}{(r_2 - r_1)} \cdot (r_2 - v) \right\} \frac{dv}{v} \tag{2.187}$$

**Fig. 2.29** Trapezoidal cross section details



$$= A - R \left[ \int_{r_1}^{r_2} b_2 \frac{dv}{v} + \int_{r_1}^{r_2} \frac{(b_1 - b_2)}{(r_2 - r_1)} \cdot (r_2) \frac{dv}{v} + \int_{r_1}^{r_2} \frac{(b_1 - b_2)}{(r_2 - r_1)} dv \right] \quad (2.188)$$

$$= A - R \left\{ b_2 \ln \left( \frac{r_2}{r_1} \right) + \frac{(b_1 - b_2)}{(r_2 - r_1)} \cdot (r_2) \ln \left( \frac{r_2}{r_1} \right) - (b_1 - b_2) \right\} \quad (2.189)$$

$$= A - R \left[ \left\{ b_2 + \frac{(b_1 - b_2)}{(r_2 - r_1)} \cdot (r_2) \right\} \ln \left( \frac{r_2}{r_1} \right) - (b_1 - b_2) \right] \quad (2.190)$$

$$m = 1 - \frac{R}{A} \left[ \left\{ b_2 + \frac{(b_1 - b_2)}{(r_2 - r_1)} \cdot (r_2) \right\} \ln \left( \frac{r_2}{r_1} \right) - (b_1 - b_2) \right] \quad (2.191)$$

$$e = R - \frac{A}{\left[ \left\{ b_2 + \frac{(b_1 - b_2)}{(r_2 - r_1)} \cdot (r_2) \right\} \ln \left( \frac{r_2}{r_1} \right) - (b_1 - b_2) \right]} \quad (2.192)$$

In the above equation, if  $b_2 = 0$  the section becomes a triangular section and if  $b_1 = b_2 = b$  the section becomes a rectangular section. The equation is also used to locate the neutral axis from the centroidal axis. These equations are useful only to obtain the stress on the extreme fibers in curved beam with large ( $R_i$ ).

## 2.6 Simplified Equations to Estimate Stresses

Following equations are valid to estimate stresses in the extreme fibre, in a simplified manner.

$$\sigma = K \frac{Mh}{I} \quad (2.193)$$

where  $K$  is a factor to be used for intrados and extrados as below:

$$K_{\text{intrados}} = \frac{\frac{M}{2I} (h_i - e)}{\frac{Mh_i}{2I}} \quad (2.194)$$

$$K_{\text{extrados}} = \frac{\frac{h_o + e}{r_o}}{\frac{Mh_o}{2I}} \quad (2.195)$$

where  $k_{\text{intrados}}$  and  $k_{\text{extrados}}$  are called as correction factors, whose values are given in Table 2.1.

**Table 2.1** Stress correction factors for intrados and extrados

Cross section	R/h	Factors		e
		K <sub>i</sub>	K <sub>o</sub>	
Circular	1.2	3.41	0.54	0.224R
	1.4	2.40	0.60	0.151R
	1.6	1.96	0.65	0.108R
	1.8	1.75	0.68	0.084R
	2.0	1.62	0.71	0.009R
	3.0	1.33	0.79	0.030R
	4.0	1.23	0.84	0.016R
	6.0	1.14	0.89	0.007R
Rectangular	1.2	2.89	0.57	0.305R
	1.4	2.13	0.63	0.204R
	1.6	1.79	0.67	0.149R
	1.8	1.63	0.70	0.112R
	2.0	1.52	0.73	0.090R
	3.0	1.30	0.81	0.041R
	4.0	1.20	0.85	0.021R
	6.0	1.12	0.90	0.0093R

## 2.7 Example Problems in Curved Beams

**Example 1** Estimate the stresses at points A, B, C, and D for the section shown in Fig. 2.30. Type of the section is rectangular; details are given in Fig. 2.31. Length of the section,  $l = 40$  mm; breadth of the section,  $b = 20$  mm; inner radius of the beam,  $r_1 = 40$  mm; load acting on the beam,  $P = 20$  kN, and angle of  $CD$  from centroidal axis,  $\Theta = 45^\circ$

**Solution:**

### A. Winkler–Bach Equation

(i) *Calculation of geometric properties:*

$$h = l/2 = 20 \text{ mm}$$

$$h_i = h_o = h = 20 \text{ mm}$$

1. Radius of the curved beam,  $R = r_1 + h = 60$  mm
2. Outer radius of the curved beam,  $r_2 = r_1 + l = 80$  mm
3. CS area of the section,  $A = l \times b = 800 \text{ mm}^2$
4. Sectional property,  $m = 1 - \left(\frac{R}{A}\right).b.\ln\left(\frac{r_2^2}{r_1^2}\right) = -0.0397$ (no unit)

**Fig. 2.30** Example problem-1 for curved beams

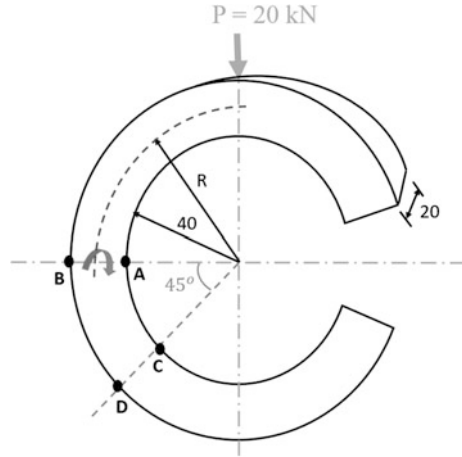
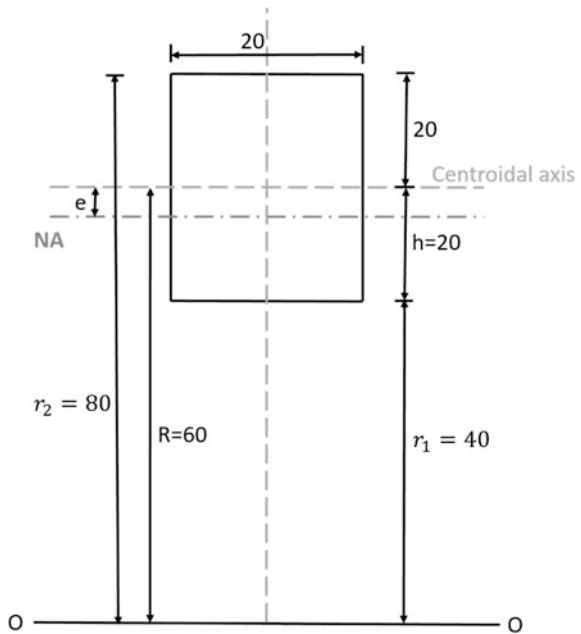


**Fig. 2.31** Cross section details of curved beam problem-1



5. Eccentricity,  $e = \left(\frac{m}{m-1}\right)R = 2.292 \text{ mm}$  (The positive value of 'e' indicates that the neutral axis will shift toward the center of curvature)
6. Moment of inertia,  $I = 1.067 \times 10^5 \text{ mm}^4$

(ii) **Section AB:**

- (a) Direct stress,  $\sigma_d = -\frac{P}{A} = -25 \text{ N/mm}^2$
- (b) Moment at CG,  $M = P \times R = 1.2 \text{ kNm}$   
 Moment about CG will cause tensile stresses in extrados and compressive stresses in intrados.
- (c) Stress at intrados,  $\sigma_i = -\frac{M}{Ae} \left( \frac{h_i - e}{r_i} \right) = -289.697 \text{ N/mm}^2$  (compressive)
- (d) Stress at extrados,  $\sigma_i = \frac{M}{Ae} \left( \frac{h_o - e}{r_o} \right) = 182.348 \text{ N/mm}^2$  (tensile)
- (e) Total stress at intrados,  $\sigma_A = \sigma_d + \sigma_i = -314.697 \text{ N/mm}^2$  (compressive)
- (f) Total stress at extrados,  $\sigma_B = \sigma_d + \sigma_o = 157.348 \text{ N/mm}^2$  (tensile)

(iii) **Section CD:**

Since the section CD is at an angle from the centroidal axis, the normal load at the section is given by (please refer to Fig. 2.32 for details):

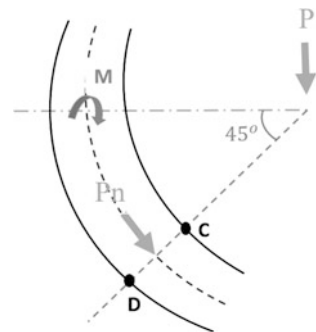
$$P_n = P \cos \theta = 14.142 \text{ kN.}$$

- (a) Direct stress,  $\sigma_d = -\frac{P_n}{A} = -17.678 \text{ N/mm}^2$
- (b) Moment at CG,  $M = M \times \cos \theta = 0.848 \text{ kNm}$
- (c) Stress at intrados,  $\sigma_i = -\frac{M}{Ae} \left( \frac{h_i - e}{r_i} \right) = -204.847 \text{ N/mm}^2$  (compressive)
- (d) Stress at extrados,  $\sigma_i = \frac{M}{Ae} \left( \frac{h_o - e}{r_o} \right) = 128.94 \text{ N/mm}^2$  (tensile)
- (e) Total stress at intrados,  $\sigma_A = \sigma_d + \sigma_i = -222.524 \text{ N/mm}^2$  (compressive)
- (f) Total stress at extrados,  $\sigma_B = \sigma_d + \sigma_o = 111.262 \text{ N/mm}^2$  (tensile)

**B. Wilson and Querean Equation:**

$$R/h = 3$$

Fig. 2.32 Resolving load



From the table,

$$k_i = 1.3.$$

$$k_o = 0.81$$

- (a) Stress at intrados,  $\sigma_i = -k_i \frac{M}{Ae} h = -292.5 \text{ N/mm}^2$  (compressive)
- (b) Stress at extrados,  $\sigma_o = k_o \frac{M}{Ae} h = 182.25 \text{ N/mm}^2$  (tensile)
- (c) Total stress at intrados,  $\sigma_A = \sigma_d + \sigma_i = -317.5 \text{ N/mm}^2$  (compressive)
- (d) Total stress at extrados,  $\sigma_B = \sigma_d + \sigma_o = 157.25 \text{ N/mm}^2$  (tensile)

**Example 2** A 10-ton crane hook is used to lift an object during commissioning of an offshore deck as shown in Fig. 2.33. Find the stresses at the intrados and extrados. Type of the section: trapezoidal section, as shown in Fig. 2.34. Height of the section,  $l = 120 \text{ mm}$ ; breadth of the section,  $b_1 = 90 \text{ mm}$ ;  $b_2 = 30 \text{ mm}$ ; inner radius of the beam,  $r_1 = 70 \text{ mm}$ , and load acting on the beam,  $P = 100 \text{ kN}$ .

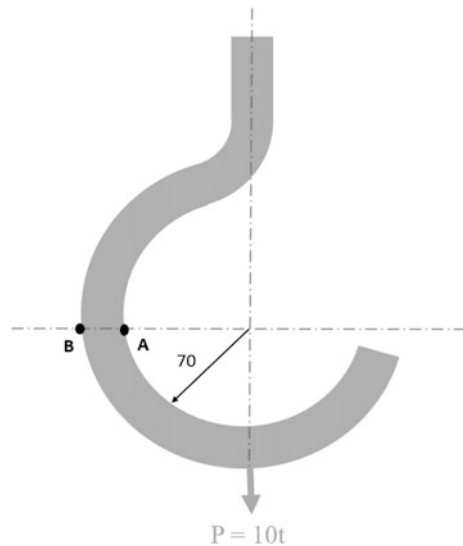
**Solution:**

**A. Winkler–Bach Equation**

- (i) *Calculation of geometric properties:*

$$b_3 = 30 \text{ mm}$$

**Fig. 2.33** Crane hook for curved beam problem-2



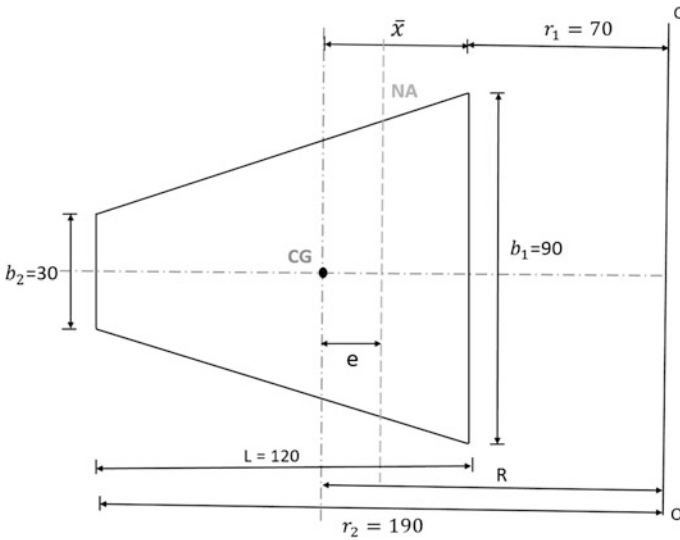


Fig. 2.34 Cross section of curved beam for problem-2

Location of the neutral axis,  $\bar{x} = \frac{\sum A\bar{x}}{\sum A} = 50 \text{ mm}$

$$h_i = x = 50 \text{ mm}$$

$$h_o = h - x = 70 \text{ mm}$$

1. Radius of the curved beam,  $R = r_1 + x = 120 \text{ mm}$
2. Outer radius of the curved beam,  $r_2 = r_1 + h = 190 \text{ mm}$
3. CS area of the section,  $A = 7200 \text{ mm}^2$
4. Sectional property,  $m = 1 - \left(\frac{R}{A}\right) \left\{ \left[ b_2 + \frac{r_2(b_1 - b_2)}{(r_2 - r_1)} \right] \cdot \ln\left(\frac{r_2}{r_1}\right) - (b_1 - b_2) \right\} = -0.0803 \text{ (no unit)}$
5. Eccentricity,  $e = \left(\frac{m}{m-1}\right)R = 8.916 \text{ mm}$  (The positive value of 'e' indicates that the neutral axis will shift toward the center of curvature)
6. Moment of inertia,  $I = 7.92 \times 10^6 \text{ mm}^4$

(ii) **Section AB:**

$$r_i = r_1 = 70 \text{ mm}$$

$$r_o = r_2 = 190 \text{ mm}$$

(a) Direct Stress,  $\sigma_d = \frac{P}{A} = 13.889 \text{ N/mm}^2$

(b) Moment at CG,  $M = -P \times R = -12 \text{ kNm}$

- (c) Stress at intrados,  $\sigma_i = -\frac{M}{Ae} \left( \frac{h_i - e}{r_i} \right) = 109.704 \text{ N/mm}^2$  (tensile)  
 (d) Stress at extrados,  $\sigma_o = \frac{M}{Ae} \left( \frac{h_o - e}{r_o} \right) = -77.637 \text{ N/mm}^2$  (compressive)  
 (e) Total stress at intrados,  $\sigma_A = \sigma_d + \sigma_i = 123.593 \text{ N/mm}^2$  (tensile)  
 (f) Total stress at extrados,  $\sigma_B = \sigma_d + \sigma_o = -63.748 \text{ N/mm}^2$  (compressive)

**B. Straight Beam Formula:**

$$\sigma = \frac{M}{I} y$$

$$y_i = 50 \text{ mm}$$

$$y_o = 70 \text{ mm}$$

- (a) Stress at intrados,  $\sigma_i = \frac{M}{I} y_i = 75.758 \text{ N/mm}^2$  (tensile)  
 (b) Stress at extrados,  $\sigma_o = \frac{M}{I} y_o = -106.06 \text{ N/mm}^2$  (compressive)  
 (c) Total stress at intrados,  $\sigma_A = \sigma_d + \sigma_i = 89.647 \text{ N/mm}^2$  (tensile)  
 (d) Total stress at extrados,  $\sigma_B = \sigma_d + \sigma_o = -92.172 \text{ N/mm}^2$  (compressive)

## 2.8 Marine Risers

Risers connect floating drilling or production platforms to the wells. The risers are used for different purposes such as drilling, production, export, and completion/work over. Riser is a large, slender, vertical cylindrical pipe. Axial tension is provided to improve total stiffness. Risers are subjected to waves and current from different direction. But for analysis, it is considered to bend in any one plane where plane of the motion of the platform traced. To account for wave direction effects in the riser analysis, a coupled analysis of the riser under different bending planes can be done. Based on the pressure, the risers are classified as low-pressure risers and high-pressure risers. Generally, risers can be grouped as follows:

- i. Bundled risers
- ii. Flexible risers
- iii. Top tensioned risers (TTR)
- iv. Steel catenary riser (SCR)
- v. Hybrid risers (a combination of steel flexible risers).

### 2.8.1 Low-Pressure Risers

These types of risers are open to the atmospheric pressure at the top end, and they are useful for drilling. They are of very large diameter, typically around 500 mm

with a lot of peripheral lines. Kill and choke lines are useful to circulate fluid when lick occurs. They are used as communicating units, located at the closure of BOP in case of gas kick. Low-pressure risers and BOP are fixed to the seafloor and also will act as communication about the BOP closure. Booster lines are useful both to inject fluid at the lower end and accelerate the flow. When risers are to be installed at water depth greater than 20 m, they need to be top tensioned in order to maintain its stability.

### **2.8.2 High-Pressure Drilling Riser**

These risers are installed when blow out preventer is located closer to the surface. Further, no additional pipelines and peripherals are required for communication with BOP. In this case, risers are designed to operate at full pressure.

### **2.8.3 Flexible Risers**

Flexible risers are useful as production risers or export risers. These are different from the low pressure, drilling risers. These risers are layered; inner metal surface is called carcass and is covered by plastic pressure sheathing to avoid fluid containment. It is further covered by steel vault, which is needed to sustain high magnitude of hoop stress. Steel armors cover this layer to improve resistance against axial tensile stresses. Whole cross section will be covered by anti-wear layer and a plastic outer sheathing, which prevents water penetration.

### **2.8.4 Top Tensioned Risers (TTR)**

Top tensioned risers are required to ensure stability. The first TTR was used in Hutton Tension Leg Platform in 1984. TTRs connect seabed through a stress joint. In addition, these risers will also have a keel joint, which is located at the keel level of the platform. One of the important design criteria is that the ratio of top tension to apparent weight be 1.2–1.8. Generally, top tensioning is required for platforms with large offset, which demands tension riser stiffness. Air cans are deployed to reduce this high tension values. As these risers are highly flexible in terms of its cross section, they undergo large deformation and finite rotations. *Top tensioned riser (TTR) force* is the sum of the weight of riser equipments, buoyancy force of the riser, and force that arises from wave and current. In case of increased water depth, top tension force would be of a very high magnitude. In order to reduce this intensity, risers are produced with buoyancy modules at the upper part of the risers. Buoyancy modules are helpful in reducing top tension force that is required for

installation of riser in deep water while they also make the riser neutrally buoyant. Installation standards (ISO 13624-1, 2009) prescribe the procedure for design, selection, operation, and maintenance of marine risers.

Consider a small segment of length ( $ds$ ) on a riser. External forces acting on the segment are  $F_{xs}$  and  $F_{ys}$  in the horizontal and vertical directions, respectively.  $F_w$  is the weight of the segment at midpoint. Internal forces that act on the segment are shear bending moment and axial force. Following conditions hold good:

$$\frac{dfs}{ds} - \frac{d\theta}{ds} \quad (2.196)$$

$$\frac{dfs}{ds} + FA \frac{d\theta}{ds} \quad (2.197)$$

$$\sum F_y = 0 : f_1 \cos \theta - f_2 \sin \theta - f_w + f_{ys} = 0 \quad (2.198)$$

$$\sum F_x = 0 : f_1 \sin \theta - f_2 \cos \theta + f_{xs} - m\ddot{x} = 0 \quad (2.199)$$

$$\sum M = 0 : \frac{dM_B}{ds} + F_s = 0 \quad (2.200)$$

where  $m$  denotes mass per unit length of the segment.

$$f_1 = \frac{dF_A}{ds} + F_s \frac{d\theta}{ds} = 0 \quad (2.201)$$

$$f_2 = \frac{dF_s}{ds} + F_A \frac{d\theta}{ds} = 0 \quad (2.202)$$

Deflection of the riser is small, and small deflection beam theory is applicable.

$$\cos \theta = \frac{dx}{ds} \quad (2.203)$$

$$\sin \theta = \frac{dy}{ds} \quad (2.204)$$

$$M_B = EI \frac{d\theta}{ds} = EI \frac{d^2x}{ds^2} \quad (2.205)$$

$$\frac{dF_A}{dy} - \frac{d}{dy} \left( F_s \frac{dx}{dy} \right) - F_w + F_{ys} = 0 \quad (2.206)$$

$$\frac{d}{dy} \left( F_A \frac{dx}{dy} \right) + \frac{dF_s}{dy} + F_{xs} - mx = 0 \quad (2.207)$$

$$\frac{d}{dy} \left( EI \frac{d^2x}{ds^2} \right) + F_s = 0 \quad (2.208)$$

Equation of motion of the riser in the horizontal plane can be obtained by combining the above equations:

$$\sec \theta \left\{ \frac{d^2}{ds^2} \left[ EI \left( \frac{d\theta}{ds} \right) \right] - F_A \left( \frac{d\theta}{ds} \right) \right\} \quad (2.209)$$

$$(F_w = F_{ys}) \tan \theta + m\ddot{x} = f_s \quad (2.210)$$

Let  $A_i$  and  $A_o$  be the internal and external areas of cross section of the riser segment. Internal segment will be under hydrostatic load pressure, and the internal fluid will oppose the hydrodynamic load arising from the external fluid. Static equivalent pressure is given by

$$f_{xp} = (A_o p_o - A_i p_i) \frac{d^2}{dy^2} - (A_o p_o - A_i p_i) g \frac{dx}{dy} \quad (2.211)$$

Equation of motion is now modified as:

$$\begin{aligned} & \frac{d^2}{dy^2} \left[ EI \frac{d^2x}{dy^2} \right] - [F_A + A_o p_o - A_i p_i] \frac{d^2x}{dy^2} - (\rho_s g) (A_o - A_i) - f_{ys} \\ & - g (A_o p_o - A_i p_i) \frac{dx}{dy} + m\ddot{x} \\ & = f_{xs} \end{aligned} \quad (2.212)$$

$$\frac{d^2}{dy^2} \left[ EI \frac{d^2x}{dy^2} \right] - \frac{d}{dy} \left[ F_e(y) \frac{dx}{dy} \right] + m(y)\ddot{x} = f_{xs}(x, y, t) \quad (2.213)$$

It is the equation of motion for the riser. The first term represents the resistance of the riser due to its flexural rigidity (EI). The second term denotes the load from the axial force (tensile-top tension) and the external/internal fluid pressure. The third term is the internal resistance of the riser. The right-hand side term is the applied horizontal force. The basic assumption is that the riser inertia force is absent, which leads to simplified static analysis.

$$\frac{d^2}{dy^2} \left[ EI \frac{d^2x}{dy^2} \right] - \frac{d}{dy} \left[ F_e(y) \frac{dx}{dy} \right] + m(y)\ddot{x} = \frac{1}{2} \rho C_D(y) D(y) |u(y)| u(y) \quad (2.214)$$

where  $u(y)$  is the current velocity, which is a function of vertical coordinates ( $y$ ) and  $C_D(y)$  is the drag coefficient, which is a function of  $y$ .

## 2.9 Members Under Vortex-Induced Vibration (VIV)

When risers are exposed to fluid flow, flow separation takes place. This results in formation of vortex shedding from the surface of the riser, which occurs mainly due to passage of fluid. During vortex-induced vibration, vortex-shedding frequencies try to lock various units of the riser, which leads to resonating condition ( $\omega = \omega_n$ ). VIV is caused by the vortex shed behind the risers in the fluid flow. Major consequences of VIV are as follows:

- i. They can cause alternating pressure field on the surface the riser.
- ii. It results in oscillating members.
- iii. In case of unsteady flow, when vortex shedding matches (even when approaches) the structural frequency, structure undergoes VIV at this stage.
- iv. When the VIV frequency matches with that of the structural frequency, resonance condition sets in. This leads to various consequences as fatigue damage, reduction of service life of system, induces large transverse motion, and causes operational difficulties.

Vortex shedding is a phenomenon that occurs over bluff bodies subjected to sustained currents, which might result in large transverse motions. When a flowing medium strikes a non-streamlined bluff object, it moves around the object generating alternating pressure forces on either side of the bluff body, as shown in Fig. 2.35.

This results in the formation of vortices, causing periodic forces, which are strong enough to set the body into oscillatory motion. Vortex-induced vibration (VIV) is the outcome of such exciting forces that are generated by vortex shedding on hull of a bluff body, causing response closer to the resonant period (Anagnostopoulos and Bearman 1992; Bearman 1984). Experimental investigations carried out on elastically mounted cylinder showed wake formation with the maximum amplitude occurring near lower limit of lock-in region. Due to VIV, structure undergoes a number of stress cycles leading to fatigue damage. Based upon the significant consequences of VIV on several mechanical systems and ocean engineering structures, VIV suppression configurations are encouraged (Sarpkaya 1978). Observation of large amplitude responses of systems that used water as working fluid necessitates the importance of VIV suppression by design (Kalak and Williamson 1991; Zdravkovich 1981). While a number of suppression techniques of VIV suppression are successfully developed, cost and difficulty of

**Fig. 2.35** Shear layers on both sides to form lee-wake vortices

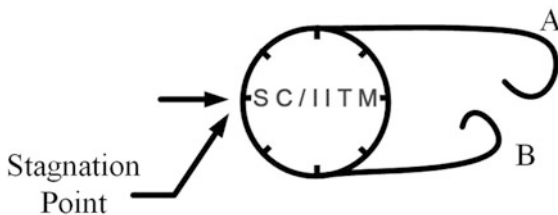
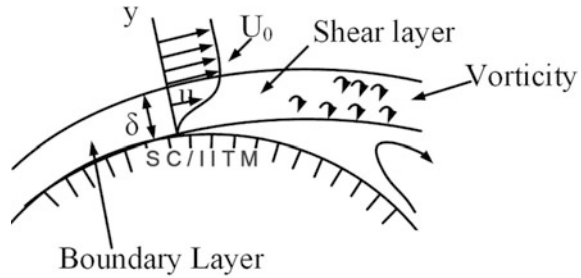


**Fig. 2.36** Flow near separation during vortex formation



implementation restricted their application (Owen and Masa 2003). In addition to suppressing VIV, use of helical strakes proved to be effective in strengthening the cylinder to resist larger bending moments that result from the increased drag. Under close examination of flow behind a pair of cylinder, pair of anti-phase streets and in-phase shedding can cause the formation of a single wake in large scale (Williamson and Govardhan 2004; Govardhan and Williamson 2000; Brika and Laneville 1993). Their applications in marine risers by modeling them as flexible cylinders are quite successful. Various flow velocities affect normalized vortex-shedding frequency (Lesage and Garthshore 1987). Figure 2.36 shows flow near separation during vortex formation. Present case study deals with the experimental investigations of a rigid cylinder that resembles cylinder of a Spar.

## 2.10 Research Case Study: Effect of Suppression System on VIV of Spar Cylinder

Flow around a cylinder is one of the classical topics in field of hydrodynamics. Recent research highlights advantages of reduction of lateral forces by providing perforated outer cover around offshore cylindrical members (Mutlu and Jorgen 2003; Chandrasekaran and Madhavi 2015a, b). In general, models proposed by several researchers consider rigid circular cylinder with a single degree of freedom in the cross-flow direction (Gabbai and Benaroya 2005; Rodolfo et al. 2011; Govardhan and Williamson 2002). Experimental investigations carried out on long and flexible cylinders indicated the formation of vortex-induced motion in the form of hysteresis loop motion in which contributions are seen from each of the vortex-shedding modes. Amongst various methods proposed to suppress VIV, strakes and shrouds are found to be effective regardless the orientation of structure to waves and current; but showed substantial increase in drag, resulting in high drift. When strakes or bumps are fixed, no regular shedding is observed on the wake side of the cylinder, while major advantage is effective suppression of amplitude of vibration of the cylinder. Recent studies also show the possibilities of suppression of vibration of multiple cylinders using rough strip (Blevins 1994). A few analytical and numerical investigations of VIV on cylinders with low mass and aspect ratio

are helpful in modeling wake oscillations and force decomposition, resulting from VIV suppression systems. Alternatively, force reduction is also achieved by providing an outer perforated cover, which alters fluid flow around cylinders in flow regime. Being undesirable, suppression of VIV shall improve safe and comfortable working environment of offshore drilling by enhancing the design life of structural members. Vortex-induced motion is characterized by the following dimensionless parameters:

$$R_e = \frac{\rho u D}{\mu} \quad (2.215)$$

$$S = \frac{f_s D}{u} \quad (2.216)$$

$$\text{Reduced velocity} = \frac{u T}{D} \quad (2.217)$$

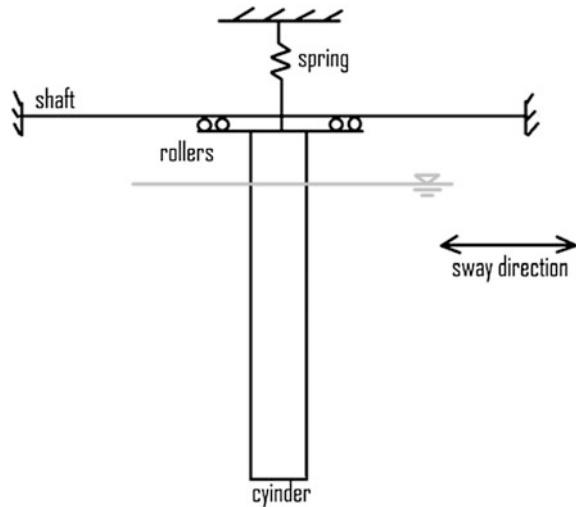
$$\text{amplitude Ratio} = \frac{A}{D} \quad (2.218)$$

where  $D$  is diameter of the cylinder,  $u$  is current velocity,  $T$  is period of the cylinder,  $f_s$  is vortex-shedding frequency,  $A$  is motion amplitude,  $\rho$  is density of fluid, and  $\mu$  is dynamic viscosity. Maximum amplitude is expected at a reduced velocity of five (0.73 m/s). Experimental investigations are carried out by idealizing the model as a single degree of freedom system; model is set free along the lift direction. Experimental setup is shown in Fig. 2.37. A cylinder of diameter 101.6 and 2 mm thickness is sealed at the bottom to make it watertight. Test setup is connected to the carriage of towing tank, where the specimen is clamped to the carriage.

While mooring system is modeled as a spring system in the towing tank, scaled model is fabricated and tested to evaluate to fluid-oscillator interaction. Total length of the specimen is 1080 mm including draft of 917 mm. Towing tank carriage is moved at the required velocity in a still water medium. Considering the fact that motion amplitude and drag force rely on the relative motion between the test section and fluid medium and not on the physical fluid flow, during experimental studies, test section is moved while water remains stationary. First set of tests are conducted on a plain cylinder of unit mass ratio, without any VIV suppression systems. Tests are conducted for velocities ranging from 0.2 to 1.2 m/s at an interval of 0.02 m/s. Amplitude of transverse vibration is measured using LVDT with its probe connected to the movable platform in which cylinder is fixed. A DC supply of 12 V is provided to a calibrated LVDT and the response data, as acquired by the oscilloscope is post-processed.

A passive method of VIV suppression is attempted. Figure 2.38 shows two steel wires, fixed parallel to the axis of the cylinder to miniature turnbuckles and stretched over small notches at the ends of the cylinder. Sufficient tensile load is applied to keep the wire tight against the cylinder wall; no glue or other adhesive are used to fix the wire against the cylinder. Steel wires of 0.3 mm in diameter are fixed at

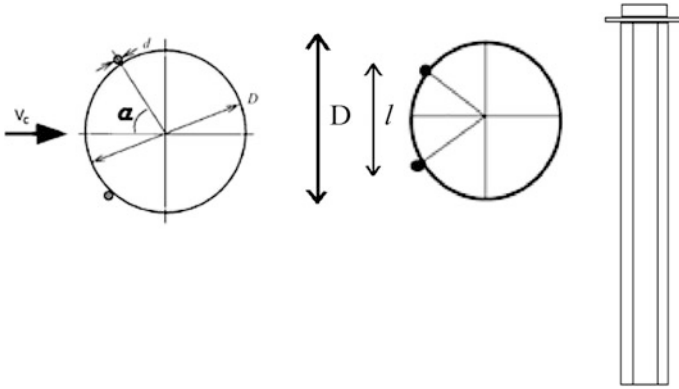
**Fig. 2.37** Experimental setup



different angles ( $\alpha$ ) with respect to the stagnation point to achieve diameter ratio ( $d/D$ ) of 0.003. Tests are repeated by attaching wires at different angles varying from  $40^\circ$  to  $80^\circ$  at an interval of  $10^\circ$ . Alternatively, helical wires of diameter 0.3 mm are wrapped around the cylinder in a helical configuration, as shown in Fig. 2.39. Experimental investigations are then carried out to assess the influence of pitch of helical strakes on VIV suppression; strakes are fixed to the cylinder at different pitch of  $5D$ ,  $7D$ , and  $10D$ , where  $D$  is the diameter of cylinder.

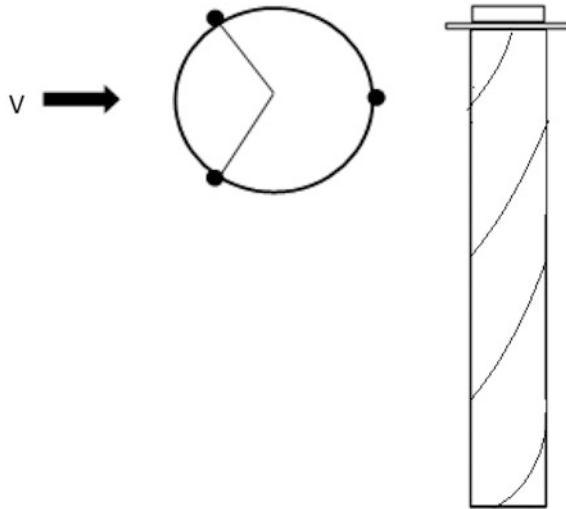
Response amplitude of bare cylinder over a wide range of reduced velocity is shown in Fig. 2.40. It is seen from figure that at lower reduced velocity, cylinder barely moves. With the increase in the reduced velocity, lock-in phenomenon occurs and results in instantaneous increase in the response of cylinder. It is seen that at a reduced velocity of 6.668 (current velocity 0.98 m/s), maximum response occurred ( $A/D = 0.87$ ). This is attributed to the fact that the cylinder undergoes vibration in the transverse direction, whose magnitude is almost equal to its own diameter. By attaching tripping wires, turbulence is generated within the laminar boundary layer. Such protrusions or attachments on the surface of bluff body have considerable effect on vortex-induced formation process and resulting oscillations of cylinder.

Figure 2.41 shows response of cylinder attached with the vertical wires. Satisfactory results are achieved when tripping wires are attached  $50^\circ$  with respect to the stagnation point. It is seen that maximum response ratio ( $A/D$ ) is reduced to about 71% in comparison to that of a bare cylinder. It is also seen that vibration is suppressed effectively throughout the chosen range of velocity. Tripping wires fixed at  $40^\circ$  show response at higher end of reduced velocity, whereas cylinders attached with  $80^\circ$  show low response at lower end of reduced velocity. Since vertical wires are unidirectional with respect to the flow direction, helical wires are attached to achieve the desired suppression under all flow directions. Figure 2.42 shows



**Fig. 2.38** Sectional view of cylinder attached with vertical wires

**Fig. 2.39** Sectional view of cylinder attached with helical wires



response of cylinder wound helically with wires. Plots show a common trend of behavior but the peak response and the velocity, at which lock-in occurs, vary slightly. As seen from the plots, one of the most effective arrangements shall be a set of three wires wound at a pitch of  $10D$ . In this case, response amplitude is reduced about 25% in comparison to that of a bare cylinder. Lock-in region starts at a reduced velocity of 4.89. As each configuration has a different pattern of suppression, overall benefits of different modifications are quantified by considering area under the curve. Table 2.2 shows a comparative assessment of the passive VIV suppression systems. As seen from Table, wires attached at  $50^\circ$  show the best reduction in vertical wires. In helical arrangement, wires wrapped at  $10D$  showed the minimum response.

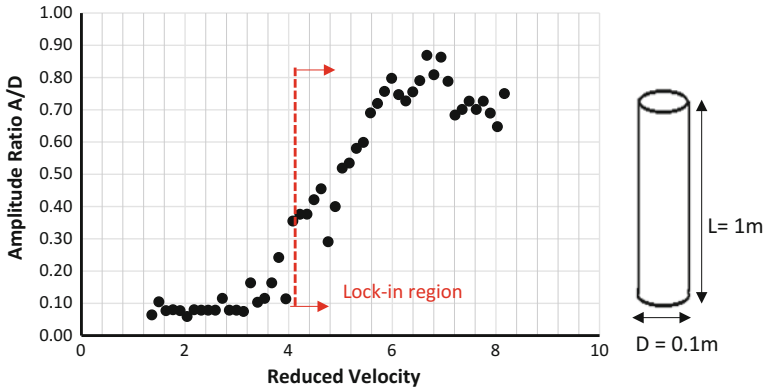


Fig. 2.40 Amplitude ratio of bare cylinder

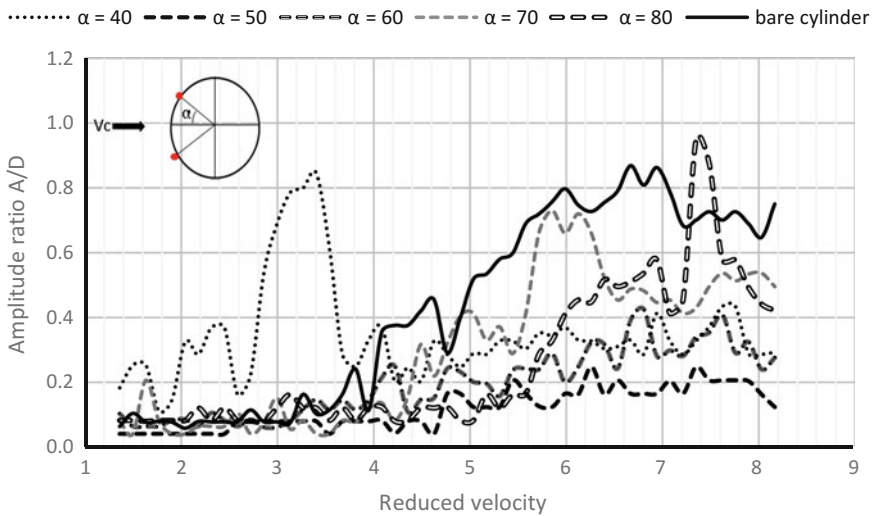


Fig. 2.41 Response of cylinders attached with vertical wires

Under the action of steady current, bare cylinder undergoes a transverse vibration whose amplitude becomes almost equal to its diameter. Passive suppression systems are effective to address VIV. When wires are arranged vertically, flow separation point has an important role in vibration of the cylinder. As the angle between wires with respect to that of the stagnation point increases, lock-in point shifts toward higher reduced velocity. Vertical wires, when placed at  $50^\circ$  and  $60^\circ$  are found to be effective in suppressing vortex-induced vibration. This has a practical application where a prominent current direction prevails. Helical configuration is symmetric with respect to that of the wave approach angle and hence provides effective suppression, irrespective of the predominant current direction in

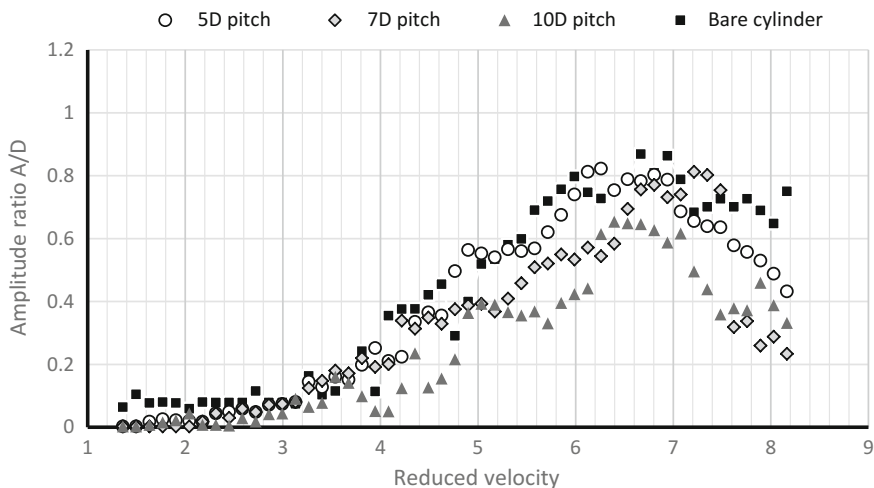


Fig. 2.42 Comparison of VIV suppression using helical wires

Table 2.2 Comparison of passive suppression systems

Vertical	Description	Area under the curve	Max amplitude ratio
	Bare cylinder	2.970	0.8685
	40°	2.378	0.8454
	50°	0.818	0.2478
	60°	1.356	0.4259
	70°	2.069	0.7304
	80°	1.790	0.9499
Helical	5D pitch	2.6791	0.8221
	7D pitch	2.2728	0.8124
	10D pitch	1.807	0.6538

the flow field. Out of helical configurations tested, wires placed at pitch equals 10 times of the diameter of the cylinder showed maximum suppression.

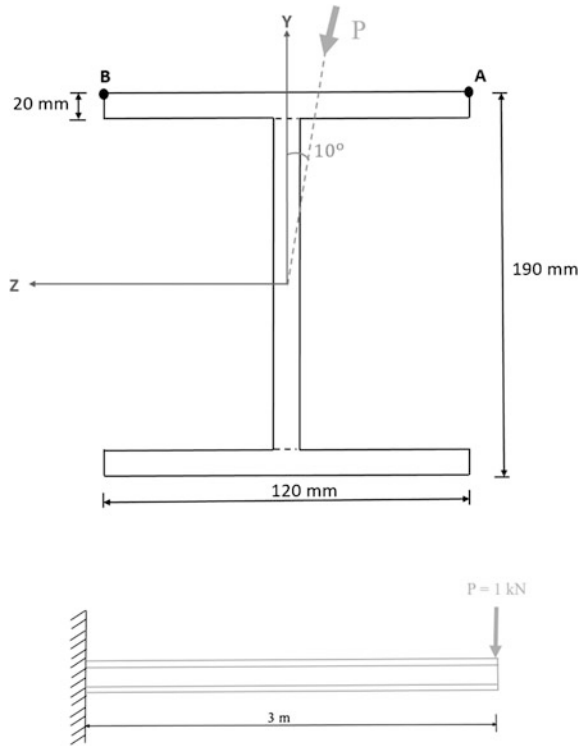
**Tutorial 5: Advanced structural analyses-I****Time: 60 min****Max marks: 20****Part A: Objective questions (5 marks)**

1. When bending takes place parallel to the plane of applied moment, \_\_\_\_\_ can be applied to compute the stresses (theory of simple bending)
2.  $\int (zy) dA = 0$  is true only when both  $ZZ$  and  $YY$  axes are \_\_\_\_\_ (Principal axes of inertia)
3. In case of unsymmetrical bending, moment will cause bending about \_\_\_\_\_ (both the principal axes of inertia)
4. To transform the problem of unsymmetrical bending to uni-planar bending, one need to locate \_\_\_\_\_ (principal axes of inertia)
5. What is the major consequence of unsymmetrical bending in design?  
If a cross section is under unsymmetrical bending, stresses in the fibers will be magnified.

**Part B: Descriptive questions (15 marks)**

1. State two conditions that should be satisfied in case of symmetric bending  
It is essential that plane containing one of the Principal axes of inertia, plane of applied moment and plane of deflection should coincide  
Neutral axis will coincide with the other Principal axis of inertia
2. What is unsymmetrical bending?
3. List the consequences of unsymmetrical bending
4. Explain how to determine bending stress at any point in a given cross-section, under unsymmetrical bending

5. Find the stresses on the cantilever beam of I section shown in the figure. The load acts at angle of  $10^\circ$  from the vertical axis.



(i) **Calculation of  $I_Z$ ,  $I_Y$ , and  $I_{ZY}$ :**

$$\bar{y} = \frac{\sum ay}{\sum a} = 95 \text{ mm}$$

$$\bar{z} = \frac{\sum az}{\sum a} = 60 \text{ mm}$$

$$I_Y = \frac{2 \times 20 \times 120^3}{12} + \frac{150 \times 20^3}{12}$$

$$= 0.586 \times 10^7 \text{ mm}^4$$

$$I_Z = 2 \left[ \frac{120 \times 20^3}{12} + 120 \times 20 \times (85)^2 \right] + \frac{20 \times 150^3}{12}$$

$$= 4.046 \times 10^7 \text{ mm}^4$$

(ii) **To locate principal axes ( $u, v$ ):**

Since I section is symmetrical,  $ZZ$  and  $YY$  axes are the principal axes  $UU$  and  $VV$ , respectively.

$$I_U = 0.586 \times 10^7 \text{ mm}^4$$

$$I_V = 4.046 \times 10^7 \text{ mm}^4$$

(iii) **To find the stresses:**

Moment about  $Z$ -axis = load  $\times$  perpendicular distance =  $1 \times 3 = -3$  kNm.

$$M_U = M_Z \cos \alpha = -2.954 \text{ kNm}$$

$$M_V = -M_Z \sin \alpha = 0.521 \text{ kNm}$$

$$\sigma_x = -\left(\frac{M_U}{I_U}v - \frac{M_V}{I_V}u\right)$$

For point  $A$ ,

$$u_A = -60 \text{ mm}$$

$$v_A = +95 \text{ mm}$$

$$\sigma_A = -\left(\frac{M_U}{I_U}v_A - \frac{M_V}{I_V}u_A\right) = 1.602 \text{ N/mm}^2 \text{ (tension)}$$

Similarly for point  $B$ ,

$$u_B = 60 \text{ mm}$$

$$v_B = 95 \text{ mm}$$

$$\sigma_B = -\left(\frac{M_U}{I_U}v_B - \frac{M_V}{I_V}u_B\right) = 12.28 \text{ N/mm}^2 \text{ (tension)}$$

**Tutorial 6: Advanced structural analyses-III**

**Time: 60 min**

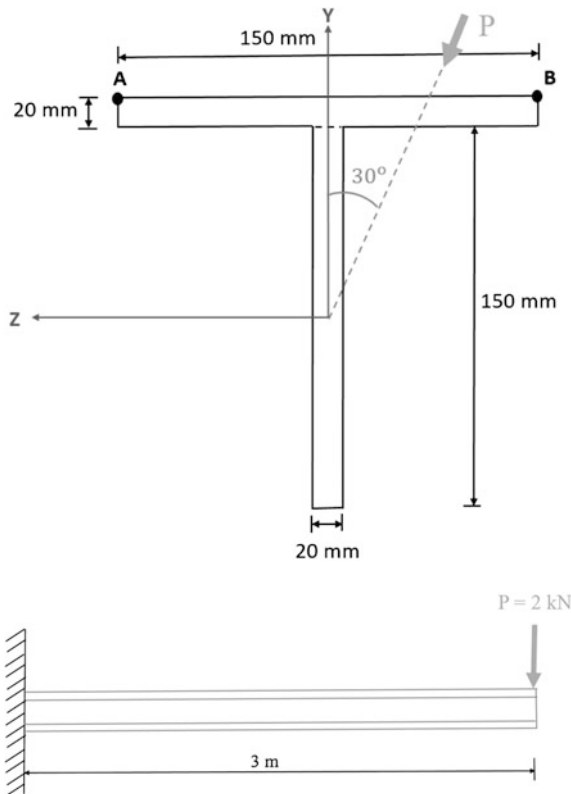
**Max marks: 20**

**Part A: Objective questions (5 marks)**

1. Draw a shear flow diagram of an I Section.
2. Define shear center  
It is the intersection of the loading plane with that of the bending axis It is also defined as the point of intersection of longitudinal axis of the member with that of line of action of transverse load.
3. If a cross-section has two axes of symmetry, their intersection shall be the \_\_\_\_\_ (shear center)
4. Load should be applied at the shear center to avoid \_\_\_\_\_ (twisting of the cross-section)
5. \_\_\_\_\_ is a special location of the cross-section (shear center).

**Part B: Descriptive questions (15 marks)**

1. List the summary about members subjected to unsymmetrical bending
2. Find the stresses on the cantilever beam shown in the figure.



(i) **Calculation of  $I_Z$ ,  $I_Y$ , and  $I_{ZY}$ :**

$$\bar{y} = \frac{\sum ay}{\sum a} = 52.5 \text{ mm}$$

$$\bar{z} = \frac{\sum az}{\sum a} = 75 \text{ mm}$$

$$I_Y = \frac{20 \times 150^3}{12} + \frac{150 \times 20^3}{12}$$

$$= 5.725 \times 10^6 \text{ mm}^4$$

$$I_Z = \frac{150 \times 20^3}{12} + 150 \times 20 \times (42.5)^2 + \frac{20 \times 150^3}{12} + 20 \times 150 \times 42.5^2$$

$$= 16.562 \times 10^6 \text{ mm}^4$$

(ii) **To locate principal axes ( $u$ ,  $v$ ):**

Since I section is symmetrical,  $ZZ$  and  $YY$  axes are the principal axes  $UU$  and  $VV$ , respectively.

$$I_U = 5.725 \times 10^6 \text{ mm}^4$$

$$I_V = 16.562 \times 10^6 \text{ mm}^4$$

(iii) **To find the stresses:**

Moment about  $Z$ -axis = load  $\times$  perpendicular distance =  $2 \times 3 = -6$  kNm.

$$M_U = M_Z \cos \alpha = -5.196 \text{ kNm}$$

$$M_V = -M_Z \sin \alpha = 3 \text{ kNm}$$

$$\sigma_X = -\left(\frac{M_U}{I_U}v - \frac{M_V}{I_V}u\right)$$

For point  $A$ ,

$$u_A = 75 \text{ mm}$$

$$v_A = 52.5 \text{ mm}$$

$$\sigma_A = -\left(\frac{M_U}{I_U}v_A - \frac{M_V}{I_V}u_A\right) = 61.234 \text{ N/mm}^2 \text{ (tension)}$$

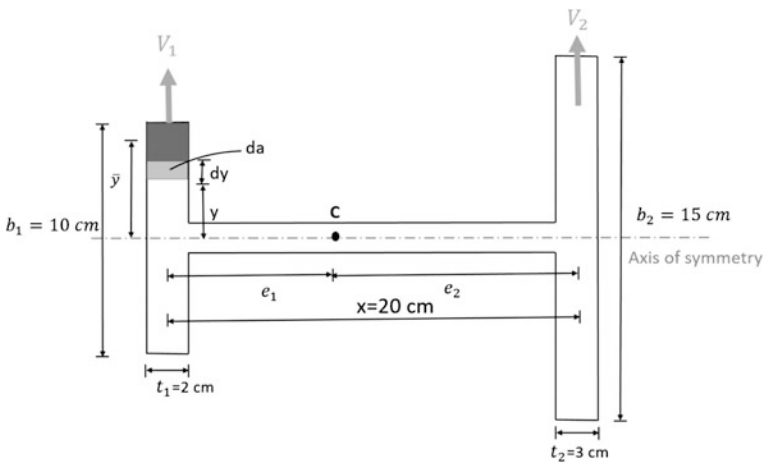
Similarly for point  $B$ ,

$$u_B = 60 \text{ mm}$$

$$v_B = 95 \text{ mm}$$

$$\sigma_B = -\left(\frac{M_U}{I_U} v_B - \frac{M_V}{I_V} u_B\right) = 34.065 \text{ N/mm}^2 \text{ (tension)}$$

3. Why shear center problem is of special interest in offshore structural design?
4. Locate the shear center 'C' for the section shown in the figure.



The shear taken by the Web is neglected. Hence,

$$V = V_1 + V_2$$

Consider a strip of thickness 'dy' in the flange at a distance 'y' from the axis of symmetry. The area of the strip is taken as 'da'.

$$da = dy(t_1)$$

The area of the section above the strip is given by

$$A = \left(\frac{b_1}{2} - y\right)t_1$$

The centroid of the section above the strip is

$$\begin{aligned}\bar{y} &= y + \frac{1}{2} \left( \frac{b_1}{2} - y \right) \\ &= y + \frac{b_1}{4} - \frac{y}{2} \\ &= \left( \frac{y}{2} + \frac{b_1}{4} \right)\end{aligned}$$

We know that,  $\tau = \frac{VA\bar{y}}{I}$

$$\begin{aligned}\tau &= \frac{V}{It_1} \left( \frac{b_1}{2} - y \right) t_1 \left( \frac{y}{2} + \frac{b_1}{4} \right) \\ &= \frac{V}{I} \left( \frac{b_1}{2} - y \right) \left( \frac{b_1}{2} + y \right) \frac{1}{2} \\ &= \frac{V}{2I} \left[ \left( \frac{b_1}{2} \right)^2 - y^2 \right]\end{aligned}\tag{1}$$

$$\begin{aligned}V_1 &= \int_{-\frac{b_1}{2}}^{\frac{b_1}{2}} \tau da \\ V_1 &= \int_{-\frac{b_1}{2}}^{\frac{b_1}{2}} \frac{V}{2I} \left[ \left( \frac{b_1}{2} \right)^2 - y^2 \right] dy t_1 \\ &= \frac{Vt_1}{2I} \times 2 \times \int_0^{\frac{b_1}{2}} \left[ \left( \frac{b_1}{2} \right)^2 - y^2 \right] dy \\ &= \frac{Vt_1}{2I} \left[ \frac{b_1^2}{4} y - \frac{y^3}{3} \right]_0^{\frac{b_1}{2}} \\ &= \frac{Vt_1}{2I} \left[ \frac{b_1^3}{8} - \frac{b_1^3}{24} \right] \\ &= \frac{V}{I} \left( \frac{t_1 b_1^3}{12} \right) \\ &= \frac{V}{I} (I_1)\end{aligned}\tag{2}$$

Similarly,

$$V_2 = \frac{V}{I}(I_2) \quad (3)$$

where

$$V = V_1 + V_2$$

' $I$ ' can be computed from the first principles.

Taking moment about  $c$ ,

$$V_1 e_1 = V_2 e_2$$

$$\frac{e_2}{e_1} = \frac{I_2}{I_1}$$

$$I_1 = \frac{t_1 b_1^3}{12} = 1.667 \times 10^6 \text{ mm}^4$$

$$I_2 = \frac{t_2 b_2^3}{12} = 8.438 \times 10^6 \text{ mm}^4$$

$$e_2 = 5.062 e_1$$

Calculate the value of  $e_1$  and  $e_2$  from the following equation:

$$x = e_1 + e_2$$

$$20 = 6.062 e_1$$

$$e_1 = 33 \text{ mm}$$

$$e_2 = 167 \text{ mm}$$

5. List the significance of estimating shear center of cross section

***Tutorial 7: Advanced structural analyse-IV***

***Time: 60 min***

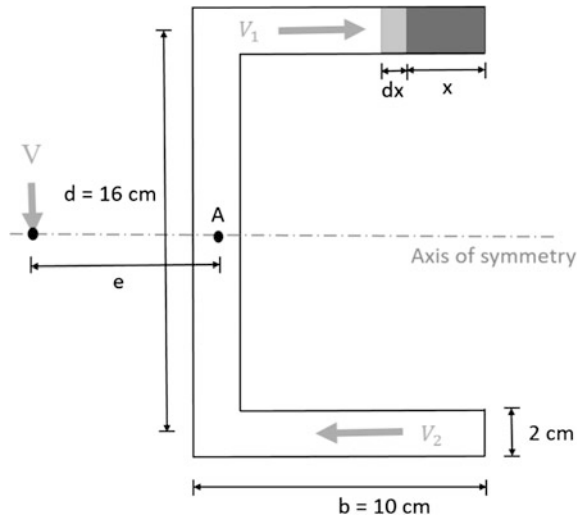
***Max marks: 20***

**Part A: Objective questions (5 marks)**

1. Load should be applied at the shear centre to avoid \_\_\_\_\_ (twisting of cross-section)
2. \_\_\_\_\_ is very vital for thin-walled sections (shear centre)
3. Curved beams can be classified as \_\_\_\_\_ and \_\_\_\_\_ (beams with small initial curvature; beams with large initial curvature)
4. If ratio of initial radius of curvature to depth of the section is lesser than 10, then the beam is classified as \_\_\_\_\_ (beams with large initial curvature)
5. If net force acting on any cross-section of the curved beam is not ZERO, it may result in \_\_\_\_\_ (warping of the cross-section)

**Part B: Descriptive questions (15 marks)**

1. List the steps involved in determining shear centre for sections with no axis of symmetry
2. List the assumptions made in the analysis of curved beams with small initial curvature
3. Locate the shear centre for the channel section.



Consider a section of thickness ‘dx’ on the flange at a distance ‘x’ from the end.

$$V_1 = \int \tau da$$

$$V_1 = \int \frac{VA\bar{y}}{It} da$$

where  $A = t x$

$$da = dx t$$

$$\bar{y} = d/2$$

$$\begin{aligned} V_1 &= \frac{V}{It} \int_0^b (tx)(dxt) \frac{d}{2} \\ &= \left[ \frac{V t^2 d x^2}{2} \right]_0^b \\ &= \frac{V t b^2 d}{4I} \end{aligned}$$

By symmetry,  $V_1 = V_2 = \frac{Vtb^2d}{4I}$

Neglecting the shear taken by the Web and taking moment about the point A on the Web,

$$Ve = V_1 \frac{d}{2} + V_2 \frac{d}{2}$$

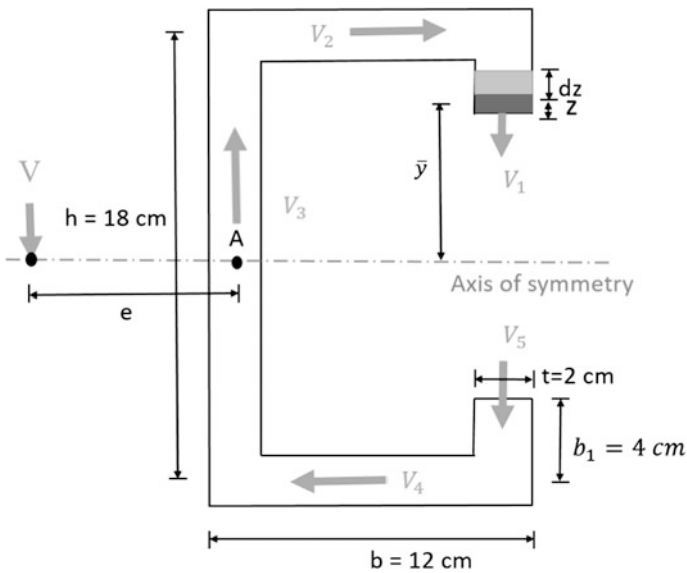
$$Ve = \frac{Vtb^2d}{4I} \times d$$

$$e = \frac{tb^2d^2}{2I}$$

Moment of Inertia,  $I = 3.031 \times 10^7 \text{ mm}^4$

$$e = 8.44 \text{ cm.}$$

4. Locate the shear center.



By symmetry,

$$V_1 = V_5$$

$$V_2 = V_4$$

(i) **To find  $V_1$ :**

Consider a strip of thickness ‘dz’ on the lip portion, at a distance ‘z’ from the end. The area of the strip is ‘da’.

$$V_1 = \int \tau da$$

$$V_1 = \int \frac{VA\bar{y}}{It} da$$

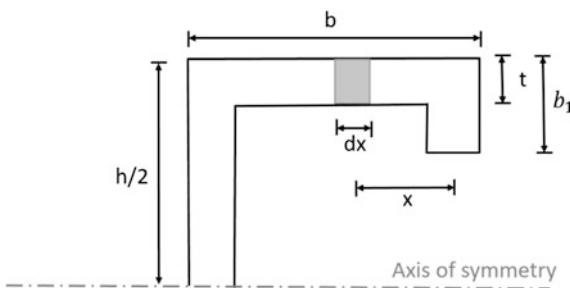
where  $A = t z$

$$da = dz t$$

$$\bar{y} = \frac{h}{2} - b_1 + \frac{z}{2}$$

$$\begin{aligned}
 V_1 &= \int_0^{b_1} \frac{V}{It} (tz)(t dz) \left( \frac{h}{2} - b_1 + \frac{z}{2} \right) \\
 &= \frac{Vt}{I} \left( \frac{h}{2} - b_1 + \frac{z}{2} \right) z dz \\
 &= \frac{Vt}{I} \left[ \frac{h}{2} \left( \frac{z^2}{2} \right) - b_1 \left( \frac{z^2}{2} \right) + \left( \frac{z^3}{6} \right) \right]_0^{b_1} \\
 &= \frac{Vt}{I} \left[ \frac{h}{2} \left( \frac{b_1^2}{2} \right) - \left( \frac{b_1^3}{2} \right) + \left( \frac{b_1^3}{6} \right) \right] \\
 &= \frac{Vt}{I} \left[ \frac{hb_1^2}{4} - \frac{b_1^3}{3} \right] \\
 &= \frac{Vtb_1^2}{I} \left( \frac{h}{4} - \frac{b_1}{3} \right)
 \end{aligned} \tag{1}$$

(ii) **To find  $V_2$ :**



Consider a strip of thickness 'dx' on the flange portion, at a distance 'x' from the lip portion. The area of the strip is 'da'.

$$\begin{aligned} a\bar{y} &= \left\{ (b_1 t) \left( \frac{h}{2} - b_1 + \frac{b_1}{2} \right) \right\} + \int xt \frac{h}{2} \\ &= \left( \frac{b_1 t h}{2} - b_1^2 t + \frac{b_1^2 t}{2} \right) + \int xt \frac{h}{2} \\ (V_2)^* &= \int \frac{VA\bar{y}}{I} da \end{aligned}$$

where  $A = t x$

$$da = dx t$$

$$\bar{y} = \frac{h}{2}$$

$$\begin{aligned} (V_2)^* &= \int_0^b \frac{V}{I} (tx) (t dx) \left( \frac{h}{2} \right) \\ &= \frac{Vth}{2I} \int_0^b x dx \\ &= \frac{Vth}{2I} \frac{b^2}{2} \\ &= \frac{Vthb^2}{4I} \end{aligned}$$

$$V_2 = \frac{Vt}{I} \left[ b_1 \left( \frac{bh}{2} \right) - \frac{b_1^2 b}{2} + \frac{b_1^2 h}{4} \right] \quad (2)$$

Taking moment about A,

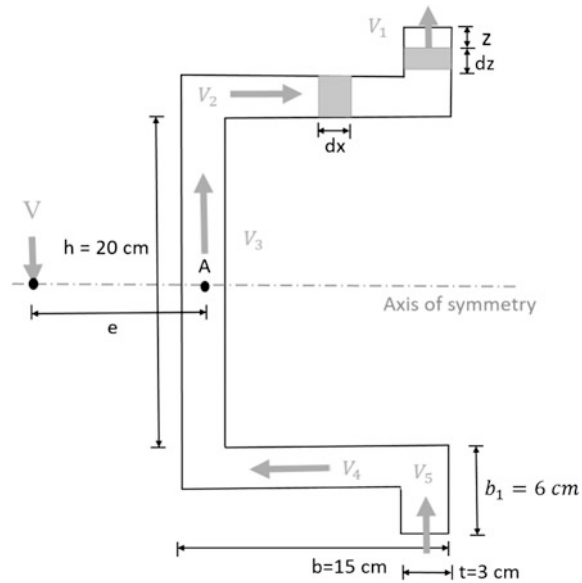
$$Ve = (V_1 + V_5)b + (V_2 + V_4) \frac{h}{2}$$

$$Ve = 2V_1 b + 2V_2 \frac{h}{2}$$

For the given section,  $I = 3.629 \times 10^8 \text{ mm}^4$

$$e = \frac{tb_1 h^2}{2I} b \left( 1 + \frac{b}{2b_1} - \frac{4}{3} \left( \frac{b_1^2}{b} \right) \right) = 3.09 \text{ mm.}$$

5. Locate the shear center for the load  $V = 10 \text{ kN}$ .



Consider a strip of thickness ‘dz’ at a distance ‘z’ from the end.

$$V_1 = \int \tau da$$

$$V_1 = \int \frac{VA\bar{y}}{It} da$$

where  $A = t z$

$$da = dz t$$

$$\bar{y} = \frac{h}{2} + b_1 - \frac{z}{2}$$

$$\begin{aligned}
 V_1 &= \int_0^{b_1} \frac{V}{It} (tz)(t dz) \left( \frac{h}{2} + b_1 - \frac{z}{2} \right) \\
 &= \frac{Vt}{I} \left[ \frac{h}{2} \left( \frac{b_1^2}{2} \right) + \left( \frac{b_1^3}{2} \right) - \left( \frac{b_1^3}{3} \right) \right] \\
 &= \frac{Vt}{I} \left[ \frac{hb_1^2}{4} + \frac{b_1^3}{3} \right] \\
 &= \frac{Vtb_1^2}{I} \left( \frac{h}{4} + \frac{b_1}{3} \right)
 \end{aligned}
 \tag{1}$$

Moment of inertia of the section is given by

$$I = \frac{th^3}{12} + \left[ \frac{tb_1^3}{12} + tb_1 \left( \frac{h}{2} + \frac{b_1}{2} \right)^2 \right] + \left( \frac{bt^3}{12} + \frac{bth^2}{4} \right) 2$$

For the section,  $I = 1.416 \times 10^8 \text{ mm}^4$ .

(ii) **To find  $V_2$ :**

Consider a strip of thickness 'dx' on the flange portion, at a distance 'x'.

$$a\bar{y} = (b_1t) \left( \frac{h}{2} + \frac{b_1}{2} \right) + tx \left( \frac{h}{2} \right)$$

$$da = t dx$$

$$\begin{aligned} V_2 &= \frac{V}{I} \int_0^b t \left( \frac{b_1h}{2} + \frac{b_1^2}{2} + \frac{xh}{2} \right) t dx \\ &= \frac{Vt}{I} \left( \frac{b_1hb}{2} + \frac{b_1^2b}{2} + \frac{hb^2}{4} \right) \end{aligned}$$

Taking moment about A,

$$(V_2 + V_4) \frac{h}{2} - (V_1 + V_5)b = Ve$$

The value of 'e' can be calculated from the above expression.

$$V_1 = V_5 = 0.0534 V$$

$$V_2 = V_4 = 0.438 V$$

Substituting the values in the above equation,

$$e = 71.69 \text{ mm.}$$

**Tutorial 8: Advanced structural analyses-IV**

**Time: 60 min**

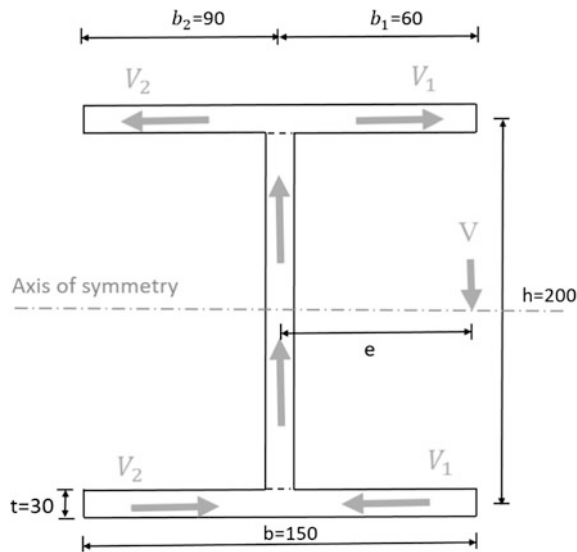
**Max marks: 20**

**Part A: Objective questions (5 marks)**

1. \_\_\_\_\_ theorem is used to derive deflection of curved beams with small initial curvature (Castigliano’s theorem)
2. \_\_\_\_\_ variations are nonlinear in curved beams with large initial curvature (stress)
3. Stresses in \_\_\_\_\_ are larger than that of extrados (intrados)
4. In curved beams with large initial curvature, stress distribution is nonlinear due to the fact that \_\_\_\_\_ shifts towards the centre of curvature (Neutral axis)
5. Winkler–Bach equation is useful to estimate stresses in curved beams with large initial curvature only at \_\_\_\_\_ (at the extreme skin layers).

**Part B: Descriptive questions (15 marks)**

1. What is the sign convention used in estimating stresses in curved beams with large initial curvature?
2. State simplified equations to estimate stresses in extreme fibers of curved beams with large initial curvature
3. Determine the location of the shear centre for an I section:  
 Flange: 150 × 30 mm  
 Web: 20 × 200 mm



Consider a section of thickness ‘dx’ on the flange at a distance ‘x’ from the end.

$$V_1 = \int \tau da$$

$$V_1 = \int \frac{VA\bar{y}}{It} da$$

where  $A = t x$

$$da = dx t$$

$$\bar{y} = h/2$$

$$\begin{aligned} V_1 &= \frac{V}{It} \int_0^{b_1} (tx)(dx t) \frac{h}{2} \\ &= \left[ \frac{V t^2 h x^2}{2} \right]_0^{b_1} \\ &= \frac{V t b_1^2 h}{4I} = 0.0546 V \end{aligned}$$

By symmetry,

$$V_2 = \frac{V t b_2^2 h}{4I} = 0.123 V$$

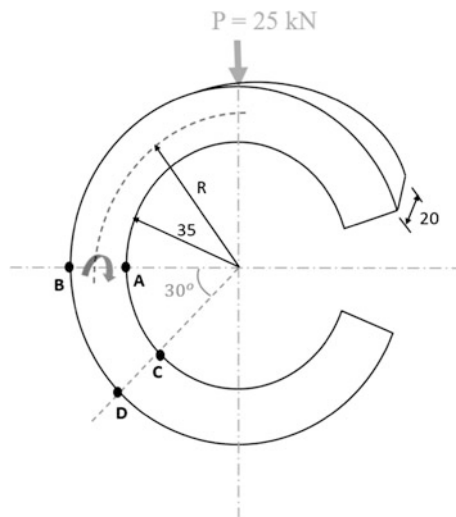
$$I = 9.886 \times 10^7 \text{ mm}^4$$

Taking moments about the center of the Web,

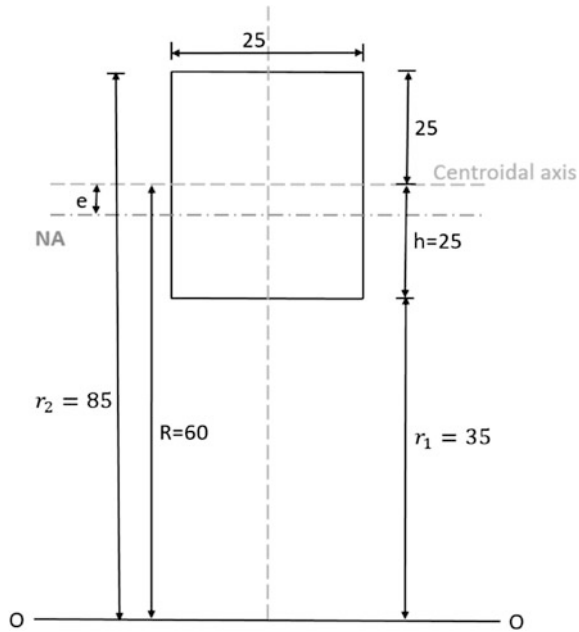
$$V e + V_1(h) - V_2(h) = 0$$

$$e = 13.66 \text{ mm}$$

4. Estimate the stresses at points A, B, C, and D.



**Given:**



Type of the section: rectangular section

Length of the section,  $l = 50$  mm

Breadth of the section,  $b = 25$  mm

Inner radius of the beam,  $r_1 = 35$  mm

Load acting on the beam,  $P = 25$  kN

Angle of  $CD$  from centroidal axis,  $\Theta = 30^\circ$

**Solution:****A. Winkler–Bach Equation****(i) Calculation of geometric properties:**

$$h = l/2 = 25 \text{ mm}$$

$$h_i = h_o = h = 25 \text{ mm}$$

1. Radius of the curved beam,  $R = r_1 + h = 60 \text{ mm}$
2. Outer radius of the curved beam,  $r_2 = r_1 + l = 85 \text{ mm}$
3. CS area of the section,  $A = l \times b = 1250 \text{ mm}^2$
4. Sectional property,  $m = 1 - \left(\frac{R}{A}\right) \cdot b \cdot \ln\left(\frac{r_2}{r_1}\right) = -0.0647$  (no unit)
5. Eccentricity,  $e = \left(\frac{m}{m-1}\right)R = 3.649 \text{ mm}$  (The positive value of 'e' indicates that the Neutral axis will shift toward the center of curvature)
6. Moment of inertia,  $I = 2.604 \times 10^5 \text{ mm}^4$

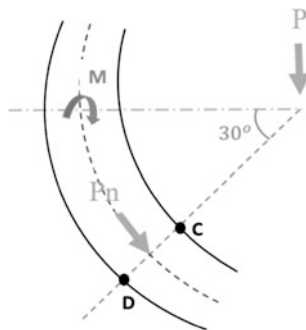
**(ii) Section AB:**

- (a) Direct stress,  $\sigma_d = -\frac{P}{A} = -20 \text{ N/mm}^2$
- (b) Moment at CG,  $M = P \times R = 1.5 \text{ kNm}$   
Moment about CG will cause tensile stresses in extrados and compressive stresses in intrados.
- (c) Stress at intrados,  $\sigma_i = -\frac{M}{Ae} \left(\frac{h_i - e}{r_i}\right) = -200.582 \text{ N/mm}^2$  (compressive)
- (d) Stress at extrados,  $\sigma_e = \frac{M}{Ae} \left(\frac{h_o - e}{r_o}\right) = 110.828 \text{ N/mm}^2$  (tensile)
- (e) Total stress at intrados,  $\sigma_A = \sigma_d + \sigma_i = -220.582 \text{ N/mm}^2$  (compressive)
- (f) Total stress at extrados,  $\sigma_B = \sigma_d + \sigma_o = 90.828 \text{ N/mm}^2$  (tensile)

**(iii) Section CD:**

Since the section CD is at an angle from the centroidal axis, the normal load at the section is given by

$$P_n = P \cos \theta = 21.651 \text{ kN.}$$



- (a) Direct stress,  $\sigma_d = -\frac{P_n}{A} = -17.321 \text{ N/mm}^2$
- (b) Moment at CG,  $M = M_x \cos \theta = 1.299 \text{ kNm}$
- (c) Stress at intrados,  $\sigma_i = -\frac{M}{Ae} \left( \frac{h_i - e}{r_i} \right) = -173.709 \text{ N/mm}^2$  (compressive)
- (d) Stress at extrados,  $\sigma_e = \frac{M}{Ae} \left( \frac{h_o - e}{r_o} \right) = 95.98 \text{ N/mm}^2$  (tensile)
- (e) Total stress at intrados,  $\sigma_A = \sigma_d + \sigma_i = -191.029 \text{ N/mm}^2$  (compressive)
- (f) Total stress at extrados,  $\sigma_B = \sigma_d + \sigma_o = 78.659 \text{ N/mm}^2$  (tensile)

**B. Wilson and Querean Equation:**

$$R/h = 2.4$$

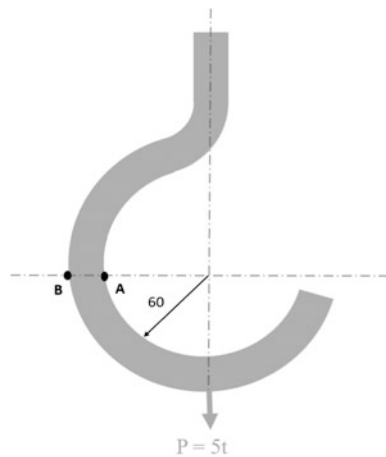
From the table,

$$k_i = 1.432.$$

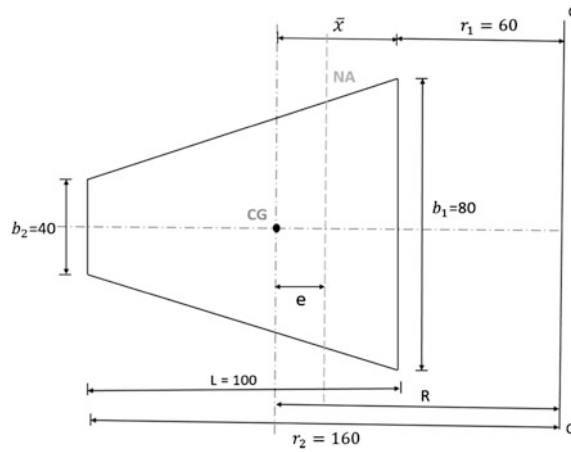
$$k_o = 0.762$$

- (a) Stress at intrados,  $\sigma_i = -k_i \frac{M}{Ae} h = -206.208 \text{ N/mm}^2$  (compressive)
- (b) Stress at extrados,  $\sigma_o = k_o \frac{M}{Ae} h = 109.728 \text{ N/mm}^2$  (tensile)
- (c) Total stress at intrados,  $\sigma_A = \sigma_d + \sigma_i = -226.208 \text{ N/mm}^2$  (compressive)
- (d) Total stress at extrados,  $\sigma_B = \sigma_d + \sigma_o = 89.728 \text{ N/mm}^2$  (tensile)

5. A 10-ton crane hook is used to lift an object during commissioning of an offshore deck. Find the stresses at the intrados and extrados.



**Given:**



Type of the section: trapezoidal section

Height of the section,  $l = 100$  mm

Breadth of the section,

$$b_1 = 80 \text{ mm}$$

$$b_2 = 40 \text{ mm}$$

Inner radius of the beam,  $r_1 = 60$  mm

Load acting on the beam,  $P = 50$  kN

**Solution:**

**A. Winkler–Bach Equation**

(i) **Calculation of geometric properties:**

$$b_3 = 20 \text{ mm}$$

$$\text{Location of the neutral axis, } \bar{x} = \frac{\sum A\bar{x}}{\sum A} = 44.44 \text{ mm}$$

$$h_i = x = 44.44 \text{ mm}$$

$$h_o = h - x = 55.56 \text{ mm}$$

1. Radius of the curved beam,  $R = r_1 + x = 104.44$  mm
2. Outer radius of the curved beam,  $r_2 = r_1 + h = 160$  mm
3. CS area of the section,  $A = 6000$  mm<sup>2</sup>

4. Sectional property,  $m = 1 - \left(\frac{R}{A}\right) \left\{ \left[ b_2 + \frac{r_2(b_1-b_2)}{(r_2-r_1)} \right] \cdot \ln\left(\frac{r_2^2}{r_1^2}\right) - (b_1 - b_2) \right\} = -0.0794$  (no unit)
5. Eccentricity,  $e = \left(\frac{m}{m-1}\right)R = 7.679$  mm (the positive value of 'e' indicates that the neutral axis will shift toward the center of curvature)
6. Moment of inertia,  $I = 4.814 \times 10^6$  mm<sup>4</sup>

(ii) **Section AB:**

$$r_i = r_1 = 60 \text{ mm}$$

$$r_o = r_2 = 100 \text{ mm}$$

- (a) Direct stress,  $\sigma_d = \frac{P}{A} = 8.333$  N/mm<sup>2</sup>
- (b) Moment at CG,  $M = -P \times R = -5.222$  kNm
- (c) Stress at intrados,  $\sigma_i = -\frac{M}{Ae} \left(\frac{h_i - e}{r_i}\right) = 69.442$  N/mm<sup>2</sup> (tensile)
- (d) Stress at extrados,  $\sigma_i = \frac{M}{Ae} \left(\frac{h_o - e}{r_o}\right) = -44.79$  N/mm<sup>2</sup> (compressive)
- (e) Total stress at intrados,  $\sigma_A = \sigma_d + \sigma_i = 77.775$  N/mm<sup>2</sup> (tensile)
- (f) Total stress at extrados,  $\sigma_B = \sigma_d + \sigma_o = -36.457$  N/mm<sup>2</sup> (compressive)

**B. Straight Beam Formula:**

$$\sigma = \frac{M}{I}y$$

$$y_i = 44.44 \text{ mm}$$

$$y_o = 55.56 \text{ mm}$$

- (a) Stress at intrados,  $\sigma_i = \frac{M}{I}y_i = 48.205$  N/mm<sup>2</sup> (tensile)
- (b) Stress at extrados,  $\sigma_o = \frac{M}{I}y_o = -60.256$  N/mm<sup>2</sup> (compressive)
- (c) Total stress at intrados,  $\sigma_A = \sigma_d + \sigma_i = 56.539$  N/mm<sup>2</sup> (tensile)
- (d) Total stress at extrados,  $\sigma_B = \sigma_d + \sigma_o = -51.923$  N/mm<sup>2</sup> (compressive).

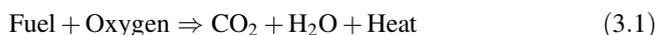
## Chapter 3

# Fire Safety in Offshore Structures

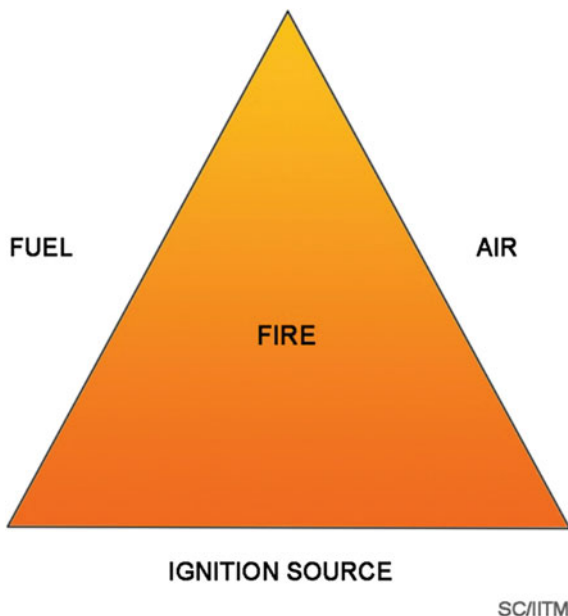
**Abstract** This chapter deals with fire safety in offshore structures. Process of fire, fire growth, and decay are discussed in detail. In addition, factors associated with fire-resistant design of structural members are dealt with reference to international codes. Examples are solved to illustrate the presented concept. Extracts of a few codal provisions are also given in this chapter for completeness of understanding.

### 3.1 Introduction

Fire is essentially a combustion phenomenon, which required three conditions to initiate: fuel, oxygen, and source of ignition. The chemistry behind a fire is represented in a generic form as given below:



As seen from Eq. (3.1), fire is an exothermic reaction, which produces heat in addition to carbon dioxide and water vapor. In case of incomplete combustion, carbon monoxide is also produced. Amount of heat produced by a particular fuel depends on its calorific value. Fuel can be in any of the forms, namely: solid, liquid, or vapor. Calorific value is defined as the total energy released when unit amount of a substance undergoes complete combustion. Amount of substance burnt is measured in moles or weight; latter is more commonly used in structural fire engineering community. While energy is measured in Joules, calorific value is measured in Joules/kg. Hydrocarbons have remarkably large calorific values compared to other combustibles. Dry and wet samples of the same material will have different apparent values of specific heat. On ignition, fire will release energy in the form of thermal radiation, which reaches its peak intensity with passage of time. Fire can also be an outcome of explosion. Offshore platforms are vulnerable to fire accidents as the exploration process itself is hazardous to a significant extent. Fire and explosion accidents can be prevented while by understanding the following, namely: (i) fire and explosion characteristics of hazardous materials; (ii) nature of fire; and (iii) explosion process. A typical fire triangle is shown in Fig. 3.1. Fire and

**Fig. 3.1** Fire triangle

explosions can be prevented by removing any one of the arms of the fire triangle. Fuel is typically organic materials derived from plants, animals, or petrochemicals. For offshore platforms, petrochemicals form the major portion of the fuel that can potentially initiate a fire. Oxygen is usually available from air.

Total energy released by a wet sample is lesser than that of the same overall weight of the dry sample. Let  $H_d$  be the calorific value of the dry sample. Net calorific value ( $H$ ) of the actual sample is given by (Eurocode 2002):

$$H = H_d(1 - 0.01u) - 0.025u \quad (3.2)$$

where  $u$  is moisture content, expressed as percentage of dry weight; ( $H$ ,  $H_d$ ) are calorific values ( $J/kg$ ). Net calorific value, which is also referred as lower calorific value of commonly encountered solid, liquid, and gaseous fuels, is well documented in several handbooks and building codes. A few of the relevant values are reproduced in Table 3.1.

Please note that for usual applications, net calorific value is used as it is not possible to ensure complete dryness of the combustible material. In particular, this is true in a marine environment due to the presence of high humidity. Once the relevant calorific values are known, total energy content of a potential fire can be computed as given below:

$$E = m \times H \quad (3.3)$$

where  $E$  is the total energy released and  $m$  is the mass of the combustible.

**Table 3.1** Calorific values of common combustibles

Fuel	MJ/kg	Fuel	MJ/kg
Gasoline	44	Diesel	41
Methanol	20	Paraffin oil	41
Butane	46	Methane	50
Acetylene	48	Carbon monoxide	10
Cellulose	17	Clothes	19
Cotton	18	Grease	41
Paper/cardboard	17	Rubber tire	32
Wood	19	Wool	23
ABS	36	Epoxy	34
Polyester	29	Polyethylene	44

**Example 1** A storage room has 10 kg of wood, 50 kg gasoline, and 60 kg diesel. What is the maximum amount of energy that can be released in the event of a fire in that room? Estimate the fire load.

**Solution:** Referring to the net calorific values of the material as given in Table 3.1, we get:

$$E = \sum_{i=1}^3 m_i H_i = 10 \times 19 + 50 \times 44 + 60 \times 41 = 435,420 \text{ MJ} \approx 435 \text{ GJ}.$$

Since  $E$  represents the maximum energy that can be released during a fire outbreak, it is also known as fire load.

## 3.2 Fire and Explosion Characteristics

Fire is a rapid exothermal oxidation of ignition fuel. Fuel can be solid, liquid, or gaseous state. Fire will release energy in the form of exothermal reaction. It takes some time for this release to reach its peak intensity. Fire can also occur due to explosion. Explosion is the rapid expansion of the gases resulting from the pressure waves or shock waves. These waves propagate very fast, and this rapidity results in the expansion. Explosion can be mechanical or chemical process. Explosion releases energy rapidly, and this causes fire. A few characteristics of flammable materials are discussed below. Figure 3.2 shows the flammability characteristics of combustible materials.

**Auto-ignition temperature (AIT)** It is the lowest temperature above which the material may not require any external source for combustion. Auto-ignition temperature is a fixed temperature above which material may not require any external source of ignition such as flame or spark for combustion. This temperature is required to supply energy that is needed for combustion. Ignition can even take

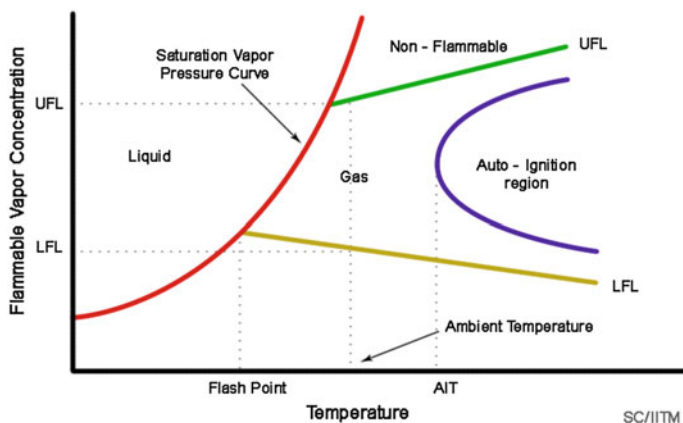


Fig. 3.2 Flammability characteristics of materials

Table 3.2 Auto-ignition temperature of selected materials

Material	Auto-ignition temperature (°C)
Gasoline	247–280
Diesel	210
Butane	405
Methane	580

place at normal atmospheric condition, when the temperature is reached. Auto-ignition temperature is also known as the *kindling point of the material*. Temperature at which a chemical ignites decreases as the pressure or oxygen concentration increases. AIT is referred as the minimum temperature required, supplying the activation energy that is needed for combustion; also referred to as self-ignition temperature. Table 3.2 gives auto-ignition temperature of selected material present in the atmosphere at 20.9% of oxygen.

**Flash point** It is the lowest temperature at which liquid gives up enough vapor to maintain continuous flame. It is the temperature at which the vapors are produced from the fluid, and they will result in ignition, if the source is present. Fluid will not burn at this temperature.

**Flammability limits** It is the range of vapor concentration that could cause combustion on meeting the ignition source. There are two flammability limits, namely: (i) lower flammability limit (LFL) and (ii) upper flammability limit (UFL). LFL is the limit below which mixture will not burn due to lean mixture. UFL is the limit above which the mixture will not catch fire as the mixture is too rich to catch fire. It is expressed in flammable limits. These are the range of vapor concentration that could cause combustion, when it is supported by the ignition source. Increase in UFL and decrease in LFL will result in the increase of flammable region. For the known values of flammable constants, flash point for liquids is given by the following relationship:

$$\mathbf{T}_f = \mathbf{a} + \frac{\mathbf{b} \left( \frac{\mathbf{c}}{\mathbf{T}_b} \right)^2 \mathbf{e}^{-\left( \frac{\mathbf{c}}{\mathbf{T}_b} \right)}}{\left[ 1 - \mathbf{e}^{-\left( \frac{\mathbf{c}}{\mathbf{T}_b} \right)} \right]^2} \quad (3.4)$$

where  $a$ ,  $b$ , and  $c$  are the flammable limits (Chandrasekaran 2016);  $\mathbf{T}_b$  is boiling point; and  $\mathbf{T}_f$  is flash point. Increase in the upper flammability limit, with the constant lower limit, is given by:

$$\text{UFL}_P = \text{UFL} + 20.6 \text{Log}(P + 1) \quad (3.5)$$

where  $P$  is the absolute pressure in MPa.

**Limiting Oxygen concentration (LOC)** It is the minimum oxygen concentration below which combustion is not possible, with any fuel mixture. It is expressed as volume percentage of oxygen. It is also called as minimum oxygen concentration (MOC) or maximum safe oxygen concentration (MSOC).

**Shock waves** These are abrupt pressure waves moving through a medium. A shock wave in open air is usually followed by wind, which is called as a blast wave. One of the most important characteristics of the shock waves is that they exhibit adiabatic characteristics under rapid increase in pressure.

**Over pressure** It is that pressure imparted on an object by shock waves.

**Fire point** It is the temperature at which fluid will sustain fire, if ignited by an external ignition source. Fire point is usually lower than the auto-ignition temperature for any hydrocarbon.

### 3.3 Best Practices in Fire Safety

Fire safety is ensured in offshore exploration and production process, not only by appropriate design but also through inherited practices of fire safety. Following points are vital to ensure fire safety in production processes:

- Fluid should be used above the flash point and fire point temperature but not above its auto-ignition temperature.
- Fluid can be used up to their maximum bulk temperature. It is important to note that bulk temperature is (much) higher than that of the flash point temperature of fluid.
- Avoid designing confined spaces with the presence of ignition source as this can result into a flash very easily.
- Through proper system design, one should ensure that there is no oxygen or air content available at the proximity of heat source. Common heat sources are namely: (i) electric heater; (ii) heat exchanger; and (iii) drilling controller.

- Fluid should be well contained within the system.
- Fluid containment should not have direct contact with the external ignition source.

### 3.3.1 Common Mistakes in Fire Accidents

Common mistakes that can lead to fire accidents are listed below:

- All heat transfer systems should be thoroughly inspected for no leak or smoke. Any negligence in their periodic inspection can result in fire accidents.
- In case of smoke, one should not disconnect the smoldering insulation. This is due to the fact that this will allow excess of air inside and result in auto-ignition.
- Do not let fluid drop on any heat sources as this will ignite the fluid instantaneously.
- If there is leakage of fluid in the flow line and it is trapped within a confined system, it may get oxidized and emit heat. Therefore, trapping of liquid should be cleaned immediately.

## 3.4 Fire Risk

The following categorization of fire risk commonly prevails in oil and gas industries:

**No fire risk:** This indicates a condition where energy source is absent in the platform (engineering) modules

**Low fire risk:** This indicates presence of modules that store/stock non-flammable equipments. Inventory, which are non-inflammable but stored in bulk also falls under this category

**Medium fire risk:** This category includes modules containing electric power, testing equipments, drilling modules etc. It also includes non-accommodation modules, which are present in the topside of the platform.

**High risk fire:** This includes modules where flammable liquid are stored. They also include the plant segments, which houses high power electrical machinery and accommodation modules.

Table 3.3 summarizes likely temperature of different types of fire.

**Table 3.3** Type of fire and temperature rise

Type of fire	Temperature (°C)
Oxyhydrogen fire	2800
Air-acetylene fire	2530
Blow under welding operation	2200
Candle burning	1000

### 3.5 Classification of Fire

Fire is triggered when leakage or spill of flammable mixture occurs in the presence of potential ignition source. Fire can be classified, namely: (i) pool fire; (ii) jet fire; (iii) fire ball; and (iv) flash fire. Subclassifications include flares, fire on sea surface, and running liquid fire. For analytical purposes, fire can be treated as follows:

- Flares can be idealized as jet fire in modeling.
- Fire on sea surface and running liquid fire can be modeled as pool fire.

#### 3.5.1 Pool Fire

It is a turbulent mode of diffusion fire, which burns above the pool of vaporizing hydrocarbon with a lesser momentum. Probability of occurrence of pool fire in offshore platform is very high due to continuous handling of hydrocarbons. Liquid fuel, which is released accidentally during the overfilling of storage tank, may also result in pool fire. It may also result from the rupture of pipelines and cracks in the pressure vessels and tanks because of corrosion of metal. Release of liquid fuel forms a pool on the surface, which subsequently vaporizes and causes pool fire by ignition. Pool diameter is equal to the diameter of the bund constructed to contain the spread of pool fire, and its lengths are given by the following relationships:

$$D_p = \sqrt{\frac{4A}{\pi}} \quad (3.6)$$

$$L = 42 D_p \left[ \frac{\text{Burning Rate}}{\rho_{\text{air}} \sqrt{9.81 D_p}} \right]^{0.61} \quad (3.7)$$

where  $A$  is the area of the bund ( $\text{m}^2$ ),  $D_p$  is diameter of pool (m), and  $\rho_{\text{air}}$  is density of air ( $\text{kg}/\text{m}^3$ ).

#### 3.5.2 Jet Fire

It is the turbulent mode of diffusion of flame resulting from the combustion of fuel, which is continuously released. Unlike pool fire, jet fire has a significant momentum to propagate in downwind side. It can cause damage to offshore installations that are located even far away from the potential source of fire. Jet fire results in release of gases in two phases of crude oil. Spread of jet fire may be either in the horizontal or in vertical direction. Out of the two, horizontal jet fire is more dangerous as it can

cause damage on downwind side extensively. This may result in consequences such as: (i) structural failure; (ii) storage failure; and (iii) failure of pipelines. Heat flux released during the jet fire depends upon the type of fuel being released and varies in the range of about 200–400 kW/m<sup>2</sup>. Primary source of jet fire in an offshore production/process platform is pressurized gas lines. In case leak occurs in the gas line, leak rate is given by the following relationship:

$$Q_o = C_D A P_o \sqrt{\frac{M V}{R T_o} \left(\frac{2}{r+1}\right)^{(r+1)(r-1)}} \quad \text{if } p_o > p_a \left(\frac{2}{r+1}\right)^{\left(\frac{r-1}{r}\right)} \quad (3.8)$$

where  $C_D$  is discharge coefficient,  $A$  is cross-sectional area (m<sup>2</sup>),  $P_o$  and  $P_a$  are pressure of gas under operational conditions and absolute pressure (Pascal), respectively,  $M$  is molecular weight of gas (gm/mol),  $V$  is rate of specific heat,  $R$  is universal gas constant (=8314 J/kg mol k), and  $T_o$  is temperature of gas under operating conditions (Kelvin). Flame length of jet fire is given by:

$$M = 11.14(Q_o)^{0.447} \quad (3.9)$$

where  $Q_o$  is the initial release rate (in kg/s). Corresponding time frame of the length of jet fire is estimated as below:

$$Q_t = Q_o e^{\left(\frac{Q_o}{M_G}\right)t} \quad (3.10)$$

$$M_G = \frac{P_o M}{0.08314} \pi r^2 L \quad (3.11)$$

where  $M_G$  is mass of gas (kg),  $r$  is radius of the pipeline (m),  $L$  is length of pipeline (m),  $t$  is time of release (s), and  $Q_t$  is gas release rate (kg/s).

### 3.5.3 Fire Ball

It is a rapid turbulent combustion of fuel, which is in the form of rising and expanding radiant ball of fire. When a fire ball attacks a vessel/tank containing pressure liquefied gas, pressure inside the vessel increases and leads to its catastrophic failure. This may lead to loss of complete inventory present in the tank. Under boiling liquid expanding vapor cloud explosion (BLEVE), released material is flammable and may ignite as well. This will result in explosion and thermal radiation hazards. Duration of heat pulse in BLEVE is about 10–20 s, while damage potential is relatively very high. Maximum emissive power that results from BLEVE are namely: (i) upwind/downwind direction is about 270–333 kW/m<sup>2</sup> and (ii) crosswind direction is about 278–413 kW/m<sup>2</sup>.

### 3.5.4 Flash Fire

It is a transient fire resulting from the ignition of gas or vapor cloud. It is a special process as there will be a delay between the release of flammable material and subsequent ignition. It initially forms a vapor cloud for a larger area, which also results in radial expansion. Cloud thus formed subsequently explodes because of ignition. Flash fire is more catastrophic and capable of causing damage to a larger area. Flash fire is characterized by a wall of flame. Similar to fire balls, flash fire can also ignite and remain as a continuous flame. Further, it can also be caused by a delayed ignition and remain for a longer time. Instantaneous effect causes thermal radiation, and the flash fire generates 'knock-on' events such as: pool fire, jet fire, and BLEVE. It is important to note that severity of flash fire is relatively higher.

### 3.5.5 Minimum Ignition Energy

Minimum ignition energy (MIE) is required to initiate combustion reaction of hydrocarbons. This depends on the factors namely: (i) combustion of the mixture; (ii) concentration (or richness) of the fuel mixture; (iii) temperature; and (iv) pressure. Table 3.4 shows minimum ignition energy of a few select chemicals; rest can be seen readily from a Chemical Engg Handbook.

## 3.6 Fire Protection in Offshore Platforms

Offshore platforms have several ignition sources that are responsible for the fire accidents. Based on the statistics carried out in the recent past, they are identified as: (i) electric sources, contributing about 23%; (ii) smoking, contributing about 18%; (iii) friction between metal surfaces, contributing about 10%; (iv) overheating of metal surfaces, contributing about 8%; (v) flames and sparks, contributing about 12%; and (vi) other sources. Offshore platforms are generally designed to be self-reliant even in case of fire. This is due to the following reasons namely:

**Table 3.4** Ignition energy of chemicals

Chemicals	MIE (mJ)
Acetylene	0.02
Benzene	0.225
Hydrogen	0.018
Methane	0.28
Propane	0.25

1. There will be no fire rescue facility available in the near vicinity of offshore platforms.
2. Fire accidents cause many significant consequences.

Many effective fire protection measures are in-built in offshore platforms to make them fire-resistant by virtue of its design. Common fire protection measures that exist are namely:

- Flame arrestors, which are passive devices, designed to prevent propagation of gas flames through pipelines.
- Fire-resistant barriers and fire walls.
- Insulation.
- Water shower.
- Foams.
- Water spray.

In case of efficient design of fire protection, it is important to identify possible source of fire; minimizing them shall improve fire protection, automatically. Sources of fire are inherently present in offshore platforms, which arise from the inflammable gases. However, preventing sparks is one of the highest priorities in fire-resistant design of offshore platforms. By design, fire protection can be provided by two methods namely: (i) fire detection system and (ii) fire extinguishing system. It is important to appreciate the fact that both the above methods are effective only when they are designed to remain automatic. High degree of reliability should be ensured through periodic service and effective maintenance of the systems.

Offshore platforms are generally aided with offshore platform support vessels (PSVs). They should be protected in case of fire. If there is a fire in PSV itself and not managed, it can result in serious consequences; probability of fire protection to the platform will be significantly reduced in such cases. Fire protection system design should be integrated with the geometric design of the platform. It is important to realize that fire protection is an integral part of the platform layout itself. All potential hotspots in the platform layout should be enveloped into the fire protection layout. Common types of fire protection systems, which are very effective in offshore platforms, are as follows:

**Foam systems** These systems are highly suitable for hydrocarbon fire. Foam systems contain air-filled bubbles, which are formed from aqueous solutions; their density is lower than the lightest flammable liquid. The types of foam systems commonly used are: (i) low expansion systems, which are highly suitable for storage tanks, helideck, and loading terminals and (ii) high expansion systems, which are highly suitable for LPG spills.

**High pressure water main** Potable water is used in these mains for fire protection. Seawater is highly corrosive and harmful to human on board, and hence potable water is sprayed at high pressure. These are highly suitable for Platform Support Vessels (PSV).

### ***3.6.1 Complications in the Fire-Resistant Design***

Design of the process and production system, in terms of its layout, is not complex but to guarantee fire resistance is highly complex. Most of the modules on the topside are located in a congested manner. This is required (or desired) to minimize the pipeline flow so that process time and other parameters like pressure, temperature can be controlled to the desired level. Unfortunately, such a congested layout of plants and equipments results in high proximity of spread of fire or blast waves from one unit to the adjacent. In case of outbreak of fire, congested layout of network of pipelines, electric mains, water mains, etc., makes the firefighting operation inefficient and inaccessible. Level of risk in such conditions is high due to the following reasons:

1. Facilities, equipment, and even the process design are unique and have to be protected.
2. Recreating the facility or retrofitting the damaged platform is very expensive and not worthy. Most of the fire accidents will result in high degree of catastrophe, both to human and equipments.

Offshore platforms operate in a remote and harsh environment, and they do not have any external support of firefighting on demand. Various complexities that arise from factors, namely: (i) congested layout of topside equipments; (ii) close network of pipelines, electric cables, water mains, etc.; (iii) remote and harsh environment; (iv) involvement of highly flammable mixture during drilling, production, and process; (v) limited availability of external support systems even in case of emergency; (vi) very high capital investment; and (vii) complex process of recommissioning a new setup confirms the fact that offshore platforms can never be designed to remain completely safe; but by intelligent design, one can improve the degree of inherent safety. They include (i) optimum design and layout of equipments; (ii) field configuration; (iii) operational feature; and (iv) fire resistance. Potential risks in offshore platforms arise from blowouts, riser and process leak, fire and explosion, vessel collision, helicopter accidents, dropped objects, structural failure due to environmental loads, and complete capsizing of the platform under worst combination of environmental loads.

It is evident that about 70% of the accidents occurred in offshore facilities are due to hydrocarbon explosion and fire whose consequences are very serious. Hence, major concern for the designers is to make the offshore platform fire-resistant. In case of LNG processing platforms, risk is even higher as their physical and chemical conditions are different from that of the liquid hydrocarbon. By ensuring high or satisfactory level of inherent safety, designers make the platform to be as low as reasonably practicable (ALARP). Risk is reduced to ALARP level, and it is not eliminated completely. Primary concerns in the fire analysis arise from two factors, namely: (i) impact caused by fire due to overpressure and explosion and (ii) effect of material characteristics at an elevated temperature.

### **3.6.2 Firefighting Equipments**

Few of the basic requirements of firefighting equipments are listed below:

- They should be simple in design and easy to operate so that the personnel on board can readily use them.
- They should be free from high-end techniques to operate.
- They should be maintained and repaired periodically to ensure their availability on demand.
- Fire drills should be conducted on regular intervals to train personnel on board. Training should incorporate use of various firefighting equipments apart from understanding their limitations to use under different types of fire.

However, there are a few factors as listed below, which make fire protection of offshore platforms very difficult.

- Congested layout of topside equipments allows very little free space for movement of firefighting equipments; it also causes cascading effect on equipments located at closer proximity in case of fire.
- They operate in a very confined and compact space.
- Offshore production equipments are generally not commissioned horizontally but vertically. This is due to the fact that vertical layout of drilling stack is compact and efficient in operations.
- There are serious space and weight limitations of the fire protection equipments to be provided on board.
- As seawater is highly corrosive, using it for fire protection may cause serious consequences to the topside equipments of the platform. Further, it can be harmful to human on board.
- Non-availability of potable water in large quantity for firefighting in offshore platforms is also one of the serious limitations.

## **3.7 Objectives of Fire Safety**

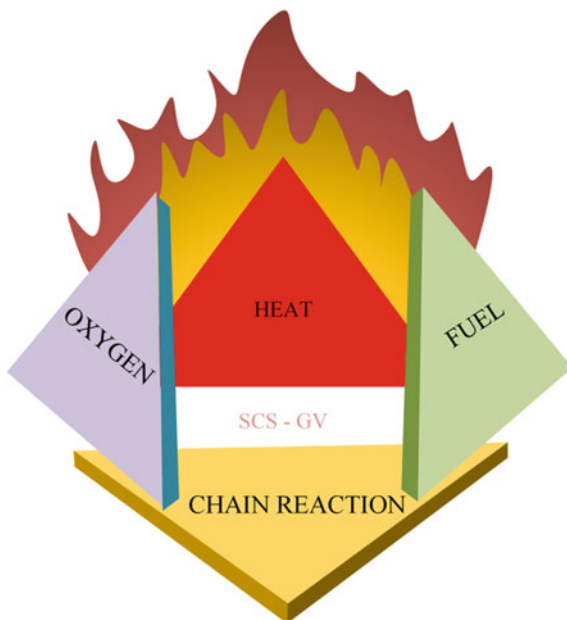
All structural systems carry a risk of being exposed to fire during their lifetime. For offshore platforms, the risk is even greater as they primarily involve handling of highly inflammable hydrocarbon materials. While probability of occurrence of fire can be considerably reduced by following good safety practices and periodic maintenance of equipment, it is difficult to rule out the possibility of fire altogether. Studies indicate that most of the major offshore fire accidents occurred in the 1980s (Technology Offshore 2016). Recent fire accidents include the 2005 fire in Mumbai High North (loss of 120,000 barrels of oil and 4.4 million cubic meters of gas per day), the 2007 Usumacinta Jack-up disaster (loss of 22 lives), the 2010 BP's Deepwater Horizon drilling rig explosion, and the 2012 Chevron Nigeria Limited

oil rig explosion (Attorney 2016). Inevitably, fire and explosions in offshore platforms result into spillage of crude or other harmful chemicals into sea or atmosphere and can pose significant environmental protection challenges. Thus, it is necessary to develop and adopt procedures and designs to minimize the losses in the event of a fire. Losses due to fire can be classified into three categories, namely: (i) loss of lives; (ii) loss of property; and (iii) degradation of environmental conditions. Use of engineering principles and understanding to prevent aforementioned losses can be termed fire safety engineering. This is an emerging multi-disciplinary field of engineering and research. It is well known that in case of a fire outbreak, smoke poses a much severe threat to life safety than that of heat and structural (Malhotra 1987; Hall 2011). Occupants usually have a few minutes after the onset of fire to escape before conditions become untenable for life. In case of fire arising from gas leaks, which are typical in offshore platforms, time available for escape can be of the order of seconds. Thus, it is essential to design effective means of egress and smoke/gas mitigation. Therefore, fire-resistant design should ensure smoke mitigation prior to control fire spread.

In the context of offshore platforms, protection should be extended to both the product (crude oil) and the asset (platform itself along with plants and equipments). Losses can easily run into multi-billion dollars in the case of fire accidents, as seen from the past accident records. Typically, protection of both is interlinked as much of the structural components of an offshore platform involve handling the product. By ensuring structural protection, one can expect to protect the product as a consequence. Steel and reinforced concrete are the main materials utilized for construction of offshore platform apart from composites, which are largely used under special cases. While concrete is a natural insulator, steel is a very good conductor. Both have their own weaknesses against fire that a designer must understand to ensure proper design. Past incidents and experiences show that connections are the most vulnerable components of a structural system and need special attention during a design process as fire-resistant member. Accidents on offshore platforms can have serious implications for the environment as well. First threat is due to long-term uncontrolled combustion of hydrocarbons that can discharge significant amount of toxic gaseous products into the environment. Second is due to spillage of crude oil on sea as a result of failure of pipelines and containment mechanisms, which can adversely affect the local ecosystem.

### **3.8 Fire Behavior and Development**

There are three elements that a fire needs to ignite: fuel (e.g., wood, hydrocarbons), oxidizing agent (oxygen for natural fire), and heat (a source of ignition). Whenever these three components are present in the right combination, a fire can occur. Removal of any one of these components leads to extinguishing of fire. After developing a better understanding of the chemical reactions occurring during a fire, it is found that a significant number of free radicals are formed during fire. They

**Fig. 3.3** Fire tetrahedron

facilitate in sustaining the ongoing exothermic reactions. Consequently, a fourth component ‘chain reaction’ is added to the existing aforementioned elements. These four elements are often represented in the form of a tetrahedron, called the fire tetrahedron, as shown in Fig. 3.3.

### 3.8.1 Fire Behavior

Behavior of fire can be well understood by plotting the fire temperature with time, typically called a time–temperature curve, as shown in Fig. 3.4. Phases are identified after ignition (a point where the right combination of fuel, oxidizer, and heat initiates a flame). First is the growth phase during which a small amount of combustibles burn or smolder. Temperature is not very high during this phase, and it is ideal if the fire can be extinguished during this phase. Rate of growth of fire during this phase is relatively modest. As the size of fire grows gradually, more and more hot gases accumulate near the upper portion of the closed containment. As shown in Fig. 3.5, this in turn heats the nearby combustible items through radiative heat transfer.

If the supply of oxygen is sufficient, due to this tremendous radiative heating, there exists a possibility when all items inside the confined space catch fire. This phase is known as ‘flashover’ and is marked by a steep rise in temperature in the time–temperature curve. After flashover, burning is fully established and

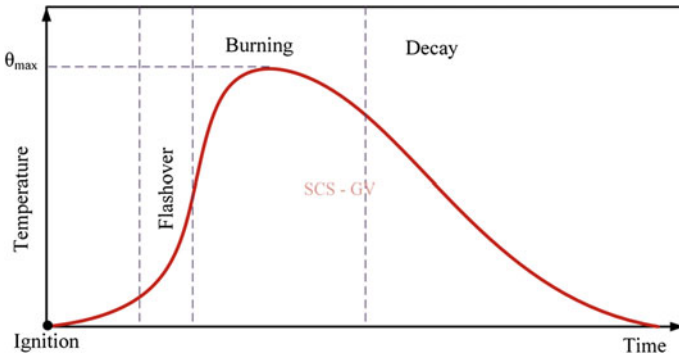


Fig. 3.4 Time–temperature curve of fire

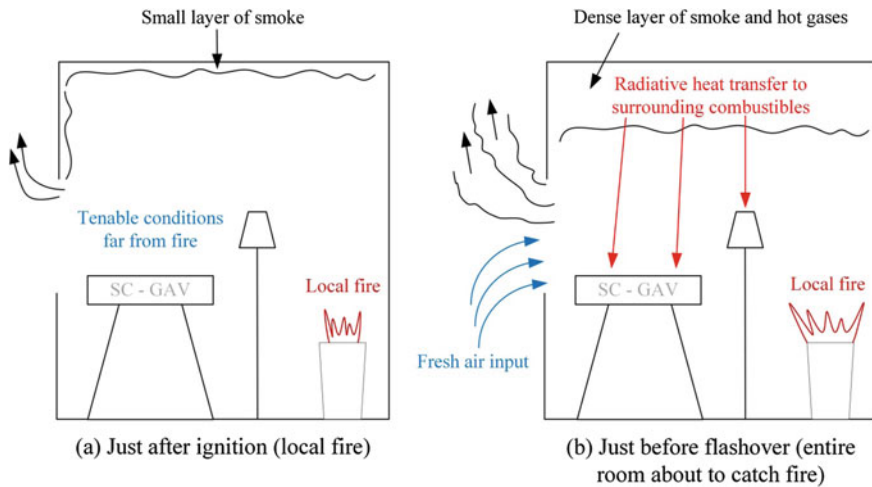


Fig. 3.5 Condition of confined space just after ignition and before flashover

temperatures rise very high; this rise can be as high as 600 °C. By flashover, conditions in the confined space become untenable for protecting loss of life due to excessive heat and high temperature. It is important to note that the extent to which the temperature rises depends on the availability of oxygen during the burning phase. If there is sufficient supply of oxygen, fire is termed as fuel-controlled; otherwise, called as ventilation-controlled. In either case, fire begins to decay after reaching a peak temperature as the total amount of fuel is limited. Behavior of fire will be much different in case of a closed space, which is filled with (leaked) gas. Entire room can potentially explode at the onset of an ignition source. Such explosions impart dynamic loads in the form of shocks to the surroundings and can be much more devastating than usual fire.

### 3.9 Egress and Human Behavior

Human behavior in the event of a fire is a key variable that has potential to significantly affect outcomes of any fire event. When managed properly, even severe fire events may result in modest losses. Early detection and availability of redundant mitigation measures are two factors that are crucial for minimizing impact of fire. While several automated products can be deployed to facilitate early fire detection, human intervention is a quintessential parameter. Training and mindset of the topside personnel of offshore platform play a vital role. It is therefore important to train offshore personnel on firefighting methods and use of equipments. Untrained and unaware occupants can easily panic in the event of a fire, leading to potentially large impact. On the other hand, if the occupants are well trained, have undergone necessary fire drills, and are aware about the safety of their surroundings, impact of fire can be minimized. Similarly, it is important for a designer to include sufficient redundancies in design to ensure easy and identifiable egress paths. Factors such as size of pathways, space between plants and equipments in the layout, locations of fire doors are very important apart from design of structural components.

### 3.10 Fire Resistance

Fire resistance is the ability of a system or a part of it to sustain fire. Topside and other parts of an offshore platform comprise of load-bearing, non-load-bearing, and partitioning components. While functional requirements of load-bearing components are to withstand service loads during a fire, partitioning components are to prevent the spread of fire to adjoining spaces. Typically, fire resistance is specified as fire ratings in three domains, namely: (i) load; (ii) insulation; and (iii) integrity. For a load-bearing member, time until which it can resist the stipulated load under standard fire is called its fire rating; this is based on its load criterion. Insulation and integrity criteria are primarily applicable for partitioning components, such as walls. Insulation criterion requires a member to prevent the rise of temperature on its unexposed side. For instance, if the maximum temperature rise on the unexposed side of a partition wall subjected to a standard fire reaches 180 °C, insulation criterion is considered to be failed and the elapsed time is termed as fire rating in insulation. Integrity refers to the ability of a partition to prevent leakage of hot gases and/or direct flames from one compartment to another.

### 3.11 Detection and Fire Control

Detection of fire is the first step toward controlling fire. Detection can be either by deploying manual techniques (for example, alarm can be raised by one of the personnel) or by deploying electronic sensors (for example, smoke detectors). Since

electronic systems enable automatic detection, they are generally preferred as they are found to be effective even in case of unmanned situations. If fire breaks out in one part of the platform, it is desirable that all occupants who can be potentially affected due to the fire are alerted as early as possible. Automatic detection systems, if centrally controlled, can offer such a mechanism. Fire sensors can be classified into three categories based on the mechanism through which they sense fire, namely heat, smoke, or radiant energy. Smoke-based sensors are preferred as they can give a very early indication of a potential fire. Heat sensors depend on sufficient build-up of hot gas near the vicinity, while radiant energy sensors work only when the fire is within their line of sight. For applications in the oil industry, it is common to use arrays of radiant energy sensors that can cover a wide area and work in a synchronous manner. Such arrays also minimizing false alarms tend to be more robust.

### ***3.11.1 Active Control of Fire***

Mechanisms that require thermal, electrical, or manual triggering to control a fire are called active systems. These include typical sprinkler systems, which are activated by heat or an electrical feedback from a smoke alarm system. Alternatively, manually operated fire extinguishers are also useful in firefighting operations. Key idea is the need of activation. Presence of active control systems can significantly reduce the risk of fire spread and damage. National Fire Protection Association (NFPA) states that in case of fire, the risk of dying is cut by about one-third when smoke alarms are present (or about half if the smoke alarms are working), while automatic fire sprinkler systems cut the risk of dying by about 80%. In a system equipped with sprinklers, average property loss per fire is cut by about 70%. Primary application of active systems is to extinguish a fire as early as possible or to maintain tenable conditions for as long as possible to enable timely egress of the occupants. Controlling the spread of fire to adjoining physical spaces is a consequence of restricting the size of fire.

### ***3.11.2 Passive Control of Fire***

Passive controlling systems are the ones that are always present, ready to offer their service whenever the need arises. These typically include the usual structural and/or architectural partitions (primarily walls of different types). Such protective mechanisms enable arresting the spread of smoke, hot gases, and open flames of a fire due to their inherent properties. The primary action of passive systems is to control the spread of fire to adjoining physical spaces and to limit the size of the fire by restricting the supply of fresh air. If the passive systems do not lose integrity for a sufficiently long time, they may lead to extinguishing of the fire due to lack of oxygen and/or complete burning of the fuel. Such partitions are typically

constructed using naturally fire-resistant materials such as concrete, masonry, gypsum boards, cement boards.

### 3.11.3 Compartmentation

Topside of offshore platform is complex by virtue of layout of various plants and equipments. They include heavy-duty equipments like drilling derricks, which cannot be accessed during outbreak of fire as they are usually circumscribed by congested layout of pipelines as well. Any closed space is formed by several enclosures, which are typically designed in accordance with the functional requirements. Such enclosures are typically partitioned using load-bearing or non-load-bearing walls that physically isolate one enclosure from another, thus forming compartments. If fire starts in one such compartment, it is desirable that it does not spread to the neighboring compartments. Such a design consideration is termed compartmentation in fire protection engineering. Physical requirements of the compartment walls depend on its fire potential. If a compartment is designed to store highly inflammable material, partition walls should be designed to sustain longer in case a fire occurs. Compartment walls are typically rated in terms of the time they can sustain a 'standard fire.'

## 3.12 Fire Load

Fire load, while an important parameter, cannot give a complete sense of the severity of fire as it does not account for the time factor. Consider two fire cases, fueled by the same energy content, but one burns itself out in 10 min while the other takes 30 min to burn completely. Of course, the first fire will be more severe and will create greater concerns in terms of structural safety. To include information about time, power or heat release rate (HRR) of fire is defined as follows:

$$Q = E/t \quad (3.12)$$

where  $t$  represents time. As expected, HRR ( $Q$ ) will have the SI units of J/s or W.

**Example 2** A storage room 50 kg of cellulosic material. A fire accident happened in the room during which the fire lasted for about 45 min. What was the average heat release rate during this fire?

$$E = mH = 50 \times 17 = 850 \text{ MJ}$$

$$Q = \frac{E}{t} = \frac{850 \text{ MJ}}{2700 \text{ s}} = 314.8 \text{ kW}$$

**Example 3** If a fire happened in the storage room mentioned in Example 1 and lasted for 30 min, what will be the average heat release rate?

$$Q = \frac{E}{t} = \frac{450 \text{ GJ}}{1800 \text{ s}} = 250 \text{ MW}$$

Another factor that becomes important, especially for room fire, is the spatial distribution of the combustible items. Consider again, two fire of same energy content but one taking place in a room with smaller floor area in comparison to the other that takes place in a room with larger floor area. In the former case, fire will be more severe as more energy is being released in a smaller area. To include this information, fire load energy density (FLED) is defined as:

$$e = E/A \quad (3.13)$$

where  $A$  represents area (some applications consider the floor area  $A_f$  while some consider the total surface area of the enclosure  $A_t$ ). FLED will be expressed in SI units as  $\text{J/m}^2$ . A measure of the energy being transmitted through a surface per unit time is called as heat flux. This is defined as the rate of heat energy transferred through a given surface per unit area and is given by the following relationship:

$$q = Q/A \quad (3.14)$$

### 3.13 Combustion of Materials

While any combustion process follows a chemical reaction given by Eq. (3.1), solids, liquids, and gases follow slightly a different physical process when they burn. Gases, when mixed with air, can burn readily. Specific arrangements such as the Bunsen burner produce a mixture of gas and air in a predefined proportion before combustion. When this mixture burns, resulting flame is called a premixed flame. Appropriate proportioning of the mixture is necessary to ensure complete combustion. Both excess and dearth of oxygen can inhibit combustion. Liquids and solids, on the other hand, do not burn directly. First, their transition into a gaseous phase takes place; subsequently, gas phase mixes with the available oxygen and then burns. Liquid and their respective vapor phases are known to coexist in liquid–vapor equilibrium, which is characterized by the physical process of evaporation. Solids usually melt into a liquid phase first before it gets converted into a gaseous phase, which then burns. There exists an intermediate phase at the burning surface of a solid, which is a combination of liquid and gaseous phases. This process is called pyrolysis.

### 3.14 Initiation of Fire

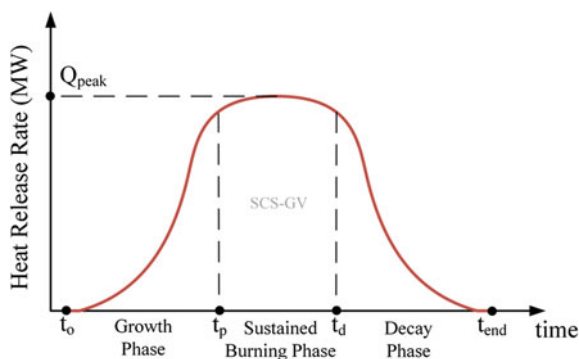
Typically, a source of ignition (consider, for example, heat from an external source) is required to start fire. There can be a variety of ignition sources such as open flames (lit matches, candles), smoldering sources (cigarettes), electrical sources (short circuit, overheating), radiant sources (sunlight, distant fire, heaters), and mechanical actions (friction). Fire can be ignited due to natural phenomena or by human action. An example of natural ignition is a forest fire, which is initiated due to high winds in a dry forest area where fire can initiate due to friction. Examples of fire initiated by human action include intentional ignitions such as burning of garbage, explosive detonation. Unintentional ignitions include a campfire, which is left unattended and likely to initiate a forest fire.

### 3.15 Open Fire

Fire that has sufficient availability of oxygen is termed as open fire. Most commonly, fire outbreak in offshore platforms initiates as open fire. They are marked by a growth phase, sustained burning phase, and decay phase. These phases can be characterized using the HRR of fire, as shown in Fig. 3.6.

As seen from the figure, ignition takes place at time  $t_0$  and the fuel begins to burn. Heat release rate increases rapidly with time until the fuel reaches a steady burning state at time  $t_p$  at which the peak ( $Q_p$ ) is registered. Peak is attained when the maximum possible surface area of the fuel is in contact with oxygen. The steady and sustained burning phase continues until this optimal fuel–oxygen interaction is not affected by the diminishing fuel quantity until time  $t_d$  at which the decay phase begins. Nature of the decay phase is usually similar to that of the growth phase. Finally, when all the fuel is consumed, fire stops and heat release rate becomes zero at time,  $t_{end}$ . A schematic of this combustion process is illustrated in Fig. 3.7. Area of the HRR versus time curve gives the total energy released during fire outbreak.

**Fig. 3.6** Heat release rate signature of fire



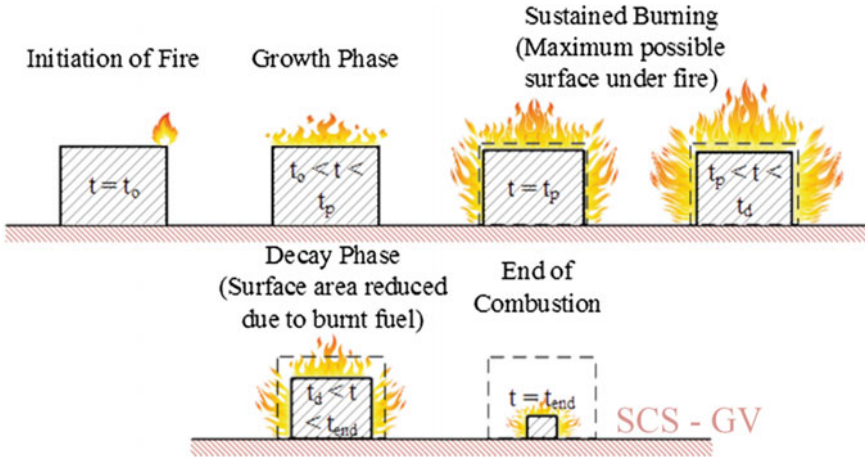


Fig. 3.7 Phases of combustion process during fire outbreak

### 3.16 *t*-Squared Fire Model

For use in design applications, heat release rate behavior of any fuel can be characterized by *t*-squared model. The heat release rate, in different phases, namely: growth, steady, and decay, are modeled as given below:

$$Q = \begin{cases} \alpha_g t^2; t = t - t_0; t_0 \leq t \leq t_p \\ Q_p; t_p \leq t \leq t_d \\ \alpha_d t^2; t = t_{end} - t; t_d \leq t \leq t_{end} \end{cases} \quad (3.15)$$

where  $\alpha_g$  and  $\alpha_d$  are fire growth and decay coefficients ( $W/s^2$ ) that are determined empirically.  $\alpha_g$  is determined using the time at which the fire reaches heat release rate of 1 MW. Time at which 1 MW heat release rate reached is given by the following relationship:

$$\alpha_g = \frac{1000}{(t_{1MW} - t_0)^2} \quad (3.16a)$$

$$\alpha_d = \frac{Q_p}{(t_{end} - t_d)^2} \quad (3.16b)$$

Maximum heat release rate is also related to other parameters. Detailed calculation methods can be found in the literature (Kim and Lilley 2000). Based on the growth rate, fire is classified as slow, medium, fast, and ultra-fast. Typical characteristics of the growth phase of fire are given in Table 3.5 and also shown in Fig. 3.8. Values of  $t_{1MW}$  and  $Q_p$  are determined experimentally (Babrauskas and Grayson 1992).

**Table 3.5** Classification of fire growth

Fire growth	$\alpha_g$ (kW/s <sup>2</sup> )	$t_{1\text{ MW}}$ (s)
Slow	0.00293	600
Medium	0.0117	300
Fast	0.0466	150
Ultra-fast	0.1874	75

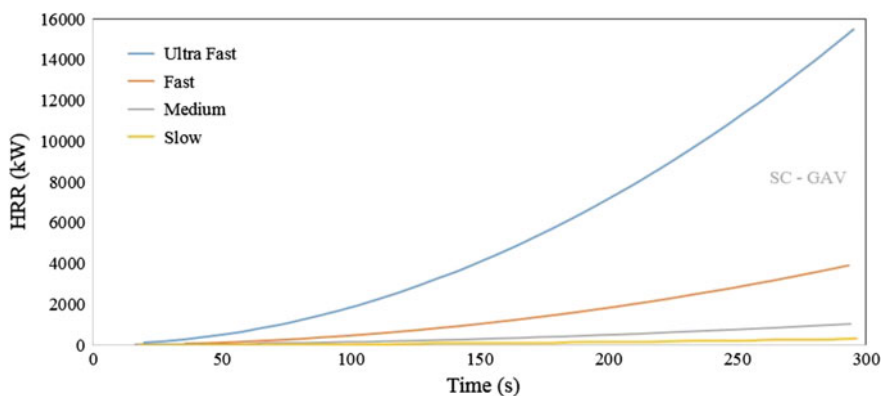


**Fig. 3.8** Fire with different growth rates

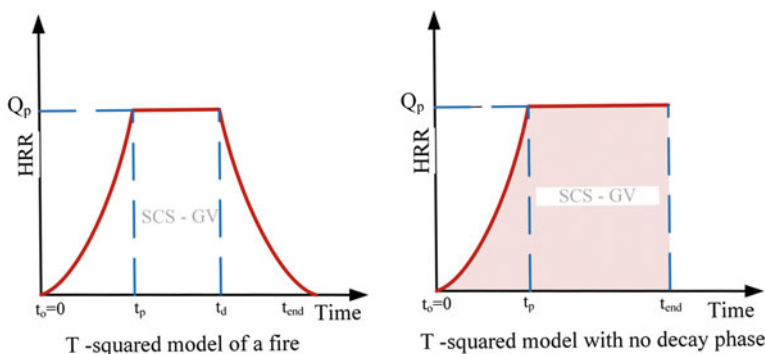


**Fig. 3.9** *t*-squared fire models

Using the *t*-squared model, characteristics of a fire are modeled as shown in Fig. 3.9. For structural engineering applications, it is typically assumed that the fire does not have a decay phase, i.e., the fire ends at its peak HRR. While this assumption may be conservative, it is not realistic. This idealization is also seen in the figure. It is important to note that total energy release (which is the area under HRR-time curve) will be same for both the cases. Typically, the *t*-squared model is used for predicting pre-flashover fire behavior for which assumption of absence of decay phase is reasonable.

Now onwards, it will be assumed that the onset of fire happens at  $t_0 = 0$  for ease of notation and calculations. Further, calculations will be carried out with respect to the *t*-squared model of fire without decay phase as it is more common from structural engineering perspective. From Fig. 3.9, energy released during the growth phase can be computed as the area under the parabola and is given by the following relationship:

$$E_1 = \frac{Q_p t_p}{3} \quad (3.17)$$

In order to use the above equation for computing the energy release, one needs to estimate the variables ( $t_p$  and  $Q_p$ ), respectively. Following steps are useful:

- First step An appropriate value of fire growth coefficient ( $\alpha_g$ ) is chosen based on the possible growth characterization of fire.
- Second step Value of  $Q_p$  is to be specified based on the available experimental data.
- Third step Variable ( $t_p$ ) can be computed as  $t_p = \sqrt{(Q_p/\alpha_g)}$ . If the fuel is known to have a total energy content  $E > E_1$ , remainder of the energy will be released in the steady burning phase and hence,  $E_2 = E - E_1$ . With this information, time of burning  $t_b$  of fire can be estimated (Pl, see Fig. 3.10). If  $E < E_1$ , i.e., the total available energy of the fuel is insufficient to reach its peak HRR, and time of burning will be given by the following relationship:

$$t_b = \sqrt[3]{\frac{3E}{\alpha_g}} \quad (3.18)$$

If  $E > E_1$ , energy release during growth phase can first be computed and the total time of burning can be computed as below:

$$t_b = t_p + \frac{E - E_1}{Q_p} \quad (3.19)$$

**Example 4** An office room has approximately 200 kg of furniture with an average calorific value of 17 MJ/kg. If a ‘medium’  $t^2$  fire takes place with a peak HRR of 9 MW, estimate the total time of burning.

**Solution:** Total energy content of the fuel,  $E = mH = 200 \times 17 = 3400$  MJ

Growth factor for medium fire,  $\alpha_g = 0.0117$  (from Table 3.5)

Time taken to reach peak HRR,  $t_p = \sqrt{Q_p/\alpha_g} = \sqrt{\frac{9000}{0.0117}} = 877$  s

Total energy released in growth phase,  $E_1 = \frac{Q_p t_p}{3} = \frac{9 \times 877}{3} = 2631$  MJ  $< E = 3400$  MJ

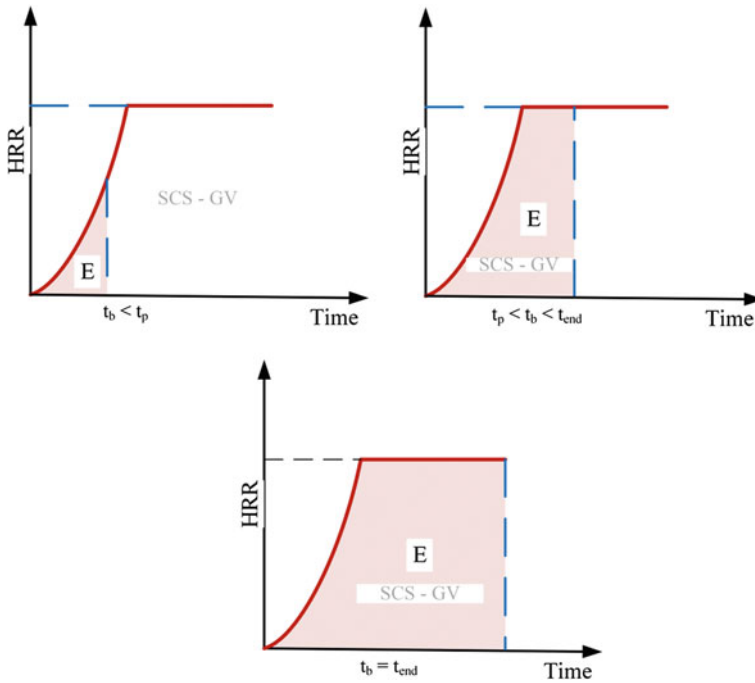


Fig. 3.10 Calculations with  $t$ -squared fire model

Thus, the fire will go to the steady-burning phase and total time of burn will be given by

$$t_b = t_p + \frac{E - E_1}{Q_p} = 877 + \frac{3400 - 2631}{9} = 877 + 85.4 = 962.4 \text{ s} \approx 16 \text{ min}$$

**Example 5** Due to a spill, approximately 100 kg of gasoline was discharged to an area of approximately 10 m<sup>2</sup>. It was decided to remove it by burning. Gasoline usually burns as an ‘ultra-fast’  $t^2$  fire and has a peak HRR of 1500 kW/m<sup>2</sup>. How much time will it take to completely burn the spilled gasoline?

**Solution:**

Total energy contents of the fuel,  $E = mH = 100 \times 44 = 4400 \text{ MJ}$ .

Growth factor for ultra-fast fire,  $\alpha_g = 0.1874$  (from Table 3.5)

Time taken to reach peak HRR,  $t_p = \sqrt{Q_p/\alpha_g} = \sqrt{\frac{44 \times 10^5}{0.1874}} = 4845.5 \text{ s} \approx 80 \text{ min}$

Peak HRR,  $Q_p = 1.5 \times 10 = 15 \text{ MW}$

Total energy released in growth phase,  $E_1 = \frac{Q_p t_p}{3} = \frac{15 \times 4845.5}{3} = 24227.5 \text{ MJ} > E = 4400 \text{ MJ}$

Thus, the fire will not reach the peak HRR and steady-burning phase.

Total time of burn will be given by:

$$t_b = t_b = \sqrt[3]{\frac{3E}{\alpha_g}} = \sqrt[3]{\frac{3 \times 4400}{0.1874}} = 41.3 \text{ s}$$

### 3.17 Compartment Fire

Any enclosure that creates physical boundaries to air circulation forms a compartment. Fire within the compartment (or enclosed space) is known as compartment fire. It is obvious to note that behavior of compartment fire will be influenced by the boundaries of the compartment. Qualitative behavior of fire can be diagnosed in four stages, namely: incipient, pre-flashover, flashover, and post-flashover. In the incipient stage, sustained burning of a single object will take place. Fire may decay if the object is too small or if it does not spread to an adjoining object. This may occur either due to low intensity of fire or greater distance of adjoining object from the burning object. Typically, fire decay, if happens in incipient stage, shall be due to the fuel being completely utilized. It is important to note that supply of oxygen is not an issue at this stage. Exception will be compartments where the oxygen concentration is maintained around 15% by mechanical means to inhibit fire growth. Fire will remain as fuel-controlled at this stage. In the pre-flashover stage, fire spreads to the adjoining objects but still not governed by availability of oxygen. In this stage, HRR can be modeled as a *t*-squared fire. Simple computer models are also available to assess temperature and layer thickness of the accumulated hot gases. Zone models such as ASET, FIRE SIMULATOR, CFAST, and FASTLite are commonly used tools to assess fire behavior in this stage. In this stage, fire still remains as spatially localized. Size of the compartment plays an important role in deciding the amount of hot gases being accumulated. During the flashover stage, a localized transition occurs and fire is transformed into a full compartment fire within a very small period of time. This occurs primarily due to radiative feedback from the hot gases that are accumulated in the compartment. Time to flashover is typically the available time for safe egress as well as the limit up to which interventions by untrained personnel can extinguish fire. The term ‘flashover’ is not relevant for open fire. This phase is usually marked a rapid increase in both time and temperature within the compartment, and the observed HRR is likely to be higher. In the last stage, namely post-flashover stage, flashover marks sustained burning of the entire contents of a compartment. Size of post-flashover is governed by either the availability of fuel or oxygen concentration. If the geometry and openings of the compartment enable sufficient oxygen supply, fire is fuel-controlled; or else, fire is ventilation-controlled. In the growth and sustained burning phase, fire is typically ventilation-controlled. In the decay phase, fire is certainly fuel-controlled.

### 3.17.1 *Pre-flashover*

Heat released and peak temperature in the pre-flashover stage of fire are typically smaller enough to be ignored for structural engineering considerations. But behavior of fire in this stage is of prime importance from life safety and egress points of view. Questions such as optimal placement of fire and smoke detectors for early fire detection, location and size of egress mechanisms require understanding of the smoke spread behavior during the pre-flashover stage. Ideally, one would like to perform a full computational fluid dynamics (CFD) analysis of the compartment. However, simpler models such as Zone model are preferred sometimes due to their computational efficiency over the very intensive CFD models. Open source software such as CFAST is available from NIST, which is capable of modeling smoke behavior during the pre-flashover stage of fire. FDS is open source software available from NIST, which is capable of carrying out full CFD analysis of compartments to yield more realistic fire scenarios.

### 3.17.2 *Flashover*

Flashover takes place if all of the following conditions are fulfilled during a compartment fire, namely: (i) sufficient availability of fuel; (ii) sufficient availability of oxygen; (iii) ability of the compartment to trap hot gases (e.g., compartments with significant openings in the ceiling may not be able to hold necessary amount of hot gases); and (iv) ability of geometry of compartment to enable radiative heat flux from hot gases to reach other combustible items. For a living compartment on topside with a single window opening, one can use Thomas's flashover criterion (Walton and Thomas 1995) to estimate the critical value of heat released (in MW), which is required for flashover. This is given by the following relationship:

$$Q_{\text{flashover}} = 0.0078 A_t + 0.378 A_v (H_v)^{0.5} \quad (3.20)$$

where  $A_t$  is the total surface area of the room ( $\text{m}^2$ ),  $A_v$  is the area of the window opening ( $\text{m}^2$ ), and  $H_v$  is the height of the window opening (m). Equation (3.20) is an empirical relation and is therefore approximate. It excludes the dependence of flashover on factors such as fuel type, fuel distribution, wall linings. If a  $t$ -squared model is used in the pre-flashover regime, Thomas criterion can be used to estimate the time to flashover. Further discussions on pre-flashover models and calculations can be found in Drysdale (1999).

**Example 6** Let us revisit Example 4. Calculations showed that the fire went to a steady burning phase and the total time of burning was approximately 16 min.

Those calculations did not consider compartment restrictions. Let the fire take place in a room shown below and other characteristics are same as in Example 4.

**Solution:**

Compartment information:  $L = 4\text{ m}$ ,  $B = 3\text{ m}$ ,  $H = 3\text{ m}$ .

Window information:  $L_v = 1.5\text{ m}$ ,  $H_v = 0.8\text{ m}$ .

Area of window,  $A_v = L_v H_v = 1.2\text{ m}^2$ .

Total surface area,  $A_t = 2(LB + LH + BH) = 66\text{ m}^2$ .

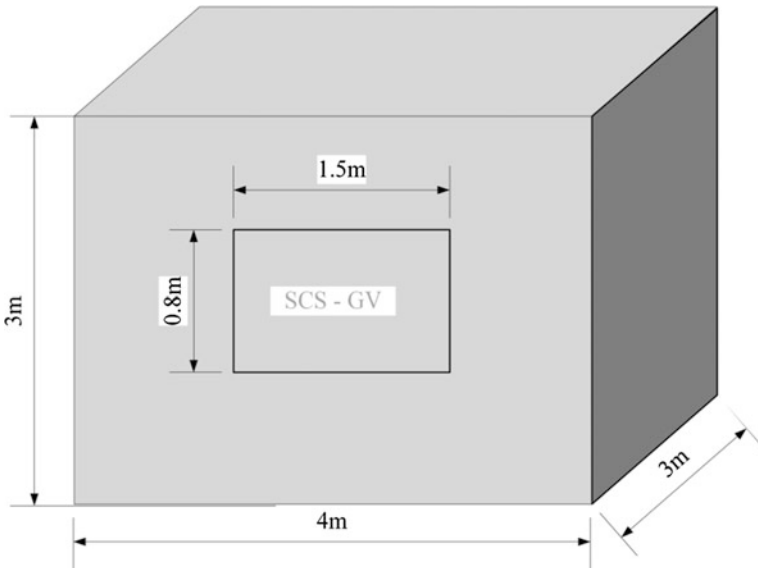
$$Q_{\text{flashover}} = 0.0078 A_t + 0.378 A_v \sqrt{H_v} = 0.0078 \times 66 + 0.378 \times 1.2 \times \sqrt{0.8} = 0.92\text{ MW}.$$

Since the peak HRR is  $9\text{ MW} > Q_{\text{flashover}}$ , the room will actually reach flashover according to this criterion.

Next, time to flashover can be computed in a manner similar to how time to peak HRR was computed in Example 4. It is reasonable to assume that flashover will take place much before the fire can reach its peak HRR (if burning in the open).

$$\text{Time to flashover, } t_{\text{flashover}} = \sqrt{Q_{\text{flashover}} / \alpha_g} = \sqrt{\frac{0.92 \times 10^3}{0.0117}} = 280\text{ s}.$$

It can be noted that the time to flashover is lesser than the time to reach peak HRR, as expected.



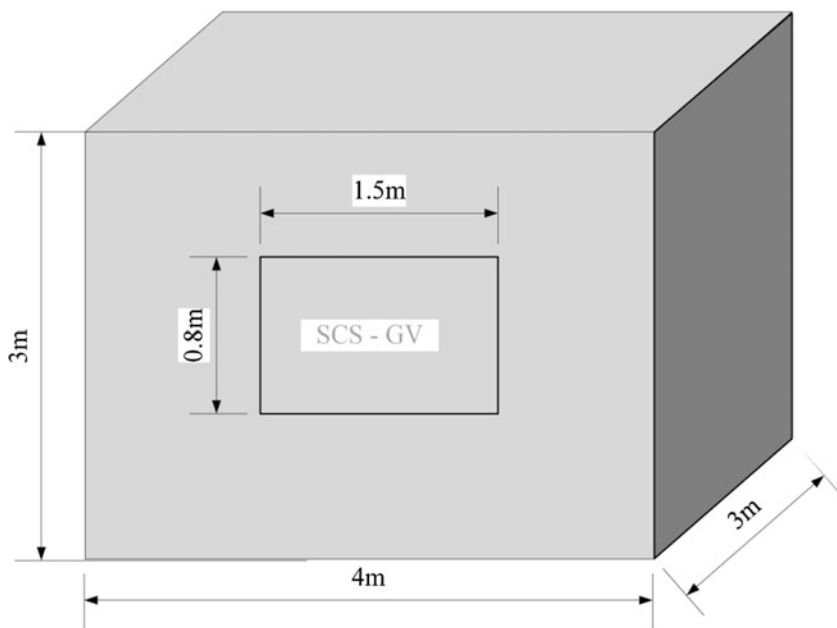
### 3.17.3 Post-flashover

After flashover, the compartment will have fully developed fire and experience very high temperature and heat flux. This is the stage, which tests the structural design of the compartment. As discussed earlier, in the post-flashover stage, fire can be either ventilation-controlled or fuel-controlled; this depends on the characteristics of the compartment. Several empirical models are developed to estimate the HRR during this phase. Primary relation being used is again proposed for a single room with one opening by Kawagoe (1958). These relations are estimated based on wood burning and are under doubt for their usefulness in general scenarios. However, due to lack of research, Kawagoe's equation still forms the basis of many post-flashover computations. Kawagoe noted that the mass burning rate of wood is directly proportional to  $A_v\sqrt{H_v}$ , i.e.,

$$\dot{m} = KA_v\sqrt{H_v} \quad (3.21)$$

where proportionality constant  $K$  is typically 0.092 for wood.

**Example 7** Let us revisit Example 6 which showed that the room with 200 kg of wood will reach flashover in about 280 s with. Determine the post-flashover HRR and duration of burning for ventilation-controlled scenario.



Mass burning rate of wood,  $\dot{m} = 0.092 A_v \sqrt{H_v} = 0.092 \times 1.2 \times \sqrt{0.8} = 0.10 \text{ kg/s}$ .

Heat of combustion of wood is 17 MJ/kg (Example 4).

Hence,  $Q = \dot{m}H = 0.1 \times 17 = 1.7 \text{ MW}$ .

Duration of burning can be computed from the total fuel estimate (note that relations related to  $t$ -squared model cannot be used in post-flashover regime).

Total energy contents of the fuel,  $E = mH = 200 \times 17 = 3400 \text{ MJ}$ .

Hence, duration of burning,  $t_b = \frac{E}{Q} = \frac{3400 \text{ MJ}}{1.7 \text{ MW}} = 2000 \text{ s} \approx 33 \text{ min}$ .

It can be observed that in an open environment, 200 kg of wood would have burnt in 16 min, while in a room, being ventilation-controlled, it will burn for about half an hour (twice as long). Further, it should be noted that in case the fire is fuel-controlled, estimates of Example 4 can be employed.

**Example 8** Again consider scenario of Example 7 but now let the room have one door and three windows with dimensions as below. Let geometry of the room remain the same. Estimate the peak HRR and duration of burning.

Entity	$L_v$ (m)	$H_v$ (m)
Door	1.5	2.0
Window 1	1.5	0.8
Window 2	1.0	1.0
Window 3	1.0	1.1

Area of openings now becomes

$$A_v = L_{v,\text{door}}H_{v,\text{door}} + L_{v,W1}H_{v,W1} + L_{v,W2}H_{v,W2} + L_{v,W3}H_{v,W3} = 6.3 \text{ m}^2$$

Since heights of all the openings are different, an area-weighted average can be used

$$H_v = \frac{A_{v,\text{door}}H_{v,\text{door}} + A_{v,W1}H_{v,W1} + A_{v,W2}H_{v,W2} + A_{v,W3}H_{v,W3}}{A_v} = 1.46 \text{ m}$$

Now, mass burning rate of wood,  $\dot{m} = 0.092 A_v \sqrt{H_v} = 0.092 \times 6.3 \times \sqrt{1.46} = 0.70 \text{ kg/s}$ .

Heat of combustion of wood is 17 MJ/kg (Example 4).

Hence,  $Q = \dot{m}H = 0.7 \times 17 = 11.9 \text{ MW}$ .

Total energy contents of the fuel,  $E = mH = 200 \times 17 = 3400 \text{ MJ}$ .

Hence, duration of burning,  $t_b = \frac{E}{Q} = \frac{3400 \text{ MJ}}{11.9 \text{ MW}} = 286 \text{ s}$ .

As expected, the fire burns much faster and the intensity is much larger. Note that the HRR predicted here is more than 9 MW, which is the maximum HRR for wood based on experiments where sufficient supply of oxygen is available. Thus, this room has sufficient openings to enable a fuel-controlled fire to take place and

calculations from Example 4 will be more relevant. Additionally, it is now difficult to say whether flashover will happen or not primarily because Thomson's formula assumes a room with one opening.

### 3.18 Fire Resistance

As seen previously, structural systems can be exposed to different types of fire during their service life. Concerns about their performance begin to arise in the post-flashover regime of fire where temperature can become as high as 1200 °C. In order to prevent collapse during a fire event, various components of a structure need to function in a certain (desired) manner so as to resist the effects of fire. A quantitative measure of such resistance is termed as fire resistance. This measure is typically given in terms of the maximum time for which a structural member can sustain in a given fire. Two questions arise naturally in these discussions, namely:

- (i) What is meant by a member 'sustaining' fire?
- (ii) Which type of fire is to be considered for assessing fire resistance?

First question will have different answers depending on the functionality of structural members. For instance, load carrying capacity of a beam before fire breakout is not affected even after fire. IN that case, it is termed as service load during fire. Similarly, a partition wall not allowing hot gases to pass from the fire compartment to the surroundings can be another definition. As such, fire resistance is specified in three domains, namely: (i) strength or stability ( $R$ ); (ii) integrity ( $E$ ); and (iii) insulation ( $I$ ). Strength or stability criterion refers to the ability of a structural member (such as beam, column, load-bearing wall, slab) to withstand the service loads during fire. It is applicable to any load-bearing member. Integrity and insulation are prescribed for partitioning components of a building such as walls and doors. Capability of a partitioning element to restrict the rise of temperature on its unexposed side is termed as insulation, while the ability to prevent hot gases to reach the unexposed side through cracks/fissures is called integrity. Fire resistance is typically measured as the time up to which a structural member satisfies the  $R$ ,  $E$ , or  $I$  criteria, as applicable, in fire; this time is termed the fire rating of the member.

The second question requires a greater discussion. In order to ensure uniformity across fire ratings prescribed in different countries, applications and codes, one needs to have a common fire exposure. As discussed earlier, real fire can be highly uncertain and vary greatly in terms of their maximum temperature, duration of burning and length of growth, sustained burning, and decay phases. To remedy this, all fire ratings are usually prescribed with respect to *standard fire*. A typical standard fire curve is shown in Fig. 3.11. Standard curve differs from that of a real fire curve in two aspects: First, the phase from ignition to the onset of flashover is

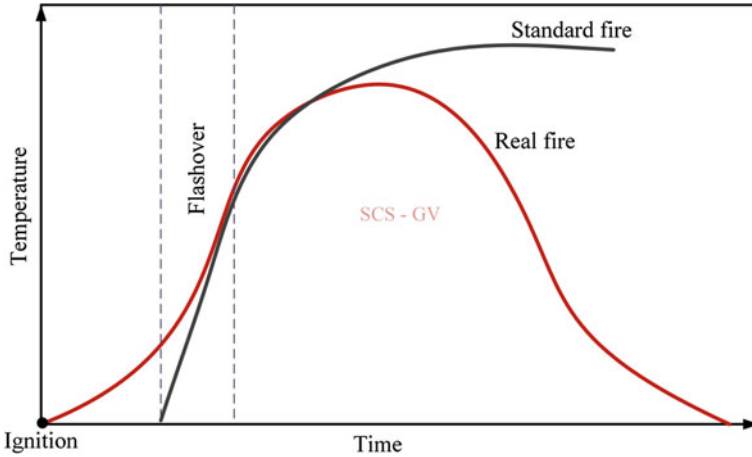


Fig. 3.11 Standard fire curve

not considered, and second, there is no decay phase in the standard curve. Both these characteristics are contingent on the fact that standard fire curve is to be used to assess ratings of structural members in fire. As discussed earlier, fire temperature, before the onset of flashover, is not sufficient to cause any threat to the structural system. It is because of this reason, it is not considered in the standard curve. Increasing nature of the standard curve (lack of decay phase) is motivated by the fact that greater fire ratings of structural members should imply their ability to fulfill relevant functional requirements for a longer duration at greater temperatures.

Various building codes adopt different versions of standard fire curve; but qualitatively, all of them are of similar in nature. In fact, most of them have a similar quantitative nature as well. Two of the most widely used standard fire curves are ISO 834 (ISO 1975) and the ASTM E119 (ASTM 1988) curves. For design of fire that originates from hydrocarbon pool fire, which is a typical case in offshore platforms, Eurocode (2002) defines a more severe version of the standard fire, called the hydrocarbon curve. Mathematical expressions for the time–temperature relationship for all of these curves are given below while their behavior is shown graphically in Fig. 3.12.

According to ISO 834 (ISO 1975) and IS 3809 (BIS 1979), standard fire is given by the following relationship:

$$T = 345 \log_{10}(8t_m + 1.0) + T_0 \tag{3.22}$$

where  $T$  is temperature of fire ( $^{\circ}\text{C}$ ),  $t_m$  is time (minutes), and  $T_0$  is ambient temperature ( $^{\circ}\text{C}$ ).

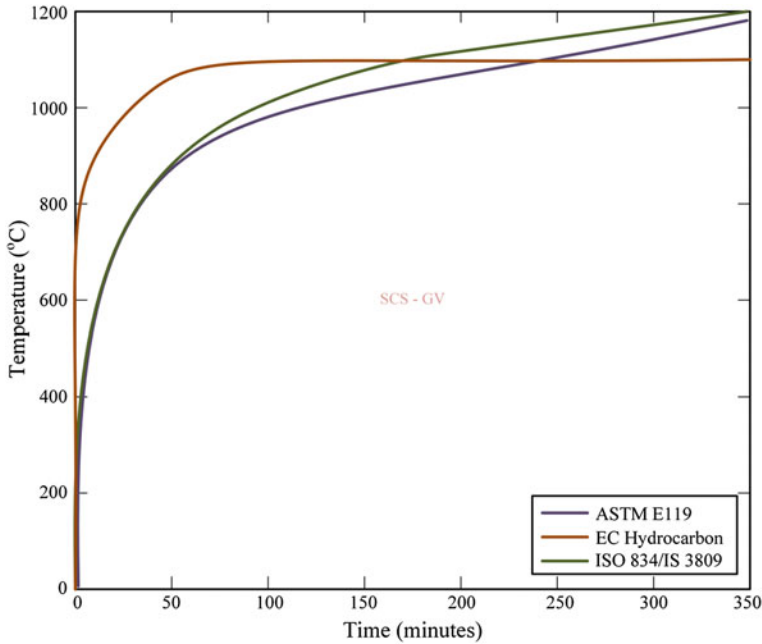


**Fig. 3.12** Standard fire curves

According to ASTM E119 (ASTM 1988), standard fire is given by:

$$T = 750[1 - \exp(-3.79553\sqrt{t_h})] + 170.41\sqrt{t_h} + T_0 \quad (3.23)$$

where  $t_h$  is time (hours).

According to Euro code (EN 1992, 2008), hydrocarbon standard fire is given by:

$$T = 1080(1 - 0.325 e^{-0.167t_m} - 0.675 e^{-2.5t_m}) + T_0 \quad (3.24)$$

where  $t_m$  is time (minutes).

### 3.19 Equivalent Fire Severity

Standard fire curves ensure uniformity in the fire-exposure perspective with respect to the prescription of structural fire ratings. However, applicability of fire ratings derived from a standard fire exposure needs to be addressed in the context of real fire scenario. This requires a notion of ‘equivalence’ between the standard fire and a potential (perhaps most severe) real fire scenario of a structure.

### 3.19.1 Area Equivalence

As the name suggests, time of exposure in a standard fire is considered equivalent to that of a real fire if the area under the time–temperature curves for both cases is the same. Figure 3.13 illustrates this concept. If  $A_r$  is the total area of the temperature–time curve of a real fire from ignition until the total time of burn  $t_b$ , equivalent exposure time  $t_e$  in a standard fire is defined as the time up to which the area under the standard fire curve  $A_s$  is same as that of the real fire. This equivalence concept is the oldest but does not have a sound theoretical basis behind it because the units of area under temperature–time curve (Kelvin second) do not have any physical meaning.

### 3.19.2 Maximum Temperature Equivalence

Maximum temperature concept considers the temperature within a protected structural steel member when exposed to a real fire in comparison to that of a standard fire. As shown in Fig. 3.14, if a protected steel member is exposed to real fire, curve attains maximum temperature at time  $t_{mr}$ . Equivalent exposure time  $t_e$  of a standard fire curve is defined as the time of standard exposure after which the same steel member attains the same temperature as it did at  $t_{mr}$  under exposure to real fire. Given that several simplified design procedures consider a critical temperature of steel as a failure criterion, this equivalence has better grounding from the point of view of its application to design.

### 3.19.3 Minimum Load Capacity Equivalence

Minimum load capacity concept has a similar grounding as that of the maximum temperature concept. Instead of considering the maximum temperature, this concept considers minimum load capacity of a structural member when exposed to fire. It is

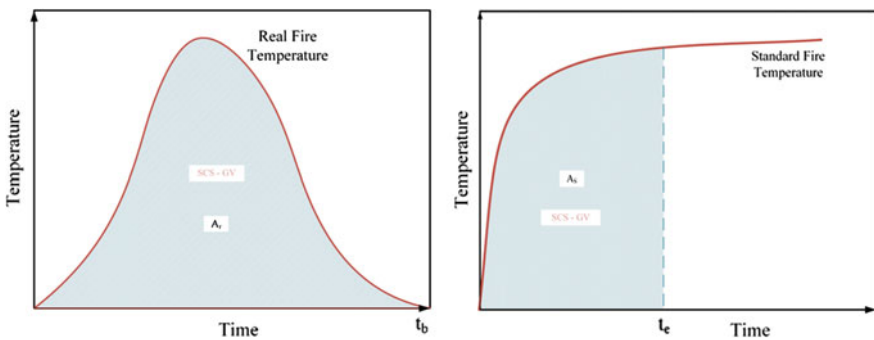


Fig. 3.13 Equivalent fire severity through area equivalence

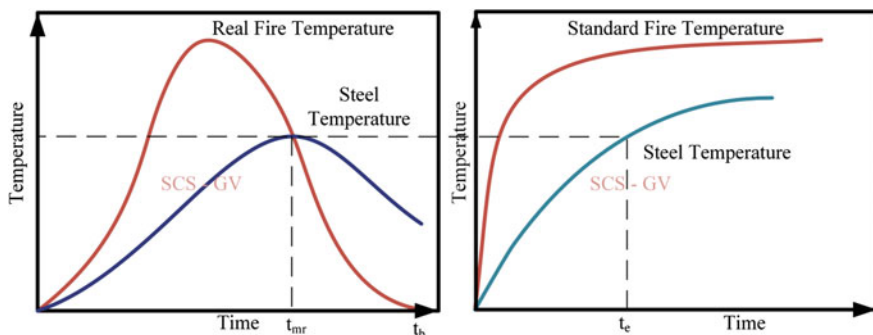


Fig. 3.14 Equivalent fire severity through maximum temperature

well known that strength of structural members degrades with the rise in temperature. This is primarily due to reduction in material properties such as yield strength and elastic modulus. Equivalent time of exposure of a standard fire  $t_e$  is defined as the time at which the structural member attains its least capacity during full real fire exposure, as shown in Fig. 3.15. This definition of exposure equivalence is the most robust as it is applicable to all structural systems.

### 3.20 Fire Resistance Tests

Fire resistance of structural and partitioning members is typically characterized through furnaces that expose the members to standard fire under certain predefined conditions. Several testing standards prescribe conditions under which such tests are to be carried out. Most common ones are ASTM E119 (ASTM 1998) and ISO 834 (ISO 1975). Testing parameters are also specified by IS 3809 (BIS 1979). Typical parameters given by such codes include furnace parameters, instrumentation details, size, specifications of test specimens, and mechanisms to assess the test results to generate fire-resistance ratings in the R, E, and I domains.

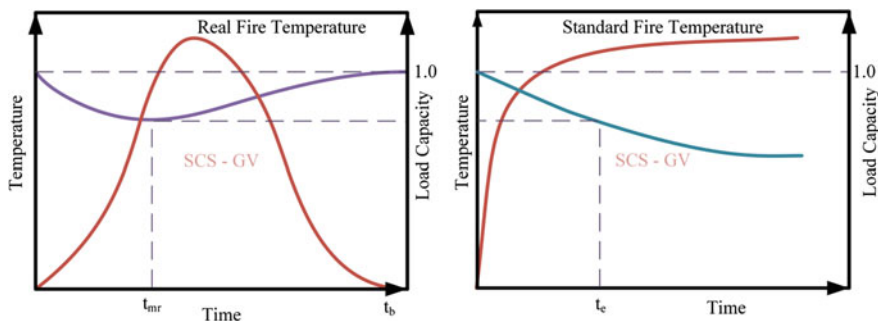


Fig. 3.15 Equivalent fire severity through minimum load capacity

### **3.20.1 Furnace Parameters**

Furnace temperature should follow the standard fire curve as closely as possible. Specifically, tolerances of a variation of  $\pm 15\%$ ,  $\pm 10\%$ , and  $\pm 5\%$  are allowed in the first 10 min, 30 min, and after 30 min of beginning of the test, respectively. An overpressure of  $10 \pm 5$  Pa shall exist in the furnace during the test. At least five thermocouples shall be used to monitor the furnace temperature. Appropriate instrumentation is required to assess temperature inside the test specimens, mechanical load application, and measurement of deflection of test specimens.

### **3.20.2 Test Specimens**

Specimens should be tested in full size as far as practical. However, when full size cannot be accommodated, it is ensured that minimum dimensions, as prescribed, should be deployed. Test specimens of walls and partitions should have minimum dimensions of width 3 m and height of 3 m. Floors and roofs, supported on two sides, should be spanned at least by 4 m and width of specimen shall be about 2 m. For floor and roof supported on all four sides, width of specimen shall be at least 3 m. Beams shall have test specimen size of 4 m span and that of columns of 3 m in height. Load-bearing specimens should be subjected to the expected service load during fire conditions at least 30 min prior to being tested. Columns are to be subjected to four-sided exposure while beams to three-sided exposure. Separating elements such as walls/slabs shall be subjected to full or one-sided exposure depending on the application.

### **3.20.3 Fire-Resistance Ratings**

Strength (R) is defined as the time at which a load-bearing element ceases to support the design load. This is also known as strength-based fire-resistance rating.

Integrity (E) is the time at which a significant crack/fissure develops in the test specimen that allows passage of hot gases through. It is termed as the integrity-based fire-resistance rating. To quantify whether the 'size' of a crack is significant or not, IS 3809 specifies assessment based on a 100-mm-square 20-mm-thick cotton pad. If such a pad, when held between 20 and 30 mm of any opening for 10–30 s, shows sustained flaming, such an opening is considered large enough to cause failure of integrity.

Insulation (I) is the temperature of an insulating element on the unexposed side which forms the basis of this criterion. As such, time at which one of the following happens is termed the insulation-based fire rating:

- Average temperature of unexposed side rises by more than 140 °C.
- Maximum temperature at any point of unexposed side rises by more than 180 °C.
- Maximum temperature of any point of unexposed side exceeds 220 °C.

Building codes of almost all countries give fire ratings of important structural elements in tabulated forms (BIS 1989). It is important to note that such ratings are usually prescribed for materials like reinforced concrete and masonry and are in terms of the overall width and cover thickness of members. Table 3.6 shows the fire resistance ratings for concrete columns and Table 3.7 shows for beams.

It should be noted that IS 1642 does not explicitly mention critical parameters such as reinforcement ratio and load levels at which the fire ratings are specified. Given that these ratings will have reference to the IS 3809 testing standard, it can be assumed that the ratings are applicable to members subjected to full design loads. This, however, may be misleading as a member is seldom subjected to full design load during a fire incident. Specifically, the live loads in a fire situation are usually lesser than those stipulated for ambient conditions. Eurocode considers these scenarios by specifying fire ratings with effect to the reinforcement ratio and various encountered load levels. Please refer to Table 5.2a, b of EC 1992-1-2 for more details.

**Table 3.6** Fire resistance ratings for reinforced concrete columns (BIS 1989)

Exposure condition		Minimum dimensions (mm), excluding any finish, for a fire resistance rating					
		½ h	1 h	1½ h	2 h	3 h	4 h
Full	Width	150	200	250	300	400	450
	Cover	20	25	30	35	35	35
50%	Width	125	160	200	200	300	350
	Cover	20	25	25	25	30	35
One face	Width	100	120	140	160	200	240
	Cover	20	25	25	25	25	25

**Table 3.7** Fire resistance ratings for concrete beams subjected to three-sided exposure (BIS 1989)

Construction/materials		Minimum dimensions (mm), excluding any finish for a fire resistance rating of					
		½ h	1 h	1½ h	2 h	3 h	4 h
Reinforced concrete, simply supported	Width	80	120	150	200	240	280
	Cover	20	30	40	60	70	80
Reinforced concrete, continuous supported	Width	80	80	120	150	200	240
	Cover	20	20	35	50	60	70
Prestress concrete, simply supported	Width	100	120	150	200	240	280
	Cover	25	40	55	70	80	90
Prestress concrete, continuous supported	Width	80	100	120	150	200	240
	Cover	20	30	40	55	70	80

**Tutorial 9: Fire resistant design-I****Time: 45 min****Max marks: 20****Part A: Objective questions (5 marks)**

1. Accidents in offshore plant can be grouped as \_\_\_\_\_, \_\_\_\_\_ and \_\_\_\_\_ (fire, explosion and toxic release)
2. Fire is \_\_\_\_\_ (rapid, exothermal oxidation) of ignition fuel
3. Rapid expansion of gases resulting from pressure waves or shock waves is \_\_\_\_\_ (explosion)
4. Define Auto-ignition temperature  
It is the lowest temperature above which material may not require any external source for combustion
5. \_\_\_\_\_ is the temperature at which fluid will not burn (Flash point)

**Part B: Descriptive questions (15 marks)**

1. What is fire?  
Fire is a rapid ex-thermal oxidation of ignition fuel. Fuel can be solid, liquid or gas. Fire releases energy in the form of exothermal radiation. It takes some time for this release to reach its peak intensity.
2. How explosion causes fire?  
Explosion results from rapid expansion of gases. Explosion can be either a mechanical or chemical process. It releases energy rapidly and this causes fire.
3. Define flash point  
Flash point is the lowest temperature at which liquid gives up enough vapor to maintain a continuous flame. It is the temperature at which vapors produced from the liquid result in ignition but fluid will not burn at this temperature.
4. List best practices of fire safety in process industries
  - Fluid should be above flash point and fire point temperatures
  - fluid can be used up to their maximum bulk temperature
  - Avoid designing confined space with the presence of ignition source as this can cause flash very easily
  - Ensure no direct oxygen contact with the heat source. This can be done through proper system design
  - Fluid should be contained within the system
  - Fluid containment should not have direct contact with the external ignition source.
5. List common mistakes that can cause fire accidents
  - All heat transfer systems should be checked for no leak or smoke
  - In case of smoke emerging, one should not isolate smoldering insulation
  - do not let fluid drop on any heat source as this can ignite fluid immediately

**Tutorial 10: Fire resistant design-II****Time: 45 min****Max marks: 20****Part A: Objective questions (5 marks)**

1. List the factors Minimum Ignition energy depends on
  - a. Composition of mixture, concentration of richness of mixture, temperature and pressure
2. List different types of industrial explosion
  - a. CVCE, VCE, BLEVE, VE and dust explosion
3. What is a pressure vessel?
  - a. Pressure vessel is typically a storage tank designed to operate at a pressure about 15lbs. It is designed to hold either liquid or gas a high pressure. If this vessel is cracked or damaged, it can result in leakage or complete rupture.
4. Name any two sources of BLEVE
  - a. Corrosion of walls of pressure vessel, Mechanical damage caused by impact loads, absence of pressure relief valves, over-heating, vapor space explosion, exposure to over pressure
5. What is fire ball?
  - a. In the presence of ignition source, vessel will result in formation of fire could due to thermal radiation or direct flame contact. This is called as fire ball.

**Part B: Descriptive questions (15 marks)**

1. How is fire categorized?
  - a. They are characterized as No fire risk, low fire risk, medium fire risk and high fire risk (DNV 2, 7-2, Offshore services Module-2013)
2. What are the common ignition sources an offshore platform have?
3. How to measure consequences of explosion damage?
4. What are possible reasons for rupture of a pressure vessel?
5. Write short notes on Flash fire.

***Tutorial 11: Blast-resistant design-I******Time: 45 min******Max marks: 20*****Part A: Objective questions (5 marks)**

1. \_\_\_\_\_ is of highest priority in fire safety of offshore platforms (preventing sparks)
2. \_\_\_\_\_ and \_\_\_\_\_ are two explosion protection methods that discharge of unacceptable material into environment (containment method and suppression method)
3. Name two types of deflagration arrestors (end-of-line arrestor; tank-vent arrestor)
4. List objectives of blast-resistant design (personnel safety, controlled shut-down and financial considerations)
5. What is the difference between blast-proof and blast-resistance  
Blast proof is non-realistic term. It is difficult to make a system completely blast-proof. On the other hand, blast-resistance should aim to protect the functional requirements of the critical systems from any irreparable damage. Blast-resistant design should ensure that the system does not undergo catastrophic damage.

**Part B: Descriptive questions (15 marks)**

1. List basic problems that make fire protection of offshore platforms very difficult
2. Explain two types of fire protection systems deployed in offshore platforms
3. What are basic functions of deflagration arrestors?  
These arrestors do not stop detonation but only control them. They reduce risk of flame propagation
4. Write short note on blast resistance
5. List blast-resistance requirements  
It should follow the standard procedure and international recommendation as per AP RP 2FB. It should address the following issues:  
Critical units should be located away from the potential hotspots  
Critical functions of the systems should be protected. Criticality order of any functional requirements should be investigated and planning be done appropriately, even in the design stage. Safety of personnel on board should be ensured, based on the expected occupancy

**Tutorial 12: Blast-resistant design-II****Time: 45 min****Max marks: 20****Part A: Objective questions (5 marks)**

1. List factors that influence blast loads
  - (i) Distance of the object from blast source; and (ii) inventory of explosive chemicals present in the plant
2. Spaces in offshore platforms that are designed to remain blast-resistant are called as \_\_\_\_\_ (protected spaces)
3. List two vital parameters of blast wave
  - (i) peak side-on positive over pressure; (ii) positive phase duration; (iii) corresponding impulse; (iv) peak side negative over pressure; and (v) associated phase duration and negative impulse
4. What is rebound load?

On passage of time, during the negative phase of the blast load, building modules will experience the effects of blast load on the opposite side to that of the primary load. Such rebound effects depend on inertia content of the peak over-pressure load. In general, negative pressure forces are ignored as they are insignificant.

5. List differences in conventional and blast loads  
In case of conventional loads, rate of load is very slow. It remains to act on the structure for a longer period in comparison to that of the natural period of the structure. Typical example are wind load, wave load etc.  
In case of blast loads, rate of loading is very rapid. It acts only for a short duration in comparison to that of the natural period of the structure. Blast loads are transient in nature. They return to ambient condition within short period.

**Part B: Descriptive questions (15 marks)**

1. How to mitigate effect of blasts in offshore facilities?
  - (a) Blast walls are one of the effective ways of mitigating blast effect in offshore facilities. Blast walls offer a safe and confined space for equipments and personnel on board. Usually, equipments of high importance are covered by blast wall on all four sides to enable protection. They are designed to resist impact caused by explosion, without undergoing serious damages.
  - (b) Blast-resistant design has two stages namely: preliminary design stage; and (ii) detailed design stage. Preliminary design is often based on design of structural members to withstand nominal over-pressure and impulse. In detailed design stage, CFD tools are used to design the system for blast loads. Basic design philosophy for blast-resistant arrives by answering a few set of questions namely: (i) what is to be protected? (ii) how to model the possible extent of damage that can be caused? and (iii) how to design a layout of structural system so that it develops inherent protection.

2. List the factors that govern blast resistance

Blast loads are extremely intense and act for a very short duration. Blast resistance is governed by two factors:

- (a) energy absorption capacity of the construction material of the member. Steel and reinforced concrete members have significant energy absorption capacity. They also show ductile behavior. In general, flexible members are less prone to severe damages. Further, it is also known that flexible members with larger periods absorb significant energy, either by allowance to undergo large displacements or to avoid reflections due to compliant nature of response.
- (b) dynamic response characteristics of the member itself  
Unfortunately, potential points on the topside could be mass points with epicenter of large equipments and machinery. Under explosion, mass points will be targeted first. Hence, blast walls around the space are constructed to confine them within a safe enclosure.

3. Define peak reflected pressure and peak dynamic pressure

Peak reflected pressure, peak dynamic pressure, shock-front velocity and blast wave length are secondary parameters of blast wave loads. They are generally derived from the primary parameters. Peak-reflected pressure is caused by reflection of the blast wave when hits the surface of the body. Surface will experience more pressure than that of the incidence side-wall pressure. Peak-reflected pressure is given by:

$$p_r = C_r p_{50}$$

where  $C_r$  is reflection coefficient, which depends on peak over-pressure, angle of incidence of wave front with respect to reflecting surface of bluff body, type of blast wave etc. For peak-overpressure up to 140 kPa, reflection coefficient is given by Newmarks method:

$$C_r = \{p_r/p_{50}\} \text{ which is approximated as } (2 + 0.0073 p_{50}).$$

Alternatively, reflection coefficient can also be obtained from the Green Book. As shock wave propagates, suction will occur after the positive phase of pressure. Duration of reflected pressure depends on (i) dimensions of the reflecting surface; (ii) maximum time of the reflected wave ( $t_d$ ) etc.

Peak dynamic pressure ( $q_0$ ) occurs as the blast wave propagates due to air movement and is given by Newmarks equation. It is approximated as  $0.0032 (p_o)^2$ .

Dynamic net-pressure on the offshore platform is given by:

$$q_n = C_d q_0$$

where  $C_d$  is drag coefficient. Drag coefficient depends on geometric shape of the body and orientation of the body with respect to dominant propagation direction. Typically, for a rectangular block, drag coefficient for front walls is +1.0 and -0.4 for side wall, rear wall and roof.

4. List differences between conventional and blast-resistant design

In conventional design, stress is limited to the elastic range. In blast-resistant design, yielding of the member (material) is acceptable. Hence, blast loads are expected to create permanent-type deformation (plastic deformation), which is permissible. It is important to note that high strain energy that is developed during blasting or explosion is balanced by strain energy of the material.

5. Write short notes on strain increase factor

In general, structural characteristics of marine steel show that average yield strength is very large in comparison to the values specified as minimum acceptable limit in conventional design. Rapid rate of load causes phenomenal increase in stress of the material. Hence, yield phenomenon of the material, under the rapid strain rate is different. It results in increase in strength. To account for this change, UFC-3-340-02 recommends strength increase factor (SIF). In general, SIF is 1.1, as applied to minimum yield strength, specified for structural steel of grade 345 Mpa and above. Steel, with such enhanced yield strength is recommended for blast-resistant design systems. Due to large ductility and deformation capacity of members that arise from high degree of redundancy, capacity of material in the conventional design is under-estimated. Steel experiences increase in strength under rapidly applied loads. But, steel, as a material cannot match its strain rate with that of rate of loading. This causes increase in yield strength and results in plastic deformation. At a faster strain rate, a higher load is required to produce same deformation as that of the lower rate. Hence, yield strength becomes partially a function of rate of loading. It is important to note that increase in yield strength is significant in low-carbon steel; but decreases with the increase in static yield strength. However, Modulus of elasticity of steel is unchanged in both elastic region and yield plateau, for both static and dynamic response of material. In strain-hardening region, slope of the stress-strain curve is different for static and dynamic responses. Some codes and design procedures neglect this difference, even though it is significant.

$$\alpha_{ult} < \alpha_{yield}$$

where  $\alpha_{ultimate}$  is the ratio of dynamic to static strength at ultimate load stage and  $\alpha_{yield}$  is the ratio of same proportion at yield stage. In such cases, it is important to note that strength is not the focus of design but deformation capacity at yield strength is the real focus.

# Chapter 4

## Analysis and Design of Members in Fire

**Abstract** This chapter deals with aspects related to analysis and design of structures in fire. Detailed design procedure of steel members, reinforced concrete members, and steel–concrete composites under fire exposure are discussed. Design examples and solved following code provisions illustrate the presented concepts in detail.

### 4.1 Material Properties at Elevated Temperatures

Thermal and mechanical properties of steel and concrete play a major role in defining their behavior at elevated temperatures. It is important to note that the properties of steel and concrete at elevated temperature are necessary and important to assess their performance under fire loads. They include yield strength and modulus of elasticity, which are influenced by the temperature range. According to the codal methods for design of structures under fire loads, yield strength and the young’s modulus must be estimated at an elevated temperature. Alternatively, if the advanced method of design is used, then stress–strain variations at elevated temperature must be completely known as an input to the designer. In both the design approaches, variation of strength of steel and concrete at elevated temperature, with respect to different strain levels, is very important to compute. Behavior of materials at elevated temperature is handled using strength reduction factor.

Strength reduction factor is a ratio of strength of steel at specific strain level to strength at ambient temperature yield stress. It is given by:

$$k_{y,\theta} = \frac{f_{y,\theta}}{f_y}$$

where  $f_{y,\theta}$  is the yield strength of steel at temperature  $\theta$  and  $f_y$  is the yield strength at an ambient temperature (usually 20 °C). Strength reduction factor is influenced by the strain level; higher the value of strain, lower the strength reduction factor is. Changes in strength reduction are significant with respect to increase in temperature. In the design procedure, it is necessary to choose the strain level, which is

appropriate to the type of loading and cross section. For design purposes, basic strength values at 2% strain can be used. In addition, suitable modification factors are applied to account for the failure cases at the lower strain levels. At an elevated temperature, two main consequences in the steel are: (i) loss of strength and (ii) loss of stiffness. Further, it also leads to the reduction of the modulus of elasticity. Most of the relevant material properties are standardized after several experimental programs and are deliberated in select building codes in detail (EN 1992-1-2, 2008; EN1993-1-2, 2005); codes address fire as a service load for design purposes. While it is expected that the reader will have access to such building codes, a few important properties of concrete and steel are discussed in this chapter with reference to the codes.

## 4.2 Thermal Properties of Concrete

### 4.2.1 Specific Heat

Specific heat of concrete is determined using the following relationships:

$$C_c = 900 \quad \text{for } 20^\circ\text{C} \leq \theta_c \leq 100^\circ\text{C} \quad (4.1a)$$

$$C_c = \{900 + (\theta_c - 100)\} \quad \text{for } 100^\circ\text{C} \leq \theta_c \leq 200^\circ\text{C} \quad (4.1b)$$

$$C_c = \{1000 + 0.5(\theta_c - 200)\} \quad \text{for } 200^\circ\text{C} \leq \theta_c \leq 400^\circ\text{C} \quad (4.1c)$$

$$C_c = 1100 \quad \text{for } 400^\circ\text{C} \leq \theta_c \leq 1200^\circ\text{C} \quad (4.1d)$$

where specific heat of concrete ( $C_c$ ) is measured in ( $\text{J kg}^{-1} \text{K}^{-1}$ ) and  $\theta_c$  is temperature of concrete measured in ( $^\circ\text{C}$ ). Relationship given in Eq. (4.1) applies to concrete constituted of both siliceous and calcareous aggregates. Variation in the range of temperature is due to the fact that presence of moisture ( $U$ ) alters the specific heat capacity of concrete; this is more significant in the temperature range of 100–200  $^\circ\text{C}$ . Figure 4.1 shows the variation of specific heat capacity of concrete with rise in temperature.

### 4.2.2 Density

Density of concrete alters with temperature primarily due to water loss and is given by the following relationships:

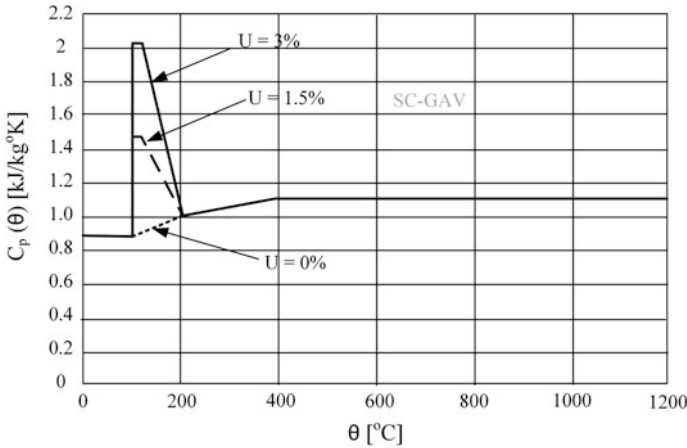


**Fig. 4.1** Influence of moisture content on specific heat capacity of concrete

$$\rho_c = \rho_{20} \quad \text{for } 20^\circ\text{C} \leq \theta_c \leq 115^\circ\text{C} \quad (4.2a)$$

$$\rho_c = \rho_{20} \left\{ 1 - \frac{0.02(\theta_c - 115)}{85} \right\} \quad \text{for } 115^\circ\text{C} \leq \theta_c \leq 200^\circ\text{C} \quad (4.2b)$$

$$\rho_c = \rho_{20} \left\{ 0.98 - \frac{0.03(\theta_c - 200)}{200} \right\} \quad \text{for } 200^\circ\text{C} \leq \theta_c \leq 400^\circ\text{C} \quad (4.2c)$$

$$\rho_c = \rho_{20} \left\{ 0.95 - \frac{0.07(\theta_c - 400)}{800} \right\} \quad \text{for } 400^\circ\text{C} \leq \theta_c \leq 1200^\circ\text{C} \quad (4.2d)$$

where  $\rho_{20}$  is density of concrete at 20 °C, expressed in (kg/m<sup>3</sup>), and  $\theta_c$  is temperature of concrete expressed in (°C), respectively.

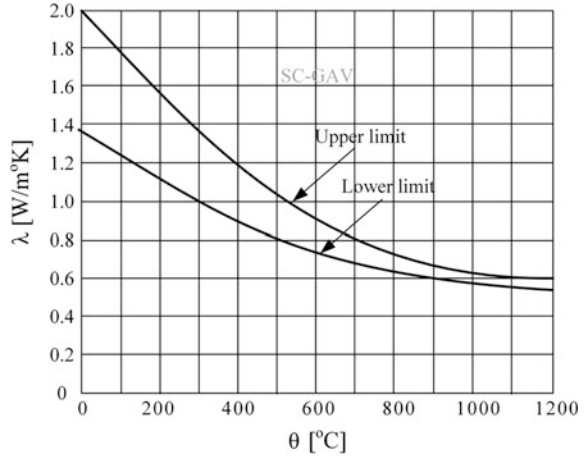
### 4.2.3 Thermal Conductivity

Thermal conductivity ( $\lambda_c$ ) of normal concrete is specified through an upper and a lower limit. Typical values of thermal conductivity lie within these limits. Upper and lower limits of thermal conductivity are given by the following relationship:

$$\lambda_c = 2 - 0.2451 \left( \frac{\theta_c}{100} \right) + 0.0107 \left( \frac{\theta_c}{100} \right)^2 \quad \text{for } 20^\circ\text{C} \leq \theta_c \leq 1200^\circ\text{C} \quad (4.3a)$$

$$\lambda_c = 1.36 - 0.136 \left( \frac{\theta_c}{100} \right) + 0.0057 \left( \frac{\theta_c}{100} \right)^2 \quad \text{for } 20^\circ\text{C} \leq \theta_c \leq 120^\circ\text{C} \quad (4.3b)$$

**Fig. 4.2** Limits of thermal conductivity of concrete



where  $\lambda_c$  is thermal conductivity of concrete (expressed in  $\text{Wm}^{-1} \text{K}^{-1}$ ) and  $\theta_c$  is temperature of concrete (expressed in  $^{\circ}\text{C}$ ). A graphical representation of the upper and the lower limits of thermal conductivity is shown in Fig. 4.2.

### 4.3 Thermal Properties of Steel

Various thermal properties are required to understand steel at different temperatures. They include specific heat, density, thermal conductivity. Time–temperature curve should be obtained from the thermal load estimates on the members. Temperature time history is dependent on the following factors, namely: (i) applied heat load, (ii) shape (size of the member and section dimensions), and (iii) presence of passive fire protection methods/techniques. Fourier equation for heat transfer, in the absence of an internal heat source, is given by:

$$\nabla(a(\nabla\theta)) = \dot{\theta} \quad (4.3c)$$

where  $\theta$  is the space-dependent temperature,  $\dot{\theta} = d\theta/dt$ , and  $a$  is the temperature-dependent thermal diffusivity. Thermal diffusivity is given by:

$$a = \frac{\lambda}{\rho C_v} \quad (4.3d)$$

where  $\lambda$  is thermal conductivity,  $\rho$  is density of material, and  $C_v$  is specific heat capacity.

### 4.3.1 Specific Heat and Density

Specific heat ( $C_s$ ) of steel is recommended at different range of temperature by international code (EN 1994-1-2). They are given by the following relationships:

$$C_s = 425 + 7.73 \times 10^{-1} \theta_s - 1.69 \times 10^{-3} \theta_s^2 + 2.22 \times 10^{-6} \theta_s^3 \quad \text{for } 20^\circ\text{C} \leq \theta_s \leq 600^\circ\text{C} \quad (4.4a)$$

$$C_s = 666 + \frac{1302}{738 - \theta_s} \quad \text{for } 600^\circ\text{C} \leq \theta_s \leq 735^\circ\text{C} \quad (4.4b)$$

$$C_s = 545 + \frac{17820}{\theta_s - 731} \quad \text{for } 735^\circ\text{C} \leq \theta_s \leq 900^\circ\text{C} \quad (4.4c)$$

$$C_s = 650 \quad \text{for } 900^\circ\text{C} \leq \theta_s \leq 1200^\circ\text{C} \quad (4.4d)$$

where  $C_s$  is specific heat (expressed in  $\text{J kg}^{-1} \text{ }^\circ\text{C}$ ) and  $\theta_s$  is temperature of steel (expressed in  $^\circ\text{C}$ ). Variation of specific heat of carbon steel with rise in temperature is shown in Fig. 4.3. For design purposes, specific heat of steel can be taken as  $600 \text{ J/kg }^\circ\text{C}$ . Density of steel is taken to be constant at  $7850 \text{ kg m}^{-3}$  at all temperatures. It is inversely proportional to thermal diffusivity.

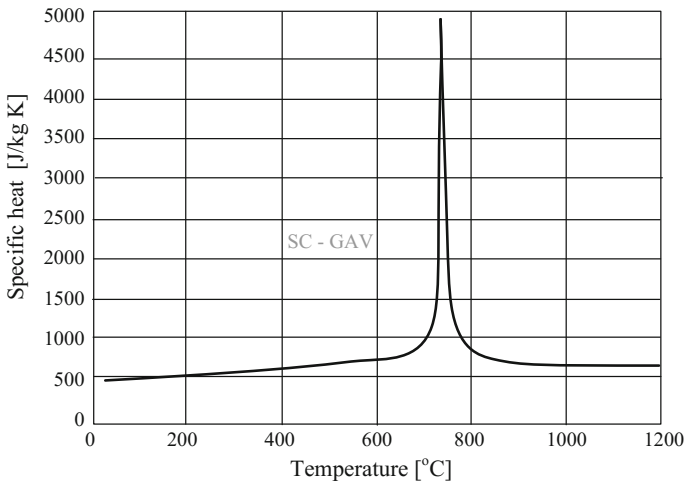


Fig. 4.3 Specific heat of carbon steel

### 4.3.2 Thermal Conductivity

Thermal conductivity depends on strength of steel, but it is not very significant. Thermal conductivity of steel is determined from the following relationship:

$$\lambda_s = 54 - 3.33 \times 10^{-3} \theta_s \quad \text{for } 20^\circ\text{C} \leq \theta_s \leq 800^\circ\text{C} \quad (4.5a)$$

$$\lambda_s = 27.3 \quad \text{for } 800^\circ\text{C} \leq \theta_s \leq 1200^\circ\text{C} \quad (4.5b)$$

where  $\lambda_s$  is thermal conductivity (expressed in  $\text{Wm}^{-1} \text{ }^\circ\text{C}^{-1}$ ) and  $\theta_s$  is temperature of steel (expressed in  $^\circ\text{C}$ ). Variation of thermal conductivity of steel with rise in temperature is shown in Fig. 4.4. For design purposes, thermal conductivity of steel can be taken as  $45 \text{ W/m } ^\circ\text{C}$ .

### 4.3.3 Thermal Diffusivity

Thermal diffusivity shows a linear relationship with temperature up to  $750^\circ\text{C}$ . It is given by:

$$a = 0.87 - 0.84 \times 10^{-3} \theta_s \quad (4.5c)$$

where  $a$  is thermal diffusivity and  $\theta_s$  is temperature ( $^\circ\text{C}$ ).

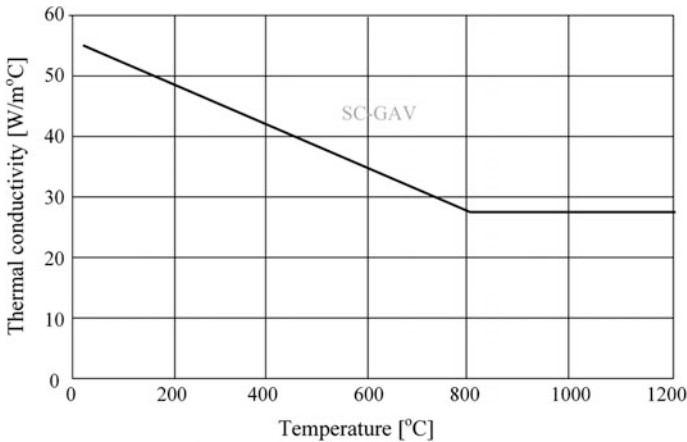


Fig. 4.4 Thermal conductivity of carbon steel

## 4.4 Mechanical Properties

### 4.4.1 Concrete

For design of concrete structures under fire, the most important mechanical property is its characteristic compressive strength,  $f_{ck}$ . As concrete is exposed to higher temperatures, its characteristic compressive strength reduces. This reduction is often expressed as strength reduction factor  $k_{c,\theta} = f_{c,\theta}/f_{ck}$ . There are two more mechanical properties that have a role in design: (i) strain at which peak compressive strength of concrete is attained,  $\varepsilon_{c1,\theta}$ , and (ii) ultimate crushing strain,  $\varepsilon_{cu1,\theta}$ . Contrary to the characteristic compressive strength, limiting values of these strains decrease with rise in temperature. Variations of the strength reduction factor, peak strain, and ultimate strain with temperature are shown in Table 4.1. It is seen from the table that compressive strength of concrete comprising calcareous aggregates is slightly greater than that of the concrete with siliceous aggregates; however, there is no difference in the variation of corresponding strain values. Further, it can also be observed that strength of concrete is reduced by about 50% at 600 °C and loses its entire strength at 1200 °C.

### 4.4.2 Steel

For design of steel structures, typically two material quantities are required, namely: (i) Young's modulus and (ii) yield stress. For ambient temperature design, Young's modulus of steel remains unchanged and the yield stress defines the grade of steel.

**Table 4.1** Reduction factors for concrete

$\theta_s$ (°C)	Siliceous aggregates			Calcareous aggregates		
	$k_{c,\theta}$	$\varepsilon_{c1,\theta}$	$\varepsilon_{cu1,\theta}$	$k_{c,\theta}$	$\varepsilon_{c1,\theta}$	$\varepsilon_{cu1,\theta}$
20	1.000	0.0025	0.0200	1.000	0.0025	0.0200
100	1.000	0.0040	0.0225	1.000	0.0040	0.0225
200	0.950	0.0055	0.0250	0.970	0.0055	0.0250
300	0.850	0.0070	0.0275	0.910	0.0070	0.0275
400	0.750	0.0100	0.0300	0.850	0.0100	0.0300
500	0.600	0.0150	0.0325	0.740	0.0150	0.0325
600	0.450	0.0250	0.0350	0.600	0.0250	0.0350
700	0.300	0.0250	0.0375	0.430	0.0250	0.0375
800	0.150	0.0250	0.4000	0.270	0.0250	0.4000
900	0.080	0.0250	0.4250	0.150	0.0250	0.4250
1000	0.040	0.0250	0.0450	0.006	0.0250	0.0450
1100	0.010	0.0250	0.0475	0.020	0.0250	0.0475
1200	0.000			0.000		

It is seen that as the temperature of a steel specimen rises, both the Young’s modulus and yield stress reduce. A convenient way to represent this reduction is through reduction factors. Reduction in yield stress is given by the following relationship:

$$k_{y,\theta} = f_{y,\theta}/f_y \tag{4.6}$$

Reduction in Young’s modulus is given by the following relationship:

$$k_{E,\theta} = E_{s,\theta}/E_s \tag{4.7}$$

Reduction in proof strength is given by the following relationship:

$$k_{p,\theta} = f_{p,\theta}/f_y \tag{4.8}$$

where  $f_{y,\theta}$ ,  $f_{p,\theta}$  and  $E_{s,\theta}$  are the yield stress, proof strength, and the Young’s modulus at temperature  $\theta$ , respectively. Values of yield strength and Young’s Modulus of steel are corresponding values in the cold conditions (at 20 °C). Variation of these reduction factors with temperature is shown in Fig. 4.5. For design calculations, reduction factors are also given in Table 4.2; values for intermediate temperatures may be calculated by linear interpolation. It is seen from the table that steel loses its entire strength at 1200 °C. However, temperature higher than 500 °C (up to 600 °C) may be considered to be critical as steel loses half of its strength during this temperature range. While the actual critical temperature of a steel member depends on its utilization factor, 600 °C is often considered to be the critical temperature of a steel member in the absence of other data.

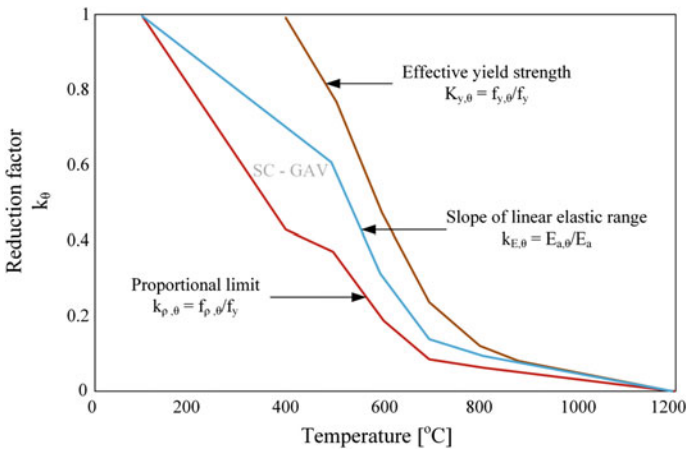


Fig. 4.5 Variation of reduction factors of steel with temperature

**Table 4.2** Reduction factors for steel at different temperatures

Steel temperature $\theta_s$ (°C)	$k_{y,\theta} = f_{y,\theta}/f_y$	$k_{p,\theta} = f_{p,\theta}/f_y$	$k_{E,\theta} = E_{s,\theta}/E_s$
20	1.000	1.000	1.0000
100	1.000	1.000	1.0000
200	1.000	0.807	0.9000
300	1.000	0.613	0.8000
400	1.000	0.420	0.7000
500	0.780	0.360	0.6000
600	0.470	0.180	0.3100
700	0.230	0.075	0.1300
800	0.110	0.050	0.0900
900	0.060	0.0375	0.0675
1000	0.040	0.0250	0.0450
1100	0.020	0.0125	0.0225
1200	0.000	0.000	0.0000

## 4.5 Constitutive Models for Concrete and Steel Under Fire

### 4.5.1 Concrete

Constitutive behavior of concrete, to be used in compression zone for advanced structural analysis under fire, is shown in Fig. 4.6. Functional form of stress–strain curves is given below:

$$\sigma(\theta) = \frac{3\epsilon f_{c,\theta}}{\epsilon_{c1,\theta} \left( 2 + \left( \frac{\epsilon}{\epsilon_{c1,\theta}} \right)^3 \right)} \quad \text{for } \epsilon \leq \epsilon_{c1,\theta} \tag{4.9}$$

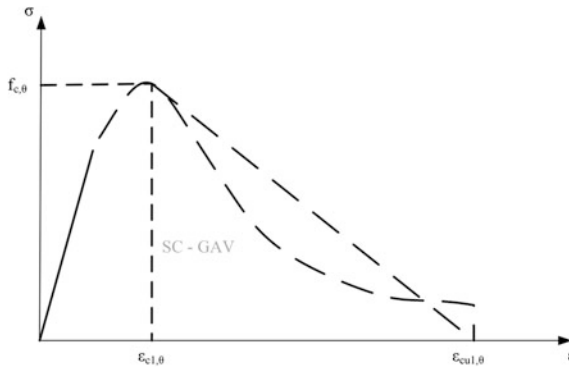


**Fig. 4.6** Temperature-dependent stress–strain behavior of concrete in compression

For other range of values like  $\varepsilon_{c1,\theta} \leq \varepsilon \leq \varepsilon_{cu1,\theta}$ , appropriate descending branch should be adopted as shown in Fig. 4.6. Tensile strength is usually ignored. In case it is required for advanced calculations, following empirical equations for estimating material degradation coefficients under tensile strength are useful:

$$f_{ck,t}(\theta) = k_{c,t}(\theta)f_{ck,t} \quad (4.10)$$

where  $f_{c,\theta}$  is temperature-dependent tensile strength,  $f_{ck,t}$  represents tensile strength of concrete at room temperature, and  $k_{c,t}(\theta)$  is given by:

$$k_{c,t}(\theta) = \begin{cases} 1 & \text{for } 20^\circ\text{C} \leq \theta \leq 100^\circ\text{C} \\ 1 - \frac{\theta-100}{500} & \text{for } 100^\circ\text{C} \leq \theta \leq 600^\circ\text{C} \end{cases} \quad (4.11)$$

### 4.5.2 Steel

Figure 4.7 gives overall stress–strain behavior of steel, which is useful in estimating resistance against tension, compression, moment and shear. Functional forms of the stress–strain relation for various ranges of strain are given below:

Strain at proportional limit ( $\varepsilon_{p,\theta}$ ) is given by:

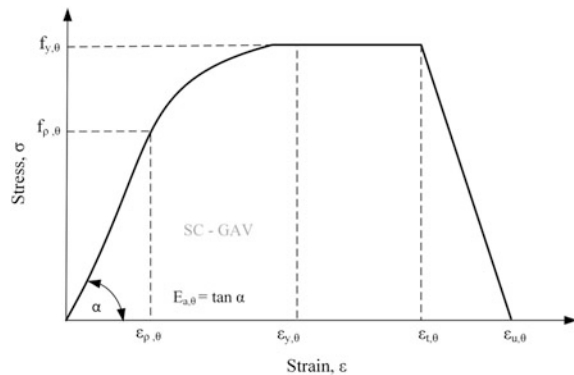
$$\varepsilon_{p,\theta} = \frac{f_{p,\theta}}{E_{a,\theta}} \quad (4.12)$$

$$\varepsilon_{y,\theta} = 0.02 \quad (4.13)$$

$$\varepsilon_{t,\theta} = 0.15 \quad (4.14)$$

$$\varepsilon_{u,\theta} = 0.20 \quad (4.15)$$

**Fig. 4.7** Stress–strain behavior of steel



where  $f_{p,\theta}$  is stress at proportional limit,  $\epsilon_{y,\theta}$  is yield strain,  $\epsilon_{t,\theta}$  is limiting strain for yield strength,  $\epsilon_{u,\theta}$  is ultimate strain, and  $E_{a,\theta}$  is Young's Modulus of steel, as described in Fig. 4.7.

(a) For strain range  $\epsilon \leq \epsilon_{p,\theta}$ , stress is given by:

$$\sigma = \epsilon E_{a,\theta} \quad (4.16)$$

where  $E_{a,\theta}$  is tangent modulus.

(b) For strain range  $\epsilon_{p,\theta} < \epsilon < \epsilon_{t,\theta}$ , stress is given by:

$$\sigma = f_{p,\theta} - c + \left\{ \frac{b}{a} \right\} \left[ a^2 - (\epsilon_{y,\theta} - \epsilon)^2 \right]^{0.5} \quad (4.17)$$

Tangent modulus is given by:

$$E_{a,\theta} = \frac{b(\epsilon_{y,\theta} - \epsilon)}{a \left[ a^2 - (\epsilon_{y,\theta} - \epsilon)^2 \right]^{0.5}} \quad (4.18)$$

(c) For strain range  $\epsilon_{y,\theta} \leq \epsilon \leq \epsilon_{t,\theta}$ , stress is given as  $f_{y,\theta}$

(d) For strain range  $\epsilon_{t,\theta} < \epsilon < \epsilon_{u,\theta}$ , stress is given by:

$$\sigma = f_{y,\theta} \left[ 1 - \frac{(\epsilon - \epsilon_{t,\theta})}{(\epsilon_{u,\theta} - \epsilon_{t,\theta})} \right] \quad (4.19)$$

For this specific range of strain, tangent modulus is not defined.

(e) For strain range  $\epsilon = \epsilon_{u,\theta}$ , stress is zero

where following parameters are useful to determine the stress values as given above:

$$a^2 = (\epsilon_{y,\theta} - \epsilon_{p,\theta}) \left( \epsilon_{y,\theta} - \epsilon_{p,\theta} + \frac{c}{E_{a,\theta}} \right) \quad (4.20a)$$

$$b^2 = c(\epsilon_{y,\theta} - \epsilon_{p,\theta})E_{a,\theta} + c^2 \quad (4.20b)$$

$$c = \frac{(f_{y,\theta} - f_{p,\theta})^2}{(\epsilon_{y,\theta} - \epsilon_{p,\theta})E_{a,\theta} - 2(f_{y,\theta} - f_{p,\theta})} \quad (4.20c)$$

where  $f_{y,\theta}$  is effective yield strength and  $E_{s,\theta}$  is slope of the stress–strain curve at linear elastic range (Young's Modulus of steel).

## 4.6 Design of Steel Members Exposed to Fire

It is a usual practice to note that structural design of members under fire is carried out for a predefined fire rating that the structural system must demonstrate during any fire event. Design procedures entail two steps, namely: (i) thermal analysis; and (ii) structural analysis. Usually, unprotected steel members perform very poor even under moderate fire. Hence, the use of exposed steel structures is discouraged. Therefore, design of steel structures against fire also includes design of insulation material to ensure the required fire rating. Fire rating is defined either on temperature-based or on strength-based criterion.

### 4.6.1 Temperature Assessment

Primary objective of temperature assessment is to compute temperature of the structural members under certain fire conditions. Temperature of the structural member is useful to assess temperature-based fire rating of the member. In addition, it serves as vital input to assess its strength-based fire rating. Heat reaches from source of fire to the surface of the member through convection and radiation. In the initial stages of fire, convection dominates, while after sustained burning, radiation is the major contributor toward heat transfer. Due to very high thermal conductivity of steel, surface temperature quickly penetrates through its entire volume. Hence, thermal gradients within the member become negligible. Under such conditions, lumped capacitance method is useful to assess temperature of structural member. Resultant heat flux is given by the following relationship:

$$h_{\text{net}} = KF(\theta_t - \theta_{a,t}) \quad (4.21)$$

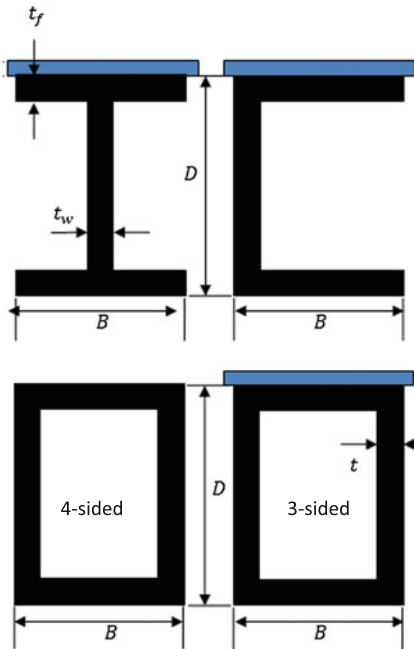
where  $K$  is coefficient of total heat transfer,  $F$  is surface area of the member exposed to fire,  $\theta_t$  is the gas temperature, and  $\theta_{a,t}$  is the temperature of steel member. Rate of heat flow into the member, in an incremental form, is given by:

$$h_{\text{net}} = c_a \rho_a V_t \frac{\Delta \theta_{a,t}}{\Delta t} \quad (4.22)$$

where  $c_a$  is the specific heat of steel,  $\rho_a$  is the density of steel, and  $V_t$  is the volume per unit length. Equating the values of heat flow in the above equations, time-variant temperature of the member can be obtained as follows:

$$\Delta \theta_{a,t} = \frac{K}{c_a \rho_a V_t} \frac{A_m}{V} (\theta_t - \theta_{a,t}) \Delta t \quad (4.23)$$

where  $A_m/V$  is the heated perimeter per unit volume of the structural member. Calculation procedure for typical steel sections is given below:



$$A_m = 2D + 4B - 2t_w \text{ for 4-sided exposure}$$

$$A_m = 2D + 3B - 2t_w \text{ for 3-sided exposure}$$

$$V = 2Bt_f + (D - 2t_f)t_w \approx 2Bt_f + Dt_w$$

$$A_m = 2D + 2B \text{ for 4-sided exposure}$$

$$A_m = 2D + B \text{ for 3-sided exposure}$$

$$V = BD - (B - 2t)(D - 2t)$$

$A_m/V$  for other configurations can be calculated for other sections similarly or can be found in EN 1993-1-2:2005 (Table 4.2). It is to be noted that usually, the calculated values of  $A_m/V$  are rounded up to the nearest 5. Heat flow in uninsulated steelwork is given by:

$$\Delta\theta_{a,t} = \frac{\alpha_c + \alpha_r}{c_a \rho_a} \frac{A_m}{V} (\theta_i - \theta_{a,t}) \Delta t \tag{4.24}$$

Here,  $\alpha_c$  is the coefficient of convective heat transfer (typical value for hydrocarbon fire is  $50 \text{ W/m}^2 \text{ }^\circ\text{C}$ ) and  $\alpha_r$  is the coefficient of radiative heat transfer and depends on factors such as the temperature of steel and gas, configuration factor, and emissivity of the structural member. For protected steel members, temperature calculations are based on the concept of thermal resistance of materials. Thermal resistance is given by:

$$R = L/kA \tag{4.25}$$

where  $L$  is thickness of the member (taken to be unity for convection and radiation modes),  $k$  is the thermal conductivity or heat convection/radiation coefficient, and  $A$  is the area of cross section. Note the one-to-one similarity between the concept of thermal and electrical resistance. Consequently, when multiple layers of different materials are encountered in heat transfer (as in protected steel members), the overall heat transfer calculations are performed by considering equivalent thermal

resistance of the constituent materials connected in series or parallel, as applicable. Typically, the ECCS method is used to calculate temperature rise in protected steelwork. In case of insulated members with negligible heat capacity, temperature rise is obtained as follows:

$$\Delta\theta_{a,t} = \frac{\lambda_p}{c_a\rho_a} \frac{A_m}{V} (\theta_t - \theta_{a,t}) \quad (4.26)$$

Here,  $\lambda_p$  is the thermal conductivity (W/m °C) and  $d_p$  is the thickness (m) of the insulation. Heat flow in members with substantial heat capacity is obtained as:

$$\Delta\theta_{a,t} = \frac{\lambda_p}{c_a\rho_a} \frac{A_m}{V} \frac{(\theta_t - \theta_{a,t})\Delta t}{1 + \frac{\phi}{2}} - \frac{\Delta\theta_t}{1 + \frac{2}{\phi}} \quad (4.27)$$

Here,  $\phi = \frac{c_p\rho_p}{c_a\rho_a} d_p \frac{A_m}{V}$  is a parameter used to define whether insulation has substantial heat capacity or not. Insulations with  $\phi > 0.5$  are considered to have substantial heat capacity and require (4.27) for temperature calculations, while for others, (4.26) is to be used.  $c_p$  and  $\rho_p$  are the specific heat and density of the insulating material, respectively.

#### 4.6.2 Eurocode Approach (EN 1993-1-2)

This approach uses the relation derived by Wickstorm (1986). Following equations apply:

$$\Delta\theta_{a,t} = \frac{\lambda_p}{c_a\rho_a} \frac{A_m}{V} \frac{(\theta_t - \theta_{a,t})\Delta t}{1 + \frac{\phi}{3}} - \left( e^{\left(\frac{\phi}{10}\right)} - 1 \right) \Delta\theta_t \quad (4.28)$$

Eurocode EN 1993-1-2 places a limit on the minimum value of  $\Delta t$  to be used for computing temperature rise as 30 s (clause 4.2.3.2). Wickstorm (1986) suggested that the limit on  $\Delta t$  should be taken as:

$$\Delta t \leq \frac{c_a\rho_a}{\lambda_p} \frac{V}{A_m} \left( 1 + \frac{\phi}{3} \right) < 60 \text{ s} \quad (4.29)$$

Above methods for computing temperature are semiempirical in nature and are derived based on the lumped capacitance and thermal resistance concepts.

### 4.6.3 Bare Steelwork

Twilt and Witteveen (1986) gave the following equation for computing the temperature rise on bare steelwork:

$$t_{fi,d} = 0.54(\theta_{a,t} - 50) \left( \frac{A_m}{V} \right)^{-0.6} \quad (4.30)$$

where  $\theta_{a,t}$  is the temperature in the steel reached at a time  $t$  (minutes). Note that the above equation only holds for  $10 \leq t_{fi,d} \leq 80$  min;  $400 \leq \theta_{a,t} \leq 600$  °C and  $10 \leq A_m/V \leq 300$  m<sup>-1</sup>.

### 4.6.4 Protected Steelwork

When steelwork is protected with dry insulation, it is found that the time to failure depends solely on the term  $(d_p/\lambda_p)(V_t/A_p)$  with the following resultant equation:

$$t_{fi,d} = 40(\theta_{a,t} - 140) \left( \frac{d_p}{\lambda_p} \frac{V}{A_m} \right)^{0.77} \quad (4.31)$$

The above equation is an empirical relation determined from tests in which insulation material was very light. When the insulation has substantial heat capacity, above equation is revised as below:

$$t_{fi,d} = 40(\theta_{a,t} - 140) \left( \frac{d_p}{\lambda_p} \left( \frac{V}{A_m} + \frac{d_p \rho_p}{\rho_a} \right) \right)^{0.77} \quad (4.32)$$

## 4.7 Fire Rating Based on Temperature Criterion

For a member to perform adequately where deflection or stability (buckling) is not critical in a fire, EN 1993-1-2 requires that the structural temperature remains below a critical temperature, i.e.,

$$\theta_a \leq \theta_{a,cr} \quad (4.33)$$

Temperature of structural members can be determined through thermal analysis as detailed above. Value of critical temperature  $\theta_{a,cr}$  is dependent on the degree of utilization  $\mu_0$  of the structural member. Relationship between  $\theta_{a,cr}$  and  $\mu_0$  has been

determined from elementary plasticity theory. Reduction in steel strength with rise in temperature is given by:

$$\theta_{a,cr} = 39.19 \ln \left( \frac{1}{0.9674 \mu_0^{3.833}} - 1 \right) + 48 \text{ subject to the limit } \mu_0 > 0.013 \quad (4.34)$$

The degree of utilization is defined as:

$$\mu_0 = \frac{E_{\bar{f},d}}{R_{\bar{f},d,0}} \quad (4.35)$$

where  $R_{\bar{f},d,0}$  is the resistance of the member at time  $t = 0$  (i.e., at the beginning of the fire) and  $E_{\bar{f},d}$  is the design effect of the structural fire actions.

## 4.8 Strength Assessment

Strength assessment of structural members under fire conditions is performed by considering the same set of design equations that are usually employed for ambient temperature; only change is to use appropriate strength reduction factors. It is important to note that classification of a structural member may change due to strength and modulus degradation at higher temperatures. For instance, a column member, which was not slender earlier, becomes slender during fire; alternatively, Class 1 section becomes Class 2 and so on. In such cases, design calculations need to be adjusted accordingly. It is usually assumed that end conditions do not change during a fire event.

### 4.8.1 Fire Rating Based on Strength Criterion

Fire rating, based on strength criterion, is defined as the time up to which the design value of the internal force to be resisted remains below the design resistance during fire. Mathematically, it is given as:

$$E_{\bar{f},d} < R_{\bar{f},d,t}. \quad (4.36)$$

This is usually calculated in accordance with the Code (EN 1993-1-2).

- (a) Section classification: This should be carried out in accordance with the code EN 1993-1-1, except the value of  $\varepsilon$  is modified to allow for the effects of temperature, as given below:

$$\varepsilon = 0.85 \left[ \frac{235}{f_y} \right]^{0.5} \quad (4.37)$$

- (b) Tension members, with a uniform temperature distribution, will have a reduced axial tensile capacity ( $N_{fi,\theta,Rd}$ ), and it is given by:

$$N_{fi,\theta,Rd} = k_{y,\theta} N_{Rd} \left[ \frac{\gamma_{M,1}}{\gamma_{M,fi}} \right] \quad (4.38)$$

where,  $k_{y,\theta}$  is the normalized strength reduction factor at a temperature of  $\theta_a$  and  $N_{Rd}$  is the ambient design resistance. For tension members with a non-uniform temperature distribution, axial capacity may be obtained by summing the contributions of discretized areas as  $N_{fi,\theta,Rd} = \sum_{i=1}^n \frac{A_i k_{y,\theta,i} f_y}{\gamma_{M,fi}}$ , where  $A_i$  and  $k_{y,\theta,i}$  are the area and the strength reduction factor of  $i$ th area. One can also use (4.38) using the maximum steel temperature reached and assuming constant temperature.

- (c) Compression members (Class 1, 2, and 3 cross sections):  
The compressive strength in fire conditions is given by:

$$N_{b,fi,t,Rd} = \chi_{fi} A k_{y,\theta} \frac{f_y}{\gamma_{M,fi}} \quad (4.39)$$

where buckling strength reduction factor  $\chi_{fi}$  is given by:

$$\chi_{fi} = \frac{1}{\phi_\theta + \sqrt{\phi_\theta^2 - \lambda_\theta^2}} \quad (4.40)$$

with  $\phi_\theta = 0.5(1 + \alpha\lambda_\theta + \lambda_\theta^2)$  and  $\alpha = 0.65\sqrt{\frac{235}{f_y}}$ .  $\lambda_\theta = \lambda\sqrt{\frac{k_{y,\theta}}{k_{E,\theta}}}$  is the non-dimensional slenderness ratio at temperature  $\theta$  with  $\lambda$  being the normalized slenderness ratio. Buckling length in fire conditions is usually calculated in a similar manner as done for ambient temperatures. For braced frames, buckling length for columns of an intermediate story is taken as 0.5 times the story height, while for columns of top story, it is taken as 0.7 times the story height.

- (d) Beams:

In case of Class 1 or 2 sections, with a uniform temperature distribution, moment capacity  $M_{fi,\theta,Rd}$  with no lateral torsional buckling may be calculated using the following relationship:

$$M_{fi,\theta,Rd} = k_{y,\theta} M_{Rd} \left[ \frac{\gamma_{M,1}}{\gamma_{M,fi}} \right] \quad (4.41)$$

For  $\gamma_{M,1} = \gamma_{M,fi} = 1.0$ , above equation reduces to the following form:

$$M_{fi,\theta,Rd} = k_{y,\theta} M_{Rd} \quad (4.42)$$

where  $k_{y,\theta}$  is the normalized strength reduction at a temperature of  $\theta_a$  and  $M_{Rd}$  is the ambient design resistance. When lateral torsional buckling can occur, the moment capacity  $M_{b,fi,t,Rd}$  is given by the following relationship:

$$M_{b,fi,t,Rd} = \chi_{L,fi} W_{pl,y} k_{y,\theta,com} \frac{f_y}{\gamma_{M,fi}} \quad (4.43)$$

where  $k_{y,\theta,com}$  is the strength reduction factor for the temperature in the compression flange, which can be conservatively based on the uniform temperature  $\theta_a$ . For members with non-uniform temperature, the capacity can be computed by discretizing the area into multiple areas and summing over the contributions of individual areas, as was described in case of tension members previously.

## 4.9 Numerical Examples

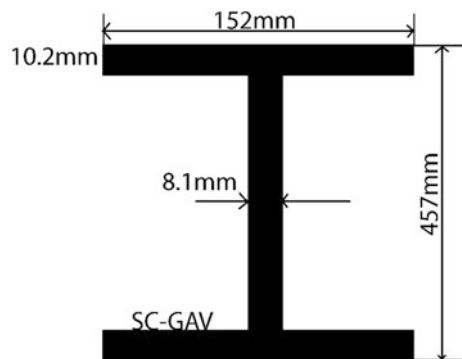
**Example 1** Evaluate the temperature profile for an unprotected I section shown in Fig. 4.8, when it is exposed to three-sided standard ISO-834 fire.

### Thermal analysis:

Increment in temperature in steel structure when exposed to fire is given by:

$$\Delta\theta_{a,t} = \frac{\alpha}{c_a \rho_a} \frac{A_m}{V_m} (\theta_t - \theta_{a,t}) \Delta t$$

**Fig. 4.8** Steel I section for Example 1



where  $c_a$  is the specific heat,  $\rho_a$  is the density of the material,  $A_m$  is the area of the unit length exposure,  $V_m$  is the volume of unit length section,  $\theta_{a,t}$  is the temperature in member,  $\theta_t$  is the gas temperature,  $\Delta t$  is the increment in time, and  $\alpha$  is the effective heat transfer coefficient given by:

$$\alpha = 25 + \frac{0.7 \times k_{sh} \times 0.56 \times 10^{-8}}{\theta_t - \theta_{a,t}} \left[ (\theta_t + 273)^4 - (\theta_{a,t} + 273)^4 \right]$$

where  $k_{sh}$  is the shielding parameter which is similar to the configuration factor and determines whether all surfaces of an exposed member receive direct radiation or certain portions of the cross-sectional shield other sections. The maximum value of shielding parameter ( $= (A_m/V)_b / (A_m/V)$ ) is unity and can be used in calculations. For I sections, Eurocode 1993-1-2 specifies  $k_{sh} = 0.9 (A_m/V)_b / (A_m/V)$ .

For this example, gas temperature is given by:

$$\theta_t = 20 + 345 \log(8t + 1)$$

For the given section,

$$\begin{aligned} \frac{A_m}{V} &= \frac{2D + 3B - 2t_w}{2Bt_f + (D - 2t_f)t_w} = \frac{2 \times 457 + 3 \times 152 - 2 \times 10.22}{2 \times 152 \times 10.22 + (457 - 2 \times 10.22) \times 8.1} \times 10^3, \\ \frac{A_m}{V} &= 1000 \times \frac{1349.56}{6643} = 203.2 \approx 205 \text{ m}^{-1}, \text{ while} \\ \left(\frac{A_m}{V}\right)_b &= \frac{2D + B}{2Bt_f + (D - 2t_f)t_w} = \frac{2 \times 457 + 152}{2 \times 152 \times 10.22 + (457 - 2 \times 10.22) \times 8.1} \times 10^3, \\ \left(\frac{A_m}{V}\right)_b &= 1000 \times \frac{1066}{6643} = 160.5 \approx 165 \text{ m}^{-1}. \end{aligned}$$

Thus,  $(A_m/V) = 205 \text{ m}^{-1}$  and  $(A_m/V)_b = 165 \text{ m}^{-1}$ . Subsequently,  $k_{sh}$  is computed as 0.72. Temperature variation of the member with respect to time is summarized in Table 4.3. Figure 4.9 shows the variation of structural temperature with time.

**Example 2** Evaluate the temperature profile for an unprotected C-Channel section of constant thickness shown in Fig. 4.10, when it is exposed to four-sided standard ISO-834 fire.

### Thermal analysis:

Increment in temperature in steel structure when exposed to fire is given by:

$$\Delta\theta_{a,t} = \frac{\alpha}{c_a \rho_a} \frac{A_m}{V_m} (\theta_t - \theta_{a,t}) \Delta t$$

**Table 4.3** Temperature in given steel section of Example 1

Time (min)	$\alpha$	$\theta_t$	$\Delta\theta$	$\theta_m$
0		20.00	0.00	20.00
0.5	25.87	261.14	32.79	52.79
1	26.32	349.21	41.01	93.80
1.5	26.75	404.31	43.66	137.46
2	27.18	444.50	43.86	181.32
2.5	27.61	476.17	42.79	224.10
3	28.05	502.29	41.01	265.11
3.5	28.49	524.53	38.85	303.96
4	28.93	543.89	36.49	340.45
4.5	29.38	561.03	34.06	374.52
5	29.82	576.41	31.65	406.16
5.5	30.25	590.36	29.29	435.45
6	30.68	603.12	27.04	462.49
6.5	31.09	614.88	24.90	487.39
7	31.49	625.78	22.91	510.30
7.5	31.88	635.94	21.05	531.35
8	32.25	645.46	19.34	550.69
8.5	32.60	654.40	17.77	568.47
9	32.95	662.85	16.34	584.81
9.5	33.27	670.84	15.05	599.86
10	33.58	678.43	13.87	613.73
0.5	25.87	261.14	32.79	52.79

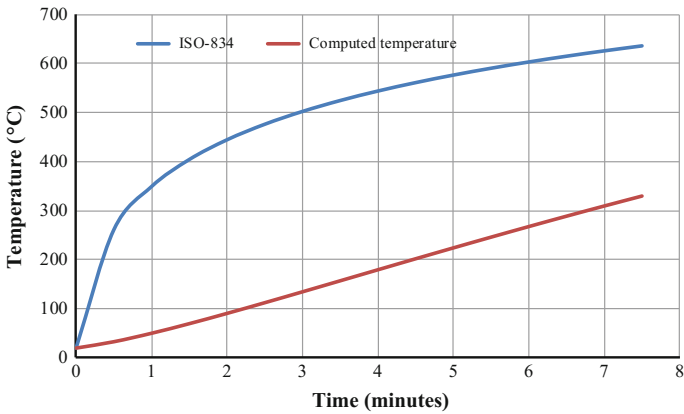
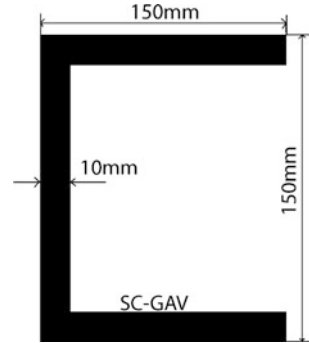


**Fig. 4.9** Temperature variation of beam section with time

**Fig. 4.10** Steel channel section for Example 2



where  $c_a$  is the specific heat,  $\rho_a$  is the density of the material,  $A_m$  is the area of the unit length exposure,  $V_m$  is the volume of unit length section,  $\theta_{a,t}$  is the temperature in member,  $\theta_t$  is the gas temperature,  $\Delta t$  is the increment in time, and  $\alpha$  is the effective heat transfer coefficient given by:

$$\alpha = 25 + \frac{0.7 \times k_{sh} \times 0.56 \times 10^{-8}}{\theta_t - \theta_{a,t}} \left[ (\theta_t + 273)^4 - (\theta_{a,t} + 273)^4 \right]$$

For the given example, the gas temperature is given by:

$$\theta_t = 20 + 345 \log(8t + 1)$$

For the given section,  $(A_m/V) = 205 \text{ m}^{-1}$ ,  $(A_m/V)_b = 140 \text{ m}^{-1}$ , and subsequently,  $k_{sh}$  is computed as 0.68. Temperature variation of the member with respect to time is summarized in Table 4.4. Figure 4.11 shows the variation of structural temperature with time.

**Example 3** Evaluate the temperature profile for I section (same web and flange thicknesses) beam protected with a 20-mm fiberboard as shown in Fig. 4.12, when exposed to a four-sided ISO-834 standard fire.

Thermal analysis:

Increment in temperature in protected steel structure when exposed to fire is given by:

$$\Delta\theta_{a,t} = \frac{\lambda_p}{c_a \rho_a} \frac{A_m}{V} \frac{(\theta_t - \theta_{a,t}) \Delta t}{1 + \frac{\phi}{3}} - \left( e^{(\frac{\phi}{10})} - 1 \right) \Delta\theta_t,$$

**Table 4.4** Temperature in given steel section of Example 2

Time	$\alpha$	$\theta_t$	$\Delta\theta$	$\theta_m$
0		20.00	0.00	20.00
0.5	25.82	261.15	8.18	28.20
1	26.18	349.21	11.04	39.20
1.5	26.47	404.31	12.70	51.90
2	26.72	444.51	13.79	65.70
2.5	26.96	476.17	14.54	80.30
3	27.18	502.29	15.08	95.30
3.5	27.40	524.53	15.45	110.80
4	27.61	543.89	15.71	126.50
4.5	27.81	561.03	15.88	142.40
5	28.01	576.41	15.98	158.40
5.5	28.22	590.36	16.02	174.40
6	28.41	603.12	16.01	190.40
6.5	28.61	614.88	15.96	206.30
7	28.81	625.78	15.88	222.20
7.5	29.01	635.94	15.77	238.00
8	29.21	645.46	15.64	253.60
8.5	29.41	654.40	15.49	269.10
9	29.61	662.85	15.32	284.40
9.5	29.81	670.84	15.14	299.60
10	30.01	678.43	14.94	314.50

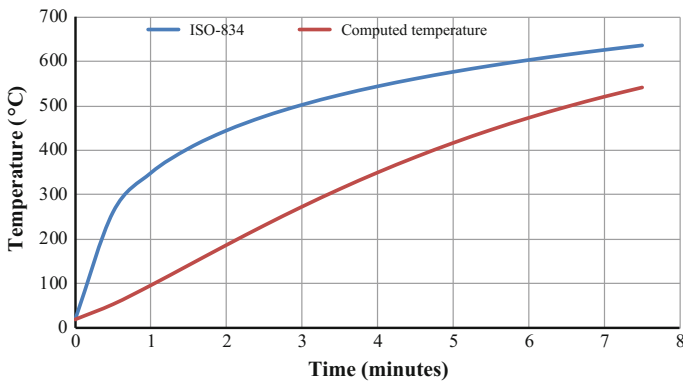
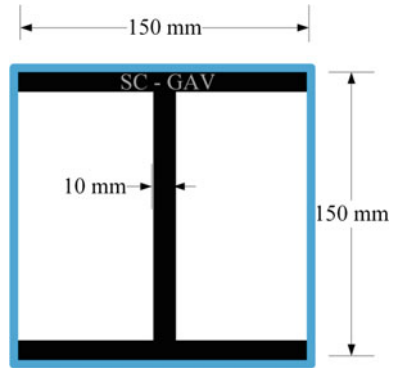


**Fig. 4.11** Temperature variation of C-section with time

Material data:

For fiberboard fire protection,  $\lambda_p = 0.25 \text{ W/m } ^\circ\text{C}$ ,  $\rho_p = 500 \text{ kg/m}^3$ ,  $p = 2\%$ ,  $c_p = 1500 \text{ J/kg } ^\circ\text{C}$ ,  $d_p = 0.020 \text{ m}$ ,  $A_p/V = 160 \text{ m}^{-1}$ ,  $\rho_a = 7850 \text{ kg/m}^3$ , and  $c_a = 600 \text{ J/kg } ^\circ\text{C}$ .

**Fig. 4.12** Box-insulated steel beam I section for Example 3



Since  $\phi = \frac{c_p \rho_p d_p A_m}{c_a \rho_a d_p A_m} \frac{A_m}{V}$  gives  $\phi = 0.50$ ,

Which gives,  $\Delta\theta_{a,t} = 0.0109(\theta_t - \theta_{a,t}) - 0.0523\Delta\theta_t$ .

For the given section,  $(A_m/V) = 160 \text{ m}^{-1}$ . Temperature variation of the member with respect to time is summarized in Table 4.5. Figure 4.13 shows the variation of structural temperature with time.

**Example 4** Evaluate the temperature profile for a C-Channel section protected with a 20-mm fiberboard protection shown in Fig. 4.14, when exposed to a four-sided ISO-834 standard fire.

**Table 4.5** Temperature in given steel section of Example 3

Time	$\theta_t$	$\Delta\theta$	$\theta_m$
0	20.00	0.00	20.00
0.5	261.14	2.60	22.63
1	349.21	3.38	26.05
1.5	404.31	3.90	29.99
2	444.50	4.27	34.29
2.5	476.17	4.54	38.88
3	502.29	4.76	43.69
3.5	524.53	4.94	48.67
4	543.89	5.08	53.80
4.5	561.03	5.21	59.06
5	576.41	5.31	64.42
5.5	590.36	5.40	69.87
6	603.12	5.47	75.39
6.5	614.88	5.54	80.97
7	625.78	5.59	86.61
7.5	635.94	5.64	92.30

(continued)

**Table 4.5** (continued)

Time	$\theta_t$	$\Delta\theta$	$\theta_m$
8	645.46	5.68	98.03
8.5	654.40	5.71	103.79
9	662.85	5.74	109.57
9.5	670.84	5.76	115.38
10	678.43	5.78	121.21
10.5	685.65	5.79	127.05
11	692.54	5.80	132.91
11.5	699.13	5.81	138.77
12	705.44	5.82	144.63
12.5	711.49	5.82	150.50
13	717.31	5.82	156.36
13.5	722.91	5.82	162.23
14	728.31	5.81	168.08
14.5	733.52	5.81	173.94
15	738.56	5.80	179.78
15.5	743.43	5.79	185.61
16	748.15	5.78	191.43
16.5	752.73	5.76	197.24
17	757.17	5.75	203.03
17.5	761.48	5.74	208.81
18	765.67	5.72	214.57
18.5	769.75	5.70	220.32
19	773.72	5.69	226.05
19.5	777.59	5.67	231.75
20	781.35	5.65	237.44
20.5	785.03	5.63	243.10
21	788.62	5.61	248.75
21.5	792.13	5.59	254.37
22	795.55	5.56	259.97
22.5	798.90	5.54	265.55
23	802.17	5.52	271.10
23.5	805.38	5.49	276.63
24	808.52	5.47	282.13
24.5	811.59	5.44	287.61
25	814.60	5.42	293.06
25.5	817.56	5.39	298.49
26	820.45	5.37	303.89
26.5	823.29	5.34	309.26
27	826.08	5.32	314.61
27.5	828.82	5.29	319.93
28	831.50	5.26	325.22

(continued)

**Table 4.5** (continued)

Time	$\theta_t$	$\Delta\theta$	$\theta_m$
28.5	834.14	5.24	330.49
29	836.74	5.21	335.72
29.5	839.29	5.18	340.93
30	841.80	5.15	346.12
30.5	844.26	5.13	351.27
31	846.69	5.10	356.40
31.5	849.08	5.07	361.49
32	851.43	5.04	366.56
32.5	853.74	5.02	371.60
33	856.02	4.99	376.61
33.5	858.26	4.96	381.60
34	860.48	4.93	386.55
34.5	862.66	4.90	391.48
35	864.80	4.88	396.37
35.5	866.92	4.85	401.24
36	869.01	4.82	406.08
36.5	871.07	4.79	410.89
37	873.10	4.76	415.67
37.5	875.11	4.73	420.43
38	877.08	4.71	425.15
38.5	879.04	4.68	429.85
39	880.96	4.65	434.51
39.5	882.87	4.62	439.15
40	884.74	4.59	443.76
40.5	886.60	4.57	448.34
41	888.43	4.54	452.90
41.5	890.24	4.51	457.42
42	892.03	4.48	461.92
42.5	893.80	4.45	466.39
43	895.55	4.43	470.83
43.5	897.27	4.40	475.24
44	898.98	4.37	479.62
44.5	900.67	4.34	483.98
45	902.34	4.32	488.31
45.5	903.99	4.29	492.61
46	905.62	4.26	496.88
46.5	907.24	4.23	501.12
47	908.84	4.21	505.34
47.5	910.42	4.18	509.53
48	911.98	4.15	513.70
48.5	913.53	4.13	517.83

(continued)

**Table 4.5** (continued)

Time	$\theta_t$	$\Delta\theta$	$\theta_m$
49	915.07	4.10	521.94
49.5	916.58	4.07	526.03
50	918.08	4.05	530.08
50.5	919.57	4.02	534.11
51	921.04	4.00	538.11
51.5	922.50	3.97	542.09
52	923.95	3.94	546.04
52.5	925.38	3.92	549.97
53	926.79	3.89	553.86
53.5	928.20	3.87	557.74
54	929.59	3.84	561.58
54.5	930.97	3.82	565.40
55	932.33	3.79	569.20
55.5	933.68	3.77	572.97
56	935.03	3.74	576.72
56.5	936.35	3.72	580.44
57	937.67	3.69	584.13
57.5	938.98	3.67	587.80
58	940.27	3.64	591.45
58.5	941.55	3.62	595.07
59	942.83	3.59	598.67
59.5	944.09	3.57	602.24
60	945.34	3.55	605.79
60.5	946.58	3.52	609.32
61	947.81	3.50	612.82
61.5	949.03	3.48	616.30
62	950.24	3.45	619.75
62.5	951.44	3.43	623.18
63	952.64	3.41	626.59
63.5	953.82	3.38	629.98
64	954.99	3.36	633.34
64.5	956.15	3.34	636.68
65	957.31	3.32	640.00
65.5	958.46	3.29	643.29
66	959.59	3.27	646.56
66.5	960.72	3.25	649.81
67	961.84	3.23	653.04
67.5	962.95	3.21	656.25
68	964.06	3.19	659.43
68.5	965.15	3.16	662.60
69	966.24	3.14	665.74

(continued)

**Table 4.5** (continued)

Time	$\theta_t$	$\Delta\theta$	$\theta_m$
69.5	967.32	3.12	668.86
70	968.39	3.10	671.96
70.5	969.46	3.08	675.03
71	970.51	3.06	678.09
71.5	971.56	3.04	681.13
72	972.61	3.02	684.14
72.5	973.64	3.00	687.14
73	974.67	2.98	690.11
73.5	975.69	2.96	693.07
74	976.70	2.94	696.00
74.5	977.71	2.92	698.91
75	978.71	2.90	701.81
75.5	979.71	2.88	704.68
76	980.69	2.86	707.54
76.5	981.67	2.84	710.37
77	982.65	2.82	713.19
77.5	983.62	2.80	715.99
78	984.58	2.78	718.77
78.5	985.53	2.76	721.53
79	986.48	2.75	724.27
79.5	987.43	2.73	726.99
80	988.37	2.71	729.69
80.5	989.30	2.69	729.21
81	990.22	2.67	731.88
81.5	991.15	2.66	734.54
82	992.06	2.64	737.17
82.5	992.97	2.62	739.79
83	993.87	2.60	742.40
83.5	994.77	2.58	744.98
84	995.67	2.57	747.55
84.5	996.55	2.55	750.10
85	997.44	2.53	752.63
85.5	998.31	2.52	755.15
86	999.19	2.50	757.65
86.5	1000.05	2.48	760.13
87	1000.92	2.47	762.60
87.5	1001.77	2.45	765.04
88	1002.63	2.43	767.48

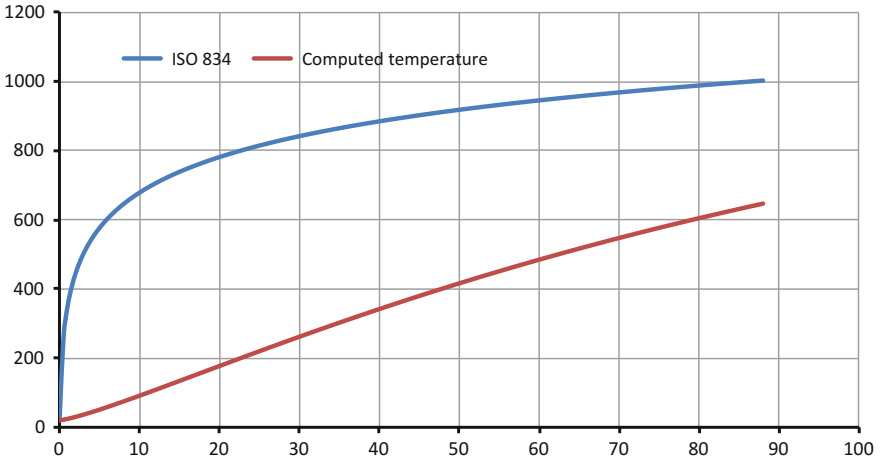
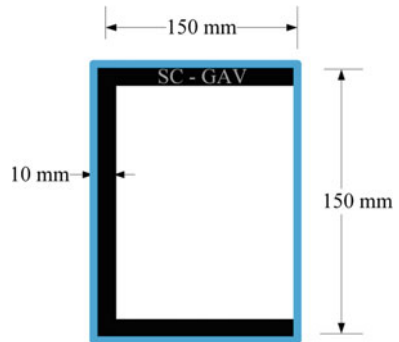


Fig. 4.13 Temperature variation of box-insulated steel beam I section with time

Fig. 4.14 Box-insulated steel beam channel section for Example 4



Thermal analysis:

Increment in temperature in steel structure when exposed to fire is given by:

$$\Delta\theta_{a,t} = \frac{\lambda_p}{c_a \rho_a} \frac{A_m}{V} \frac{(\theta_t - \theta_{a,t}) \Delta t}{1 + \frac{\phi}{3}} - \left( e^{\left(\frac{\phi}{10}\right)} - 1 \right) \Delta\theta_t$$

Material data:

$\lambda_p = 0.25 \text{ W/m } ^\circ\text{C}$ ,  $\rho_p = 500 \text{ kg/m}^3$ ,  $p = 2\%$ ,  $c_p = 1500 \text{ J/kg } ^\circ\text{C}$ ,  $d_p = 0.020 \text{ m}$ ,  $A_m/V = 160 \text{ m}^{-1}$ ,  $\rho_a = 7850 \text{ kg/m}^3$ , and  $c_a = 600 \text{ J/kg } ^\circ\text{C}$ .

Thus,  $\phi = 0.50$  and, therefore,  $\Delta\theta_{a,t} = 0.0109(\theta_t - \theta_{a,t}) - 0.0523\Delta\theta_t$ .

Details of temperature variation in the member with respect to time are summarized in Table 4.5. Figure 4.15 shows variation of structural temperature with time (Table 4.6).

**Example 5** Evaluate the fire rating of the unprotected I section subjected to a dead load of 17.8 kN/m and live load of 9.375 kN/m, as shown in Fig. 4.16, when exposed to three-sided standard ISO-834 fire.

*Structural Analysis:*

For the given beam, load combination for fire is considered as per EN 1991-1-2 and is given by:

$$1 \times \text{P.L} + 0.3 \times \text{I.L.}$$

Design moment on the structure,  $M_{fi,ED}$ , is computed as follows:

$$= 3.75 \times (17.8 + 0.3 \times 0.375) \times 8^2/8 = 165 \text{ kN/m.}$$

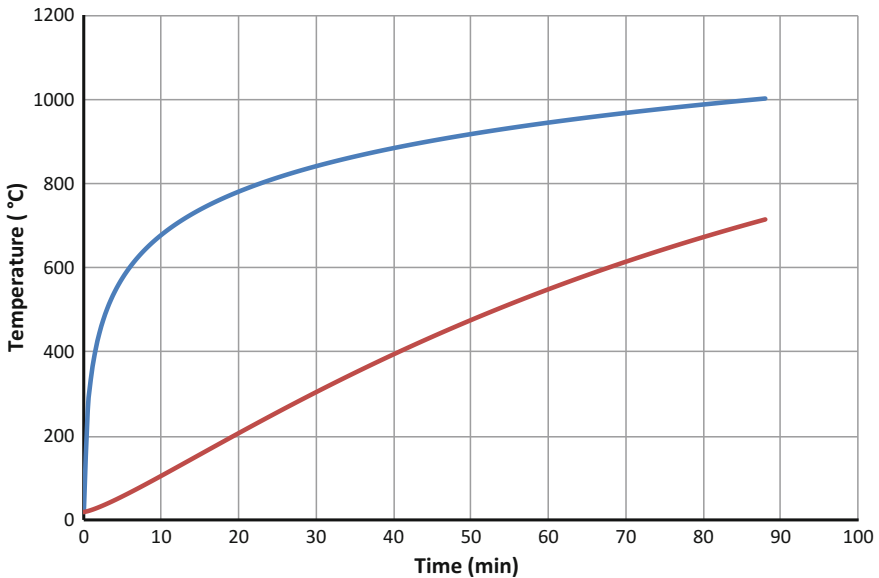


**Fig. 4.15** Temperature variation of box-insulated channel section with time

**Table 4.6** Temperature in given steel section of Example 4

Time	$\theta_t$	$\Delta\theta$	$\theta_m$
0	<b>20.00</b>	<b>0.00</b>	<b>20.00</b>
0.5	261.14	2.60	22.63
1	349.21	3.38	26.05
1.5	404.31	3.90	29.99
2	444.50	4.27	34.29
2.5	476.17	4.54	38.88
3	502.29	4.76	43.69
3.5	524.53	4.94	48.67
4	543.89	5.08	53.80
4.5	561.03	5.21	59.06
5	576.41	5.31	64.42
5.5	590.36	5.40	69.87
6	603.12	5.47	75.39
6.5	614.88	5.54	80.97
7	625.78	5.59	86.61
7.5	635.94	5.64	92.30
8	645.46	5.68	98.03
8.5	654.40	5.71	103.79
9	662.85	5.74	109.57
9.5	670.84	5.76	115.38
10	678.43	5.78	121.21
10.5	685.65	5.79	127.05
11	692.54	5.80	132.91
11.5	699.13	5.81	138.77
12	705.44	5.82	144.63
12.5	711.49	5.82	150.50
13	717.31	5.82	156.36
13.5	722.91	5.82	162.23
14	728.31	5.81	168.08
14.5	733.52	5.81	173.94
15	738.56	5.80	179.78
15.5	743.43	5.79	185.61
16	748.15	5.78	191.43
16.5	752.73	5.76	197.24
17	757.17	5.75	203.03
17.5	761.48	5.74	208.81
18	765.67	5.72	214.57
18.5	769.75	5.70	220.32
19	773.72	5.69	226.05
19.5	777.59	5.67	231.75
20	781.35	5.65	237.44

(continued)

**Table 4.6** (continued)

Time	$\theta_t$	$\Delta\theta$	$\theta_m$
20.5	785.03	5.63	243.10
21	788.62	5.61	248.75
21.5	792.13	5.59	254.37
22	795.55	5.56	259.97
22.5	798.90	5.54	265.55
23	802.17	5.52	271.10
23.5	805.38	5.49	276.63
24	808.52	5.47	282.13
24.5	811.59	5.44	287.61
25	814.60	5.42	293.06
25.5	817.56	5.39	298.49
26	820.45	5.37	303.89
26.5	823.29	5.34	309.26
27	826.08	5.32	314.61
27.5	828.82	5.29	319.93
28	831.50	5.26	325.22
28.5	834.14	5.24	330.49
29	836.74	5.21	335.72
29.5	839.29	5.18	340.93
30	841.80	5.15	346.12
30.5	844.26	5.13	351.27
31	846.69	5.10	356.40
31.5	849.08	5.07	361.49
32	851.43	5.04	366.56
32.5	853.74	5.02	371.60
33	856.02	4.99	376.61
33.5	858.26	4.96	381.60
34	860.48	4.93	386.55
34.5	862.66	4.90	391.48
35	864.80	4.88	396.37
35.5	866.92	4.85	401.24
36	869.01	4.82	406.08
36.5	871.07	4.79	410.89
37	873.10	4.76	415.67
37.5	875.11	4.73	420.43
38	877.08	4.71	425.15
38.5	879.04	4.68	429.85
39	880.96	4.65	434.51
39.5	882.87	4.62	439.15
40	884.74	4.59	443.76
40.5	886.60	4.57	448.34

(continued)

**Table 4.6** (continued)

Time	$\theta_t$	$\Delta\theta$	$\theta_m$
41	888.43	4.54	452.90
41.5	890.24	4.51	457.42
42	892.03	4.48	461.92
42.5	893.80	4.45	466.39
43	895.55	4.43	470.83
43.5	897.27	4.40	475.24
44	898.98	4.37	479.62
44.5	900.67	4.34	483.98
45	902.34	4.32	488.31
45.5	903.99	4.29	492.61
46	905.62	4.26	496.88
46.5	907.24	4.23	501.12
47	908.84	4.21	505.34
47.5	910.42	4.18	509.53
48	911.98	4.15	513.70
48.5	913.53	4.13	517.83
49	915.07	4.10	521.94
49.5	916.58	4.07	526.03
50	918.08	4.05	530.08
50.5	919.57	4.02	534.11
51	921.04	4.00	538.11
51.5	922.50	3.97	542.09
52	923.95	3.94	546.04
52.5	925.38	3.92	549.97
53	926.79	3.89	553.86
53.5	928.20	3.87	557.74
54	929.59	3.84	561.58
54.5	930.97	3.82	565.40
55	932.33	3.79	569.20
55.5	933.68	3.77	572.97
56	935.03	3.74	576.72
56.5	936.35	3.72	580.44
57	937.67	3.69	584.13
57.5	938.98	3.67	587.80
58	940.27	3.64	591.45
58.5	941.55	3.62	595.07
59	942.83	3.59	598.67
59.5	944.09	3.57	602.24
60	945.34	3.55	605.79
60.5	946.58	3.52	609.32
61	947.81	3.50	612.82

(continued)

**Table 4.6** (continued)

Time	$\theta_t$	$\Delta\theta$	$\theta_m$
61.5	949.03	3.48	616.30
62	950.24	3.45	619.75
62.5	951.44	3.43	623.18
63	952.64	3.41	626.59
63.5	953.82	3.38	629.98
64	954.99	3.36	633.34
64.5	956.15	3.34	636.68
65	957.31	3.32	640.00
65.5	958.46	3.29	643.29
66	959.59	3.27	646.56
66.5	960.72	3.25	649.81
67	961.84	3.23	653.04
67.5	962.95	3.21	656.25
68	964.06	3.19	659.43
68.5	965.15	3.16	662.60
69	966.24	3.14	665.74
69.5	967.32	3.12	668.86
70	968.39	3.10	671.96
70.5	969.46	3.08	675.03
71	970.51	3.06	678.09
71.5	971.56	3.04	681.13
72	972.61	3.02	684.14
72.5	973.64	3.00	687.14
73	974.67	2.98	690.11
73.5	975.69	2.96	693.07
74	976.70	2.94	696.00
74.5	977.71	2.92	698.91
75	978.71	2.90	701.81
75.5	979.71	2.88	704.68
76	980.69	2.86	707.54
76.5	981.67	2.84	710.37
77	982.65	2.82	713.19
77.5	983.62	2.80	715.99
78	984.58	2.78	718.77
78.5	985.53	2.76	721.53
79	986.48	2.75	724.27
79.5	987.43	2.73	726.99
80	988.37	2.71	729.69
80.5	989.30	2.69	729.21
81	990.22	2.67	731.88
81.5	991.15	2.66	734.54

(continued)

**Table 4.6** (continued)

Time	$\theta_t$	$\Delta\theta$	$\theta_m$
82	992.06	2.64	737.17
82.5	992.97	2.62	739.79
83	993.87	2.60	742.40
83.5	994.77	2.58	744.98
84	995.67	2.57	747.55
84.5	996.55	2.55	750.10
85	997.44	2.53	752.63
85.5	998.31	2.52	755.15
86	999.19	2.50	757.65
86.5	1000.05	2.48	760.13
87	1000.92	2.47	762.60
87.5	1001.77	2.45	765.04
88	1002.63	2.43	767.48

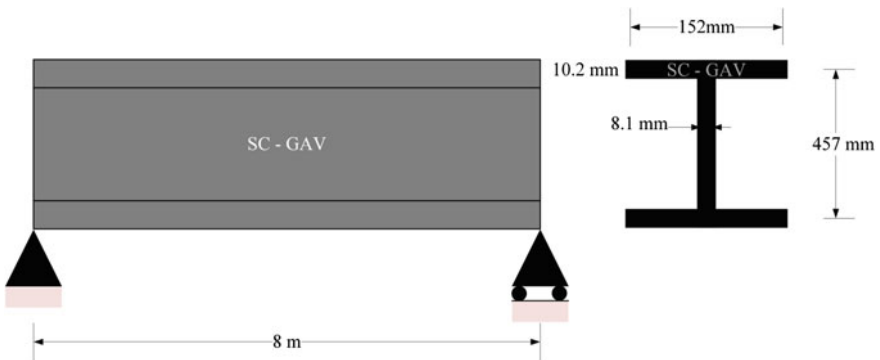


**Fig. 4.16** Unprotected steel I section for Example 5

Section classification:

$$\varepsilon = 0.85 \left[ \frac{235}{f_y} \right]^{0.5} = 0.85 \left[ \frac{235}{275} \right]^{0.5} = 0.786$$

Class of flange:

$$\varepsilon = 0.85 \left[ \frac{235}{f_y} \right]^{0.5} = 0.85 \left[ \frac{235}{275} \right]^{0.5} = 0.786$$

$$c = 0.5[b - 2.t_f - t_w] = 62.6 \text{ mm}$$

$$\frac{c}{t_f} = 4.71$$

Limiting value for Class 1 is  $9\varepsilon = 9 \times 0.786 = 7.07$ . Hence, flange is Class 1  
Class of web:

$$c = 407.6 \text{ mm}$$

$$\frac{c}{t_w} = 50.3$$

Limiting value for Class 1 is  $9\varepsilon = 72 \times 0.786 = 56.6$ . Hence, web is Class 1.

Evaluation of fire rating in accordance with EN 1993 1-2:

Strength-based fire resistance:

Design moment of resistance  $M_{RD} = 275 \times 1287 \times 10^3/1.0 = 354 \text{ kNm}$ .

$$k_{y,\theta} = \frac{M_{fi,ED}}{M_{RD}} = \frac{163}{354} = 0.460$$

As it is a three-sided exposure, effective value of  $k_{y,\theta}$  is obtained by further dividing with 0.85 as 0.541. From Table 4.2, it can be found using linear interpolation that this value of  $k_{y,\theta}$  is obtained at a temperature of 577 °C.

Thermal analysis:

Increment in temperature in steel structure when exposed to fire is given by:

$$\Delta\theta_{a,t} = \frac{\alpha}{c_a \rho_a} \frac{A_m}{V_m} (\theta_t - \theta_{a,t}) \Delta t$$

where  $c_a$  is the specific heat,  $\rho_a$  is the density of the material,  $A_m$  is the area of the unit length exposure,  $V$  is the volume of unit length section,  $\theta_{a,t}$  is the temperature in member,  $\theta_t$  is the gas temperature,  $\Delta t$  is the increment in time, and  $\alpha$  is the effective heat transfer coefficient given by:

$$\alpha = 25 + \frac{0.7 \times k_{sh} \times 0.56 \times 10^{-8}}{\theta_t - \theta_{a,t}} \left[ (\theta_t + 273)^4 - (\theta_{a,t} + 273)^4 \right]$$

where  $k_{sh}$  is the shielding parameter given by  $(A_m/V)_m/(A_m/V)$ . For the given example, the gas temperature is given by:

$$\theta_t = 20 + 345 \log(8t + 1)$$

For the given section,  $(A_m/V)_m = 205 \text{ m}^{-1}$  and  $(A_m/V)_b = 165 \text{ m}^{-1}$ . Subsequently,  $k_{sh}$  is computed as 0.72. Detailed member temperature with 0.5-min time interval is shown in Table 4.7. Critical temperature of the beam is 598 °C. Temperature obtained from strength-based criteria for beam is 577 °C. Failure of the beam will happen at lower of the two temperatures, i.e., at 577 °C. Thus, the fire rating of the beam is approximately 20 min as shown in Fig. 4.17 and highlighted in Table 4.7.

**Example 6** Consider the same beam and fire scenario as in Example 5 but protected with a 20-mm fiberboard fire protection. Evaluate its fire rating (Fig. 4.18).

**Table 4.7** Temperature in the steel section of Example 5

Time	$\alpha$	$\theta_t$	$\Delta\theta$	$\theta_m$
0.0		20.00	0.00	20.00
0.5	25.963	261.15	8.23	28.23
1.0	26.384	349.21	11.13	39.36
1.5	26.727	404.31	12.82	52.17
2.0	27.029	444.51	13.94	66.11
2.5	27.308	476.17	14.72	80.82
3.0	27.572	502.29	15.27	96.10
3.5	27.825	524.53	15.67	111.76
4.0	28.073	543.89	15.94	127.70
4.5	28.315	561.03	16.12	143.83
5.0	28.555	576.41	16.23	160.06
5.5	28.793	590.36	16.28	176.34
6.0	29.03	603.12	16.28	192.62
6.5	29.266	614.88	16.24	208.86
7.0	29.503	625.78	16.16	225.02
7.5	29.74	635.94	16.06	241.08
8.0	29.977	645.46	15.93	257.01
8.5	30.215	654.40	15.78	272.79
9.0	30.453	662.85	15.61	288.40
9.5	30.693	670.84	15.43	303.83
10.0	30.933	678.43	15.23	319.05
10.5	31.174	685.65	15.02	334.07
11.0	31.415	692.54	14.80	348.87
11.5	31.657	699.13	14.57	363.44
12.0	31.899	705.44	14.34	377.78
12.5	32.142	711.49	14.10	391.87
13.0	32.385	717.31	13.85	405.72
13.5	32.628	722.91	13.60	419.32
14.0	32.871	728.31	13.35	432.67
14.5	33.114	733.52	13.09	445.76
15.0	33.356	738.56	12.83	458.59
15.5	33.598	743.43	12.58	471.17
16.0	33.839	748.15	12.32	483.49
16.5	34.079	752.73	12.06	495.54
17.0	34.318	757.17	11.80	507.34
17.5	34.556	761.48	11.54	518.88
18.0	34.793	765.67	11.28	530.17
18.5	35.029	769.75	11.03	541.20
19.0	35.262	773.72	10.78	551.97
19.5	35.495	777.59	10.52	562.49
20.0	<b>35.725</b>	<b>781.36</b>	<b>10.28</b>	<b>572.77</b>

(continued)

**Table 4.7** (continued)

Time	$\alpha$	$\theta_t$	$\Delta\theta$	$\theta_m$
20.5	35.954	785.03	10.03	582.80
21.0	36.181	788.62	9.79	592.58
21.5	36.405	792.13	9.55	602.13
22.0	36.628	795.55	9.31	611.44
22.5	36.848	798.90	9.08	620.52
23.0	37.066	802.174	8.848	629.365
23.5	37.281	805.379	8.623	637.988
24.0	37.494	808.517	8.402	646.390
24.5	37.705	811.591	8.185	654.576
25.0	37.913	814.603	7.973	662.548

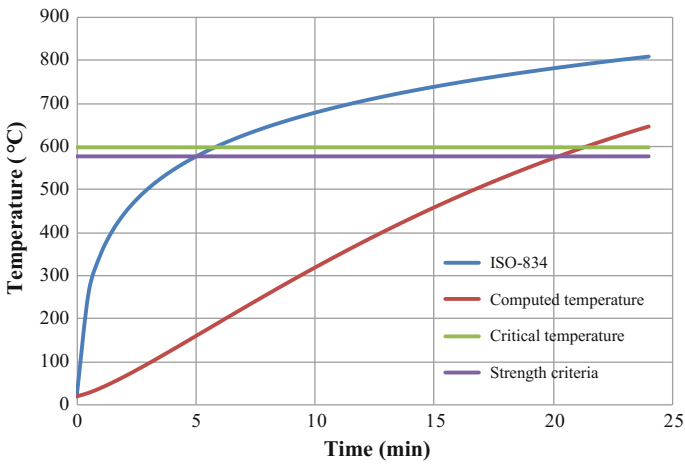


**Fig. 4.17** Temperature variation for computing fire rating of steel I section

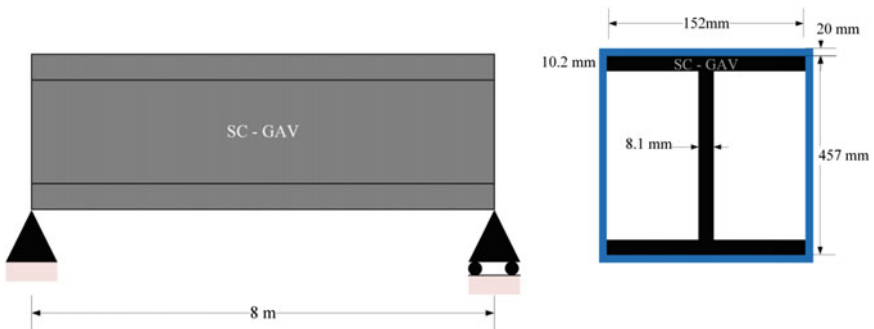


**Fig. 4.18** Box-insulated steel I section for Example 6

Structural calculations will be same as that of Example 5, i.e.,  $M_{fi,ED} = 165 \text{ kN/m}$ , and both web and flange are of Class 1,  $M_{RD} = 354 \text{ kNm}$ , and  $k_{y,\theta} = 0.541$ , which is attained at a temperature of  $577 \text{ }^\circ\text{C}$ . Thermal analysis can also be performed in manner similar to previous examples with  $\lambda_p = 0.25 \text{ W/m }^\circ\text{C}$ ,  $\rho_p = 500 \text{ kg/m}^3$ ,  $p = 2\%$ ,  $c_p = 1500 \text{ J/kg }^\circ\text{C}$ ,  $A_p/V = 170 \text{ m}^{-1}$ ,  $\rho_a = 7850 \text{ kg/m}^3$ , and  $c_a = 600 \text{ J/kg }^\circ\text{C}$ .

Temperature variation is shown in Fig. 4.19 and in Table 4.8. Similar to Example 5, critical temperature is  $577 \text{ }^\circ\text{C}$  (from strength criterion). Thus, the fire rating is about 54 min. Notice that when the same beam was not protected (in Example 5), its fire rating was 20 min. Adding 20 mm of fiberboard protection has increased the fire rating of the beam by almost 3 times.

**Example 7** Evaluate the fire rating for an unprotected column subjected to a dead load of 300 kN and a live load of 2333 kN and having an effective length of 3.5 m with section shown in Fig. 4.20, exposed to four-sided standard ISO-834 fire.

The ambient design gives  $\lambda = 0.612$  with  $N_{RD} = 3112 \text{ kN}$ . At ambient,  $N_{ED} = 2850 \text{ kN}$ .

Section classification:

$$\varepsilon = 0.85 \left[ \frac{235}{f_y} \right]^{0.5} = 0.85 \left[ \frac{235}{275} \right]^{0.5} = 0.786$$

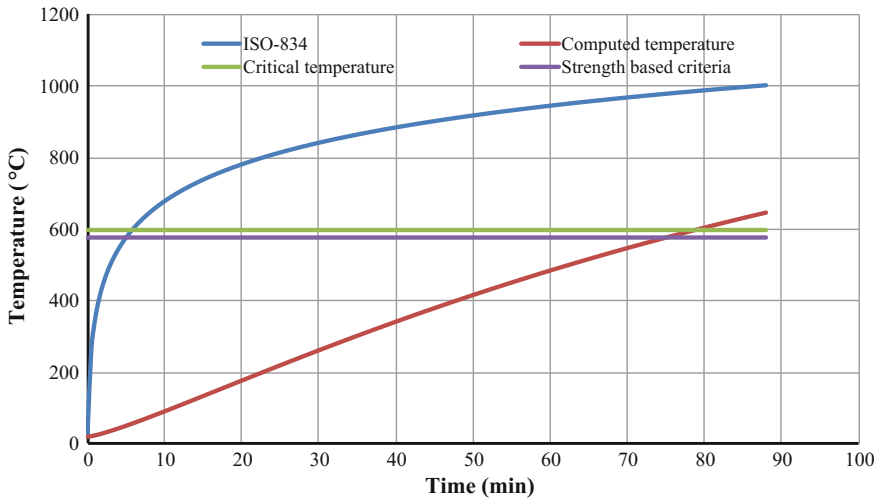


Fig. 4.19 Temperature variation for computing fire rating of box-insulated steel I section

**Table 4.8** Temperature in the steel section of Example 6

Time	$\theta_t$	$\Delta\theta$	$\theta_m$
0	20.00	0.00	20.00
0.5	261.14	2.77	22.77
1	349.21	3.59	26.35
1.5	404.31	4.13	30.49
2	444.50	4.52	35.01
2.5	476.17	4.81	39.81
3	502.29	5.04	44.85
3.5	524.53	5.22	50.07
4	543.89	5.37	55.44
4.5	561.03	5.50	60.94
5	576.41	5.60	66.54
5.5	590.36	5.69	72.24
6	603.12	5.77	78.01
6.5	614.88	5.83	83.84
7	625.78	5.89	89.73
7.5	635.94	5.94	95.67
8	645.46	5.97	101.64
8.5	654.40	6.01	107.65
9	662.85	6.03	113.68
9.5	670.84	6.05	119.73
10	678.43	6.07	125.80
10.5	685.65	6.08	131.88
11	692.54	6.09	137.97
11.5	699.13	6.10	144.07
12	705.44	6.10	150.17
12.5	711.49	6.10	156.26
13	717.31	6.09	162.36
13.5	722.91	6.09	168.45
14	728.31	6.08	174.53
14.5	733.52	6.07	180.60
15	738.56	6.06	186.66
15.5	743.43	6.05	192.71
16	748.15	6.03	198.74
16.5	752.73	6.02	204.76
17	757.17	6.00	210.76
17.5	761.48	5.98	216.74
18	765.67	5.96	222.70
18.5	769.75	5.94	228.64
19	773.72	5.92	234.56
19.5	777.59	5.90	240.46
20	781.35	5.87	246.33

(continued)

**Table 4.8** (continued)

Time	$\theta_t$	$\Delta\theta$	$\theta_m$
20.5	785.03	5.85	252.18
21	788.62	5.83	258.01
21.5	792.13	5.80	263.81
22	795.55	5.77	269.58
22.5	798.90	5.75	275.33
23	802.17	5.72	281.05
23.5	805.38	5.69	286.74
24	808.52	5.67	292.41
24.5	811.59	5.64	298.05
25	814.60	5.61	303.66
25.5	817.56	5.58	309.24
26	820.45	5.55	314.79
26.5	823.29	5.52	320.31
27	826.08	5.49	325.80
27.5	828.82	5.46	331.26
28	831.50	5.43	336.70
28.5	834.14	5.40	342.10
29	836.74	5.37	347.47
29.5	839.29	5.34	352.81
30	841.80	5.31	358.12
30.5	844.26	5.28	363.40
31	846.69	5.25	368.65
31.5	849.08	5.22	373.86
32	851.43	5.19	379.05
32.5	853.74	5.15	384.20
33	856.02	5.12	389.33
33.5	858.26	5.09	394.42
34	860.48	5.06	399.48
34.5	862.66	5.03	404.51
35	864.80	5.00	409.51
35.5	866.92	4.97	414.47
36	869.01	4.94	419.41
36.5	871.07	4.90	424.31
37	873.10	4.87	429.19
37.5	875.11	4.84	434.03
38	877.08	4.81	438.84
38.5	879.04	4.78	443.62
39	880.96	4.75	448.37
39.5	882.87	4.72	453.09
40	884.74	4.69	457.77
40.5	886.60	4.66	462.43

(continued)

**Table 4.8** (continued)

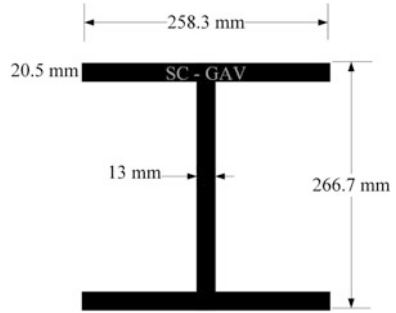
Time	$\theta_t$	$\Delta\theta$	$\theta_m$
41	888.43	4.63	467.06
41.5	890.24	4.60	471.65
42	892.03	4.56	476.22
42.5	893.80	4.53	480.75
43	895.55	4.50	485.25
43.5	897.27	4.47	489.73
44	898.98	4.44	494.17
44.5	900.67	4.41	498.58
45	902.34	4.38	502.97
45.5	903.99	4.35	507.32
46	905.62	4.32	511.65
46.5	907.24	4.30	515.94
47	908.84	4.27	520.21
47.5	910.42	4.24	524.45
48	911.98	4.21	528.65
48.5	913.53	4.18	532.83
49	915.07	4.15	536.98
49.5	916.58	4.12	541.11
50	918.08	4.09	545.20
50.5	919.57	4.06	549.26
51	921.04	4.04	553.30
51.5	922.50	4.01	557.31
52	923.95	3.98	561.29
52.5	925.38	3.95	565.24
53	926.79	3.93	569.17
53.5	928.20	3.90	573.07
54	<b>929.59</b>	3.87	576.94
54.5	930.97	3.84	580.78
55	932.33	3.82	584.60
55.5	933.68	3.79	588.39
56	935.03	3.76	592.15
56.5	936.35	3.74	595.89
57	937.67	3.71	599.60
57.5	938.98	3.68	603.29
58	940.27	3.66	606.95
58.5	941.55	3.63	610.58
59	942.83	3.61	614.19
59.5	944.09	3.58	617.77
60	945.34	3.56	621.33
60.5	946.58	3.53	624.86
61	947.81	3.51	628.36

(continued)

**Table 4.8** (continued)

Time	$\theta_t$	$\Delta\theta$	$\theta_m$
61.5	949.03	3.48	631.85
62	950.24	3.46	635.30
62.5	951.44	3.43	638.74
63	952.64	3.41	642.14
63.5	953.82	3.38	645.53
64	954.99	3.36	648.89
64.5	956.15	3.34	652.22
65	957.31	3.31	655.54
65.5	958.46	3.29	658.83
66	959.59	3.27	662.09
66.5	960.72	3.24	665.33
67	961.84	3.22	668.55
67.5	962.95	3.20	671.75
68	964.06	3.17	674.92
68.5	965.15	3.15	678.08
69	966.24	3.13	681.20
69.5	967.32	3.11	684.31
70	968.39	3.08	687.40
70.5	969.46	3.06	690.46
71	970.51	3.04	693.50
71.5	971.56	3.02	696.52
72	972.61	3.00	699.52
72.5	973.64	2.98	702.49
73	974.67	2.96	705.45
73.5	975.69	2.93	708.38
74	976.70	2.91	711.30
74.5	977.71	2.89	714.19
75	978.71	2.87	717.06
75.5	979.71	2.85	719.91
76	980.69	2.83	722.74
76.5	981.67	2.81	725.56
77	982.65	2.79	728.35
77.5	983.62	2.77	731.12
78	984.58	2.75	733.87
78.5	985.53	2.73	736.60
79	986.48	2.71	739.32
79.5	987.43	2.69	742.01
80	988.37	2.67	744.69

**Fig. 4.20** Steel column I section for Example 7



Class of flange:

$$c = 0.5 [b - 2.t_f - t_w] = 110.3 \text{ mm}$$

$$\frac{c}{t_f} = 5.38$$

Limiting value for Class 1 is  $9\varepsilon = 9 \times 0.786 = 7.07$ . Hence, flange is Class 1  
 Class of web:

$$c = 200.3 \text{ mm}$$

$$\frac{c}{t_w} = 15.6$$

Limiting value for Class 1 is  $9\varepsilon = 72 \times 0.786 = 56.6$ . Hence, web is Class 1.

As the exact end conditions are not known, buckling length in the fire limit state is assumed as 3.5 m. Taking  $\psi = 0.3$  on the variable load gives the following value:

$$N_{ED,fi} = 1.0 \times 770 + 0.3 \times 770 = 1000 \text{ kN}$$

$$k_{y,\theta} = \frac{N_{fi,ED}}{N_{RD,fi}} = \frac{1300}{2850} = 0.57$$

**Strength-based fire rating:**

From Table 4.2, this strength degradation is obtained at a temperature of 565 °C. Degradation in modulus of elasticity at that temperature is given by  $k_{E,\theta} = 0.4115$ . Subsequently, slenderness ratio at 565 °C is computed as computed below:

$$\lambda_{\theta} = \lambda \left[ \frac{k_{y,\theta}}{k_{E,\theta}} \right]^{0.5} = 0.725.$$

The buckling strength reduction factor  $\chi_{fi}$  is determined from the following relationship:

$$\chi_{fi} = \frac{1}{\phi_{\theta} + \sqrt{\phi_{\theta}^2 - \lambda_{\theta}^2}},$$

$$\phi_{\theta} = 0.5 \left[ 1 + 0.65 \sqrt{\frac{235}{f_y} \lambda_{\theta} + \lambda_{\theta}^2} \right].$$

Subsequently, axial resistance at elevated temperatures is computed as given below:

$$N_{b,fi,t,RD} = \chi_{fi} A k_{y,\theta} \frac{f_y}{\gamma_{m,fi}} = 1657 \text{ kN}$$

The detailed calculations are given in Table 4.9 (refer Fig. 4.21 for the temperature variation with respect to time). The fire rating is between 30 and 35 min and can be said to be 30 min, conservatively.

**Example 8** Consider the same column and fire scenario as in Example 7 but with a fiberboard protection of 30 mm. Evaluate its fire rating (Fig. 4.22).

Design at ambient temperature gives  $\lambda = 0.612$  with  $N_{RD} = 3112$  kN. At ambient,  $N_{ED} = 2850$  kN.

Section classification:

$$\varepsilon = 0.85 \left[ \frac{235}{f_y} \right]^{0.5} = 0.85 \left[ \frac{235}{275} \right]^{0.5} = 0.786$$

**Table 4.9** Temperature in the steel section of Example 7

Time (min)	Temperature	$k_{y,\theta}$	$k_{E,\theta}$	$\lambda_{\theta}$	$\phi_t$	$\chi_{fi}$	$N_R$	$N$
0	20.00	1.00	1.00	0.52	0.79	0.72	2674.05	1000
5	101.71	1.00	1.00	0.52	0.79	0.72	2673.00	1000
10	204.92	1.00	0.90	0.55	0.82	0.70	2614.22	1000
15	307.33	1.00	0.79	0.59	0.85	0.68	2544.82	1000
20	403.21	0.99	0.70	0.62	0.88	0.66	2452.08	1000
25	490.36	0.80	0.61	0.60	0.86	0.68	2017.09	1000
30	567.95	0.57	0.40	0.62	0.88	0.67	1408.80	1000
35	636.00	0.38	0.25	0.65	0.91	0.65	924.23	1000
40	694.94	0.24	0.14	0.69	0.94	0.63	566.87	1000

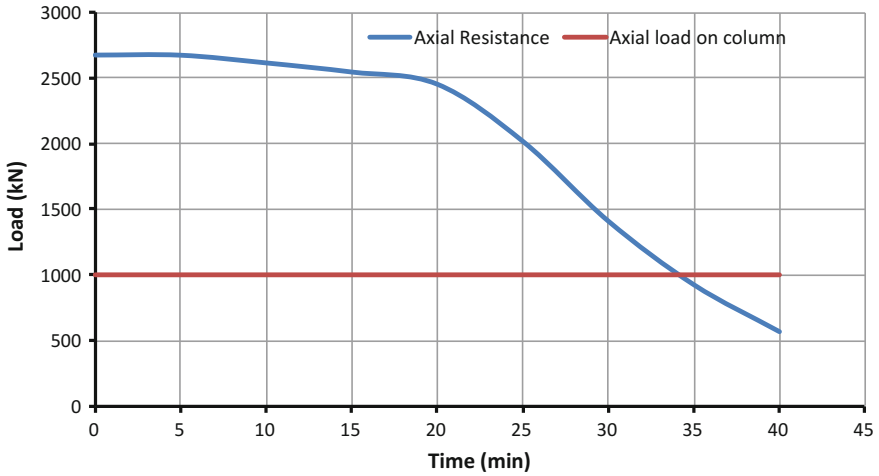
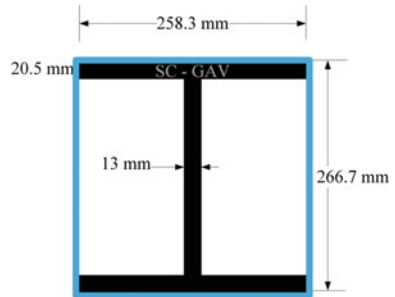


Fig. 4.21 Load versus time graph for unprotected column I section

Fig. 4.22 Protected box column I section for Example 8



Class of flange:

$$c = 0.5 [b - 2.t_f - t_w] = 110.3 \text{ mm}$$

$$\frac{c}{t_f} = 5.38$$

Limiting value for Class 1 is  $9\epsilon = 9 \times 0.786 = 7.07$ . Hence, flange is Class 1  
 Class of web:

$$c = 200.3 \text{ mm}$$

$$\frac{c}{t_w} = 15.6$$

Limiting value for Class 1 is  $9\epsilon = 72 \times 0.786 = 56.6$ . Hence, web is Class 1.

As the exact end conditions are not known, buckling length in the fire limit state is assumed as 3.5 m. Taking  $\psi = 0.3$  on the variable load gives the following:

$$N_{ED,fi} = 1.0 \times 770 + 0.3 \times 770 = 1000 \text{ kN}$$

$$k_{y,\theta} = \frac{N_{fi,ED}}{N_{RD,fi}} = \frac{1300}{2850} = 0.57$$

### Strength-based fire rating:

From Table 4.10, aforementioned strength degradation is obtained at a temperature of 565 °C. The degradation in modulus of elasticity at that temperature is given by  $k_{E,\theta} = 0.4115$ . Subsequently, slenderness ratio at 565 °C is computed as below:

$$\lambda_{\theta} = \lambda \left[ \frac{k_{y,\theta}}{k_{E,\theta}} \right]^{0.5} = 0.725.$$

The buckling strength reduction factor  $\chi_{fi}$  is determined from the following relationship:

**Table 4.10** Temperature in the steel section of Example 8

Time (min)	Temperature	$k_{y,\theta}$	$k_{E,\theta}$	$\lambda_{\theta}$	$\phi_t$	$\chi_{fi}$	$N_R$	$N$
0	20.00	1.00	1.00	0.52	0.79	0.72	2674.05	1000
5	50.65	1.00	1.00	0.52	0.79	0.72	2674.05	1000
10	91.00	1.00	1.00	0.52	0.79	0.72	2674.05	1000
15	133.74	1.00	0.97	0.53	0.80	0.71	2655.77	1000
20	176.93	1.00	0.92	0.54	0.81	0.71	2629.41	1000
25	219.71	1.00	0.88	0.56	0.82	0.70	2604.79	1000
30	261.58	1.00	0.84	0.57	0.83	0.69	2578.40	1000
35	302.38	1.00	0.80	0.59	0.85	0.69	2547.79	1000
40	341.65	1.00	0.76	0.60	0.86	0.68	2519.38	1000
45	379.59	1.00	0.72	0.62	0.87	0.67	2486.20	1000
50	416.30	0.96	0.68	0.62	0.88	0.67	2380.22	1000
55	451.00	0.89	0.65	0.61	0.87	0.67	2214.10	1000
60	484.57	0.81	0.62	0.60	0.86	0.68	2044.18	1000
65	516.64	0.73	0.55	0.60	0.86	0.68	1836.91	1000
70	547.30	0.63	0.46	0.61	0.87	0.67	1579.95	1000
75	576.59	0.54	0.38	0.63	0.88	0.66	1332.11	1000
80	604.54	0.46	0.30	0.65	0.90	0.65	1116.61	1000
85	631.23	0.40	0.25	0.65	0.91	0.65	953.46	1000
90	656.67	0.33	0.21	0.66	0.91	0.65	794.29	1000

$$\chi_{fi} = \frac{1}{\phi_{\theta} + \sqrt{\phi_{\theta}^2 - \lambda_{\theta}^2}},$$

$$\phi_{\theta} = 0.5 \left[ 1 + 0.65 \sqrt{\frac{235}{f_y} \lambda_{\theta} + \lambda_{\theta}^2} \right].$$

Subsequently, axial resistance at elevated temperatures is computed as below:

$$N_{b,fi,t,RD} = \chi_{fi} A k_{y,\theta} \frac{f_y}{\gamma_{m,fi}} = 1657 \text{ kN}$$

The calculations involved are presented in Table 4.10 (refer Fig. 4.23 for temperature variation in the member with respect to time). Fire rating of this column can be said to be 80 min. Notice that addition of fire protection has more than doubled the fire rating of the column.

**Example 9** A beam is simply supported over a span of 8 m as shown in Fig. 4.24. It carries a permanent loading of 17.8 kN/m and an imposed load of 9.375 kN/m. Design a material board for this beam for a 60-min fire rating when subjected to ISO-834 standard fire exposure on three sides.

Structural Analysis:

For the given beam, load combination for fire is considered as per EN 1991-1-2 and is given by:

$$= 1 \times \text{P.L} + 0.3 \times \text{I.L.}$$

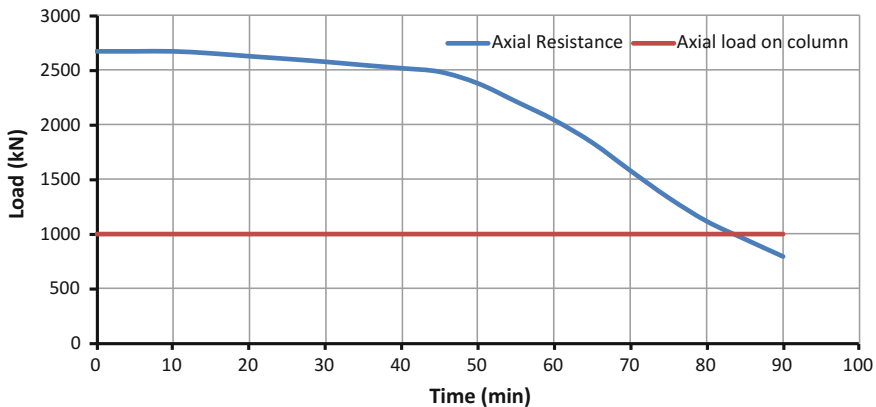


Fig. 4.23 Load versus time graph for protected column I section

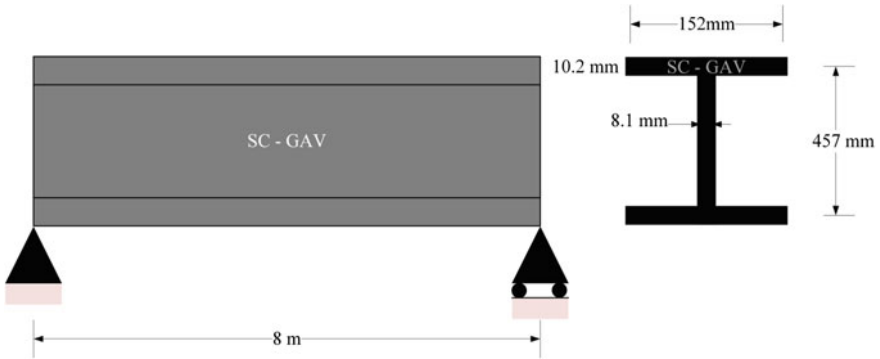


Fig. 4.24 Simply supported I section for Example 9

Design moment on the structure,  $M_{fi,ED}$ , is computed as below:

$$= 3.75 \times (17.8 + 0.3 \times 9.375) \times 8^2/8 = 163 \text{ kN/m.}$$

Section classification:

$$\varepsilon = 0.85 \left[ \frac{235}{f_y} \right]^{0.5} = 0.85 \left[ \frac{235}{275} \right]^{0.5} = 0.786$$

Class of flange:

$$\varepsilon = 0.85 \left[ \frac{235}{f_y} \right]^{0.5} = 0.85 \left[ \frac{235}{275} \right]^{0.5} = 0.786$$

$$c = 0.5 [b - 2.t_f - t_w] = 62.6 \text{ mm}$$

$$\frac{c}{t_f} = 4.71$$

Limiting value for Class 1 is  $9\varepsilon = 9 \times 0.786 = 7.07$ . Hence, flange is Class 1  
 Class of web:

$$c = 407.6 \text{ mm}$$

$$\frac{c}{t_w} = 50.3$$

Limiting value for Class 1 is  $9\varepsilon = 72 \times 0.786 = 56.6$ . Hence, web is Class 1.

**Evaluation of fire rating in accordance with EN 1993 1-2:**

**Strength-based fire resistance:**

Design moment of resistance  $M_{RD} = 275 \times 1287 \times 10^3/1.0 = 354 \text{ kNm}$ .

$$k_{y,\theta} = \frac{M_{fi,ED}}{M_{RD}} = \frac{163}{354} = 0.460$$

As it is a three-sided exposure, effective value of  $k_{y,\theta}$  is obtained by further dividing with 0.85 as 0.541. From Table 4.2, this strength degradation is obtained at a temperature of 577 °C.

Fire protection data:

Following data can be used for mineral fiber: (i.e.,  $q_p = 500 \text{ kg/m}^3$ ,  $p = 2\%$ ,  $c_p = 1500 \text{ J/kgC}$ ,  $\lambda_p = 0.25 \text{ W/mC}$ ). For box protection,  $A_m/V = 165 \text{ m}^{-1}$ . As per Wickstorm's method, thickness of the required protection board is computed as:

$$d_p = \frac{\frac{V}{\lambda_p A_m} + \sqrt{\left(\frac{V}{\lambda_p A_m}\right)^2 + 4 \frac{\rho_p}{\rho_a \lambda_p} \left[\frac{t_{fi,d}}{40(\theta_{a,t} - 140)}\right]^{1/3}}}{2 \frac{\rho_p}{\rho_a \lambda_p}}$$

where  $d_p$  is the thickness of protection,  $\rho_a$  is the density of the material,  $\rho_p$  is the density of the protection material  $A_m$  is the area of the unit length exposure,  $V$  is the volume of unit length section,  $\theta_{a,t}$  is the temperature in member,  $\lambda_p$  is the coefficient of thermal conductivity of the protection, and  $t_{fi,d}$  is the time of exposure. Upon substitution, thickness of protection is found to be 0.021 m. Let us provide 25-mm-thick board for protection. Temperature variation with this protection, as calculated by methods discussed earlier, is given in Table 4.11. It can be observed that steel temperature at 60 min is 540 °C which is lesser than the critical temperature of 577 °C as governed by strength degradation. Hence, the beam with 25 mm protection will have a rating of 60 min.

**Example 10** A  $254 \times 254 \times 107$  UC beam carries a permanent load and a variable axial load both equal to 1270 kN at ambient conditions. The effective length of the column is 3.5 m. Design box protection is to ensure a 90-min fire rating for the column. Section is shown in Fig. 4.25.

Conventional design at ambient temperature gives  $\lambda = 0.612$  with  $N_{RD} = 3112 \text{ kN}$  and  $N_{ED} = 2850 \text{ kN}$ .

**Table 4.11** Temperature in the steel section of Example 9

Time	$\theta_t$	$\Delta\theta$	$\theta_m$
0	20.00	0.00	20.00
0.5	261.14	2.18	22.18
1	349.21	2.80	24.98
1.5	404.31	3.23	28.21
2	444.50	3.53	31.74
2.5	476.17	3.77	35.51
3	502.29	3.95	39.46
3.5	524.53	4.10	43.56
4	543.89	4.23	47.79
4.5	561.03	4.34	52.13
5	576.41	4.43	56.56
5.5	590.36	4.51	61.07
6	603.12	4.58	65.65
6.5	614.88	4.64	70.29
7	625.78	4.69	74.98
7.5	635.94	4.74	79.71
8	645.46	4.78	84.49
8.5	654.40	4.81	89.30
9	662.85	4.84	94.14
9.5	670.84	4.87	99.01
10	678.43	4.89	103.90
10.5	685.65	4.91	108.81
11	692.54	4.93	113.74
11.5	699.13	4.94	118.68
12	705.44	4.95	123.63
12.5	711.49	4.96	128.59
13	717.31	4.97	133.56
13.5	722.91	4.97	138.53
14	728.31	4.98	143.51
14.5	733.52	4.98	148.49
15	738.56	4.98	153.47
15.5	743.43	4.98	158.44
16	748.15	4.98	163.42
16.5	752.73	4.97	168.39
17	757.17	4.97	173.36
17.5	761.48	4.96	178.32
18	765.67	4.96	183.28
18.5	769.75	4.95	188.22
19	773.72	4.94	193.16
19.5	777.59	4.93	198.09
20	781.35	4.92	203.01

(continued)

**Table 4.11** (continued)

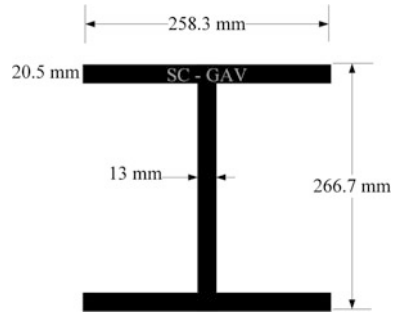
Time	$\theta_t$	$\Delta\theta$	$\theta_m$
20.5	785.03	4.91	207.92
21	788.62	4.90	212.82
21.5	792.13	4.89	217.71
22	795.55	4.87	222.59
22.5	798.90	4.86	227.45
23	802.17	4.85	232.30
23.5	805.38	4.83	237.13
24	808.52	4.82	241.95
24.5	811.59	4.81	246.76
25	814.60	4.79	251.55
25.5	817.56	4.77	256.32
26	820.45	4.76	261.08
26.5	823.29	4.74	265.82
27	826.08	4.73	270.55
27.5	828.82	4.71	275.26
28	831.50	4.69	279.95
28.5	834.14	4.67	284.63
29	836.74	4.66	289.28
29.5	839.29	4.64	293.92
30	841.80	4.62	298.54
30.5	844.26	4.60	303.15
31	846.69	4.58	307.73
31.5	849.08	4.57	312.30
32	851.43	4.55	316.85
32.5	853.74	4.53	321.37
33	856.02	4.51	325.88
33.5	858.26	4.49	330.38
34	860.48	4.47	334.85
34.5	862.66	4.45	339.30
35	864.80	4.43	343.73
35.5	866.92	4.41	348.14
36	869.01	4.39	352.54
36.5	871.07	4.37	356.91
37	873.10	4.35	361.27
37.5	875.11	4.33	365.60
38	877.08	4.31	369.91
38.5	879.04	4.29	374.21
39	880.96	4.27	378.48
39.5	882.87	4.25	382.74
40	884.74	4.23	386.97
40.5	886.60	4.21	391.19

(continued)

**Table 4.11** (continued)

Time	$\theta_t$	$\Delta\theta$	$\theta_m$
41	888.43	4.19	395.38
41.5	890.24	4.17	399.56
42	892.03	4.15	403.71
42.5	893.80	4.13	407.84
43	895.55	4.11	411.96
43.5	897.27	4.09	416.05
44	898.98	4.07	420.12
44.5	900.67	4.05	424.18
45	902.34	4.03	428.21
45.5	903.99	4.01	432.22
46	905.62	3.99	436.22
46.5	907.24	3.97	440.19
47	908.84	3.95	444.14
47.5	910.42	3.93	448.08
48	911.98	3.91	451.99
48.5	913.53	3.89	455.88
49	915.07	3.87	459.75
49.5	916.58	3.85	463.61
50	918.08	3.83	467.44
50.5	919.57	3.81	471.25
51	921.04	3.79	475.05
51.5	922.50	3.77	478.82
52	923.95	3.75	482.58
52.5	925.38	3.73	486.31
53	926.79	3.72	490.03
53.5	928.20	3.70	493.72
54	929.59	3.68	497.40
54.5	930.97	3.66	501.06
55	932.33	3.64	504.69
55.5	933.68	3.62	508.31
56	935.03	3.60	511.91
56.5	936.35	3.58	515.49
57	937.67	3.56	519.05
57.5	938.98	3.54	522.59
58	940.27	3.52	526.12
58.5	941.55	3.50	529.62
59	942.83	3.49	533.11
59.5	944.09	3.47	536.57
60	945.34	3.45	540.02

**Fig. 4.25** Steel column I section for Example 10



Section classification:

$$\varepsilon = 0.85 \left[ \frac{235}{f_y} \right]^{0.5} = 0.85 \left[ \frac{235}{275} \right]^{0.5} = 0.786$$

Class of flange:

$$c = 0.5 [b - 2.t_f - t_w] = 110.3 \text{ mm}$$

$$\frac{c}{t_f} = 5.38$$

Limiting value for Class 1 is  $9\varepsilon = 9 \times 0.786 = 7.07$ . Hence, flange is Class 1  
 Class of web:

$$c = 200.3 \text{ mm}$$

$$\frac{c}{t_w} = 15.6$$

Limiting value for Class 1 is  $9\varepsilon = 72 \times 0.786 = 56.6$ . Hence, web is Class 1.  
 Taking  $\psi = 0.3$  on the variable, load is computed as:

$$N_{ED,fi} = 1.0 \times 1270 + 0.3 \times 1270 = 1653 \text{ kN}$$

$$k_{y,\theta} = \frac{N_{fi,ED}}{N_{RD,fi}} = \frac{1300}{2850} = 0.57$$

**Strength-based fire rating:**

From Table 4.2, this strength degradation is obtained at a temperature of 565 °C. Degradation in modulus of elasticity at that temperature is given by  $k_{E,\theta} = 0.4115$ . Subsequently, slenderness ratio at 565 °C is computed as below:

$$\lambda_{\theta} = \lambda \left[ \frac{k_{y,\theta}}{k_{E,\theta}} \right]^{0.5} = 0.725.$$

The buckling strength reduction factor  $\chi_{fi}$  is determined from the following relationship:

$$\chi_{fi} = \frac{1}{\phi_{\theta} + \sqrt{\phi_{\theta}^2 - \lambda_{\theta}^2}},$$

$$\phi_{\theta} = 0.5 \left[ 1 + 0.65 \sqrt{\frac{235}{f_y}} \lambda_{\theta} + \lambda_{\theta}^2 \right].$$

Subsequently, axial resistance at elevated temperatures is computed as below:

$$N_{b,fi,t,RD} = \chi_{fi} A k_{y,\theta} \frac{f_y}{\gamma_{m,fi}} = 1657 \text{ kN}$$

Fire protection data:

Mineral fiber (i.e.,  $\rho_p = 500 \text{ kg/m}^3$ ,  $p = 2\%$ ,  $c_p = 1500 \text{ J/kgC}$ ,  $\lambda_p = 0.25 \text{ W/mC}$ ). For a four-sided box,  $A_m/V = 85 \text{ m}^{-1}$ . As per Wickstorm's method, thickness of protection required is given by the following relationship:

$$d_p = \frac{\frac{V}{\lambda_p A_m} + \sqrt{\left(\frac{V}{\lambda_p A_m}\right)^2 + 4 \frac{\rho_p}{\rho_a \lambda_p} \left[ \frac{t_{fi,d}}{40(\theta_{a,t} - 140)} \right]^{1/3}}}{2 \frac{\rho_p}{\rho_a \lambda_p}}$$

where  $d_p$  is the thickness of protection,  $\rho_a$  is the density of the material,  $\rho_p$  is the density of the protection material,  $A_m$  is the area of the unit length exposure,  $V$  is the volume of unit length section,  $\theta_{a,t}$  is the temperature in member,  $\lambda_p$  is the coefficient of thermal conductivity of the protection, and  $t_{fi,d}$  is the time of exposure. Upon substitution of above, thickness of protection is 0.01984 m. Let us provide 20-mm-thick board. Temperature variation with this protection, as calculated by methods discussed earlier, is given in Table 4.11. It can be observed that steel temperature at 90 min is 517 °C which is lesser than the critical temperature of 565 °C as governed by strength degradation. Hence, the beam with 25 mm protection will have a rating of 90 min (Table 4.12).

**Table 4.12** Temperature in the steel section of Example 10

Time	$\theta_t$	$\Delta\theta$	$\theta_m$
0.5	261.14	1.17	21.17
1	349.21	1.56	22.73
1.5	404.31	1.80	24.53
2	444.50	1.98	26.51
2.5	476.17	2.12	28.63
3	502.29	2.23	30.86
3.5	524.53	2.33	33.19
4	543.89	2.40	35.59
4.5	561.03	2.47	38.07
5	576.41	2.53	40.60
5.5	590.36	2.59	43.19
6	603.12	2.64	45.82
6.5	614.88	2.68	48.50
7	625.78	2.72	51.22
7.5	635.94	2.75	53.97
8	645.46	2.78	56.75
8.5	654.40	2.81	59.57
9	662.85	2.84	62.40
9.5	670.84	2.86	65.27
10	678.43	2.88	68.15
10.5	685.65	2.91	71.06
11	692.54	2.92	73.98
11.5	699.13	2.94	76.92
12	705.44	2.96	79.88
12.5	711.49	2.97	82.85
13	717.31	2.98	85.83
13.5	722.91	3.00	88.83
14	728.31	3.01	91.84
14.5	733.52	3.02	94.86
15	738.56	3.03	97.89
15.5	743.43	3.04	100.92
16	748.15	3.04	103.97
16.5	752.73	3.05	107.02
17	757.17	3.06	110.08
17.5	761.48	3.06	113.14
18	765.67	3.07	116.21
18.5	769.75	3.07	119.28
19	773.72	3.08	122.36
19.5	777.59	3.08	125.44
20	781.35	3.09	128.53
20.5	785.03	3.09	131.62

(continued)

**Table 4.12** (continued)

Time	$\theta_t$	$\Delta\theta$	$\theta_m$
21	788.62	3.09	134.71
21.5	792.13	3.09	137.80
22	795.55	3.09	140.89
22.5	798.90	3.09	143.99
23	802.17	3.10	147.08
23.5	805.38	3.10	150.18
24	808.52	3.10	153.28
24.5	811.59	3.10	156.37
25	814.60	3.10	159.47
25.5	817.56	3.10	162.57
26	820.45	3.09	165.66
26.5	823.29	3.09	168.75
27	826.08	3.09	171.84
27.5	828.82	3.09	174.93
28	831.50	3.09	178.02
28.5	834.14	3.09	181.11
29	836.74	3.08	184.19
29.5	839.29	3.08	187.27
30	841.80	3.08	190.35
30.5	844.26	3.08	193.43
31	846.69	3.07	196.50
31.5	849.08	3.07	199.57
32	851.43	3.07	202.64
32.5	853.74	3.06	205.70
33	856.02	3.06	208.76
33.5	858.26	3.05	211.81
34	860.48	3.05	214.86
34.5	862.66	3.05	217.91
35	864.80	3.04	220.95
35.5	866.92	3.04	223.99
36	869.01	3.03	227.02
36.5	871.07	3.03	230.05
37	873.10	3.02	233.08
37.5	875.11	3.02	236.10
38	877.08	3.01	239.11
38.5	879.04	3.01	242.12
39	880.96	3.00	245.13
39.5	882.87	3.00	248.13
40	884.74	2.99	251.12
40.5	886.60	2.99	254.11
41	888.43	2.98	257.09

(continued)

**Table 4.12** (continued)

Time	$\theta_t$	$\Delta\theta$	$\theta_m$
41.5	890.24	2.98	260.07
42	892.03	2.97	263.04
42.5	893.80	2.97	266.01
43	895.55	2.96	268.97
43.5	897.27	2.96	271.92
44	898.98	2.95	274.87
44.5	900.67	2.94	277.82
45	902.34	2.94	280.75
45.5	903.99	2.93	283.68
46	905.62	2.93	286.61
46.5	907.24	2.92	289.53
47	908.84	2.91	292.44
47.5	910.42	2.91	295.35
48	911.98	2.90	298.25
48.5	913.53	2.89	301.14
49	915.07	2.89	304.03
49.5	916.58	2.88	306.91
50	918.08	2.87	309.78
50.5	919.57	2.87	312.65
51	921.04	2.86	315.51
51.5	922.50	2.85	318.37
52	923.95	2.85	321.22
52.5	925.38	2.84	324.06
53	926.79	2.83	326.89
53.5	928.20	2.83	329.72
54	929.59	2.82	332.54
54.5	930.97	2.81	335.36
55	932.33	2.81	338.16
55.5	933.68	2.80	340.97
56	935.03	2.79	343.76
56.5	936.35	2.79	346.55
57	937.67	2.78	349.33
57.5	938.98	2.77	352.10
58	940.27	2.77	354.87
58.5	941.55	2.76	357.63
59	942.83	2.75	360.38
59.5	944.09	2.75	363.12
60	945.34	2.74	365.86
60.5	946.58	2.73	368.59
61	947.81	2.72	371.32
61.5	949.03	2.72	374.03

(continued)

**Table 4.12** (continued)

Time	$\theta_t$	$\Delta\theta$	$\theta_m$
62	950.24	2.71	376.74
62.5	951.44	2.70	379.45
63	952.64	2.70	382.14
63.5	953.82	2.69	384.83
64	954.99	2.68	387.51
64.5	956.15	2.67	390.19
65	957.31	2.67	392.85
65.5	958.46	2.66	395.51
66	959.59	2.65	398.17
66.5	960.72	2.65	400.81
67	961.84	2.64	403.45
67.5	962.95	2.63	406.08
68	964.06	2.62	408.71
68.5	965.15	2.62	411.32
69	966.24	2.61	413.93
69.5	967.32	2.60	416.54
70	968.39	2.60	419.13
70.5	969.46	2.59	421.72
71	970.51	2.58	424.30
71.5	971.56	2.57	426.87
72	972.61	2.57	429.44
72.5	973.64	2.56	432.00
73	974.67	2.55	434.55
73.5	975.69	2.55	437.10
74	976.70	2.54	439.64
74.5	977.71	2.53	442.17
75	978.71	2.52	444.69
75.5	979.71	2.52	447.21
76	980.69	2.51	449.72
76.5	981.67	2.50	452.22
77	982.65	2.49	454.71
77.5	983.62	2.49	457.20
78	984.58	2.48	459.68
78.5	985.53	2.47	462.15
79	986.48	2.47	464.62
79.5	987.43	2.46	467.08
80	988.37	2.45	469.53
80.5	989.30	2.44	471.97
81	990.22	2.44	474.41
81.5	991.15	2.43	476.84
82	992.06	2.42	479.26

(continued)

**Table 4.12** (continued)

Time	$\theta_t$	$\Delta\theta$	$\theta_m$
82.5	992.97	2.42	481.68
83	993.87	2.41	484.09
83.5	994.77	2.40	486.49
84	995.67	2.39	488.89
84.5	996.55	2.39	491.27
85	997.44	2.38	493.65
85.5	998.31	2.37	496.03
86	999.19	2.37	498.39
86.5	1000.05	2.36	500.75
87	1000.92	2.35	503.11
87.5	1001.77	2.35	505.45
88	1002.63	2.34	507.79
88.5	1003.47	2.33	510.12
89	1004.32	2.32	512.44
89.5	1005.15	2.32	514.76
90	1005.99	2.31	517.07

**Example 11** An I section beam is simply supported over a span of 8 m as with a depth of 452 mm, width of 157 mm, and thickness of 10.2 mm. It carries a permanent loading of 4.75 kN/m<sup>2</sup> and an imposed load of 0.75 kN/m<sup>2</sup>. Evaluate the thickness of fire proof board required such that the fire rating when subjected to hydrocarbon fire exposure is 90 min.

Structural Analysis:

For the given beam, load combination for fire is considered as per EN 1991-1-2 and is given by:

$$= 1 \times \text{P.L} + 0.3 \times \text{I.L.}$$

Design moment on the structure,  $M_{fi,ED}$ , is computed as below:

$$= 3.75 \times (4.75 + 0.3 \times 2.5) \times 8^2/8 = 163 \text{ kN/m.}$$

Section classification:

$$\varepsilon = 0.85 \left[ \frac{235}{f_y} \right]^{0.5} = 0.85 \left[ \frac{235}{275} \right]^{0.5} = 0.786$$

Class of flange:

$$\varepsilon = 0.85 \left[ \frac{235}{f_y} \right]^{0.5} = 0.85 \left[ \frac{235}{275} \right]^{0.5} = 0.786$$

$$c = 0.5[b - 2.t_f - t_w] = 62.6 \text{ mm}$$

$$\frac{c}{t_f} = 4.71$$

Limiting value for Class 1 is  $9\varepsilon = 9 \times 0.786 = 7.07$ . Hence, flange is Class 1  
Class of web:

$$c = 407.6 \text{ mm}$$

$$\frac{c}{t_w} = 50.3$$

Limiting value for Class 1 is  $9\varepsilon = 72 \times 0.786 = 56.6$ . Hence, web is Class 1.

### Evaluation of fire rating in accordance with EN 1993 1-2:

#### Strength-based fire resistance:

Design moment of resistance  $M_{RD} = 354 \text{ kNm}$  and  $k_{y,\theta} = \frac{163}{354} = 0.46 \text{ kNm}$

As it is a three-sided exposure, effective value of  $k_{y,\theta}$  is obtained by further dividing with 0.85 as 0.54. From Table, aforementioned strength degradation is obtained at a temperature of  $577 \text{ }^\circ\text{C}$ . Hydrocarbon fire curve is given by the following relationship:

$$T = 20 + 1080(1 - 0.325 e^{-0.167t} - 0.675 e^{-2.5t})$$

Thickness required for a fire rating of 90 min is obtained as 45 mm from the relation used in previous examples. Results of thermal analysis of the section with 45-mm fiberboard protection are shown below:

Time	(Am/Vm)	$\theta_t$	$\Delta\theta$	$\theta_m$
0	195	20	0	20
5	195	949.4253	3.69	53.63
10	195	1035.803	3.88	91.82
20	195	1089.539	3.78	168.98
30	195	1099.654	3.52	241.99
40	195	1101.558	3.25	309.62
50	195	1101.917	3.00	371.99
60	195	1101.984	2.76	429.46
70	195	1101.997	2.54	482.42
80	195	1101.999	2.34	531.20
90	195	1102	2.16	576.14

It can be observed that at 90 min, temperature of the beam is  $576.14 \text{ }^\circ\text{C}$  which is lesser than the critical temperature of  $577 \text{ }^\circ\text{C}$ . Hence, the protected beam will have the desired 90 min of fire rating.

**Example 12** A Grade S275 C-Channel section beam is simply supported over a span of 8 m as with a depth of 400 mm, width of 150 mm, and thickness of 10 mm.

It carries a permanent loading of  $2.75 \text{ kN/m}^2$  and an imposed load of  $0.75 \text{ kN/m}^2$ . Evaluate the thickness of fire proof board required such that the fire rating when subjected to hydrocarbon standard fire exposure is 90 min.

Structural Analysis:

For the given beam, load combination for fire is considered as per EN 1991-1-2 and is given by:

$$= 1 \times \text{P.L} + 0.3 \times \text{I.L.}$$

Design moment on the structure,  $M_{\text{fi,ED}}$ , is computed as

$$= 3.75 \times (2.75 + 0.3 \times 2.5) \times 8^2 / 8 = 110 \text{ kNm.}$$

Section classification:

$$\varepsilon = 0.85 \left[ \frac{235}{f_y} \right]^{0.5} = 0.85 \left[ \frac{235}{275} \right]^{0.5} = 0.786$$

Class of flange:

$$\varepsilon = 0.85 \left[ \frac{235}{f_y} \right]^{0.5} = 0.85 \left[ \frac{235}{275} \right]^{0.5} = 0.786$$

$$c = 0.5 [b - 2.t_f - t_w] = 62.6 \text{ mm}$$

$$\frac{c}{t_f} = 4.71$$

Limiting value for Class 1 is  $9\varepsilon = 9 \times 0.786 = 7.07$ . Hence, flange is Class 1  
Class of web:

$$c = 407.6 \text{ mm}$$

$$\frac{c}{t_w} = 50.3$$

Limiting value for Class 1 is  $9\varepsilon = 72 \times 0.786 = 56.6$ . Hence, web is Class 1.

**Evaluation of fire rating in accordance with EN 1993 1-2:**

**Strength-based fire resistance:**

Design moment of resistance  $M_{\text{RD}} = 200.4 \text{ kNm}$  and  $k_{y,\theta} = \frac{110}{200.4} = 0.55 \text{ kNm}$

As it is a three-sided exposure, effective value of  $k_{y,\theta}$  is obtained by further dividing with 0.85 as 0.64. From Table, aforementioned strength degradation is obtained at a temperature of  $620 \text{ }^\circ\text{C}$ .

The hydrocarbon fire curve is given by the following equation:

$$T = 20 + 1080 * (1 - 0.325 * e^{-0.167*t} - 0.675 * e^{-2.5*t})$$

After iterative thermal analysis, thickness required for a fire rating of 90 min is obtained as 40 mm. Thermal analysis with 40 mm protection is shown in the table below:

Time	$\theta_t$	$\Delta\theta$	$\theta_m$
0	20.00	0.00	20.00
5	949.42	3.78	54.41
10	1035.80	3.98	93.58
20	1089.54	3.87	172.64
30	1099.65	3.60	247.29
40	1101.56	3.32	316.28
50	1101.92	3.05	379.76
60	1101.98	2.80	438.13
70	1102.00	2.58	491.78
80	1102.00	2.37	541.10
90	1102.00	2.18	586.43

It can be observed that steel temperature at 90 min is lesser than the critical temperature of 620 °C.

## 4.10 Design of Concrete Members Under Fire

Similar to design of steel structures, fire-resistant design of concrete structures proceeds through temperature and strength assessments. Fire ratings are computed based on both temperature and strength criteria. Temperature criterion is applied on the maximum temperature of any tension rebar of a beam, while strength criterion is applicable to all concrete structures. It provides a measure of the time up to which a structural member can sustain the imposed loads when exposed to a standard fire.

### 4.10.1 Temperature Analysis

Temperature distribution within any given reinforced cement concrete section (RCC) can be computed using both numerical (finite element method and finite difference method) and empirical methods. Empirical methods are easy to implement than the former ones. Two such available empirical methods for the determination of temperature profile are discussed below. Please note that unlike steel, thermal conductivity of concrete is very low. Hence, highly nonlinear thermal gradients can form within deep concrete members. Obviously, lumped capacity

assumption cannot be used for concrete structures. Due to low thermal conductivity, even for members of reasonable cross section, temperatures far from the surface take very long time to rise. This enables idealization of the cross section of the structural member as a semi-infinite body with one face exposed to fire and the other face at infinity. Such an idealization allows analytical closed-form solutions of the heat transfer equation. This approach is used to develop both the semianalytical methods of assessing temperature rise within concrete sections, as detailed below.

### 4.10.2 Wickstrom's Method

Temperature rise ( $\Delta\theta$ ) above the ambient temperature in a normal weight concrete element is given by the following relationships:

(a) For uniaxial heat flow,

$$\Delta\theta = n_x n_w \Delta\theta_f \quad (4.44)$$

(b) For biaxial heat flow,

$$\Delta\theta_{xy} = (n_w(n_x + n_y - 2n_x n_y) + n_x n_y) \Delta\theta_f \quad (4.45)$$

where  $n_x$ ,  $n_y$ , and  $n_w$  are thermal properties of concrete and given by:

$$n_x = 0.18 \ln u_x - 0.81, \quad n_y = 0.18 \ln u_y - 0.81 \quad (4.46)$$

$$n_w = 1 - 0.0616t^{-0.88} \quad (4.47)$$

with

$$u_x = \frac{a}{a_c} \frac{t}{x^2} \quad (4.48)$$

where  $a$  is the thermal diffusivity of the concrete and  $a_c$  is the reference thermal diffusivity of normal weight concrete given by Wickstrom ( $a_c = 0.417 \times 10^{-6} \text{ m}^2/\text{s}$ ).

When  $a = a_c$ , following equations are valid:

$$n_x = 0.18 \ln \frac{t}{x^2} - 0.81 \quad (4.49)$$

with  $x$  subject to the limit:  $x \geq 2h - 3.6\sqrt{0.0015t}$

where  $t$  is time in hours,  $(x, y)$  are depths into the member ( $m$ ), and  $h$  is the overall depth of the considered section.

### 4.10.3 Hertz's Method

The unidirectional time-dependent temperature increment  $\Delta\theta(x, t)$  is given by the following relationship:

$$\Delta\theta(x, t) = f_1(x, t) + f_2(x, t) + f_3(x, t) \quad (4.50)$$

where the above functions are solutions to the heat transfer equation for particular boundary conditions, as discussed previously. The functions are given as follows:

$$f_1(x, t) = E \left( 1 - \frac{x}{3.363\sqrt{at}} \right)^2 \quad (4.51)$$

$$f_2(x, t) = D e^{-x\sqrt{\frac{\pi}{2Ca}}} \sin \left( \frac{\pi t}{C} - x\sqrt{\frac{\pi}{2Ca}} \right) \quad (4.52)$$

$$f_3(x, t) = \frac{D + E}{2(e^{LC} - 1)} \left( 1 - e^{(L(t-C) - x\sqrt{\frac{L}{a}})} \right) \quad (4.53)$$

where  $a$  is the thermal conductivity. Above functions are set equal to zero, respectively, if the following conditions are satisfied:

$$1 - \frac{x}{3.363\sqrt{at}} \leq 0 \quad (4.54)$$

$$\frac{\pi t}{C} - x\sqrt{\frac{\pi}{2Ca}} \leq 0 \quad (4.55)$$

$$L(t - C) - x\sqrt{\frac{L}{a}} \leq 0 \quad (4.56)$$

where  $L$  is dependent on the temperature curve during cooling and is given by the following relationship:

$$L = \frac{2}{C} \ln \left( \frac{3D}{E - 2D} \right) \quad (4.57)$$

where  $E$ ,  $D$ , and  $C$  parameters are dependent on the heating regime. It is to be noted that one of the parameters (namely  $L$ ) does not demand detailed computation as  $f_3$  is always zero when exposed to standard furnace temperature–time curve. Parametric values of  $C$ ,  $D$ , and  $E$  are given in Table 4.13, for exposure to standard furnace curve. It is to be noted that  $C$  is equal to twice of that of the required time period. Above calculations are for one-dimensional heat flow. For two-dimensional heat flow, temperature increment is given by the following relationship:

**Table 4.13** Parameters for temperature analysis of concrete members under standard conditions

Time (h)	C (h)	D (°C)	E (°C)
0.5	1.0	150	600
1.0	2.0	220	600
1.5	3.0	310	600
2.0	4.0	360	600
3.0	6.0	410	600
4.0	8.0	460	600

$$\Delta\theta(x, y, t) = \Delta\theta_0(\xi_{\theta,x} + \xi_{\theta,y} - \xi_{\theta,x}\xi_{\theta,y}) \quad (4.58)$$

where  $\Delta\theta_0$  is the surface temperature rise at time ( $t$ ),  $\xi_{\theta,x}\Delta\theta_0$  is the temperature rise at the point being considered assuming one-dimensional heat flow on the  $x$  direction, and  $\xi_{\theta,y}\Delta\theta_0$  is the temperature rise for heat flow on the  $y$  direction.

## 4.11 Strength Assessment of Concrete Members Under Fire

EN 1991-1-2 provides two semiempirical methods for determining the section resistance: (i) 500 °C isotherm method and (ii) method of slices given by Hertz. Both the methods effectively utilize the same principles employed for calculation of capacity of structural members at ambient temperatures. Effects of temperature are incorporated through relevant strength reduction factors and related idealizations.

### 4.11.1 500 °C Isotherm Method

This is also called as reduced section method. Anderberg proposed this method following the analysis of a number of fire tests carried out on flexural reinforced concrete elements. As the name suggests, this method utilizes the isotherm of 500 °C as a basis for design calculations. Isotherms can be computed using results from temperature assessment. Eurocode provides temperature contours for certain cross-sectional dimensions, which can also be utilized to determine the 500 °C isotherm. The following assumptions are made during design calculations:

- (1) Concrete within the 500 °C isotherm retains its full strength, while that beyond the 500 °C contour has zero strength.
- (2) Consequently, a reduced cross section of the structural member is considered in design calculations.
- (3) All rebars are considered for strength calculations with appropriate strength reduction factors as given in Tables 4.14 and 4.15, for strains less than 2% and

**Table 4.14** Strength reduction factors for compression and tension reinforcement ( $\epsilon_{s,fi} < 2\%$ )

Temperature (°C)	$k_s(\theta)$
$0 \leq T \leq 20$	1
$100 \leq T \leq 400$	$0.7 - 0.3 \left( \frac{\theta - 400}{300} \right)$
$400 \leq T \leq 500$	$0.5 - 0.13 \left( \frac{\theta - 500}{100} \right)$
$500 \leq T \leq 700$	$0.1 - 0.47 \left( \frac{\theta - 700}{200} \right)$
$700 \leq T \leq 1200$	$0.1 \left( \frac{1200 - \theta}{500} \right)$

**Table 4.15** Strength reduction factors for tension reinforcement ( $\epsilon_{s,fi} > 2\%$ )

Temperature (°C)	$k_s(\theta)$
$20 \leq T \leq 400$	1
$400 \leq T \leq 500$	$0.77 - 0.22 \left( \frac{\theta - 500}{200} \right)$
$500 \leq T \leq 600$	$0.47 - 0.31 \left( \frac{\theta - 600}{100} \right)$
$600 \leq T \leq 700$	$0.23 - 0.24 \left( \frac{\theta - 700}{100} \right)$
$700 \leq T \leq 800$	$0.11 - 0.12 \left( \frac{\theta - 800}{100} \right)$
$800 \leq T \leq 1200$	$0.11 \left( \frac{1200 - \theta}{400} \right)$

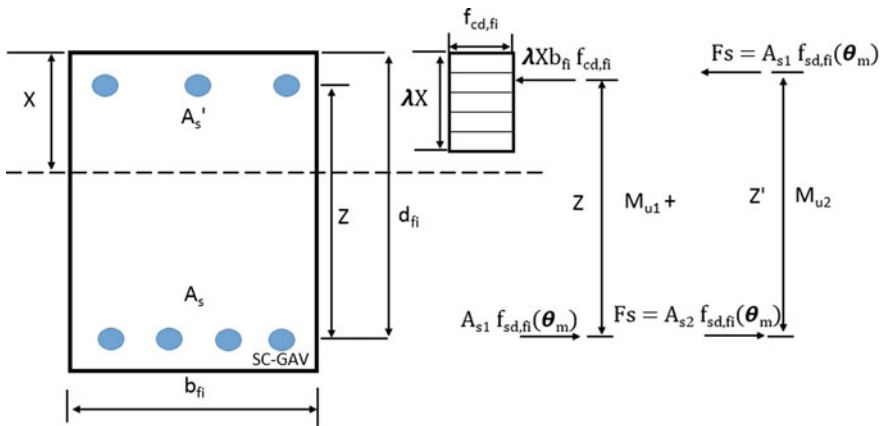


**Fig. 4.26** Stress distribution at ultimate limit state for a rectangular cross section with compression reinforcement (EN 1992-1-2)

greater than 2%, respectively. Temperature of rebars is assessed during computation of the 500 °C isotherm for the cross section of the member.

In accordance with EN 1992-1-1, depth of the concrete compressive stress block is taken as  $\lambda x$ , as shown in Fig. 4.26, where  $x$  is the depth of the neutral axis and  $\lambda$  is given by the following relationship:

$$\lambda = 0.8 - \frac{f_{ck} - 50}{200} \leq 0.8 \quad (4.59)$$

Strength of concrete is taken as  $\eta f_{cd}$ , where  $\eta$  is given by:

$$\eta = 1.0 - \frac{f_{ck} - 50}{200} \leq 1.0 \quad (4.60)$$

Subsequently, moment capacity of the section  $M_u$  is given by the following relationship:

$$M_u = M_{u1} + M_{u2} \quad (4.61)$$

where  $M_{u1}$  is due to the balanced concrete–steel section and  $M_{u2}$  is due to the compression reinforcement and the corresponding balancing tension reinforcement. These moment capacities are given as follows:

$$M_{u1} = A_{s1} f_{sd,fi}(\theta_m) z \quad (4.62)$$

$$M_{u2} = A_{s2} f_{scd,fi}(\theta_m) z' \quad (4.63)$$

Mechanical reinforcement ratio  $\omega_k$  is given by:

$$\omega_k = \frac{A_{s1} f_{sd,fi}(\theta_m)}{b_{fi} d_{fi} f_{cd,fi}(20)} \quad (4.64)$$

The total tension steel area  $A_s = A_{s1} + A_{s2}$ . The values shown in the above equation, namely  $f_{scd,fi}(\theta_m)$  and  $f_{sd,fi}(\theta_m)$ , are the temperature-reduced strengths of the reinforcement at a mean temperature  $\theta_m$  in a given layer. Where the reinforcement is in layers, the mean temperature reduced strength is computed as below:

$$k(\phi) f_{sd,fi} = \frac{\sum [k_s(\theta_i) f_{sd,i} A_i]}{\sum A_i} \quad (4.65)$$

Effective axis distance  $a$  is given by the following relationship:

$$a = \frac{\sum [a_i k_s(\theta_i) f_{sd,i} A_i]}{k_s(\theta_i) f_{sd,i} A_i} \quad (4.66)$$

### 4.11.2 Zone Method (Method of Slices)

According to this method, heat-affected concrete is divided into a series of slices and temperature ( $\theta$ ) is determined at the mid-depth of each slice. Compressive strength of concrete in each slice is considered using appropriate strength reduction factors discussed earlier. Mean concrete strength reduction factor ( $k_{c,m}$ ) for all slices is computed as below:

$$k_{c,m} = \frac{1 - \frac{0.2}{n}}{n} \sum_{i=1}^n k_c(\theta_i) \quad (4.67)$$

In the above equation, a factor of  $(1 - 0.2/n)$  is used to compensate for the fact that  $k_c(\theta_i)$  is determined at the center of a strip, where  $n$  is the total number of slices. Effective width of a uniform stress block is determined by calculating the width of the damage zone  $a_z$  and is given by the following relationships:

(a) For columns:

$$a_z = w \left[ 1 - \left( \frac{k_{c,m}}{k_c(\theta_m)} \right)^{1.3} \right] \quad (4.68)$$

(b) For beams and slabs:

$$a_z = w \left[ 1 - \left( \frac{k_{c,m}}{k_c(\theta_m)} \right) \right] \quad (4.69)$$

Strength reduction factor  $k_c(\theta_m)$  is determined at the center of the member, and  $w$  is the half width for exposure on opposite faces (thickness of a slab). For columns,  $2w$  is the smaller cross-sectional dimension. Strength reduction factors for reinforcements are the same as those used in the 500 °C isotherm method. Code imposes a restriction on the zone method that it may be used for exposure to the standard fires.

## 4.12 Numerical Example for Concrete Members Under Fire

**Example 1** Evaluate the temperature profile for the given cross section of the beam (160 × 300) exposed to standard fire curve using Wickstorm's method and compare against experimental temperature profile available in EN 1992-1-2 (Fig. 4.27).

**Solution** The temperature profile at 30 min and 60 min is calculated at certain coordinate points using Wickstorm's method as discussed earlier. Corresponding

**Fig. 4.27** Cross section of RC beam (160 × 300) under standard fire

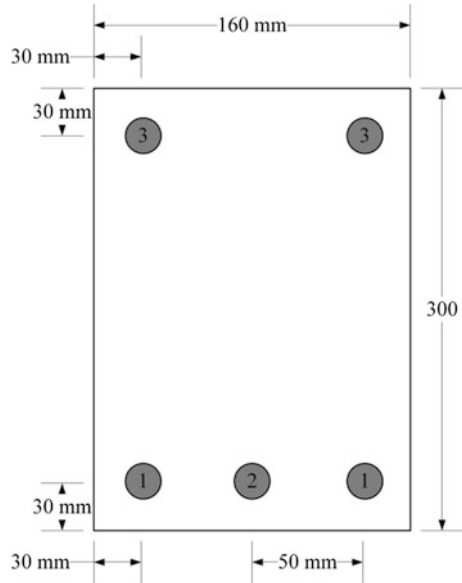


**Table 4.16** Temperature profile for beam section of 160 × 300 mm

X, Y coordinates	EN 1992-1-2		Wickstorm's method	
	60 min	30 min	60 min	30 min
20, 20	760	550	738	533
20, 40	650	420	662	451
40, 20	650	420	640	428
40, 40	500	280	530	318

temperature at those coordinates as available through EN 1992-1-2 is compared and tabulated in Table 4.16 for 30 and 60 min.

**Example 2** Evaluate the temperature profile for the given cross section of the beam (300 × 600), exposed to standard fire curve using Wickstorm's method, and compare against temperature profile available in EN 1992-1-2 (Fig. 4.28).

**Solution** Temperature profile calculated at 60 and 90 min for different coordinate points is summarized in Table 4.17.

**Example 3** Evaluate the temperature profile for the given cross section of a column (300 × 300), exposed to standard fire curve using Wickstorm's method, and compare against temperature profile available in EN 1992-1-2 (Fig. 4.29). The temperature profile calculated at 30 and 60 min at above calculated points is tabulated and compared against experimental temperature profile as in EN 1992-1-2 in Table 4.18.

**Fig. 4.28** Cross section of RC beam (300 × 600) under standard fire

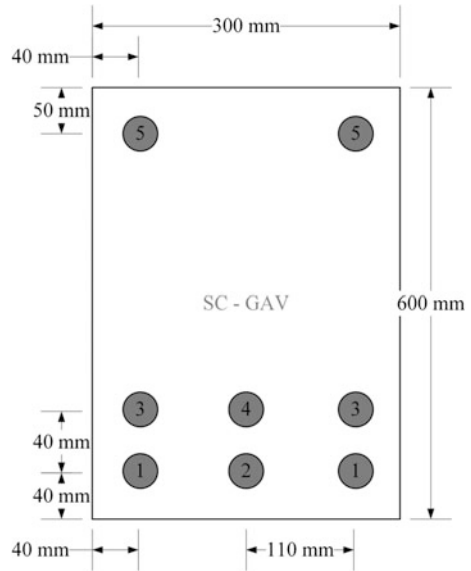


**Table 4.17** Temperature profile for beam section of 300 × 600 mm

X, Y coordinates	EN 1992-1-2		Wickstorm's method	
	60 min	90 min	60 min	90 min
20, 20	760	860	785	891
20, 40	650	780	671	795
40, 20	630	780	700	821
40, 40	500	630	495	625

**Fig. 4.29** Cross section of RC column (300 × 300) under standard fire

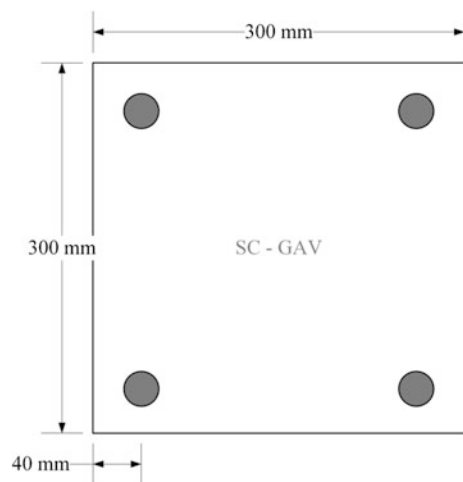


**Table 4.18** Temperature profile for column section of 300 × 300 mm

X, Y coordinates	EN 1992-1-2		Wickstorm's method	
	30 min	60 min	30 min	60 min
20, 20	550	750	537	741
20, 40	420	650	469	682
40, 20	420	650	469	682
40, 40	260	500	301	513

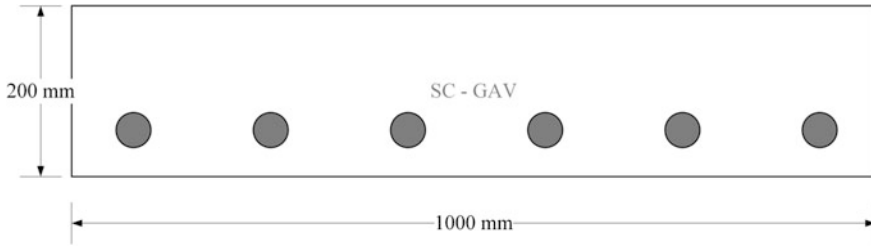


**Fig. 4.30** Cross section of RC slab (200 mm thick) under standard fire

**Table 4.19** Temperature profile for slab section (200 mm thick)

X, Y coordinates	EN 1992-1-2		Wickstorm's method	
	30 min	60 min	30 min	60 min
20, 20	320	510	306	469
20, 40	160	300	152	286
40, 20	320	510	306	469
40, 40	160	300	152	286

**Example 4** Evaluate the temperature profile for the given cross section of a slab (200 mm thick), exposed to standard fire curve using Wickstorm's method, and compare against experimental temperature profile available in EN 1992-1-2 (Fig. 4.30).

The temperature profile calculated at 30 and 60 min at above calculated points is tabulated and compared against temperature profile given in EN 1992-1-2 in Table 4.19.

**Example 5** A simply supported concrete slab of dimensions (5 × 2 m) of M25 concrete is located over an underground storage pit, which stores hazardous waste. Other required details of the slab are given in Table 4.20. Determine the fire rating of the given slab when exposed to standard fire curve (Fig. 4.31).

**Solution**

Ignoring loads that arise from partitions/finishes and no variable load acting on the underground slab, structural loading in the fire limit state is given by:

**Table 4.20** Details of the cover slab

Width ( <i>b</i> )	1000 mm
Depth ( <i>D</i> )	150 mm
Length	2 m
Variable load <i>q<sub>k</sub></i>	0
<i>f<sub>y</sub></i>	500 N/mm <sup>2</sup>
<i>f<sub>ck</sub></i>	25 N/mm <sup>2</sup>
<i>A<sub>st</sub></i>	261 mm <sup>2</sup>
Thermal diffusivity	$0.417 \times 10^{-6} \text{ m}^2/\text{s}$
Cover	25 mm
Bar diameter	10 mm
Exposure	Single-sided

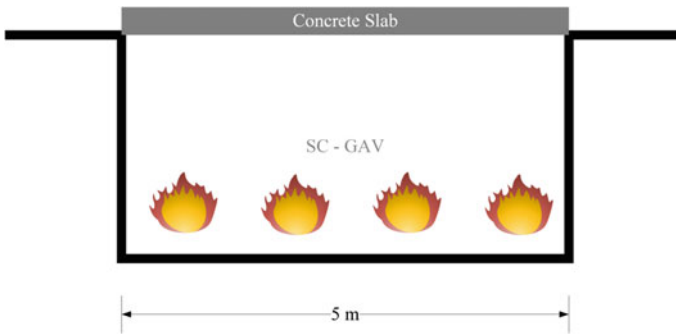


**Fig. 4.31** Details of RC slab cover of underground pit

$$0.125 \times 25 + 0.3 \times 0 = 3.75 \text{ kPa}$$

Demand factored moment  $M_{Ed,fi} = 1.35 \times 3.75 \times 2^2/8 = 2.53 \text{ kNm/m}$

Sample calculation of reduced moment capacity for a particular time of fire exposure is presented below:

Using Wickstrom’s method to determine temperatures, time of exposure  $t = 2 \text{ h}$

Temperature in steel:

The centroid of the reinforcement is at  $25 + 10/2 = 30 \text{ mm}$

$$n_w = 1 - 0.0616t^{-0.88} = 0.967$$

$$n_x = 0.18 \ln u_x - 0.81 = 0.58$$

$$\Delta\theta_g = 345 \log(480t + 1) = 1029 \text{ }^\circ\text{C}$$

$$\Delta\theta = n_x n_w \Delta\theta_g = 574 \text{ }^\circ\text{C, or}$$

$$\theta_s = 574 + 20 = 594 \text{ }^\circ\text{C} \text{ (assuming an ambient temperature of } 20 \text{ }^\circ\text{C)}$$

Strength reduction factor for  $\epsilon_{s,fi} > 2\%$

From Table 4.3,  $k_s = 0.489$ .

Tension force  $F_s$  is:

$$F_s = 500 \times 261 \times 0.489 = 63,762 \text{ N}$$

For Grade M 25 concrete,  $\lambda = 0.8$  and  $\eta = 1$

$$F_c = \eta f_{cd,fi}(20) \lambda x b$$

$$F_c/x = 24,000$$

$$x(\text{mm}) = 2.66$$

$$M_{u1} = F_s(d - 0.5\lambda x) = 7.58 \text{ kNm}$$

$M_{u1} > M_{Ed,fi}$  (OK) not exceeded demand

Similarly, calculation of reduced section capacity needs to be done for different time exposure until section is no longer able to resist the demand. Table 4.21 shows values of reduced section capacity for different time of fire exposure. It can be observed that the section capacity becomes lesser than the demand at 3.5 h. This variation is also plotted in Fig. 4.32. The fire rating of the slab can be said to be around 3.4 h.

**Example 6** A simply supported slab in a multi-span structure is designed and detailed as given in Table 4.22. The cover provided is that to satisfy durability only. Assume that the usage of structure is as an office and no continuity steel in the top face is provided. Assess the fire rating (Fig. 4.33).

**Solution** Considering 1 kPa partition and finishes load and variable loading of 3.5 kPa, structural loading in the fire limit state is given by:

$$0.125 \times 25 + 0.3 \times 3.5 + 1 = 5.175 \text{ kPa}$$

$$\text{Demand factored moment } M_{Ed,fi} = 1.35 \times 5.175 \times 2.7^2/8 = 6.37 \text{ kNm/m}$$

**Table 4.21** Reduced section capacity with increasing fire exposure time

Fire rating		
Time (h)	Reduced moment capacity of section (kNm)	Demand Moment (kNm)
0.5	15.38	2.53
1	13.34	2.53
1.5	11.29	2.53
2	7.58	2.53
2.5	5.15	2.53
3	3.36	2.53
3.5	2.49	2.53

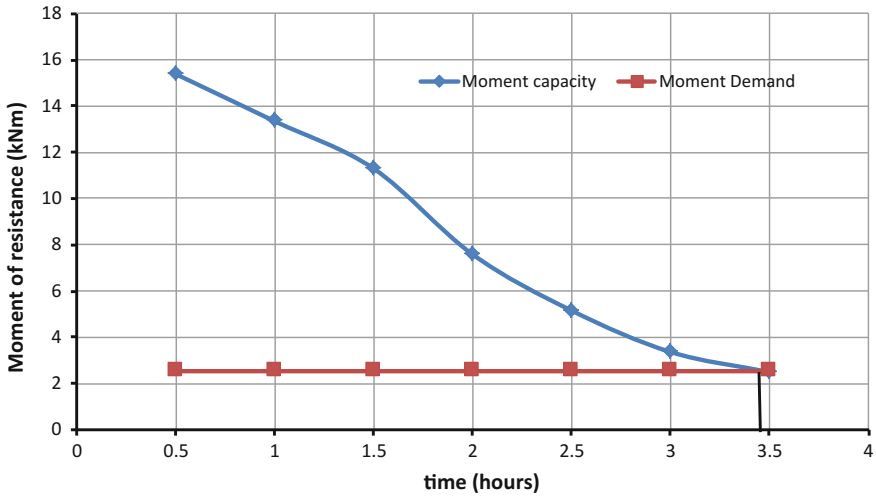


Fig. 4.32 Strength degradation curve for determining fire rating of cover slab

Table 4.22 Details of the simply supported slab

Notation	Value
Width ( $b$ )	1000 mm
Depth ( $D$ )	125 mm
Length	2700 mm
Variable coefficient	0.3
Variable load $q_k$	3.5
$f_y$	415 N/mm <sup>2</sup>
$f_{ck}$	25 N/mm <sup>2</sup>
$A_{st}$	452 mm <sup>2</sup>
Thermal diffusivity	$0.417 \times 10^{-6}$ m <sup>2</sup> /s
Cover	25 mm
Bar diameter	12 mm
Exposure	Single-sided
Specific weight	25 kN/m <sup>3</sup>
Partitions and finishes load	1 kPa

Calculation of the reduced moment-carrying capacity of the section is required, which is similar as shown in Example 1. Table 4.23 shows the values of calculated moment of resistance of section after different times of fire exposure. The same variation is also shown in Fig. 4.34. The fire rating can be said to be just below 2.5 h, say 2.4 h.

**Example 7** Determine the load-carrying capacity over a complete range of standard furnace exposures, and check the duration of fire resistance the beam can last. Data for the example is given in Fig. 4.35.

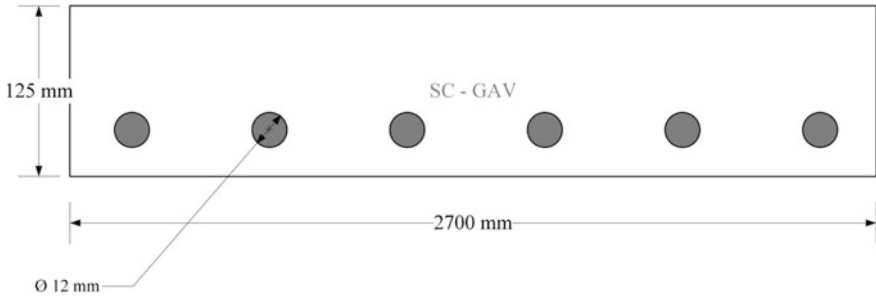


Fig. 4.33 Details of simply supported slab for determining fire rating

Table 4.23 Reduced section capacity with increasing fire exposure time

Fire rating		
Time (h)	Reduced moment capacity of section (kNm)	Demand moment (kNm)
0.5	17.23	6.37
1	14.99	6.37
1.5	12.7	6.37
2	8.57	6.37
2.5	5.83	6.37
3	3.81	6.37

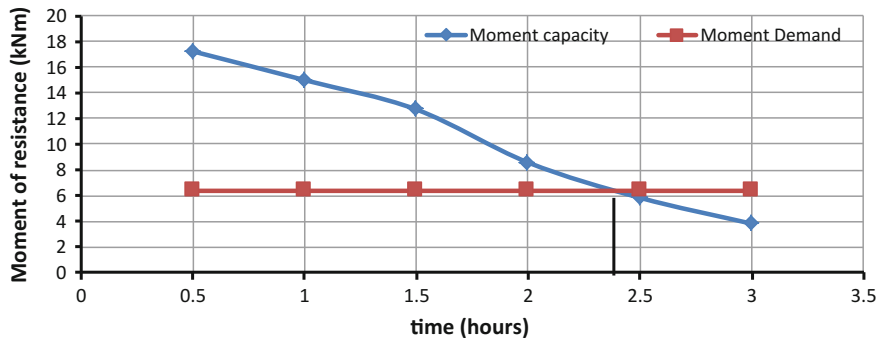


Fig. 4.34 Strength degradation curve for determining fire rating of simply supported slab

Input data: grade of concrete—c40/37; density of concrete—2500 kg/m<sup>3</sup>; type of structure—office building; diameter of tension reinforcement—16 mm; diameter of compression reinforcement—12 mm; grade of steel—Fe 415.

**Solution**

Load combination LC: 1 × D.L + 0.3 × L.L

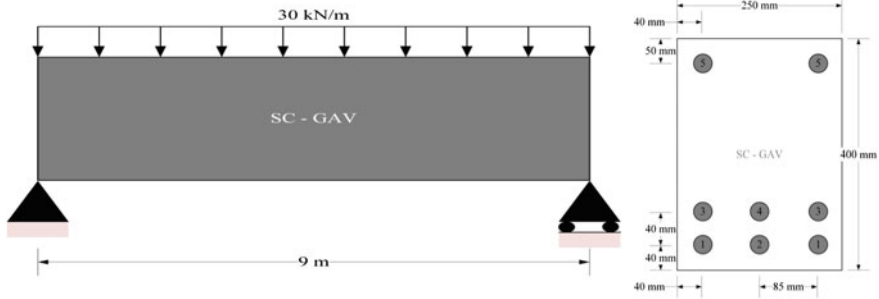


Fig. 4.35 Simply supported beam section for 9 m span for Example 7

Table 4.24 Temperatures and strength reduction factors for rebars

Time (h)	Rebar 1		Rebar 2		Rebar 3		Rebar 4		Rebar 5	
	T (°C)	$k_s(T)$								
0.25	83	1	30	1	73	1	20	1	73	1
0.5	263	1	124	1	179	1	20	1	179	0.921
0.75	385	1	196	1	259	1	24	1	256	0.844
1	476	0.7964	253	1	351	1	69	1	318	0.782
1.25	547	0.6343	300	1	425	0.8525	108	1	368	0.732
1.5	606	0.4556	355	1	486	0.7854	159	1	412	0.6844
1.75	656	0.3356	408	0.8712	538	0.6622	212	1	451	0.6337
2	699	0.2324	455	0.8195	584	0.5196	260	1	485	0.5895
2.25	737	0.1856	497	0.7733	624	0.4124	302	1	516	0.468
2.5	771	0.1448	535	0.6715	661	0.3236	340	1	545	0.41
2.75	802	0.10945	569	0.5661	693	0.2468	375	1	571	0.358
3	829	0.102025	600	0.47	723	0.2024	407	0.8723	595	0.31

Permanent load  $w_d = 0.25 \times 0.4 \times 25 = 2.5 \text{ kN/m}$

$$M_d = 2.5 \times 9^2/8 = 25.3125 \text{ kNm}$$

Live load  $w_l = 0.3 \times 30 = 9 \text{ kN/m}$

$$M_l = 9 \times 9^2/8 = 91.125 \text{ kNm}$$

Total applied moment = 116.4375 kNm

Using 500 °C isotherm method, temperature in reinforcement is determined. Values are given in Table 4.24. As all the reinforcement is the same size, strength reduction factor reduces to the following equation:

$$k(\phi) = \frac{1}{n} \sum k_s(\theta_i)$$

The above equation is expanded as per the cross-sectional details:

$$k(\phi) = \frac{k_s(\theta_1) + k_s(\theta_2) + k_s(\theta_3) + k_s(\theta_4)}{4}$$

Effective axis distance  $a$  reduces to the following relationship:

$$a = \frac{\sum [a_i k_s(\theta_i)]}{\sum k_s(\theta_i)}$$

Equation for effective axis distance expands to the following relationship:

$$a = \frac{68[k_s(\theta_1) + k_s(\theta_3)] + 13,268[k_s(\theta_2) + k_s(\theta_4)]}{4k(\phi)}$$

$$b_{fi} = b - 2x_{500} = 250 - 2x_{500}$$

$$F_s = A_s f_{scd,fi}(\theta_m) = A_{sc} k(\theta_5) f_{yk} = 226 \times 415 k(\theta_5) = 93,790 k(\theta_5)$$

$$A_{sif,fi}(\theta) = A_s f_{sd,fi}(\theta_m) - F_{sc} = 1608 \times 415 k(\phi) = 667,320 k(\phi) \text{ MN}$$

$$x = A_{sif,fi}(\theta) / (0.8 \times f_{cd}(20) \times b_{fi})$$

$$= A_{sif,fi}(\theta) / (0.8 \times 40 \times b_{fi}) = A_{sif,fi}(\theta) / (24 \times b_{fi})$$

$$M_{u1} = A_{sif,fi}(\theta) [h - a - 0, 4x] = A_{sif,fi}(\theta) [400 - a - 0, 4x]$$

$$M_{u2} = F_{sc} [h - a - 85] = F_{sc} [315 - a].$$

The values of  $M_{u1}$ ,  $M_{u2}$ , and  $M$  are determined in Table 4.25. As seen from the table, moment-carrying capacity of the section reduces with increasing fire exposure time. Figure 4.36 shows the reduced capacity versus demand curve (strength degradation curve) which gives fire rating of about 1.75 h.

**Example 8** Determine the load-carrying capacity history of 10 m span beam over the complete range of standard furnace exposures, and check the duration the beam can last (refer Fig. 4.37 for data).

Input data: grade of concrete—c30/37; density of concrete—2400 kg/m<sup>3</sup>; diameter of tension reinforcement—16 mm; diameter of compression reinforcement—10 mm; grade of steel—Fe 415.

**Solution** Load combination LC:  $1 \times \text{D.L} + 0.3 \times \text{L.L}$

Permanent load  $w_d = 0.16 \times 0.3 \times 24 = 1.152 \text{ kN/m}$

$$M_d = 1.152 \times 10^2 / 8 = 14.4 \text{ kNm}$$

Live load  $w_l = 0.3 \times 20 = 6 \text{ kN/m}$

$$M_l = 6 \times 10^2 / 8 = 75 \text{ kNm}$$

Total applied moment = 89.4 kNm

Determination of reinforcement temperatures is done in the similar way as in Example 3 and is summarized in Table 4.26. Values of moments  $M_{u1}$ ,  $M_{u2}$ , and  $M$  are determined and summarized in Table 4.27.

**Table 4.25** Moment of resistance of section with increasing fire exposure

Time (t) (h)	$k$ (T)	$a$ (mm)	$x_{500}$	$b_{fi}$ (mm)	$f_s$ (MN)	$f_{sc}$ (MN)	$f_{sr}$ (MN)	$x$ (mm)	$M_{u1}$ (kNm)	$M_{u2}$ (kNm)	$M_r$ (kNm)
0.250	1.000	60.000	6.250	237.500	0.334	0.094	0.240	31.565	126.513	42.430	168.942
0.500	1.000	60.000	12.500	135.000	0.334	0.086	0.247	57.247	127.883	39.078	166.961
0.750	1.000	60.000	18.750	122.500	0.334	0.079	0.255	64.933	130.838	35.811	166.649
1.000	0.949	61.073	25.000	110.000	0.317	0.073	0.243	69.138	124.427	33.101	157.528
1.250	0.872	61.252	25.000	110.000	0.291	0.069	0.222	63.133	114.113	30.972	145.085
1.500	0.810	62.035	31.250	97.500	0.270	0.064	0.206	66.085	105.471	28.908	134.379
1.750	0.717	63.175	37.500	85.000	0.239	0.059	0.180	66.142	91.818	26.699	118.517
2.000	0.643	63.638	37.500	85.000	0.215	0.055	0.159	58.541	81.677	24.811	106.488
2.250	0.593	63.825	43.750	72.500	0.198	0.044	0.154	66.350	78.449	19.689	98.138
2.500	0.535	64.741	43.750	72.500	0.179	0.038	0.140	60.374	71.590	17.214	88.804
2.750	0.481	65.943	50.000	60.000	0.160	0.034	0.127	66.040	64.367	14.990	79.357
3.000	0.412	66.105	50.000	60.000	0.137	0.029	0.108	56.408	55.379	12.976	68.355

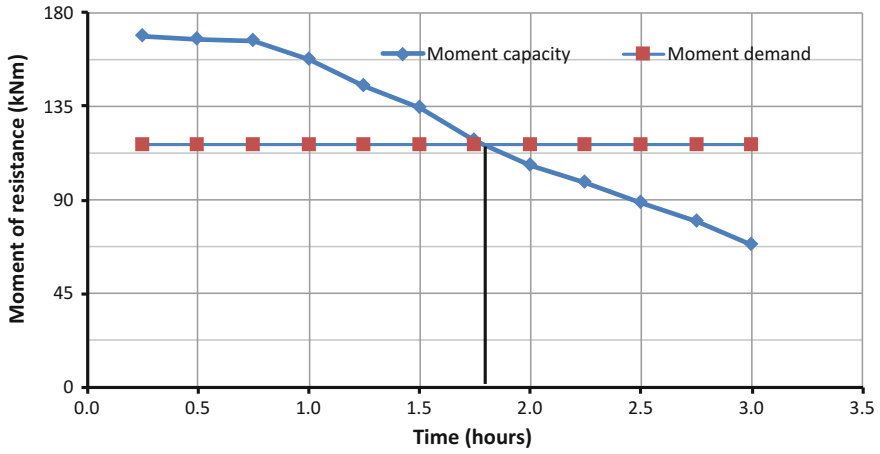


Fig. 4.36 Strength degradation curve for determining fire rating of 9 m span beam

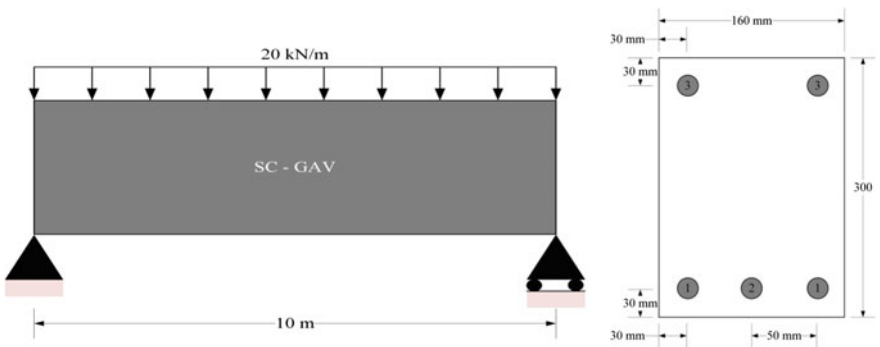


Fig. 4.37 Simply supported beam section of 10 m span

Table 4.26 Temperatures and strength reduction factors for rebars

Time (h)	Rebar 1		Rebar 2		Rebar 3	
	$T$ ( $^{\circ}\text{C}$ )	$k_s(T)$	$T$ ( $^{\circ}\text{C}$ )	$k_s(T)$	$T$ ( $^{\circ}\text{C}$ )	$k_s(T)$
0.25	44	1	20	1	29	1
0.5	157	1	20	1	139	0.961
0.75	238	1	20	1	218	0.882
1	302	1	64	1	281	0.819
1.25	412	0.802	163	1	376	0.724
1.5	520	0.513	274	1	450	0.547

**Table 4.27** Moment of resistance of section with increasing fire exposure

Time (t) (h)	k (T)	a (mm)	x <sub>500</sub>	b <sub>fi</sub> (mm)	f <sub>s</sub> (MN)	f <sub>sc</sub> (MN)	f <sub>sr</sub> (MN)	x (mm)	M <sub>u1</sub> (kNm)	M <sub>u2</sub> (kNm)	M <sub>r</sub> (kNm)
0.250	1.000	30.000	4.000	152.000	0.334	0.065	0.269	73.622	145.178	31.421	176.599
0.500	1.000	30.000	12.000	136.000	0.334	0.058	0.276	84.481	147.857	27.964	175.821
0.750	0.894	30.000	16.000	128.000	0.298	0.053	0.246	80.021	132.251	25.388	157.639
1.000	0.802	30.000	24.000	112.000	0.268	0.049	0.219	81.474	117.694	23.408	141.102
1.250	0.603	30.000	28.000	104.000	0.201	0.045	0.156	62.649	85.213	21.668	106.881
1.500	0.487	30.000	32.000	96.000	0.162	0.041	0.121	52.624	66.558	19.830	86.388
1.750	0.365	30.000	36.000	88.000	0.122	0.038	0.084	39.881	46.667	18.196	64.862
2.000	0.285	30.000	40.000	80.000	0.095	0.033	0.062	32.488	34.744	15.842	50.587
2.250	0.221	30.000	44.000	72.000	0.074	0.025	0.049	28.389	27.405	11.940	39.345
2.500	0.175	30.000	48.000	64.000	0.058	0.021	0.038	24.415	21.010	10.117	31.127
2.750	0.144	30.000	52.000	56.000	0.048	0.017	0.031	22.799	17.186	8.421	25.607
3.000	0.126	30.000	56.000	48.000	0.042	0.014	0.028	24.283	15.673	6.787	22.460

As seen from the table, moment-carrying capacity of the section reduces with the increase in fire exposure time. Figure 4.38 shows the reduced capacity versus demand curve (strength degradation curve) which indicates fire rating of about 1.5 h.

**Example 9** Determine the fire resistance of a short reinforced concrete column (300 × 300) reinforced with 4–16-mm-diameter bars having a cover of 40 mm (Fig. 4.27).

Input data: The concrete is Grade c50/60; density of concrete—2400 kg/m<sup>3</sup>; grade of steel—Fe 415;  $A_c = 89,196 \text{ mm}^2$  (Fig. 4.39).

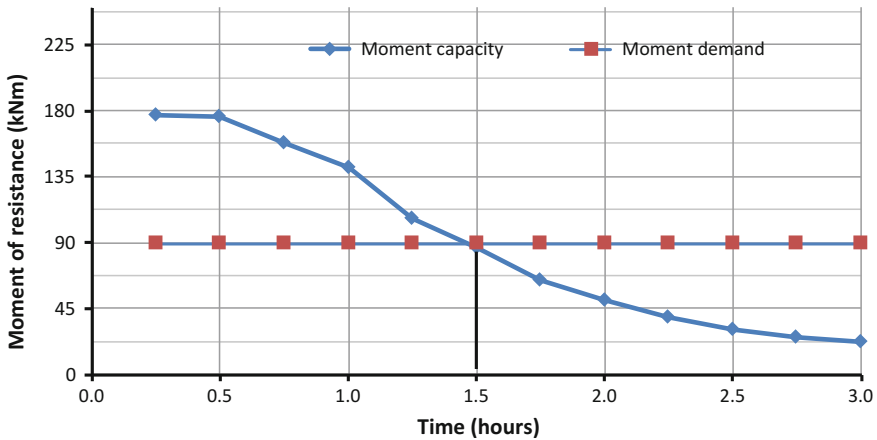


Fig. 4.38 Strength degradation curve for determining fire rating of 10 m span beam

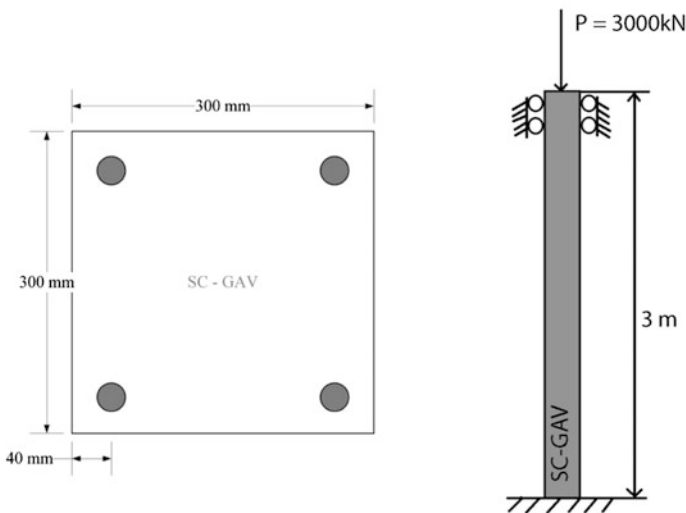


Fig. 4.39 RC column (300 × 300) with axial load demand of 3000 kN

**Solution** Axial load demand is 3000 kN. For determining reduced axial capacity of the section, values of  $x_{500}$  are calculated using Wickstrom's method. Temperatures in the reinforcement are computed and summarized in Table 4.28; rounding effects of isotherms are neglected (Table 4.29).

Results of load-carrying capacity are summarized in Table 4.30. As both  $\alpha_{cc}$  and  $\gamma_{mc}$  are equal to 1.0 in the fire limit state, concrete capacity in compression effectively becomes as follows:

$$N_{c,fi} = b_{fi}d_{fi}f_{ck}$$

**Table 4.28** Temperature of reinforcement and strength reduction factor

Rebar-1		
Time (h)	T (°C)	$k_s(T)$
0.25	51	1
0.5	227	0.873
0.75	348	0.752
1	439	0.6493
1.25	511	0.478
1.5	570	0.36
1.75	621	0.258
2	664	0.172
2.25	703	0.0994
2.5	737	0.0926
2.75	768	0.0864
3	797	0.0806

**Table 4.29** Axial load-carrying capacity of the section with increasing fire exposure time

Time (h)	$b_{fi}$ (mm)	$d_{fi}$ (mm)	$N_{c,fi}$ (kN)	$N_{s,fi}$ (kN)	$N_{rd,fi}$ (kN)
0.25	285	285	4061.25	402.12	4463.37
0.5	270	270	3645.00	351.05	3996.05
0.75	255	255	3251.25	302.40	3553.65
1	240	240	2880.00	261.10	3141.10
1.25	225	225	2531.25	192.22	2723.46
1.5	210	210	2205.00	144.76	2349.76
1.75	195	195	1901.25	103.75	2005.00
2	180	180	1620	69.16	1689.16
2.25	165	165	1361.25	39.97	1401.22
2.5	135	135	911.25	37.24	948.49
2.75	120	120	720	34.74	754.74
3	90	90	405	32.41	437.411

**Table 4.30** Temperature of reinforcement bars and strength reduction factor

Time (h)	Rebar 1		Rebar 2	
	$T$ (°C)	$k_s(T)$	$T$ (°C)	$k_s(T)$
0.25	28	1	28	1
0.5	202	0.898	121	0.979
0.75	322	0.778	192	0.908
1	413	0.6831	249	0.851
1.25	485	0.5895	296	0.804
1.5	545	0.41	337	0.763
1.75	595	0.31	374	0.726
2	640	0.22	406	0.6922
2.25	678	0.144	436	0.6532
2.5	713	0.0974	463	0.6181
2.75	745	0.091	488	0.5856
3	773	0.0854	511	0.478

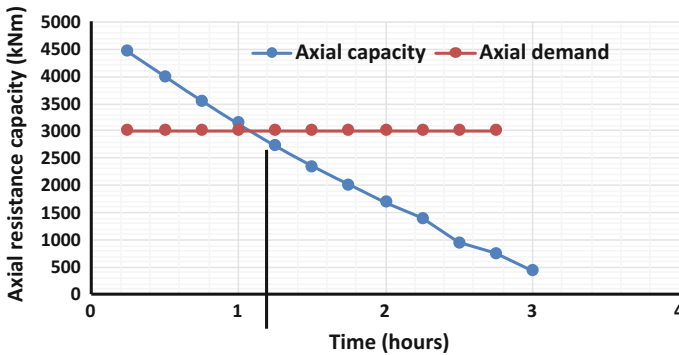


**Fig. 4.40** Strength degradation curve for determining fire rating of column (300 × 300)

Compression capacity of the reinforcement with  $\gamma_{m,s} = 1.0$  is given by:

$$N_{s,fi} = 804 \times 500(k_s(\theta_1) + k_s(\theta_2)) = 402,000(k_s(\theta_1) + k_s(\theta_2))$$

Reduced capacity of the column section is calculated as  $N_{Rd,fi} = N_{c,fi} + N_{s,fi}$  at all time exposure. Figure 4.40 shows the strength degradation curve, which provides fire rating as 1.15 h.

**Example 10** Determine the fire resistance of a short reinforced concrete column (600 × 450), reinforced with a cover of 45 mm (Fig. 4.41).

Input data: The concrete is Grade c60/60; density of concrete—2500 kg/m<sup>3</sup>; grade of steel—Fe 500;  $A_c = 266,781 \text{ mm}^2$

**Solution** Axial load demand is 12,000 kN. Determine the reduced axial capacity of the section. Values of  $x_{500}$  are calculated using Wickstrom’s method, and

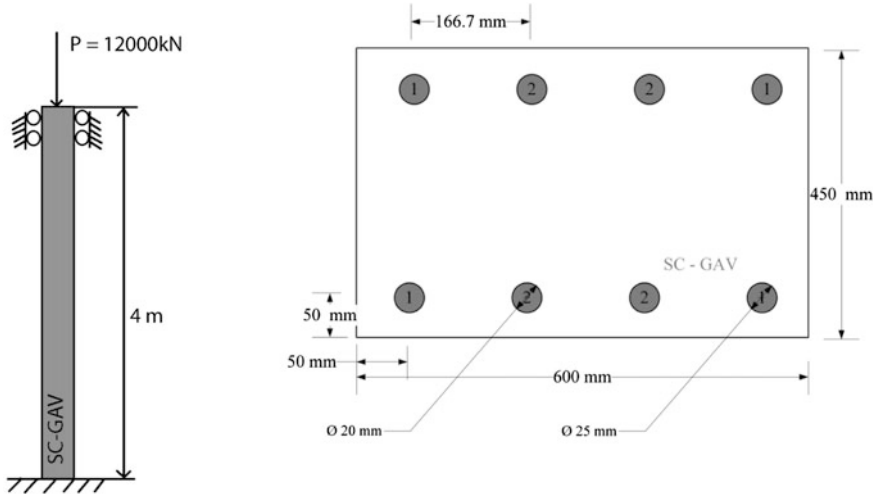


Fig. 4.41 RC column (600 × 450) with axial load demand of 12,000 kN

Table 4.31 Axial load-carrying capacity of column (600 × 450) with fire exposure

Time (h)	$b_{fi}$ (mm)	$d_{fi}$ (mm)	$N_{c,fi}$ (kN)	$N_{s,fi}$ (kN)	$N_{rd,fi}$ (kN)
0.25	600	450	16,200	1610.07	17810.07
0.5	570	427.5	14620.5	1496.73	16117.23
0.75	570	405	13,851	1334.31	15185.31
1	540	405	13,122	1205.33	14327.33
1.25	540	405	13,122	1083.91	14205.91
1.5	540	382.5	12,393	881.92	13274.92
1.75	510	382.5	11704.5	760.50	12465.00
2	510	382.5	11704.5	650.91	12355.41
2.25	510	360	11,016	551.79	11567.79
2.5	480	360	10,368	483.99	10851.99
2.75	480	360	10,368	457.28	10825.28
3	450	337.5	9112.5	384.18	9496.68

temperatures in the reinforcement are summarized in Table 4.30. Rounding effects of isotherms are neglected.

Results of the determination of load-carrying capacity are summarized in Table 4.31. As both  $\alpha_{cc}$  and  $\gamma_{mc}$  are unity in the fire limit state, concrete capacity in compression effectively becomes as follows:

$$N_{c,fi} = b_{fi}d_{fi}f_{ck}$$

Compression capacity of the reinforcement with  $\gamma_{m,s} = 1.0$  is given by:

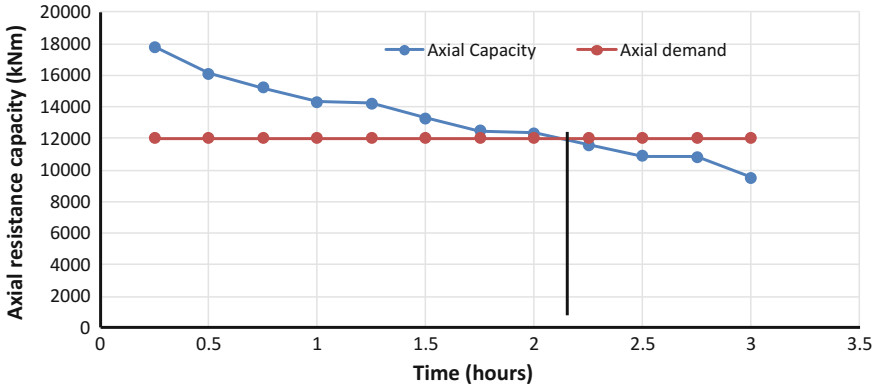


Fig. 4.42 Strength degradation curve for determining fire rating of column (600 × 450)

$$N_{S,fi} = 500(1256 \times k_s(\theta_1) + 1962 \times k_s(\theta_2))$$

Reduced capacity of the column section is calculated as  $N_{Rd,fi} = N_{c,fi} + N_{s,fi}$  at all time exposure. Figure 4.42 shows the strength degradation curve, which provides fire rating of 2.2 h.

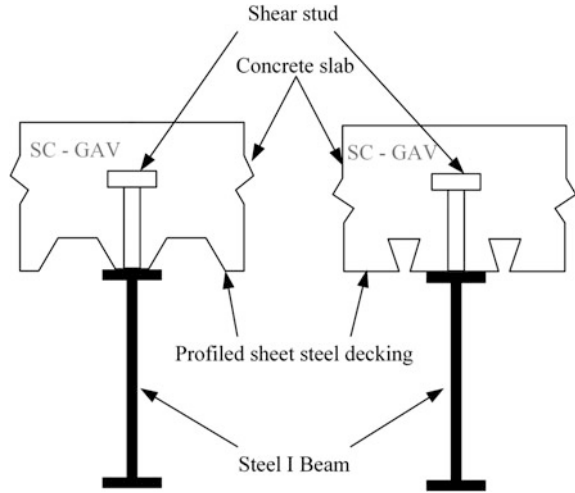
### 4.13 Composite Structures Under Fire

This section presents detailed discussions on the design of steel–concrete composite structures under fire. It covers mainly two types of composite structures, namely: (i) composite beams where the composite action is obtained from welded shear studs on to the top flange of beam and (ii) concrete-filled steel columns. Structural design of these structures for fire is carried out for the required fire rating, which is evaluated from two criteria, namely: (i) critical temperature and (ii) strength-based approach.

#### 4.13.1 Composite Beams

In this section, two types of composite beams are considered as shown in Fig. 4.43. They are designated as trapezoidal decking and dovetail decking composite beam, respectively. For evaluation of fire rating, EN 1994-1-2 considers two approaches, namely: (i) critical temperature-based approach and (ii) full moment capacity approach. In both the approaches, thermal analysis utilizes empirical equations developed for non-composite steelworks that assume no thermal gradients.

**Fig. 4.43** Composite beams.  
**a** Trapezoidal profile steel decking and **b** dovetail profile steel decking



### 4.13.2 Critical Temperature-Based Approach

This approach can be employed under certain conditions: (i) when depth of the beam is lesser than 500 mm; (ii) depth of slab  $h_c$  is greater than 120 mm; and (iii) beam is simply supported. Critical temperature  $\theta_{cr}$  for a fire resistance period of R30 is evaluated corresponding to a critical strength of steel  $f_{ay,\theta_{cr}}$  and is given by:

$$0.9\eta_{fi,t} = \frac{f_{ay,\theta_{cr}}}{f_{ay}}, \quad (4.44)$$

For cases not covered in the assumptions mentioned above, the following relationship is valid:

$$\eta_{fi,t} = \frac{f_{ay,\theta_{cr}}}{f_{ay}} \quad (4.45)$$

where  $f_{ay}$  is the ambient yield strength, and load level  $\eta_{fi,t}$  is given by:

$$\eta_{fi,t} = \frac{E_{fi,d,t}}{R_d} \quad (4.46)$$

where  $R_d$  is the resistance of the member at time  $t = 0$  and  $E_{fi,d,t}$  is the design effect of the structural fire actions.

### 4.14 Moment Capacity-Based Approach

Moment capacity is determined from plastic theory for all classifications of sections except Class 4. In case of slabs with shear connectors, compression flange is taken as Class 1. Temperatures across the steel member are computed assuming both flanges are at uniform temperatures and compression zone of slab is thermally inert. For evaluating the temperature profile of unprotected members, the section factor  $A_m/V$  is computed as discussed below (Fig. 4.44):

- (1) Top flange with 85% of the concrete slab is in contact with the upper flange and voids filled with non-combustible material:

$$\frac{A}{V} = \frac{b_2 + 2e_2}{b_2e_2} \tag{4.47}$$

- (2) Top flange with less than 85% of concrete slab is in contact:

$$\frac{A}{V} = 2 \frac{b_2 + e_2}{b_2e_2} \tag{4.48}$$

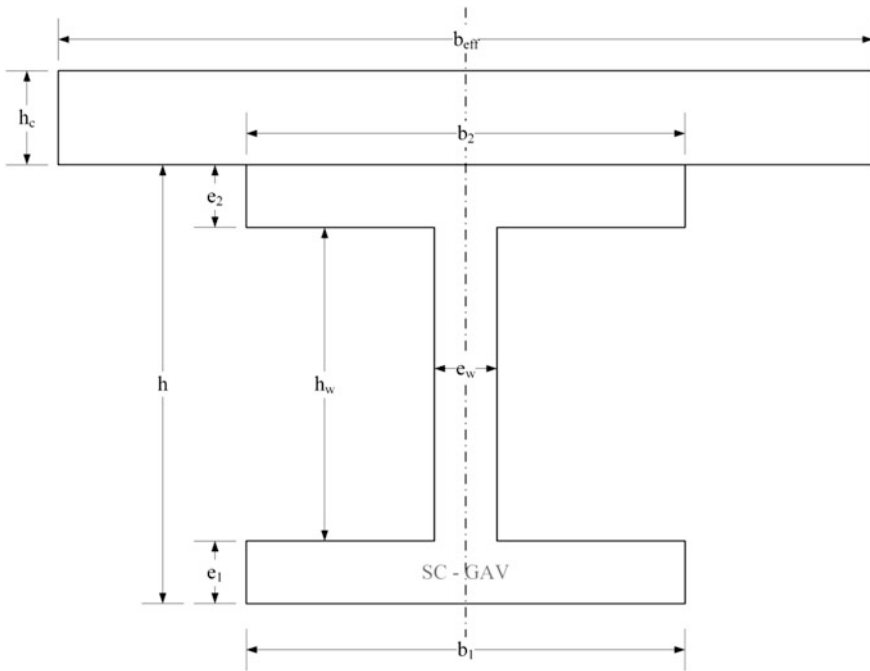


Fig. 4.44 Composite beam under consideration

(3) Bottom flange is:

$$\frac{A}{V} = 2 \frac{b_1 + e_1}{b_1 e_1} \quad (4.49)$$

where  $(b_1, e_1, b_2, e_2)$  are widths and thickness, corresponding to the bottom and top flanges. When overall depth is lesser than 500 mm, web temperature is taken equal to that of the flange. For box protection, a uniform temperature is assumed over entire cross section with the  $A/V$  value taken same as that for the box. For unprotected composite steel beam, shadow factor  $k_{sh}$  is computed as:

$$k_{sh} = 0.9 \frac{e_1 + e_2 + \frac{b_1}{2} + \sqrt{h_w^2 + \frac{(b_1 - b_2)^2}{4}}}{h_w + b_1 + \frac{b_2}{2} + e_1 + e_2 - e_w} \quad (4.50)$$

The tensile capacity of the steel beam is calculated as:

$$T = \frac{f_{ay, \theta_1} b_1 e_1 + f_{ay, \theta_w} b_w e_w + f_{ay, \theta_2} b_2 e_2}{\gamma_{m, fi, a}} \quad (4.51)$$

The lever arm of the tensile force from the bottom of the beam is calculated as:

$$y_T = \frac{f_{ay, \theta_1} \frac{b_1 e_1^2}{2} + f_{ay, \theta_w} b_w e_w \left( e_1 + \frac{h_w}{2} \right) + f_{ay, \theta_2} b_2 e_2 \left( h - \frac{e_2}{2} \right)}{T \gamma_{m, fi, a}} \quad (4.52)$$

Limiting value of the tensile force  $T$  is given by:

$$T \leq NP_{fi, Rd} \quad (4.53)$$

where  $N$  is the number of shear connectors and  $P_{fi, Rd}$  is the reduced capacity of the shear connectors, which is dependent on temperature. The tensile force is resisted by force in compression regime of concrete, and depth of compression zone is given by:

$$h_u = \frac{T \gamma_{m, fi, c}}{b_{eff} f_{ck}} \quad (4.54)$$

where  $b_{eff}$  is effective width of slab. Subsequently,  $h_{cr}$  is computed as per the code (EN-194-1-2). If  $h_c - h_u > h_{cr}$ , temperature in concrete is lesser than 250 °C and full strength can be taken for design consideration. Alternatively, some layers of concrete have temperature greater than 250 °C and calculation of  $T$  becomes iterative. This is given by:

$$T = \frac{b_{\text{eff}}(h_c - h_{\text{cr}}) + \sum_{i=2}^{n-1} 10b_{\text{eff}}f_{\text{cf},\theta i} + h_{u,n}f_{\text{ck},\theta n}}{\gamma_{m,\text{fi},c}} \quad (4.55)$$

$$h_u = (h_c - h_{\text{cr}}) + 10(n - 2) + h_{u,n}$$

Subsequently, moment-carrying capacity is defined as:

$$M_{\text{fi,Rd}} = T \left( h + h_c - y_T - \frac{h_u}{2} \right) \quad (4.56)$$

The shear stud capacity must be checked, and design shear stud capacity is minimum of the following relationships:

$$P_{\text{fi,Rd}} = \begin{cases} 0.8k_{u,\theta}P_{\text{Rd}} \\ k_{c,\theta}P_{\text{Rd}} \end{cases} \quad (4.57)$$

where  $k_{u,\theta}$  is degradation factor for ultimate strength of steel,  $k_{c,\theta}$  is degradation factor for characteristic compressive strength of concrete and  $P_{\text{Rd}}$  is calculated according to EN-1994-1-2.

## 4.15 Numerical Example on Composite Section Under Fire

**Example 1** Evaluate the thickness of gypsum plaster protection for 90-min fire resistance of composite beam of span 4 m as shown in Fig. 4.45 for an ISO-834 exposure. It is to be noted that dovetail decking is running normal to the beam span. Permanent Load:

Dead load: 2.75 (self-weight) + 2 (finishes) (kN/m<sup>2</sup>); live load: 4 (kN/m<sup>2</sup>)

(a) Moment capacity-based approach

For the given beam, load combination for fire is taken from EN 1991-1-2 as:

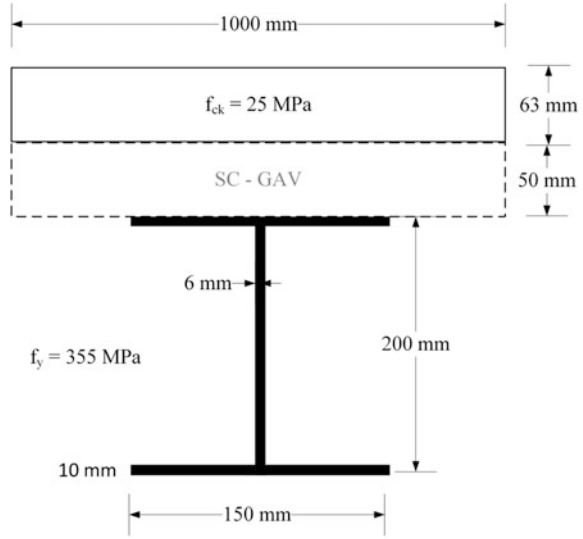
$$= 1 \times \text{P.L} + 0.3 \times \text{I.L.}$$

Design moment on the structure,  $M_{\text{fi,ED}}$ , is computed as:

$$\begin{aligned} &= 2.98 \times (4.75 + 0.3 \times 4) \times 4^2/8 \\ &= 33.3 \text{ kN/m.} \end{aligned}$$

$A/V$  for bottom flange = 213 m<sup>-1</sup> and  $A/V$  for top flange = 113 m<sup>-1</sup>. Since the beam depth is lesser than 500 mm, web temperature can be taken to be same as that

**Fig. 4.45** Composite beam under consideration for Example 1



of the lower (bottom) flange temperatures. A protection board of thickness 15 mm is assumed to be provided with material properties such as  $\rho_p = 500 \text{ kg/m}^3$ ,  $p = 2\%$ ,  $c_p = 1500 \text{ J/kg } ^\circ\text{C}$ ,  $\lambda_p = 0.25 \text{ W/m } ^\circ\text{C}$ . Subsequently, thermal analysis is performed. At 90 min of exposure, temperature of bottom flange, web, and top flange is obtained as 800, 800, and 657  $^\circ\text{C}$ , respectively.

Tension in steel is computed as:

$$T = \frac{f_{ay,01} b_1 e_1 + f_{ay,0w} b_w e_w + f_{ay,02} b_2 e_2}{\gamma_{m,fi,a}}$$

$$= \frac{355 \times 150 \times 10 \times 0.091 + 355 \times 180 \times 6 \times 0.091 + 355 \times 150 \times 10 \times 0.253}{1} = 219 \text{ kN}$$

Lever arm  $y_T$  is computed as:

$$y_T = 355 \times \frac{0.091 \frac{150 \times 10^2}{2} + 0.091 \times 180 \times 6 \left(10 + \frac{180}{2}\right) + 0.25 \times 150 \times 10 \left(200 - \frac{10}{2}\right)}{219,000}$$

$$= 135 \text{ mm}$$

Taking effective width of slab as 1000 mm  $h_u$  is computed as:

$$h_u = \frac{T \gamma_{m,fi,c}}{b_{eff} f_{ck}} = \frac{219,000}{1000 \times 25} = 8.76 \text{ mm}$$

$h_c - h_u$  is computed as 91 mm and is greater than  $h_{cr}$  which is computed as 37 mm from the code. Subsequently, moment of resistance at 90 min is computed as:

$$M_{fi,Rd} = T \left( h + h_c - y_T - \frac{h_u}{2} \right) = 36 \text{ kNm}$$

Moment capacity of composite beam is greater than the applied moment, so it is safe. In the ambient design, 19-mm studs were placed in each trough at a spacing of 150 mm. Temperature in the stud is taken as 80% of that of the top flange temperature, i.e.,  $0.8 \times 657 = 525$  °C. Concrete temperature is taken as 40%, i.e.,  $0.4 \times 657 = 268$  °C. Shear stud capacity is computed as 50.1 kN and limiting value of  $T$  as 333 kN. Hence, it is seen that the section capacity is not limited due to shear studs.

Critical temperature-based approach cannot be applied to the present example as minimum thickness of concrete slab for this approach is 120 mm.

## 4.16 Composite Columns

Eurocode (EN-1994-1-2) provides simple calculation methods for design of composite columns. From Annexure H (1), design axial load on composite columns is given by:

$$\begin{aligned} N_{fi,Rd} &= N_{fi,cr} \leq N_{fi,pl,Rd} \\ N_{fi,cr} &= \left( \frac{\pi}{l_\theta} \right)^2 [E_{a,\theta,\sigma} I_a + E_{c,\theta,\sigma} I_c + E_{r,\theta,\sigma} I_r] \end{aligned} \quad (4.58)$$

where  $l_\theta$  is the effective length of composite column;  $E_{a,\theta,\sigma}$ ,  $E_{c,\theta,\sigma}$ , and  $E_{r,\theta,\sigma}$  are the tangent modulus of steel, concrete, and reinforcement at stress level  $\sigma$ ; and  $I_a$ ,  $I_c$ , and  $I_r$  represent moment of inertia of steel, concrete, and reinforcement. The plastic axial load capacity is given by:

$$N_{fi,pl,Rd} = A_a \frac{\sigma_{a,\theta}}{\gamma_{M,fi,a}} + A_c \frac{\sigma_{c,\theta}}{\gamma_{M,fi,c}} + A_r \frac{\sigma_{r,\theta}}{\gamma_{M,fi,r}} \quad (4.59)$$

where  $A_a$ ,  $A_c$ , and  $A_r$  represent areas of steel, concrete, and reinforcement and  $\sigma_{a,\theta}$ ,  $\sigma_{c,\theta}$ , and  $\sigma_{r,\theta}$  represent temperature-dependent stress in constituent materials. Above-mentioned design method needs to be aided with numerical tools like FEA or FDM for the evaluation of temperature response history. Empirical methods have also been applied for simplified design of composite columns subjected to fire. Kodur and Lie (2) suggested empirical equation for fire endurance of rectangular and circular composite columns as:

$$t_{fi,Rd} = f_1 \frac{f_{ck} - 20}{l_\theta - 1000} \frac{D^{2.5}}{\sqrt{N_{fi,Ed}}} \quad (4.60)$$

where  $l_\theta$  is the buckling length (mm),  $D$  is the diameter of a circular column or side length of a square column (mm),  $N_{fi,Ed}$  is the applied load in the fire limit state (kN), and  $f_1$  is a factor. Table 4.32 shows values for  $f_1$  factor.

**Example 1** Evaluate the fire endurance of concrete-filled steel column as shown in Fig. 4.46, cast with siliceous aggregates and steel box section of yield strength 400 MPa.

For the given beam, load combination for fire is taken form EN 1991-1-2 as:

$$= 1 \times P.L + 0.3 \times I.L.$$

Design axial force on the structure  $N_{fi,Ed}$  is computed as 1340 kN.

Fire endurance is computed as below:

$$t_{fi,Rd} = f_1 \frac{f_{ck} - 20}{l_\theta - 1000} \frac{D^{2.5}}{\sqrt{N_{fi,Ed}}}$$

$$t_{fi,Rd} = 0.075 \frac{25 - 20}{1900 - 1000} \frac{420^{2.5}}{\sqrt{1340}} = 41 \text{ min}$$

**Table 4.32**  $f_1$  factor for composite columns

Aggregate type	Column type	Plain concrete	Fiber concrete	Reinforcement ratio and cover			
				<3%		>3%	
				<25	>25	<25	>25
Siliceous	CHS	0.07	0.075	0.075	0.08	0.08	0.085
	SHS	0.06	0.065	0.065	0.07	0.07	0.075
Carbonate	CHS	0.08	0.07	0.085	0.09	0.09	0.095
	SHS	0.06	0.065	0.075	0.08	0.08	0.085

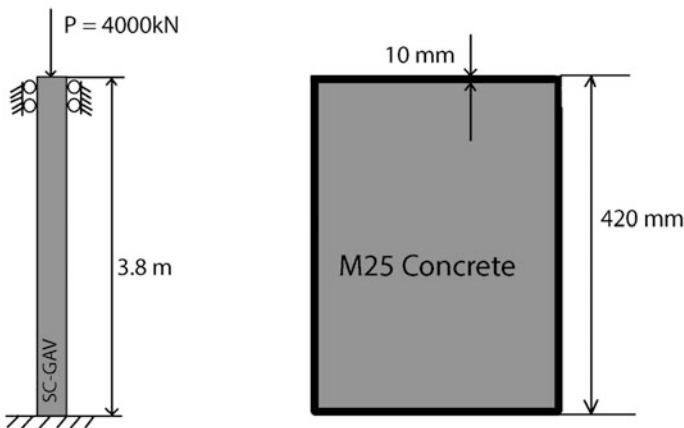


**Fig. 4.46** Concrete-filled steel column (Example 2)

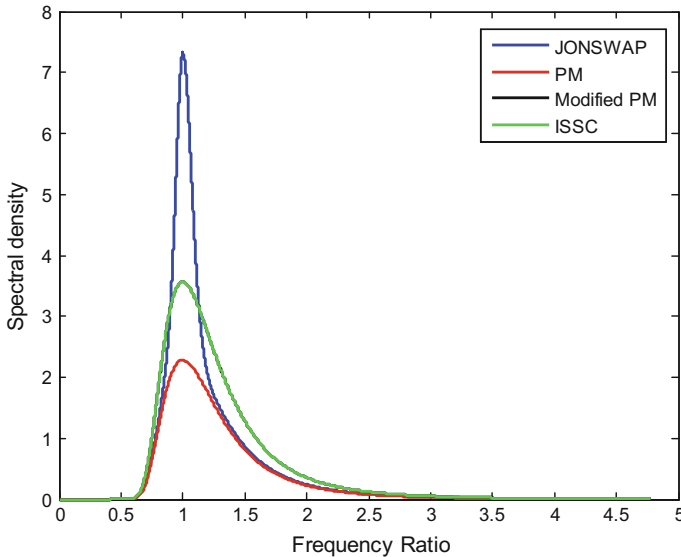
**Model exam paper-1****Design aids for offshore structures under special environmental loads including fire resistance****Time: 3 h Max marks: 100****Section A: Each question carries one mark. Use appropriate key words to answer**

1. Offshore structures are preferably function-dominant. State true/false and validate the statement.
2. Compliant structures and fixed structures resist the lateral loads by \_\_\_\_\_ and \_\_\_\_\_, respectively.
3. Continuous rotation of the spud-can arrangement in the guyed towers will lead to \_\_\_\_\_.
4. Give the expression for the resisting moment in articulated towers.
5. Ball joints restrain \_\_\_\_\_ and allow \_\_\_\_\_ from the buoyant leg to the deck.
6. When the mean square value is unique across the ensemble, the process is said to be \_\_\_\_\_.
7. Ice loads on conical structures cause less response. State true/false and validate the statement.
8. The interaction of ice on the structure will cause \_\_\_\_\_, which is measured by monitoring \_\_\_\_\_.
9. \_\_\_\_\_ is used for the analysis of the offshore structures under earthquake loads.
10. \_\_\_\_\_ is caused by second-order waves in mild and severe sea state; and \_\_\_\_\_ is caused by extremely high steep waves.
11. Non-impact waves cause \_\_\_\_\_ response on TLP which will lead to \_\_\_\_\_.
12. When the trace of the plane of applied moment does not coincide with any of the principal axes of inertia, then the bending is said to be \_\_\_\_\_.
13. Write the expression for finding the shear stress on the section.
14. Winkler–Bach equation is useful in estimating the stresses in the curved beams with large initial curvature only at \_\_\_\_\_.
15. When risers are exposed to the fluid flow, \_\_\_\_\_ takes place which results in the formation of \_\_\_\_\_.
16. \_\_\_\_\_ is required to maintain the stability of the riser, when installed in greater water depth.
17. \_\_\_\_\_ is the lowest temperature at which the liquid gives up enough vapor to maintain the continuous flame.

18. \_\_\_\_\_ reduces the risk of flame propagation.
19. High-strength steel does not have a \_\_\_\_\_ and the yield region is \_\_\_\_\_.
20. A turbulent diffusion of flame resulting from the combustion of the fuel and propagating in a particular direction with significant momentum is called \_\_\_\_\_.

**Section B: Each question carries Two marks. Answer briefly**

1. List the uncertainties in estimating the environmental loads.
2. Does the lateral load acting on the compliant platforms gets reduced by the structural action of the platform? Explain.
3. Write the following degrees of freedom in descending order based on the time period of the Spar platform: Pitch, heave, surge.
4. Find the period of a Tension Leg Platform in surge degree of freedom. The platform has eight tethers made up of steel, with 1.5 MN initial pretension each and 250 m long, 0.9 m diameter. The mass of TLP in surge is  $1.5 \times 10^7$  kg.
5. Name the essential features of buoyant leg structure that makes the structure insensitive to ultra-deep waters.
6. Compare the different wave spectra and write the inferences based on the following spectral density curves.

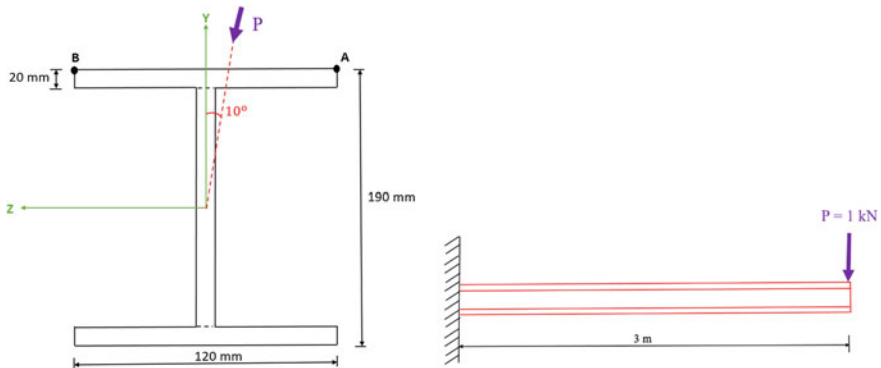


7. List the various ice conditions.
8. What are the factors that affect the dynamic modulus of elasticity?
9. How the orientation of the platform is chosen based on the wave approach angle?

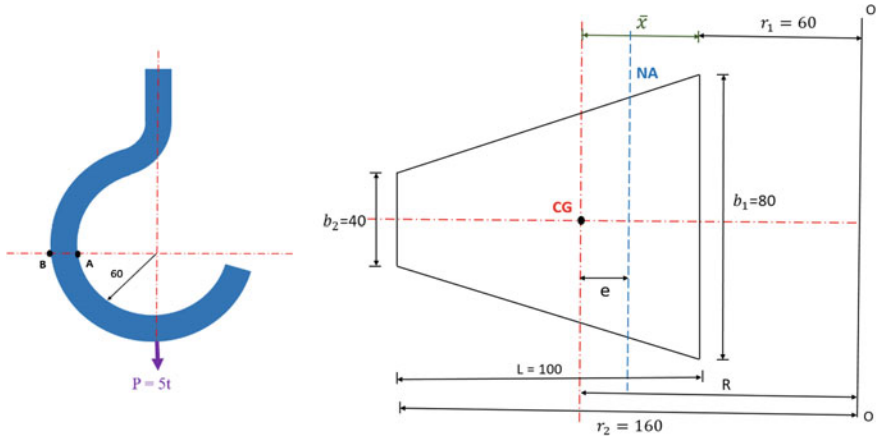
10. What is the effect of springing and ringing waves on the structures?
11. When symmetrical bending occurs in the members?
12. How do you classify the curved beams? What is the condition for the classification?
13. What are the types of failure that may occur on the chain links used as moorings in the offshore structures?
14. List the different group of risers.
15. What are the consequences of vortex-induced vibration on the structure?
16. What are the common mistakes that lead to fire accidents in offshore platforms?
17. Define BLEVE and what are the primary causes of it?
18. Explain blast wave structure interaction.
19. Differentiate the terms blast proof and blast resistant.
20. Name the principal parameters of the blast wave that has to be defined to estimate the blast load.

**Section C: Each question carries five marks. Answer in detail. Draw figures, wherever necessary to support your answer**

1. Elaborate the following: FEED, FPSO, FSRU, BLSRP, JONSWAP, AIT, CVCE, TNT, NFPA, and PSV.
2. Mention the advantages and disadvantages of Spar platform.
3. How do you calculate the total wave force acting on the pile of the jacket leg platform?
4. Find the stresses on the cantilever beam ( $l = 3$  m) of I section at points A and B, shown in the figure below. The load of 1 kN acts at angle of  $10^\circ$  from the vertical axis.



5. A 10-ton crane hook is used to lift an object during commissioning of an offshore deck. Find the stresses at the intrados and extrados using Winkler–Bach equation and Straight Beam formula. The details of the cross section are shown in the figure below:



6. Describe vortex-induced vibration (ViV) and the ways to suppress the effect of it on the structure.
7. List the best practices for fire safety in offshore platforms.
8. Describe the different types of blast waves.

### Key to model exam paper-1

#### Section A:

1. Offshore structures are preferably function-dominant. State true/false and validate the statement.  
*False. Offshore structures are form-dominant.*
2. Compliant structures and fixed structures resist the lateral loads by self-weight and relative displacement, respectively.
3. Continuous rotation of the spud-can arrangement in the guyed towers will lead to fatigue failure of the joint.
4. Give the expression for the resisting moment in articulated towers.  
$$\text{Resisting moment} = \{[(B\rho - M_B)gl_B] - [M_Dgl_D]\}\theta$$
  
*where*  
 $B = \text{Buoyancy provided by the buoyancy tank.}$   
 $l_D = \text{Distance of CG of the deck from the articulated joint.}$   
 $l_B = \text{Distance of center of buoyancy from the articulated joint.}$   
 $\theta = \text{degree of freedom.}$   
 $M_B = \text{Mass of the buoyancy tank.}$   
 $M_D = \text{Mass of the deck.}$
5. Ball joints restrain rotation and allow translation from the buoyant leg to the deck.
6. When the mean square value is unique across the ensemble, the process is said to be stationary process.
7. Ice loads on conical structures cause less response. State true/false and validate the statement.  
*True. Well-defined cone can change the ice failure mode from crushing to bending.*
8. The interaction of ice on the structure will cause ice-induced vibration, which is measured by monitoring the acceleration of the deck.
9. Kanai-Tajimi power spectrum is used for the analysis of the offshore structures under earthquake loads.
10. Springing response is caused by second-order waves in mild and severe sea state, and ringing response is caused by extremely high steep waves.
11. Non-impact waves cause heave response on TLP which will lead to fatigue failure.
12. When the trace of the plane of applied moment does not coincide with any of the principal axes of inertia, then the bending is said to be unsymmetrical.
13. Write the expression for finding the shear stress on the section.

$$\tau = \frac{V\bar{a}\bar{y}}{It}$$

14. Winkler-Bach equation is useful in estimating the stresses in the curved beams with large initial curvature only at the extreme skin layer.

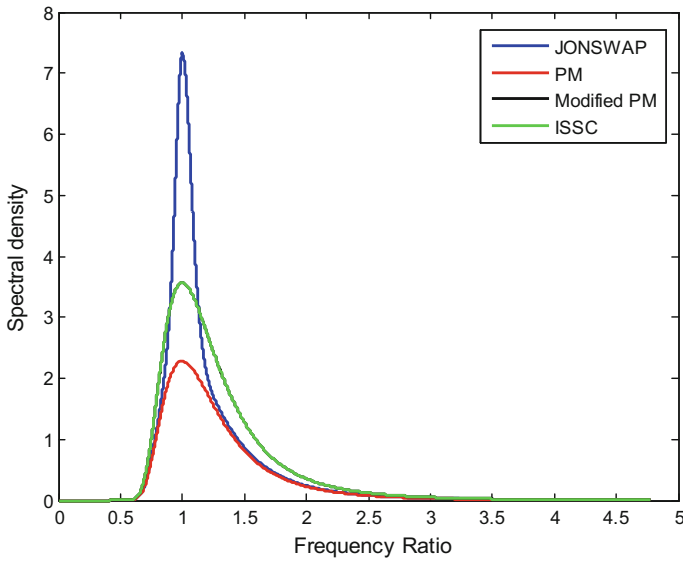
15. When risers are exposed to the fluid flow, flow separation takes place which results in the formation of vortex shedding.
16. Top tensioning is required to maintain the stability of the riser, when installed in greater water depth.
17. Flash point is the lowest temperature at which the liquid gives up enough vapor to maintain the continuous flame.
18. Deflagration arresters reduce the risk of flame propagation.
19. High-strength steel does not have a well-developed yield point, and the yield region is nonlinear.
20. A turbulent diffusion of flame resulting from the combustion of the fuel and propagating in a particular direction with significant momentum is called jet fire.

### **Section B:**

1. List the uncertainties in estimating the environmental loads.
  - *Estimation of direction of approach.*
  - *Estimation of magnitude of loads.*
  - *Return period of the maximum event.*
  - *Non-availability of data.*
2. Does the lateral load acting on the compliant platforms get reduced by the structural action of the platform? Explain.  
*The lateral loads get reduced. Since the compliant platforms are position restrained by tethers or tendons, the horizontal component of the tension in the deflected tendon will reduce the lateral load acting on the platform.*
3. Write the following degrees of freedom in descending order based on the time period of the Spar platform: pitch, heave, surge
  - *Surge: 100–120 s*
  - *Pitch: 60 s*
  - *Heave: 25–40 s*
4. Find the time period of a Tension Leg Platform in surge degree of freedom. The platform has 8 tethers made up of steel, with 1.5 MN initial pretension each and 250 m long, 0.9 m diameter. The mass of TLP in surge is  $1.5 \times 10^7$  kg.

$$(T)_{surge} = 2\pi \sqrt{\frac{m_{surge} l_t}{nT_t}} = 111.07 \text{ s}$$

5. Name the essential features of buoyant leg structure that makes the structure insensitive to ultra-deep waters.
  - *Deep draft*
  - *High stability*
6. Compare the different wave spectra and write the inferences based on the following spectral density curves.



- *The peak value of all the spectrum lies on the same frequency.*
- *JONSWAP spectrum exhibits the highest peak value.*
- *PM spectrum describes a fully developed sea condition and it has the lowest energy.*

7. List the various ice conditions.

- *Level ice*
- *Broken ice*
- *Ice ridges*
- *Ice bergs*

8. What are the factors that affect the dynamic modulus of elasticity?

- *Material on which the experiment is carried out.*
- *Type of test used to find the dynamic modulus of elasticity.*
- *Shape of the specimen used in the experimental setup.*

9. How the orientation of the platform is chosen based on the wave approach angle?

*The orientation is chosen in such a way that the members should have less projected area on the encountered wave direction.*

10. What is the effect of springing and ringing waves on the structures?

- *Generation of high-frequency force.*
- *Builds up resonance-type responses within the period of TLP.*
- *The frequency of the ringing waves seems closer to the natural frequency of the Tension Leg Platforms.*

11. When symmetrical bending occurs in the members?
- *The plane containing one of the principal axes of inertia, plane of applied moment, and plane of deflection should coincide.*
  - *The neutral axis should coincide with the principal axis of inertia.*
12. How do you classify the curved beams? What is the condition for the classification?
- *Beam with small initial curvature.*
  - *Beam with large initial curvature.*
  - *For the beams with small initial curvature, the ratio of the initial radius of curvature to the depth of the section should be greater than 10.*
13. What are the types of failure that may occur on the chain links used as moorings in the offshore structures?
- *Failure due to fatigue crack at the inter-grip area.*
  - *Distortion in the dimensions of the chain along the length.*
  - *Fatigue damage at the weld.*
  - *Erosion at the inter-grip area.*
14. List the different group of risers.
- *Bundled risers.*
  - *Flexible risers.*
  - *Top Tensioned Risers.*
  - *Steel catenary risers.*
  - *Hybrid risers.*
15. What are the consequences of vortex-induced vibration?
- *They can cause alternating pressure field on the surface of the riser.*
  - *Reduction of service life of the system.*
  - *Fatigue damage.*
  - *Induce large transverse motion.*
  - *Cause operational difficulties.*
16. Write the expression for Reynolds number and reduced velocity.
- $$\text{Re} = \frac{\rho u D}{\mu}$$
- $$\text{Reduced Velocity} = \frac{uT}{D}$$
17. Define BLEVE and what are the primary causes of it?
- BLEVE—Boiling Liquid Expanding Vapor Explosion.*  
*This is caused due to the sudden release of large amount of vapor through a narrow opening under pressurized conditions.*
18. Explain blast wave structure interaction.
- When the blast wave hits the structure, the following occurs:*
- *Reflection of waves.*
  - *Refraction of waves.*

- *Vortex formation.*
  - *Diffraction of waves.*
19. Differentiate the terms blast proof and blast resistant.
- *Blast proof is the non-realistic term, and it is difficult to provide a system with complete blast protection.*
  - *Blast resistance should aim to protect the functional requirements of the critical systems from any irreparable damage that leads to catastrophic damage.*
  - *The platform should remain functional even after the blast event.*
20. Name the principal parameters of the blast wave that has to be defined to estimate the blast load.
- *Peak side-on overpressure.*
  - *Phase duration.*
  - *Impulse.*
  - *Peak side-on negative pressure (suction).*
  - *Negative phase duration.*
  - *Associated negative impulse.*

### **Section C:**

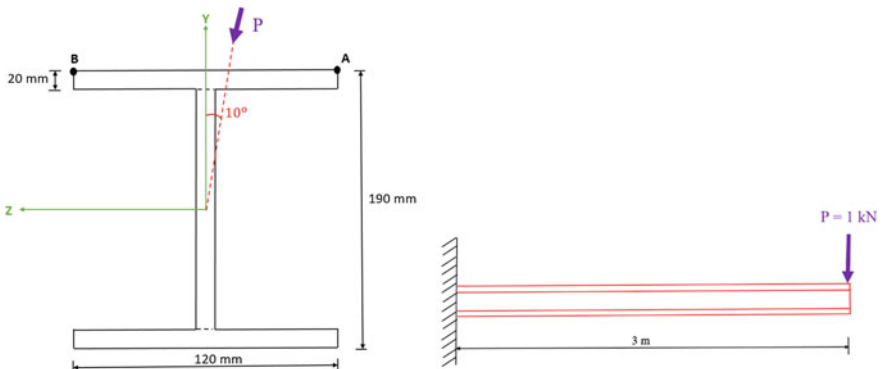
1. Elaborate the following:
- FEED—*Front End Engineering Design.*
- FPSO—*Floating Production Storage and Offloading system.*
- FSRU—*Floating, Storage, Regasification Unit.*
- BLSRP—*Buoyant Leg Storage and Regasification Unit.*
- JONSWAP—*Joint North Sea Wave Project.*
- AIT—*Auto-Ignition Temperature.*
- CVCE—*Confined Vapor Cloud Explosion.*
- TNT—*Tri-Nitro-Toluene.*
- PSV—*Platform Support Vessels.*
- NFPA—*National Fire Protection Association.*
2. Mention the advantages and disadvantages of Spar platform.
- Advantages:*
- *It is a free floating system more or less, and the response in heave and pitch is lesser.*
  - *The drilling risers are protected by the cylinder of the Spar from the wave action.*
  - *Simple fabrication.*
  - *Unconditional stability because the mass center is always located lower than the center of buoyancy.*
  - *Stability is ensured even when the mooring lines are disconnected.*

*Disadvantages:*

- *Installation is difficult compared to other platform, because the topside of the platform can only be placed after upending the cylinder of the Spar.*
  - *Little storage capacity.*
  - *Spar can be used only for storage and offloading.*
  - *It is prone to corrosion.*
3. How do you calculate the total wave force acting on the pile of the jacket leg platform?
- *On a pile member, combined inertia and drag forces will act.*
  - *Forces on the pile member arise due to velocity and acceleration components of the water particles.*
  - *The forces vary with time.*
  - *The combined inertia and drag forces can be found out from the Morison's equation.*
  - *In order to find the maximum forces, the phase angle at which this will occur should be calculated first, which can be calculated by:*

$$\frac{dF_t}{d\theta} = 0$$

- *The maximum force can now be calculated from Morison's equation for the above value of phase angle.*
4. Find the stresses on the cantilever beam ( $l = 3 \text{ m}$ ) of I section at points A and B, as shown in the figure below. The load of 1 kN acts at angle of  $10^\circ$  from the vertical axis.



(i) **Calculation of  $I_z$ ,  $I_y$ , and  $I_{zy}$ :**

$$\bar{y} = \sum \frac{ay}{a} = 95 \text{ mm}$$

$$\bar{z} = \sum \frac{az}{a} = 60 \text{ mm}$$

$$I_y = \frac{2 \times 20 \times 120^3}{12} + \frac{150 \times 20^3}{12} = 0.586 \times 10^7 \text{ mm}^4$$

$$I_z = 2 \left[ \frac{120 \times 20^3}{12} + 120 \times 20 \times (85)^2 \right] + \frac{20 \times 150^3}{12} = 4.046 \times 10^7 \text{ mm}^4$$

(ii) **To locate principal axes ( $u$ ,  $v$ ):**

*Since I section is symmetrical, ZZ and YY axes are the principal axes of UU and VV, respectively.*

$$I_U = 0.586 \times 10^7 \text{ mm}^4$$

$$I_V = 4.046 \times 10^7 \text{ mm}^4$$

(iii) **To find the stresses:**

*Moment about Z-axis = load  $\times$  perpendicular distance =  $1 \times 3 = -3 \text{ kNm}$ .*

$$M_U = M_Z \cos \alpha = -2.954 \text{ kNm}$$

$$M_V = -M_Z \sin \alpha = 0.521 \text{ kNm}$$

$$\sigma_X = - \left( \frac{M_U}{I_U} v - \frac{M_V}{I_V} u \right)$$

*For point A,*

$$u_A = -60 \text{ mm}$$

$$v_A = +95 \text{ mm}$$

$$\sigma_A = - \left( \frac{M_U}{I_U} v_A - \frac{M_V}{I_V} u_A \right) = 1.602 \text{ N/mm}^2 \text{ (tension)}$$

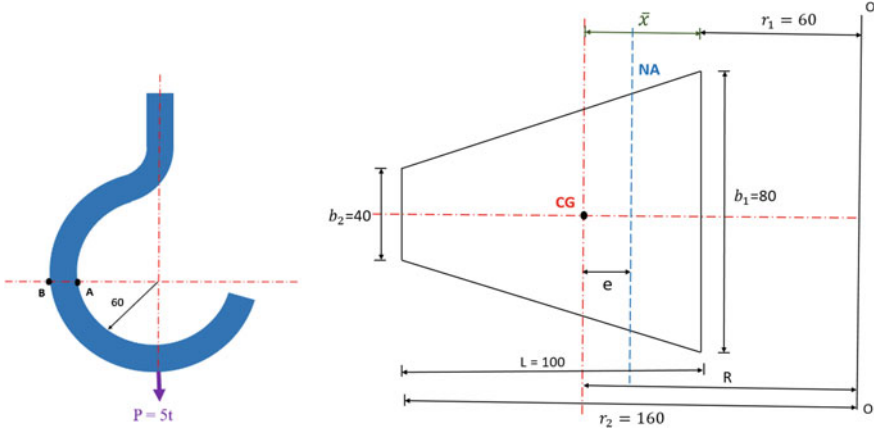
*Similarly for point B,*

$$u_B = 60 \text{ mm}$$

$$v_B = 95 \text{ mm}$$

$$\sigma_B = - \left( \frac{M_U}{I_U} v_B - \frac{M_V}{I_V} u_B \right) = 12.28 \text{ N/mm}^2 \text{ (tension)}$$

5. A 10-ton crane hook is used to lift an object during commissioning of an offshore deck. Find the stresses at the intrados and extrados using Winkler–Bach equation and Straight Beam formula. The details of the cross section are shown in the figure below.



**A. Winkler–Bach Equation**

(i) **Calculation of Geometric properties:**

$$b_3 = 20 \text{ mm}$$

$$\text{Location of the neutral axis, } \bar{x} = \frac{\sum A\bar{x}}{\sum A} = 44.44 \text{ mm}$$

$$h_i = x = 44.44 \text{ mm}$$

$$h_o = h - x = 55.56 \text{ mm}$$

1. Radius of the curved beam,  $R = r_1 + x = 104.44 \text{ mm}$

2. Outer radius of the curved beam,  $r_2 = r_1 + h = 160 \text{ mm}$

3. CS area of the section,  $A = 6000 \text{ mm}^2$

4. Sectional property,  $m$

$$m = 1 - \left(\frac{R}{A}\right) \left\{ \left[ b_2 + \frac{r_2(b_1 - b_2)}{(r_2 - r_1)} \right] \cdot \ln\left(\frac{r_2^2}{r_1^2}\right) - (b_1 - b_2) \right\} = -0.0794 \text{ (no unit)}$$

5. Eccentricity,  $e = \left(\frac{m}{m-1}\right)R = 7.679 \text{ mm}$  (The positive value of 'e' indicates that the Neutral axis will shift toward the center of curvature)

6. Moment of Inertia,  $I = 4.814 \times 10^6 \text{ mm}^4$

(ii) **Section AB:**

$$r_i = r_1 = 60 \text{ mm}$$

$$r_o = r_2 = 100 \text{ mm}$$

(a) Direct Stress,  $\sigma_d = \frac{P}{A} = 8.333 \text{ N/mm}^2$

(b) Moment at CG,  $M = -P \times R = -5.222 \text{ kNm}$

(c) Stress at intrados,  $\sigma_i = -\frac{M}{Ae} \left(\frac{h_i - e}{r_i}\right) = 69.442 \text{ N/mm}^2$  (tensile)

(d) Stress at extrados,  $\sigma_e = \frac{M}{Ae} \left(\frac{h_e - e}{r_e}\right) = -44.79 \text{ N/mm}^2$  (compressive)

- (e) *Total stress at intrados,  $\sigma_A = \sigma_d + \sigma_i = 77.775 \text{ N/mm}^2$  (tensile)*  
 (f) *Total stress at extrados,  $\sigma_B = \sigma_d + \sigma_o = -36.457 \text{ N/mm}^2$  (compressive)*

**B. Straight Beam Formula:**

$$\sigma = \frac{M}{I}y$$

$$y_i = 44.44 \text{ mm}$$

$$y_s = 55.56 \text{ mm}$$

- (a) *Stress at intrados,  $\sigma_i = \frac{M}{I}y_i = 48.205 \text{ N/mm}^2$  (tensile)*  
 (b) *Stress at extrados,  $\sigma_s = \frac{M}{I}y_s = -60.256 \text{ N/mm}^2$  (compressive)*  
 (c) *Total stress at intrados,  $\sigma_A = \sigma_d + \sigma_i = 56.539 \text{ N/mm}^2$  (tensile)*  
 (d) *Total stress at extrados,  $\sigma_B = \sigma_d + \sigma_s = -51.923 \text{ N/mm}^2$  (compressive)*

6. Describe vortex-induced vibration and the ways to suppress the effect of it on the structure.

- *As the fluid passes the body, flow separation occurs. This results in the formation of vortex behind the body.*
- *Vortex shedding frequency tries to lock-in with the natural frequency of the riser, which leads to resonating condition.*

*Consequences of VIV:*

- *They can cause alternating pressure field on the surface of the riser.*
- *Reduction of service life of the system.*
- *Fatigue damage.*
- *Induce large transverse motion.*
- *Cause operational difficulties.*

*VIV suppression:*

- *By providing surface protrusion—helical strakes.*
- *By attaching the projected plates called near-wake stabilizers.*
- *By providing shroud, which is a perforated cover around the member.*
- *Changing the geometric shape of the platform.*
- *By ensuring smooth surface of the members.*
- *By connecting external dampers.*

7. List the best practices for fire safety in offshore platforms.

- *Fluid should be used above the flash point temperature and the fire point temperature, but not above AIT.*
- *Fluid can be used up to their maximum bulk temperature, which is higher than the flash and fire point temperature of the fluid.*
- *Avoid designing confined space with the presence of ignition source, because that can result in flash fire easily.*

- *Through proper system design, one can ensure that no oxygen content is available at the heat source.*
- *Fluid should be well contained within the system.*
- *Fluid containment should not have direct contact with the external ignition source.*

8. Describe the different types of blast waves.

*Shock wave:*

- *Leads to instantaneous shoot up of pressure above the ambient temperature.*
- *The peak side-on pressure then gradually returns to the ambient conditions.*
- *This also results in negative pressure wave, following the positive phase of the shock wave.*

*Pressure wave:*

- *Gradual rise in the pressure to reach the peak side-on overpressure.*
- *It then gradually decays without any negative phase.*
- *Shock waves are the consequences of extremely energetic vapor cloud explosion.*
- *Vapor cloud deflagration will result in rise of pressure waves in the near field.*
- *They will further propagate to the far field as a shock wave.*
- *Negative phase of the shock wave is weaker, but sometimes a suction pressure can also cause significant damage.*

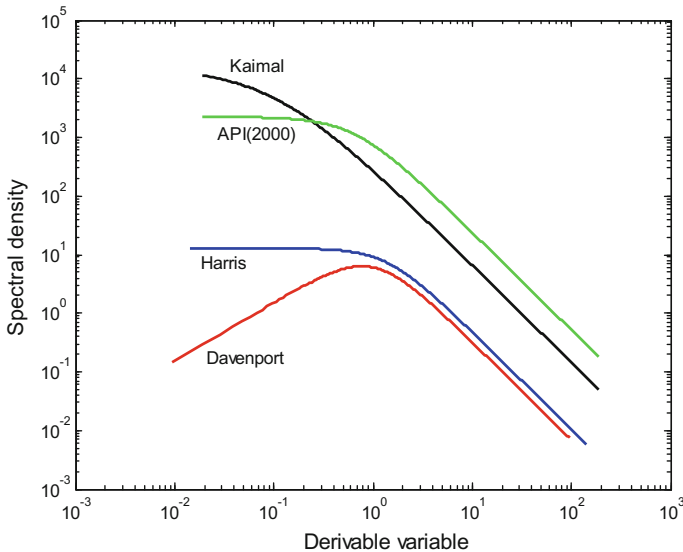
**Model exam paper-2****Design aids for offshore structures under special environmental loads including fire resistance****Time: 3 h Max marks: 100****Section A: Each question carries one mark. Use appropriate key words to answer**

1. Offshore structures are unique by \_\_\_\_\_ and \_\_\_\_\_.
2. Fixed structures trigger \_\_\_\_\_ mode of failure.
3. In Spar platform, helical strakes are provided around the cylinder to reduce \_\_\_\_\_.
4. Wave direction does not influence the response of triceratops platform. State true/false.
5. Airy's theory is valid only up to \_\_\_\_\_ and stretching modifications should be accounted for \_\_\_\_\_.
6. The wind spectra applicable for the offshore structures are \_\_\_\_\_ and \_\_\_\_\_.
7. If the return period of the event is reduced, the probability of exceedance of the event will \_\_\_\_\_.
8. Any sample from the process which represents the average statistical properties of the entire process is said to be \_\_\_\_\_.
9. Earthquake loads affect the superstructure of the Tension Leg Platforms indirectly by inducing \_\_\_\_\_.
10. Triangular geometry of TLP is advantageous compared to square geometry. Why?
11. Pitch response of triangular TLP is \_\_\_\_\_ than the square TLP.
12. \_\_\_\_\_ is used for the simulation of the extreme waves in square TLP.
13. Due to unsymmetrical bending, thin sections will undergo \_\_\_\_\_ under transverse loads.
14. If a section has one axis of symmetry, the shear center will lie on \_\_\_\_\_.
15. Write the Winkler-Bach equation
16. \_\_\_\_\_ should be introduced in the chain link when the stress in the links is greater than the permissible limits.
17. The inner metal surface of the layered riser is called \_\_\_\_\_.
18. AIT is also known \_\_\_\_\_ and \_\_\_\_\_.
19. If the ignition source is present, and the vessel is in contact with the ignition source, then it will result in the formation of \_\_\_\_\_.
20. Rear wall load tends to \_\_\_\_\_ the overall blast wave force.

**Section B: Each question carries two marks. Answer briefly**

1. Elaborate the following:

- DPS
  - BLS
  - VIV
  - BLEVE
2. Explain the structural action of the spud-can arrangement with neat sketch.
  3. Find the stiffness and time period of the Spar platform of 30 m diameter and mass in heave degree of freedom is  $60,000r$ .
  4. Platforms' remaining stiff in heave degree of freedom is advisable. Why?
  5. Write the expression for horizontal and vertical water particle velocities based on Airy's theory.
  6. Why aerodynamic admittance function is used? State the reasons.
  7. State the inferences for the following wind spectra.



8. How uncertainties in the analysis and design of the structures are grouped?
9. What are the assumptions made in the earthquake analysis of the offshore structures?
10. Write the classification of loads.
11. Mention the effect of impact waves and non-impact waves on TLP.
12. What are the consequences of transverse loading on the structural members?
13. What is the advantage of using buoyancy modules in the risers?
14. What are the ways through which VIV suppression can be achieved in the structure?

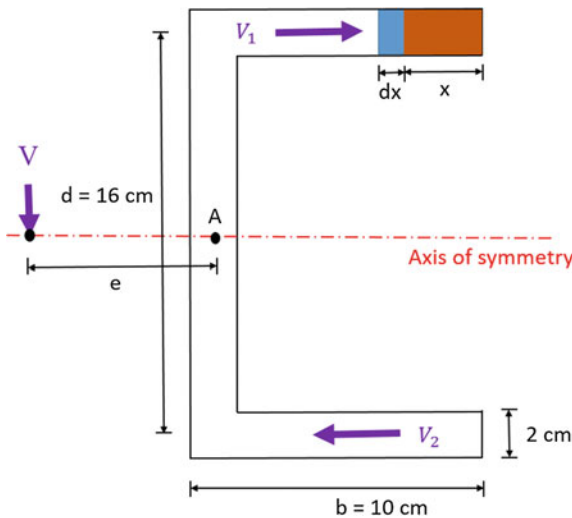
15. Differentiate fire and explosion.
16. Arrange the following in ascending order based on their temperature.  
Oxyhydrogen fire, simple candle, air acetylene fire, blow torch under welding operation.
17. How the consequences due to the explosion damage can be measured?
18. List the general design requirements of fire protection in the offshore platforms.
19. Define peak-reflected pressure and peak dynamic pressure.
20. Name the different types of fire.

**Section C: Each question carries five marks. Answer in detail. Draw figures, wherever necessary to support your answer**

1. Match the following:

1	Fixed structures	A	Exploratory drilling
2	Articulated towers	B	Deck-isolated platforms
3	Tethers	C	Turret mooring
4	Guyed towers	D	Tethered Spar
5	Compliant structures	E	Attract more forces
6	FPSO	F	DPS
7	Jack-up rig	G	Skirt piles
8	Drill ships	H	Position restraint
9	Gravity-based structure	I	Recentering is gentle
10	Jacket platforms	J	Spud-can
11	BLS	K	Seabed scouring
12	Triceratops	L	Better under cyclic loads

2. Explain the structural action of TLP.
3. Locate the shear center for the channel section as shown in figure.



4. Write a short note on different types of risers.
5. Describe the steps involved in the identification of explosion damage.
6. Mention the basic problems in the offshore platforms that make fire protection very difficult.
7. Compute the front wall loading due to blast waves traveling horizontally on the building module of offshore platform. Length = 15 m, breadth = 30 m, height = 5 m, and the blast wave approaches the building in the direction parallel to the length of the building. The peak side-on overpressure is 50 kPa for the duration of 0.06 s.
8. Write a case study on the piper alpha accident and deepwater horizon accident.

### Key to model exam paper-2

#### Section A:

1. Offshore structures are unique by innovative design and functional requirements.
2. Fixed structures triggers brittle mode of failure.
3. In Spar platform, helical strakes are provided around the cylinder to reduce vortex-induced vibration.
4. Wave direction does not influence the response of triceratops platform. State true/false.  
*True because the legs of the platform are symmetrically placed.*
5. Airy's theory is valid only up to mean sea level and stretching modifications should be accounted for the actual level of submergence.
6. The wind spectra applicable for the offshore structures are Kaimal spectrum and API spectrum.
7. If the return period of the event is reduced, the probability of exceedance of the event will increase.
8. Any sample from the process which represents the average statistical properties of the entire process is said to be ergodic.
9. Earthquake loads affect the superstructure of the Tension Leg Platforms indirectly by inducing tether tension variation.
10. Triangular geometry of TLP is advantageous compared to square geometry. Why?
  - *Increased tolerance for the position of foundation.*
  - *Increased drought and heat tolerance.*
11. Pitch response of triangular TLP is lesser than the square TLP.
12. Freak wave model is used for the simulation of the extreme waves in square TLP.
13. Due to unsymmetrical bending, thin sections will undergo twisting under transverse loads.
14. If a section has one axis of symmetry, the shear center will lie on the axis of the section.
15. Write the Winkler–Bach equation.

$$\sigma = \frac{M}{AR} \left[ 1 - \frac{1}{m} \left( \frac{y}{R+y} \right) \right]$$

16. Central stud should be introduced in the chain link when the stress in the links is greater than the permissible limits.
17. The inner metal surface of the layered riser is called carcass.
18. AIT is also known as self-ignition temperature and kindling point of the material.
19. If the ignition source is present, and the vessel is in contact with the ignition source, then it will result in the formation of fire ball.

20. Rear wall load tends to reduce the overall blast wave force.

**Section B:**

1. Elaborate the following:

DPS—*Dynamic Positioning System.*

BLS—*Buoyant Leg Structure.*

VIV—*Vortex-Induced Vibration.*

BLEVE—*Boiling Liquid Expanding Vapor Explosion.*

2. Explain the structural action of the spud-can arrangement with neat sketch.

- *Spud-can is similar to the inverted cone placed under suction.*
- *When the spud-can arrangement is placed on the seabed with high pressure, partial vacuum will develop inside the cone arrangement.*
- *The partial vacuum space is the filled by the soil particles surrounding the spud-can, and hence, high pressure is required to remove the spud-can from its position.*

3. Find the stiffness and time period of the Spar platform of 30 m diameter and mass in heave degree of freedom is  $60,000t$ .

$$\text{Stiffness} = \rho g \pi R^2 = 1025 \times 9.81 \times \pi \times (15)^2 = 7.1 \times 10^6 \text{ N/m}$$

$$m = 6 \times 10^7 \text{ kg}$$

$$\omega = \sqrt{k/m} = 0.344$$

$$T = \frac{1}{\omega} = 2.907 \text{ s}$$

4. Platforms' remaining stiff in heave degree of freedom is advisable. Why?

- *For operational convenience.*
- *To reduce the change in tension in the tethers and to avoid fatigue failure.*
- *To reduce the consequences of change in buoyancy by the added mass.*

5. Write the expression for horizontal and vertical water particle velocities based on Airy's theory.

$$\dot{u}(x, t) = \frac{\omega H \cos h ky}{2 \sin h kd} \cos(kx - \omega t)$$

$$\dot{v}(x, t) = \frac{\omega H \sin h ky}{2 \sin h kd} \sin(kx - \omega t)$$

where

$\dot{u}$  *horizontal water particle velocity.*

$\dot{v}$  *vertical water particle velocity.*

$k$  *wave number =  $2\pi/\omega$ .*

$H$  *wave amplitude.*

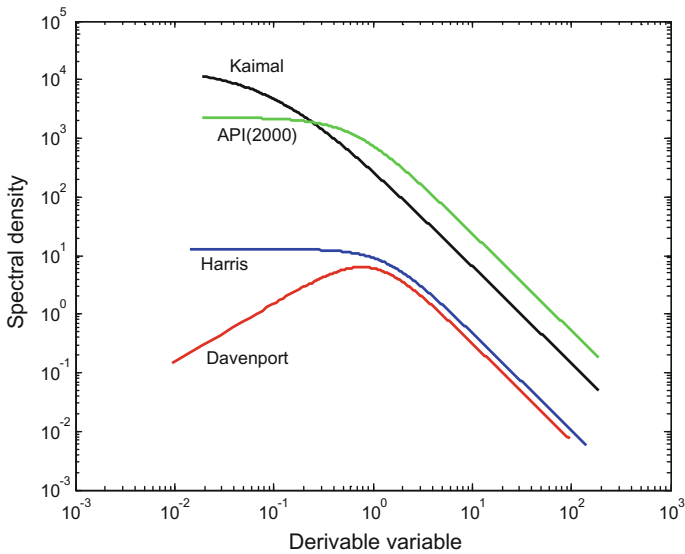
$d$  *water depth.*

$Y$  *depth at which the velocity is measured*

6. Why aerodynamic admittance function is used? State the reasons.

- *Aerodynamic admittance function is used to find the equivalent total wind load acting on the members.*
- *It is used to bypass the rigorous random variable.*
- *The value can be found experimentally.*

7. State the inferences for the following wind spectra.



- *The variation among the spectrum is considerable at lower frequencies.*
- *The variation between API and Kaimal spectra is considerably low.*
- *Davenport spectrum and Harris spectrum are not applicable to offshore structures, and they found to have lower peak value.*

8. How uncertainties in the analysis and design of the structures are grouped?

- Group I: related to material characteristics.
- Group II: related to load estimation.
- Group III: arises due to mathematical modeling and method of analysis.

9. What are the assumptions made in the earthquake analysis of the offshore structures?

- *Seabed movement is horizontal.*
- *The movement of seabed is very low, and second-order forces generated due to the seabed movement is generally neglected.*
- *Radiation damping is neglected for the slender structures.*

10. Write the classification of loads.

- *P class loads—permanent loads.*
- *L class loads—live loads.*
- *D class loads—deformation loads.*
- *E class loads—environmental loads.*
- *A class loads—accidental loads.*

11. Mention the effect of impact waves and non-impact waves on TLP.

*Impact waves:*

- *Cause ringing response.*
- *Pitch dof is influenced.*
- *Challenge the operability of the platform.*
- *Lead to tether pull-out and stability issues.*

*Non-impact waves:*

- *Cause springing response.*
- *Heave dof is influenced.*
- *Lead to fatigue failure of tethers.*

12. What are the consequences of transverse loading on the structural members?

- *Members will have premature failure due to twisting before bending.*
- *Plasticization of twisted members.*

13. What is the advantage of using buoyancy modules in the risers?

- *They are helpful in reducing the top tension force, which is required in the installation of the risers.*
- *They make the risers neutrally buoyant.*

14. What are the ways through which VIV suppression can be achieved in the structure?

- *Surface protrusion—helical strakes.*
- *Helically wound wire.*
- *Projected plates.*
- *Shrouds.*
- *Proper design.*
- *Smooth surface.*

15. Differentiate fire and explosion.

*Fire:*

- *It is a rapid exothermal oxidation of the ignition fuel.*

*Explosion:*

- *Rapid expansion of gases resulting from the pressure waves or shock waves.*
- *Explosion releases energy very rapidly.*

16. Arrange the following in ascending order based on their temperature.  
 Oxyhydrogen fire, simple candle, air acetylene fire, blow torch under welding operation.  
 2-4-3-1
17. How the consequences due to the explosion damage can be measured?
- *One of the common methods used to measure the consequences of explosion damage is TNT equivalence method.*
  - *TNT is an important explosive, which rapidly changes its form from solid to hot expanding gas.*
18. List the general design requirements of fire protection in the offshore platforms.
- *They should be compact in size and weight.*
  - *They should be easy to operate.*
  - *They should be rapid activation systems.*
  - *They should be accessible.*
19. Define peak-reflected pressure and peak dynamic pressure.  
*Peak-reflected pressure:*
- *When the blast wave hits the surface of the bluff body, it reflects back.*
  - *The effect of this reflection depends upon the surface characteristics of the body.*
  - *Surface will experience more pressure than the incident side-on pressure.*
  - $P_r = C_r P_{so}$
- where*  
 $C_r$  *is the reflection coefficient.*  
*Peak dynamic pressure:*
- *Blast wave moves due to the air movement.*
  - *Wind pressure depends upon the magnitude of peak over pressure of the blast wave.*
20. Name the different types of fire.
- *Pool fire.*
  - *Jet fire.*
  - *Fire ball.*
  - *Flash fire.*

**Section C:**

1. Match the following:

1	Fixed structures	A	Exploratory drilling
2	Articulated towers	B	Deck-isolated platforms
3	Tethers	C	Turret mooring
4	Guyed towers	D	Tethered Spar
5	Compliant structures	E	Attract more forces
6	FPSO	F	DPS
7	Jack-up rig	G	Skirt piles
8	Drill ships	H	Position restraint
9	Gravity-based structure	I	Recentering is gentle
10	Jacket platforms	J	Spud-can
11	BLS	K	Seabed scouring
12	Triceratops	L	Better under cyclic loads

1-e, 2-i, 3-h, 4-j, 5-b, 6-c, 7-a, 8-f, 9-k, 10-g, 11-d, 12-b

2. Explain the structural action of TLP.

- *The structure is vertically restrained while it is compliant in the horizontal direction, permitting surge, sway, and yaw motion. The structural action results in low vertical force in rough seas, which is the key design factor.*

$$W \lll F_B$$

$$W + T_s = F_B$$

where

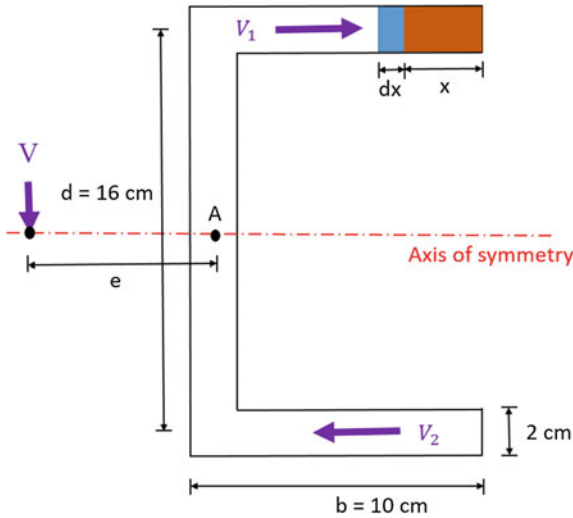
$W$  weight of the platform.

$T_o$  initial axial pretension which was set initially in the structure to hold the platform down (20% of total weight).

$F_B$  buoyancy force

- *Due to lateral forces, the platform moves along the wave direction. Horizontal movement is called **offset**.*
- *Due to horizontal movement, the platform also has the tendency to have increased immersed volume of members. Thus, the platform will undergo **set-down** effect.*
- *The lateral movement increases the tension in the tethers. The horizontal component of tensile force counteracts the wave action, and the vertical component increases the weight which will balance the additional weight imposed by set down.*

3. Locate the shear center for the channel section as shown in the figure below:



Consider a section of thickness 'dx' on the flange at a distance 'x' from the end.

$$V_1 = \int \tau da$$

$$V_1 = \int \frac{VA\bar{y}}{I} da$$

where  $A = t x$   
 $da = dx t$   
 $\bar{y} = d/2$

$$V_1 = \frac{V}{I} \int_0^b (tx)(dxt) \frac{d}{2} = \left[ \frac{V t^2 d x^2}{I t 2} \right]_0^b$$

$$= \frac{V t b^2 d}{4I}$$

By symmetry,  $V_1 = V_2 = \frac{V t b^2 d}{4I}$

Neglecting the shear taken by the web and taking moment about the point A on the web,

$$V e = V_1 \frac{d}{2} + V_2 \frac{d}{2}$$

$$V e = \frac{V t b^2 d}{4I} \times d$$

$$e = \frac{t b^2 d^2}{2I}$$

Moment of inertia,  $I = 3.031 \times 10^7 \text{ mm}^4$

$e = 8.44 \text{ cm}$ .

4. Write a short note on different types of risers.

*Low-pressure risers:*

- Large diameter risers that are open to the atmospheric pressure at the top end.
- They are useful for drilling.

- They also have a lot of peripheral lines.
- Kill and choke lines are useful to circulate the fluid when kick occurs.
- They are also useful in communicating with the well about the closure of BOP.
- Booster lines are useful to inject fluid at the lower end and to accelerate the flow.
- When the risers are installed at greater water depth, they need top tensioning.

*High-pressure risers:*

- These risers are installed when the blow-out preventer is located closer to the surface.
- These risers do not require any additional peripheral lines which are essentially useful for communicating with the BOP.
- These risers are designed to operate at full pressure.

*Flexible risers:*

- They are useful as production risers.
- Flow lines.

*Top Tensioned Risers:*

- These are required to ensure stability.
- They connect the seabed through a stress joint.
- In addition, these risers will also have keel joint, which is located at keel level of the platform.
- As these risers are highly flexible in terms of its cross section, they undergo large deformation.

5. Describe the steps involved in the identification of explosion damage.

*One of the common methods to estimate the consequences of explosion damage is TNT equivalence method. The steps involved are as follows:*

- Calculation of total mass of the fluid involved.
- Calculation of explosion energy.
- Computation of TNT equivalence.

$$m_{\text{TNT}} = \eta \frac{m\Delta H_c}{E}$$

- Calculation of scaled distance.

$$Z_e = \frac{r}{\sqrt[3]{m_{\text{TNT}}}}$$

- Calculation of peak overpressure.

6. Mention the basic problems in the offshore platforms that make fire protection very difficult.

- *Offshore platforms generally have congested layout of topside module.*
  - *They operate in a very confined and compact space.*
  - *Offshore production equipment is not laid horizontally but laid vertically.*
  - *They impose extensive weight and space limitation for fire protection equipment to be provided on board.*
  - *Usage of seawater for fire protection may lead to corrosion.*
  - *Pure water to be used for fire protection system in offshore platforms.*
7. Compute the front wall loading due to blast waves traveling horizontally on the building module of offshore platform. Length = 15 m, breadth = 30 m, height = 5 m, and the blast wave approaches the building in the direction parallel to the length of the building. The peak side-on overpressure is 50 kPa for the duration of 0.06 s.

(i) *Shock wave parameters:*

- a. *shock wave velocity,  $u = 345 (1 + 0.0083P_{so})^{0.5} = 410.39$  m/s.*
- b. *length of the pressure wave  $= u \cdot t_d = 24.623$  m.*
- c. *peak dynamic wind pressure,  $q_s = 0.0032(P_{so})^2 = 8$  kPa.*

(ii) *Front wall loading:*

*Reflected overpressure,  $C_r = 2 + 0.0073P_{so} = 2.365$*

*$P_r = C_r P_{so} = 118.25$  kPa.*

*Clearing distance is the least of  $B_H = 5$  m and  $B_W/2 = 5$  m.*

*$S = 5$  m*

*Reflected overpressure clearing time,  $t_c = 3S/u = 0.0366$ .*

*Drag coefficient = 1.0*

*Stagnation pressure,  $P_s = P_{so} + C_d q_s = 58$  kPa.*

*Front wall impulse,  $I_w = 0.5(P_r - P_s)t_c + 0.5P_s t_d = 2.84$  kPa s*

*Effective duration,  $t_e = \frac{2I_w}{P_r} = 0.048$  s.*

8. Write a case study on the piper alpha accident and deepwater horizon accident.  
*Piper alpha accident:*

- *July 6, 1998, in the North Sea.*
- *Fire and explosion occurred.*
- *The consequences are highly severe. 167 people died and financial loss of about 3.4 billion US dollars in 1998.*
- *Accident occurred due to human error during operation/maintenance and faulty design of the platform.*

*Deepwater horizon:*

- *It is a semisubmersible MODU.*
- *Accident occurred on April 20, 2010, in Gulf of Mexico.*
- *It caused severe human and environmental impact.*
- *Fire and explosion occurred which leads to capsizing of the vessel and oil spill.*
- *Reason for the explosion is faulty design.*

# References

- Adams AJ, Baltrop NDP (1991) Dynamics of fixed marine structures. Butterworth-Heinemann Ltd., London
- Adrezin R, Benaroya H (1999) Non-linear stochastic dynamics of tension leg platforms. *J Sound Vib* 220(1):27–65
- Adrezin R, Bar-Avi P, Benaroya H (1996) Dynamic response of compliant offshore structures—review. *J Aerosp Eng* 9(4):114–131
- Agarwal AK, Jain AK (2002) Dynamic behavior of offshore spar platforms under regular sea waves. *Ocean Eng* 30:487–516
- Ahmad S (1996) Stochastic TLP response under long crested random sea. *Comput Struct* 61(6):975–993
- Aktan AE, Catbas FN, Turer A, Zhang ZF (1998) Structural identification: analytical aspects. *J Struct Eng* 124(7):817–829
- Anagnostopoulos SA (1982) Dynamic response of offshore structures to extreme waves including fluid-structure interaction. *Eng Struct* 4:179–185
- Anagnostopoulos P, Bearman PW (1992) Response characteristics of a vortex-excited cylinder at low Reynolds numbers. *J Fluids Struct* 6:39–50
- API RP 2T (1997) Recommended practice for planning, designing, and constructing tension leg platforms, 2nd edn
- API RP WSD (2005) Recommended practice for planning, designing and constructing fixed offshore platforms-working stress design. American Petroleum Institute, Washington
- Arnott AD, Greated CA, Incecik A, McLeary A (1997) An investigation of extreme wave behavior around the model TLP. *Int J Offshore Polar Eng* 8(1), ISOPE-98-08-1-051
- ASTM E119-88 (1988) Standard test methods for fire tests of building construction and materials. American Society for Testing and Materials, ASTM E119-88
- Attorney (2016) Oil Rig Explosion, <http://www.oilrigexplosionattorneys.com/Oil-Rig-Explosions/History-of-Offshore-Accidents.aspx>. Accessed Dec 2016.
- Babrauskas V, Grayson SJ (eds) (1992) Heat release in fires. Elsevier Applied Science, Amsterdam
- Bai Y (2001) Pipelines and risers, vol 3. Elsevier Ocean Engineering Book Series, Amsterdam
- Bar Avi P (1999) Nonlinear dynamic response of a tension leg platform. *J Offshore Mech Arct Eng* 121:219–226
- Bar-Avi P, Benaroya H (1996) Non-linear dynamics of an articulated tower in the ocean. *J sound Vib* 190(1):77–103
- Bea RG, Xu T, Stear J, Ramas R (1999) Wave forces on decks of offshore platforms. *J Waterw Port Coast Ocean Eng* 125(3):136–144
- Bearman PW (1984) Vortex shedding from oscillating bluff bodies. *Annu Rev Fluid Mech* 16:195–222
- Blevins RD (1994) Flow induced vibration, 2nd edn. Krieger Publishing, Malabar

- Boaghe OM, Billings SA, Stansby PK (1998) Spectral analysis for non-linear wave forces. *J Appl Ocean Res* 20:199–212
- Booton M, Joglekar N, Deb M (1987) The effect of tether damage on tension leg platform dynamics. *J Offshore Mech Arct Eng* 109:186–192
- Brika D, Laneville A (1993) Vortex-induced vibrations of a long flexible circular cylinder. *J Fluid Mech* 250:481–508
- BS 5950 (2003) Structural use of steel works in buildings, part 8: code of practice of fire-resistant design, British Standards, London
- BS6235 (1982) Code of practice for fixed offshore structures. British Standards Institution, London
- Buchner B, Bunnik T (2007) Extreme wave effects on deepwater floating structures. In: *Offshore Technology Conference*, OTC 18493, Houston, Texas, 30 Apr–3 May
- Buchner B, Wichers JEW, de Wilde JJ (1999) Features of the state-of-the-art deepwater offshore basin. In: *Offshore Technology Conference*, OTC 10841, Houston, Texas, 3–6 May
- Burrows R, Tickell RG, Hames D, Najafian G (1992) Morison wave forces co-efficient for application to random seas. *J Appl Ocean Res* 19:183–199
- Capanoglu CC, Shaver CB, Hirayama H, Sao K (2002) Comparison of model test results and analytical motion analyses for buoyant leg structure. In: *Proceedings of the Twelfth International Offshore and Polar Engineering Conference*. Kitakyushu, Japan, 26–31 May, pp 46–53
- Chakrabarthi SK (2005) *Handbook of offshore engineering, offshore structure analysis*, vol II, Inc., Plainfield, Illinois, USA
- Chakrabarti SK (1971) Non-deterministic analysis of offshore structures. *J Eng Mech ASCE* 97
- Chakrabarti SK (1980) In line forces on fixed vertical cylinder in waves. *J Waterw Port Coast Ocean Eng ASCE* 106:145–155
- Chakrabarti SK (1984) Steady drift force on vertical cylinder—viscous vs. potential. *Appl Ocean Res* 6(2):73–82
- Chakrabarti SK (1987) *Hydrodynamics of offshore structures*. Springer publication co, Singapore
- Chakrabarti SK (1990) *Non-linear methods in offshore engineering*. Elsevier Science Publisher, The Netherlands
- Chakrabarti SK (1994) *Offshore structure modeling*. World Scientific, Singapore
- Chakrabarti SK (1998) Physical model testing of floating offshore structures. In: *Dynamic Positioning Conference*, Session Index, Design, 13–14 Oct, Houston, Texas
- Chang FK (ed) (1997) *Proceeding of 1st International Workshop on Structural Health Monitoring*, Stanford, California.
- Chang FK (ed) (1999) *Prof. of 2nd International Workshop on Structural Health Monitoring*, Stanford, California
- Chakrabarti SK, Tam WA (1975) Wave height distribution around vertical cylinder. *J Waterw Harbor Coast Eng Div ASCE* 101:225–230
- Chakrabarti SK, Wolbert AL, Tam AW (1976) Wave force on the vertical cylinder. *J Waterw Harbor Coast Eng Div ASCE* 10(2):203–221
- Chakrabarti SK, Libby AR, Kompare DJ (1987) Dynamic pressures around a vertical cylinder in waves. In: *Offshore Technology Conference*. OTC 5102, pp 193–199
- Chandrasekaran S (2007) Influence of wave approach angle on TLP's response. *Ocean Eng* 34:1322–1327
- Chandrasekaran S (2013a) *Advanced marine structures*, video course on National Program on Technology Enhanced Learning (NPTEL) portal, Min. Human Resource Dev., Govt. of India. Available at <http://nptel.ac.in/courses/114106037/>
- Chandrasekaran S (2013b) *Dynamics of ocean structures*, Video Course on National Program on Technology Enhanced Learning (NPTEL) portal, Min. Human Resource Dev., Govt. of India. Available at <http://nptel.ac.in/courses/114106036/>

- Chandrasekaran S (2013c) Ocean structures and materials, Video course on National Program on Technology Enhanced Learning (NPTEL) portal, Min. Human Resource Dev., Govt. of India. Available at <http://nptel.ac.in/courses/114106035/>
- Chandrasekaran S (2015) Dynamic analysis of offshore structures, Video course on Massive Open Online Course (MOOC), National Program on Technology Enhanced Learning (NPTEL) portal, Min. Human Resource Dev., Govt. of India. Available at [https://onlinecourses.nptel.ac.in/noc15\\_oe01/preview](https://onlinecourses.nptel.ac.in/noc15_oe01/preview)
- Chandrasekaran S (2016) Risk and Reliability of offshore structures, Video course on Massive Open Online Course (MOOC), National Program on Technology Enhanced Learning (NPTEL) portal, Min. Human Resource Dev., Govt. of India. Available at [https://onlinecourses.nptel.ac.in/noc16\\_oe01](https://onlinecourses.nptel.ac.in/noc16_oe01)
- Chandrasekaran S (2017) Offshore structures under special loads including fire resistance, Video course on Massive Open Online Course (MOOC), National Program on Technology Enhanced Learning (NPTEL) portal, Min. Human Resource Dev., Govt. of India. Available at [https://onlinecourses.nptel.ac.in/noc17\\_oe01/preview](https://onlinecourses.nptel.ac.in/noc17_oe01/preview)
- Chandrasekaran S, Gaurav S (2008) Offshore triangular TLP earthquake motion analysis under distinctly high sea waves. *Ship Offshore Struct* 3(3):173–184
- Chandrasekaran S, Jain AK (2002) Dynamic behavior of square and triangular offshore tension leg platform under regular waves. *Ocean Eng* 29(3):279–313
- Chandrasekaran S, Jain AK (2002) Triangular configuration tension leg platform behavior under random sea wave loads. *Ocean Eng* 29(15):1895–1928
- Chandrasekaran S, Jain AK (2004) Aerodynamic behavior of offshore triangular tension leg platforms. In: *Proceeding ISOPE; 2004 May 23–28; Toulon, France*. pp 564–569
- Chandrasekaran S, Khader SA (2016) Hydrodynamic performance of a moored barge in irregular wave. *Int J Environ Chem Ecol Eng* 10(1):47–54
- Chandrasekaran S, Yuvraj K (2013) Dynamic analysis of a tension leg platform under extreme waves. *J Naval Architect Mar Eng* 10:59–68
- Chandrasekaran S, Yuvraj K (2013) Dynamic analysis of a tension leg platform under extreme waves. *J Naval Arch Mar Engg* 10:5968. <https://doi.org/10.3329/jname.v10i1.14518>
- Chandrasekaran S, Lognath RS (2015) Dynamic analyses of buoyant leg storage regasification platform (BLSRP) under regular waves: experimental investigations. *Ships Offshore Struct*. <https://doi.org/10.1080/17445302.2015.1131006>
- Chandrasekaran S, Lognath RS (2017) Dynamic analyses of buoyant leg storage and regasification platforms: numerical studies. *J Mar Syst Ocean Tech*. <https://doi.org/10.1007/s40868-017-0022-6>
- Chandrasekaran S, Madavi N (2014) Retrofitting of offshore structural member using perforated cylinders. *SFA Newsletter* 13:10–11
- Chandrasekaran S, Madhavi N (2014) Hydrodynamic performance of retrofitted structural member under regular waves. *Int J Forensic Eng, Inder Sci* 2(2):100–121
- Chandrasekaran S, Madhavi N (2014) Numerical study on geometrical configurations of perforated cylindrical structures. *J Perform Constr Facil ASCE* 30(1):04014185. [https://doi.org/10.1061/\(ASCE\)CF.1943-5509.0000687](https://doi.org/10.1061/(ASCE)CF.1943-5509.0000687)
- Chandrasekaran S, Madhavi N (2015) Design aids for offshore structures with perforated members. *Ship Offshore Struct* 10(2):183–203. <https://doi.org/10.1080/17445302.2014.918309>
- Chandrasekaran S, Madhavi N (2015) Retrofitting of offshore cylindrical structures with different geometrical configuration of perforated outer cover. *Int J Shipbuilding Prog* 62(1–2):43–56
- Chandrasekaran S, Madhavi N (2015) Design aids for offshore structures with perforated members. *Ship Offshore Struct* 10(2):183–203
- Chandrasekaran S, Madhavi N (2015) Flow field around a outer perforated circular cylinder under regular waves: numerical study. *Int J Mar Syst Ocean Technol*. <https://doi.org/10.1007/s40868-015-0008-1>

- Chandrasekaran S, Madhavi N (2015) Retrofitting of offshore cylindrical structures with different geometrical configuration of perforated outer cover. *Int J Shipbuilding Prog* 62(1–2):43–56. <https://doi.org/10.3233/ISP-150115>
- Chandrasekaran S, Madhavi N (2015) Variation of flow field around twin cylinders with and without outer perforated cylinder: numerical studies. *China Ocean Eng* 30(5):763–771
- Chandrasekaran S, Madhuri S (2015) Dynamic response of offshore triceratops: numerical and experimental investigations. *Ocean Eng* 109(15):401–409. <https://doi.org/10.1016/j.oceaneng.2015.09.042>
- Chandrasekaran S, Madhuri S (2015) Dynamic response of offshore triceratops: numerical and Experimental investigations. *Ocean Eng* 109(15):401–409. <https://doi.org/10.1016/j.oceaneng.2015.09.042>
- Chandrasekaran S, Mayank S (2016) Dynamic analyses of stiffened triceratops under regular waves: experimental investigations. *Ships Offshore Struct* 12(5):697–705
- Chandrasekaran S, Nannaware M (2013) Response analyses of offshore triceratops to seismic activities. *Ship Offshore Struct* 9(6):633–642. <https://doi.org/10.1080/17445302.2013.843816>
- Chandrasekaran S, Nassery J (2015) Springing and Ringing response of offshore triceratops. In: *Proceeding of 34th International Conference on Ocean, Offshore and Arctic Engineering (OMAE 2015)*, St. John's, NL, Canada, 31 May–5 Jun, 2015. OMAE2015-41551
- Chandrasekaran S, Pannerselvam R (2009) Offshore structures: materials, analysis, design and construction. In: *Proceeding of Short Course on Offshore Structures and Materials*, IITM, Chennai, Dec 14–18, p 156
- Chandrasekaran S, Parameswara Pandian S (2011) Response behavior of perforated cylinders in regular waves. In: *Proceeding 30th International Conference on Ocean, Offshore and Arctic Engineering, OMAE 2011*, Rotterdam, The Netherlands, 19–24 June, 2011, OMAE 2011-49839
- Chandrasekaran S, Roy A (2006) Seismic evaluation of multi-storey RC frames using modal pushover analysis. *Int J Nonlinear Dyn* 43(4):329–342
- Chandrasekaran S, Saha N (2011) Reliability of offshore structures, short term course. Department of Ocean Engineering, IIT, Madras
- Chandrasekaran S, Seeram M (2012) Stability studies on offshore triceratops. *Int J Res Dev* 1 (10):398–404
- Chandrasekaran S, Sharma A (2010) Potential flow based numerical study for the response of floating offshore structures with perforated columns. *Ships Offshore Struct* 5(4):327–336
- Chandrasekaran S, Jain AK, Chandak NR (2004) Influence of hydrodynamic coefficients in the response behavior of triangular TLPs in regular waves. *Ocean Eng* 31(17–18):2319–2342
- Chandrasekaran S, Jain AK, Chandak NR (2006) Seismic analysis of offshore triangular tension leg platforms. *Int J Struct Stab Dyn* 6(1):1–24
- Chandrasekaran S, Chandak NR, Anupam G (2006) Stability analysis of TLP tethers. *Ocean Eng* 33(3):471–482
- Chandrasekaran S, Jain AK, Chandak NR (2007) Response behavior of triangular TLPs under regular waves using Stokes non-linear wave theory. *J Waterw Port Coast Ocean Eng ASCE* 133(3):230–237
- Chandrasekaran S, Jain AK, Gupta A, Srivastava A (2007) Response behavior of triangular tension leg platforms under impact loading. *Ocean Eng* 34(1):45–53
- Chandrasekaran S, Sharma A, Srivastava S (2007) Offshore triangular TLP behavior using dynamic Morison equation. *Struct Eng* 34(4):291–296
- Chandrasekaran S, Sharma A, Srivastava S (2007) Offshore triangular TLP behavior using dynamic Morison equation. *Struct Eng* 34(4):291–296
- Chandrasekaran S, Jain AK, Gupta A (2007) Influence of wave approach angle on TLP's response. *Ocean Eng* 8–9(34):1322–1327
- Chandrasekaran S, Jain AK, Gupta A, Srivastava A (2007) Response behavior of triangular tension leg platforms under impact loading. *Ocean Eng* 34(1):45–53

- Chandrasekaran S, Gaurav S, Srivastava S (2008) Structural response of offshore TLPs under seismic excitations. *Int Eng Technol J Civil Struct* 1(1):07–12
- Chandrasekaran S, Gaurav S, Srivastava S (2008) Structural response of Offshore TLPs under seismic excitations. *Int Eng Technol J Civil Struct* 1(1):07–12
- Chandrasekaran S, Bhaskar K, Harilal L, Brijit R (2010) Dynamic response behavior of multi-legged articulated tower with and without TMD. In: *Proceeding International Conference of Marine Technology MARTEC-2010*, 11–12 Dec, Dhaka, Bangladesh, pp 131–136
- Chandrasekaran S, Gaurav S, Jain AK (2010) Ringing response of offshore compliant structures. *Int J Ocean Clim Syst* 1(3–4):133–144
- Chandrasekaran S, Bhaskar K, Hashim M (2010b) Experimental study on dynamic response behavior of multi-legged articulated tower. In: *Proceeding 29th International Conference on Ocean, Offshore and Arctic Engineering, OMAE 2010*, 6–11 Jun, Shanghai, China
- Chandrasekaran S, Seeram M, Jain AK, Gaurav S (2010) Dynamic response of offshore triceratops under environmental loads. In: *Proceeding of International Conference on Maritime Technology*, Dhaka, Bangladesh, pp 131–136
- Chandrasekaran S, Gaurav G, Serino G, Miranda S (2011) Ringing and springing response of triangular TLPs. *Int J Shipbuilding Prog* 58:141–163
- Chandrasekaran S, Jain AK, Madhuri S (2013) Aerodynamic response of offshore triceratops. *Ships Offshore Struct* 8(2):123–140. <https://doi.org/10.1080/17445302.2012.691271>
- Chandrasekaran S, Kumar D, Ramanathan R (2013) Dynamic response of tension leg platform with tuned mass dampers. *J Naval Archit Mar Eng* 10(2):149–156
- Chandrasekaran S, Natarajan M, Sampath S (2013) Hydrodynamic response of offshore tension leg platforms with perforated members. *Int J Ocean Clim Syst* 4(3):182–196
- Chandrasekaran S, Lognath RS, Jain A (2015) Dynamic analysis of buoyant leg storage and regasification platform under regular waves. In: *Proceeding of 34th International Conference on Ocean, Offshore and Arctic Engineering (OMAE 2015)*, St. John's, NL, Canada, 31 May–5 June, 2015. OMAE2015-41554
- Chandrasekaran S, Ranjani R, Kumar D (2015) Response control of tension leg platform with passive damper: experimental investigations. *Ships Offshore Struct*. <https://doi.org/10.1080/17445302.2015.1119666>
- Chandrasekaran S, Mayank S, Jain A (2015) Dynamic response behavior of stiffened triceratops under regular waves: experimental investigations. In: *Proceeding of 34th International Conference on Ocean, Offshore and Arctic Engineering (OMAE 2015)*, St. John's, NL, Canada, 31 May–5 Jun, 2015. OMAE2015-41376
- Charles WN, Robert CW, Capanoglu C (2005) Triceratops: an effective platform for developing oil and gas fields in deep and ultra-deep water. In: *Proceedings of the fifteenth International Offshore and Polar Engineering Conference*, Seoul, Korea, 19–24 Jun, pp 133–139
- Chaudhary GK, Dover WD (1985) Fatigue analysis of offshore platforms subjected to sea wave loading. *Int J Fatigue* 7:13
- Chen X, Ding Y, Zhang J, Liagre P, Neidzwecki J, Teigen P (2006) Coupled dynamic analysis of a mini TLP: comparison with measurements. *Ocean Eng* 33:93–117
- Cheng FP, Kodur VKR, Wang TC (2004) Stress-strain curves for high strength concrete at elevated temperature. *J Mater Eng ASCE* 16(1):84–90
- Choi HS, Lou JYK (1991) Nonlinear behavior of an articulated offshore loading platform. *Appl Ocean Res* 13(2):63–74
- Chou FS (1980) Analytical approach to the design of a tension leg platform. In: *Proceeding Offshore Technology Conference, OTC 3883*, Houston, Texas, 5–8 May, pp 287–296
- Clauss GF, Birk L (1996) Hydrodynamic shape optimization of large offshore structures. *J Appl Ocean Res* 18:157–171
- Clauss GT et al (1992) *Offshore structures, vol 1: conceptual design and hydromechanics*. Springer, London

- Copple RW, Capanoglu CC (1995) A buoyant leg structure for the development of marginal fields in deep water. In: Proceedings of the fifth International Offshore and Polar Engineering Conference, The Hague, The Netherlands, 11–16 Jun, p 163
- Copson AG (1985) Semi-Submersible marine platform. U. S. Patent No. 4,556,008
- Davenport AG (1961) The application of statistical concepts to the wind loading of structures. *Proc Inst Civil Eng* 19:449–471
- Dawson TH (1983) *Offshore structural engineering*. Prentice-Hall Inc., Upper Saddle River
- de Boom WC, Pinkste JA, Tan PSG (1984) Motion and tether force prediction of a TLP. *J Waterw Port Coast Ocean Eng* 110(4):472–486
- Dean RG, Dalrymple RA (2000) *Water wave mechanics for engineers and scientists, advanced series on Ocean Engineering, vol 2*. World Scientific, Singapore
- Demirbilek Z (1990) Design formulae for offset, set down and tether loads of a tension leg platform (TLP). *Ocean Eng* 17(5):517–523
- DNV (1982) Rules for the design, construction and inspection of offshore structures. Det Norske Veritas, Oslo.
- DNV-RP-F205 (2010) Global performance analysis of deep water floating structures. Det Norske Veritas.
- DOE-OG (1985) *Offshore installation: guidance on design and construction*. Department of Energy, London, UK
- Donely MG, Spanos PD (1991) Stochastic response of a tension leg platform to viscous drift forces. *J Offshore Mech Arct Eng* 113:148–155
- Drysdale D (1999) *An introduction to fire dynamics*. Wiley, Hoboken
- El-Gamal AR, Essa A, Ismail A (2013) Effect of tethers tension force in the behavior of a tension leg platform subjected to hydrodynamic force. *Int J Civil Struct Constr Archit Eng* 7(12): 645–652
- EN1992-1-2 (2008) Eurocode. Design of concrete structures: part 1-2: General rules—structural fire design, European Comm for Standardization
- EN1993-1-2 (2005) Eurocode 3. Design of Steel structures: part 1-2: General rules—structural fire design
- EN-1991-1-2 (2002) Eurocode 1. Actions on structures: part 1-2: General actions on structures exposed to fire. European Comm for Standardization
- EN-1994-1-2 (2005) Eurocode 4. Design of composite steel and concrete structures: part 1-2: General rules for structural fire design, European Comm for Standardization
- Ertas A, Eskwaro-Osire S (1991) Effect of Damping and wave parameters on offshore structure under random excitation. *Nonlinear Dyn* 2:119–136
- Ertas A, Lee J-H (1989) Stochastic response of tension leg platform to wave and current forces. *J Energy Res Technol* 111:221–230
- Ertas A, Lee J-H (1989) Stochastic response of tension leg platform to wave and current forces. *J Energy Res Technol* 111:221–230
- Eurocode 1 (2002) Actions on structures: part 1-2: General actions—actions on structures exposed to fire
- Eurocode 3 (2005) Design of steel structures, part 1-2, general rules: fire resistant design, Document CEN, European Commission of Standardization, U.K.
- Faltinsen OM (1998) *Sea loads on ships and offshore structures*, Cambridge ocean technology series. Cambridge University Press, New York
- Faltinsen OM, Newman JN, Vinje T (1995) Nonlinear wave loads on a slender vertical cylinder. *J Fluid Mech* 289:179–198
- Finn LD, Maher JV, Gupta H (2003) The cell spar and vortex induced vibrations. In: *Offshore Technology Conference*, OTC 15244, Houston, Texas, 5–8 May, pp 1–6
- Freudenthal AM, Gaither WS (1969) Design criteria for fixed offshore structures. In: *Proceeding of Offshore Technology Conference*, Houston, paper OTC 1058
- Gabbai RD, Benaroya H (2005) An overview of modeling and experiments of vortex-induced vibration of circular cylinders. *J Sound Vib* 282:575–616

- Gadagi MM, Benaroya H (2006) Dynamic response of an axially loaded tendon of a tension leg platform. *J Sound Vib* 293:38–58
- Gasim MA, Kurian VJ, Narayanan SP, Kalaikumar V (2008) Responses of square and triangular TLPs subjected to random waves. In: *Proceeding of International Conference on Construction and Building Technology*. ICCBT 2008), Universit Teknologi Petronas, 16–20 Jun, Kuala Lumpur, Malaysia
- Gerwick B Jr (1986) *Construction of offshore structures*. Wiley, New York
- Gie TS, De Boom W (1981) The Wave induced motion of a tension leg platform in deep water. In: *13th Annual Ocean Technology Conference in Houston, Texas, May 4–7*
- Glanville RS, Paulling JR, Halkyard JE, Lehtinen TJ (1991) Analysis of the spar floating, drilling, production and storage structure. In: *Proceeding Offshore Technology Conference, OTC 6701, Houston, 6–9 May*, pp 57–68
- Gonçalves RT, Rosetti GF, ALC Fajarra (2011) Experimental comparisons to assure the similarity between VIM (Vortex-Induced Motion) and VIV (Vortex-Induced Vibration) Phenomena. In: *Proceeding of OMAE, 19–24 Jun, Rotterdam, The Netherlands*
- Govardhan R, Williamson CHK (2000) Modes of vortex formation and frequency response of a freely vibrating cylinder. *J Fluid Mech* 420:85–130
- Govardhan R, Williamson CHK (2002) Resonance forever: existence of a critical mass and an infinite regime of resonance in vortex-induced vibration. *J Fluid Mech* 473:147–166
- Graff WJ (1981) *Introduction to offshore structures: design, fabrication and installation*. Gulf Publishing Co, Tokyo
- Guo B, Song S, Chacko J, Ghilamber A (2005) *Offshore pipelines*. Gulf Professional Publishing, Houston
- Gurley KR, Kareem A (1998) Simulation of ringing in offshore systems under viscous loads. *J Eng Mech ASCE* 124(5):582–586
- Halkyard JE, Davies RL, Glanville RS (1991) The tension buoyant tower: a design for deep water. In: *23rd Annual Offshore Technology Conference, OTC 6700. Houston, Texas, 6–9 May*, pp 41–55
- Hall JR Jr (2011) *Fatal effects of fire*. National Fire Protection Association, Fire Analysis and Research Division, Quincy
- Haritos N (1985) Modeling the response of tension leg platforms to the effects of wind using simulated traces. *Math Comput Simul* 27:231–240
- Helvacioğlu IH, Incecik A (2004) *Dynamics of double articulated towers, integrity of offshore structures*, vol 4. Elsevier, Amsterdam
- Herbich JB (1991) *Handbook of coastal and ocean engineering*. Gulf Publishing Company, Houston
- Hitchings GA, Bradshaw H, Labiosa TD (1976) Planning and execution of offshore site investigations for North Sea Gravity platform. In: *Proceeding of Offshore Technology Conference, Paper No. 2430*
- Hoeg K (1976) Foundation engineering for fixed offshore structures. In: *Prof. of First International Conference in Behaviour of Offshore Structures, vol 1*, pp 39–69
- Høeg K, Tong WH (1977) Probabilistic considerations in the foundation engineering for offshore structures. In: *2nd International Conference on Structural Safety and Reliability, Munich, Germany*, pp 267–296
- Hogben N, Standing RG (1974) Wave loads on large bodies. In: *Proceedings of the International Symposium on the Dynamics of Marine, Vehicles and Structures in Waves, University College, London*, pp 258–277
- Hove K, Foss I (1974) Quality assurance for offshore concrete gravity structures. In: *Proceeding Offshore Technology Conference, Paper No. 2113*
- Hsu HT (1981) *Applied offshore structural engineering*. Gulf Publishing Co., Houston
- IS 1642-1989 *Fire safety of buildings (general): details of construction-code of practice*, Bureau of Indian Standards, New Delhi, India
- IS 3809-1979 *Fire resistance test of structures*. Bureau of Indian Standards, New Delhi, India

- ISO 834-1975 Fire resistance tests elements of building construction. International Organization for Standardization
- Issacson M, St. Det Q (1982) Non-linear wave effects on fixed and floating bodies. *J Fluid Mech* 120:267–281
- James J, O’Kane AW, Thiagarajan TroeschandKrish P (2002) Hull component interaction and scaling for TLP hydrodynamic coefficients. *Ocean Eng* 29:513–532
- Jefferys ER, Patel MH (1982) Dynamic analysis models of tension leg platforms. *J Energy Res Technol* 104:217–223
- Jefferys ER, Rainey RCT (1994) Slender body models of TLP and GBS ‘ringing’. BOSS, McGraw-Hill Inc, New York
- Kareem A (1983) Nonlinear dynamic analysis of compliant offshore platforms subjected to fluctuating winds. *J Wind Eng Ind Aerodyn* 14:345–356
- Kareem A (1985) Wind induced response analysis of tension leg platforms. *J Struct Eng* 111(1):37–55
- Kareem A, Dutton C (1982) Dynamic effects of wind on TLP. In: *Proceedings of Offshore Technology Conference, OTC-4229(1)*, pp 749–757
- Kareem A, Zhao J (1994) Analysis of non-gaussian surge response of tension leg platforms under wind loads. *J Offshore Mech Arct Eng* 116:13–144
- Karimirad M, Meissonnier Q, Moan Z, Moan T (2011) Hydroelastic code-to code comparison for a tension leg spar-type floating wind turbine. *Mar Struct* 24:412–435
- Kawagoe K (1958) Fire behaviour in rooms. Tokyo, Japan: Building Research Institute, Report No. 27
- Kenny FM, James JD, Melling TH (1976) Non-linear wave force analysis of perforated marine structures. In: *Offshore Technology Conference, OTC 2501*, pp 781–796
- Ker W-K, Lee C-P (2002) Interaction of waves and a porous tension leg platform. *J Waterw Port Coast Ocean Eng* 128(2):88–95
- Khalak A, Williamson CHK (1991) Motions, forces and mode transitions in vortex induced vibrations at low mass-damping. *J Fluids Struct* 13:813–851
- Kim H-J, Lilley DG (2000) Heat release rates of burning items in fire. In: *Proceeding of 38th Aerospace Sciences Meeting & Exhibit*
- Kim CH, Zou J (1995) A universal linear system model for kinematics and forces affected by nonlinear irregular waves. *Int J Offshore Polar Eng* 5(3):166–170
- Kim C-H, Lee C-H, Goo J-S (2007) A dynamic response analysis of tension leg platform including hydrodynamic interaction in regular waves. *Ocean Eng* 34(11–12):1680–1689
- Kjeldsen SP, Myrhaug D (1979) Wave-wave interactions and wave-current interactions in deep water. In: *Proceeding 5th POAC Conference, Trondheim, Norway, vol 111*, p 179
- Kobayashi M, Shimada K, Fujihira T (1987) Study on dynamic responses of a TLP in waves. *J Offshore Mech Arct Eng* 109:61–66
- Kodur VKR (2000) Spalling in high strength concrete exposed to fire: concerns, causes, critical parameters and cures. In: *Proceeding ASCE Structures Congress, Philadelphia*
- Kodur VKR (2005) Guidelines for fire resistance design of high strength concrete columns. *J Fire Prot Eng* 15(2):93–106
- Kodur VKR, Lie TT (1997) Fire resistance of fibre-reinforced concrete: present and future. Canadian Society of Civil Engineers, Montreal
- Kodur VKR, Lie TT (1997) Evaluation of fire resistance of rectangular steel columns filled with fibre-reinforced concrete. *Can J Civil Eng* 24(3):339
- Koo BK, Kim MH, Randall RE (2004) Mathieu instability of a spar platform with mooring and risers. *Ocean Eng* 31:2175–2208
- Kurian VJ, Gasim MA, Narayan SP, Kalaikumar V (2008) Parametric study of TLPs subjected to random waves. In: *International Conference on Construction and Building Technology, 16–20 Jun 2008, Kuala Lumpur, Malaysia, vol 19*, pp 213–222
- Lee HH, Juang HH (2012) Experimental study on the vibration mitigation of offshore tension leg platform system with UWTLCD. *Smart Struct Syst* 9(1):71–104

- Lee HH, Pei-Wen W (2000) Dynamic behavior of tension-leg platform with net cage system subjected to wave forces. *Ocean Eng* 28:179–200
- Lee HH, Wang P-W, Lee C-P (1999) Dragged surge motion of tension leg platforms and strained elastic tethers. *Ocean Eng* 26(6):575–594
- Leffler WL, Pattarozzi R, Sterling G (2011) Deep-water petroleum: exploration and production. Pennwell Corp, Tulsa, p 350
- Leonard JW, Young RA (1985) Coupled response of compliant offshore platforms. *Eng Struct* 7:21–31
- Lesage F, Garthshore LS (1987) A method of reducing drag and fluctuating side force on bluff bodies. *J Wind Eng Ind Aerodyn* 25:229–245
- Liagre PF, Niedzwecki JM (2003) Estimating nonlinear coupled frequency-dependent parameters in offshore engineering. *Appl Ocean Res* 25:1–19
- Logan BL, Naylor S, Munkejordand T, Nyhgaard C (1996) Atlantic alliance: the next generation tension leg platform. In: Proceedings of the Offshore Technology Conference, OTC 8264
- Low YM (2009) Frequency domain analysis of a tension leg platform with statistical linearization of the tendon restoring forces. *Mar Struct* 22:480–503
- Majumdar P, Marchertas A (1997) Heat moisture transport and induced stresses in porous materials under rapid heating. *Numer Heat Transfer A* 32:111–130
- Malhotra HL (1956) Effect of temperature on compressive strength of concrete. *Mag Concr Res* 8:85–94
- Malhotra HL (1982) Design of fire-resistant structures. Surrey University Press, Glasgow
- Malhotra HL (1987) Fire safety in buildings. Garston
- Marthinsen T, Winterstein SR, Ude TC (1992) TLP fatigue due to second-order springing. In: Probabilistic Methods and Structural and Geotechnical Reliability, Proceeding Specialty Conference, pp 455–458
- Masciola M, Nahon M (2008) Modeling and simulation of a tension leg platform. In: Proceedings of the Eighteenth International Offshore and Polar Engineering Conference, Vancouver, BC, Canada, 6–11 Jul
- Mather A (2000) Offshore engineering: an introduction, 2nd edn. Witherby, Livingston
- Mei CC (1966) Radiation and scattering of transient gravity waves by vertical plates. *Quart J Mech Appl Math* 19:417–440
- Mei CC (1983) The applied dynamics of ocean surface waves. Wiley, New York
- Mei CC, Liu PLF, Ippen AT (1974) Quadratic head loss and scattering of long waves. *J Waterw Harbours Coast Eng Div ASCE* 100:217–239
- Mekha BB, Johnson CP, Roesset MJ (1996) Implication of tendon modeling on nonlinear response of TLP. *J Struct Eng* 122(2):142–149
- Mekha BB, Johnson CP, Roesset JM (1996) Implication of tendon modeling on nonlinear response of TLP. *J Struct Eng* 122(2):142–149
- Melinek SJ (1989) Prediction of fire resistance of insulated steel. *Fire Saf J* 14:127–134
- Mercier JA (1982) Evolution of tension leg platform technology. In: Proceeding 3rd International Conference on the Behaviour of Offshore Structures, MIT
- Meyerhof GG (1976) Concepts of safety in foundation engineering ashore and offshore. In: Boss '76, University of Trondheim, Norway, vol 1, pp 900–911
- Michel WH (1999) Sea spectrum revisited. *Mar Technol* 36(4):211–227
- Moan T, Sigbjørnson R (1977) Stochastic sea load effect analysis for probabilistic design of fixed offshore platforms. In: 2nd International Conference on Structural Safety and Reliability, Munich, Germany, pp 227–246
- Moe G, Verley RLP (1980) Hydrodynamic damping of offshore structures in wave and currents. In: Offshore Technology Conference, 12th Annual OTC, Houston, Texas, pp 37–44
- Mogridge GR, Jamieson WW (1975) Wave forces on a circular caisson: theory and experiment. *Can J Civil Eng* 2:540–548
- Moharrami M, Tootkaboni M (2014) Reducing response of offshore platforms to wave loads using hydrodynamic buoyant mass dampers. *Eng Struct* 81:162–174

- Montasir OA, Kurian VJ (2011) Effect of slowly varying drift forces on the motion characteristics of truss spar platforms. *Ocean Eng* 38:1417–1429
- Montasir OAA, Kurian VJ, Narayanan SP, Mubarak MAW (2008) Dynamic response of Spar platforms subjected to waves and current. In: *International Conference on Construction and Building Technology, ICCBT 2008*, 16–20 Jun, Kuala Lumpur, Malaysia
- Morison JR (1953) The force distribution exerted by surface waves on piles. ASTIA File Copy, University of California, Institute of Engineering Research, Berkeley, California. AD No. 654
- Morison JR, O'Brien MP, Johnson JW, Schaaf SA (1950) The force exerted by surface waves on piles. *Petrol Trans* 189:149–154 T.P 2846
- Moses F (1976) Reliability of structural systems. In: *Boss '76*, University of Trondheim, Norway, vol 1, pp 912–923
- Moses F (1977) Safety and reliability of offshore structures. In: *International Research Seminar on Safety of Structures under Dynamic Loading*, Trondheim, Norway
- Moses F, Stevenson J (1970) Reliability-based structural design. *J Struct Div* 96:221–244
- Munkejord T (1996) The Heidrun TLP and concept development for deep water. In: *Proceeding of ISOPE, Los Angeles, USA, May*, pp 1–11
- Muren J, Flugstad P, Greiner B, D'Souza R, Solberg IC (1996) The 3 column TLP-A cost efficient deepwater production and drilling platform. In: *Proceedings of the Offshore Technology Conference, OTC 8045*
- Murray JJ, Mercier RS (1996) Model tests on a tension leg platform using truncated tendons. In: *Workshop on Model Testing of Deep Sea Offshore Structures, IITC*, pp 162–168
- Naess A, Moan T (2013) *Stochastic dynamics of Marine structures*. Cambridge University Press, New York
- Natvig VJ (1996) TLP installation without motion compensation. In: *Proceeding ISOPE, Los Angeles, USA, vol 1*, pp 228–231
- Newman JN (1963) The motions of spar buoy in regular waves. Report 1499, David Taylor Model Basin
- Niedzwecki JM, Huston JR (1992) Wave interaction with tension leg platforms. *Ocean Eng* 19(1):21–37. [https://doi.org/10.1016/0029-8018\(92\)90045-6](https://doi.org/10.1016/0029-8018(92)90045-6)
- Niedzwecki JM, van de Lindt JW, Gage JH, Teigen PS (2000) Design estimates of surface wave interaction with compliant deepwater platforms. *Ocean Eng* 27:867–888
- Nobuyoshi Y (1976) Experimental and theoretical studies of a tension leg platform in deep water. In: *Offshore Technology Conference, OTC 2690-MS*, 3–6 May, Houston, Texas, pp 849–856
- Nordgren RP (1987) Analysis of high frequency vibration of tension leg platforms. *J Offshore Mech Arct Eng* 109:119–125
- Owen JC, Brankovic M (2003) Experimental studies of passive control of vortex-induced vibration. *J Fluids Struct* 15:597–605
- Paik I, Roesset JM (1996) Use of quadratic transfer functions to predict response of tension leg platforms. *J Eng Mech* 122(9):882–889
- Paik JK, Thayamballi AK (2007) *Ship-shaped offshore installations: design, building and operations*. Cambridge University Press, Cambridge
- Patel MH (1989) *Dynamics of offshore structures*. Butterworths, London
- Patel MH, Lynch EJ (1983) Coupled dynamics of tensioned buoyant platforms and mooring tethers. *Eng Struct* 5:299–308
- Patel MH, Park HI (1995) Combined axial and lateral responses of tensioned buoyant platform tethers. *Eng Struct* 17(10):687–695
- Patel MH, Witz JA (1991) *Compliant offshore structures*. Butterworth-Heinemann Ltd., Oxford
- Perrett GR, Webb RM (1980) Tethered buoyant platform production system. In: *12th Annual Offshore Technology Conference, OTC 3881*, Houston, Texas, 5–8 May, pp. 261–274
- Perryman SR, Horton EE, Halkyard JE (1995) Tension buoyant tower for small fields in deep waters. In: *Offshore Technology Conference, OTC 7805*, Houston, Texas, 1–4 May, pp 13–22
- Purkiss JA (1984) Steel fibre reinforced concrete at elevated temperature. *Int J Cem Compos Light Weight Concrete* 6:3

- Ran Z, Kim MH, Niedzwecki JM, Johnson RP (1996) Response of a spar platform in random waves and currents (experiments vs. theory). *Int J Offshore Polar Eng* 6(1)
- Reddy DV, Arockiasamy M (1991) *Offshore structures*, vol 1. Kriger Publishing Co., Malabar
- Rijken OR, Niedzwecki JM (1991) A knowledge base approach to the design of tension leg platform. *Offshore technology center*, pp 24–100
- Roitman N, Andrade RFM, Batista RC (1992) Dynamic response analysis of small scale model tension leg platform. *Mar Struct* 5:491–513
- Sadehi K (1989) *Design and analysis of marine structures*. Khajeh Nasirroddin Tsi University of Technology, Tehran, Iran
- Sadehi K (2001) *Coasts, ports and offshore structures engineering*. Power and Water University of Technology, Tehran, Iran
- Sadehi K (2007) Offshore and petroleum platforms for Cyprus oil/Gas fields. *GAU J Soc Appl Sci* 2(4):1–16
- Sarpkaya T (1978) Fluid forces on oscillating cylinders. *J Waterw Port Coast Ocean Div ASCE* 104:275–290
- Sellers LL, Niedzwecki JM (1992) Response characteristics of multi-articulated offshore towers. *Ocean Eng* 19(1):1–20
- Shaver CB, Capanogluand CC, Serrahn CS (2001) Buoyant leg structure preliminary design, constructed cost and model test results. In: *Proceedings of the 11th International Offshore and Polar Engineering Conference*, Stavanger, Norway, 17–22 Jun, pp 432–439
- Simiu E, Leigh SD (1984) Turbulent wind and tension leg platform surge. *J Struct Eng* 110 (4):785–802
- Soding H, Blok JJ, Chen HH, Hagiwara K, Issacson M, Jankowski J, Jefferys ER, Mathisen J, Rask I, Richer J-P, Romeling JU, Varsta P (1990) Environmental forces on offshore structures: a state-of-the-art review. *Mar Struct* 3:59–81
- Spanos PD, Agarwal VK (1984) Response of a simple tension leg platform model to wave forces calculated at displaced position. *J Energy Res Technol* 106(4):437–443
- Srinivasan C, Thomas M (2016) Suppression system for offshore cylinders under vortex induced vibration. *Vibroengineering Procedia* 7:01–06
- Srinivasan C, Thailammai C, Khader SA (2016) Structural health monitoring of offshore structures using wireless sensor networking under operational and environmental variability. *Int J Environ Chem Ecol Engg* 10(1):33–39
- Stansberg CT, Ormberg H, Oritsland O (2002) Challenges in deep water experiments: hybrid approach. *J Offshore Mech Arct Eng* 124:90–96
- Stansberg CT, Karlsten SI, Ward EG, Wichersand JEW, Irani MB (2004) Model testing for ultra-deep waters. In: *Offshore Technology Conference*, OTC 16587, Houston, Texas, pp 1–9
- Stoke's G (1880) On the theory of oscillatory waves. *Math Phys Pap* 1:225–228
- Sumer BM, Fredsøe J (2003) *Hydrodynamics around cylindrical*, Revised edition. World Scientific Publishing Co., Pte. Ltd, Singapore
- Tabeshpour MR (2013) Conceptual discussion on free vibration analysis of tension leg platforms. *Dev Appl Oceanic Eng DAOE* 2(2):45–52
- Tabeshpour MR, Golafshani AA, Seif MS (2006) Comprehensive study on the results of tension leg platform responses in random sea. *J Zhejiang Univ Sci* 7(8):1305–1317
- Taflanidis AA, Scruggs JT, Angelides DC (2008) Robust design optimization of mass dampers for control of tension leg platforms. In: *Proceedings of the Eighteenth International Offshore and Polar Engineering Conference*, ISOPE-I-08-326, Vancouver, BC, Canada, 6–11 Jul
- Taflanidis AA, Angelides DC, Scruggs JT (2009) Simulation-based robust design of mass dampers for response mitigation of tension leg platforms. *Eng Struct* 31(4):847–857. <https://doi.org/10.1016/j.engstruct.2008.11.014>
- Thiagarajan KP, Troesch AW (1998) Effects of appendages and small currents on the hydro dynamic heave damping of TLP columns. *J Offshore Mech Arct Eng* 120:37–42

- Tromans T, Swan C, Masterton S (2006) Nonlinear potential flow forcing: the ringing of concrete gravity based structures, Research Report No. 468, Ocean Wave Engg Ltd, Heath & Safety Executive Publication, Norwich, U.K.
- Twilt T (1991) Stress-strain relationship of reinforcing steel at elevated temperatures. TNO-Rep., B1-91-015, TNO Building and Construction Res., Delft, The Netherlands
- Ursell F, Dean RG, Yu YS (1960) Forced small amplitude water waves: a comparison of theory and experiment. *J Fluid Mech* 7:33–752
- Vannucci P (1996) Simplified optimal design of tension leg platform TLP. *Struct Optim* 12: 265–268
- Venkataramana K, Toyoda S, Kawano K (1993) Dynamics of TLPs under current and earthquake forces. In: *Proceedings of ISOPE, Singapore*, pp 341–344
- Vickery PJ (1990) Wind & wave loads on a tension leg platform: theory and experiment. *J Wind Eng Ind Aerodyn* 36:905–914
- Vickery PJ (1995) Wind induced response of tension leg platform: theory and experiment. *J Struct Eng* 121(4):651–663
- Walton WD, Thomas PH (1995) Estimating temperatures in compartment fires. *SFPE Handbook of Fire Protection Engineering*, Society of Fire Protection Engineers, USA
- Wickstorm U (1986) Temperature analysis of heavy-insulated steel. *Fire Saf J* 9:281
- Williamson CHK, Govardhan R (2004) Vortex induced vibrations. *Annual Rev of Fluid Mech* 36:413–455
- Wilson JF (1984) *Dynamics of offshore structures*. Wiley Inter Science Publications, New York
- Wilson JF (2003) *Dynamics of offshore structures*. Wiley, Hoboken
- Witz JA, Patel MH, Harrison JH (1986) On the hydrodynamics of semisubmersibles with articulated members. In: *Proceeding of Royal Society of London, Series A, Mathematical and Physical Sciences* vol 403, pp 81–109
- Yan F, Zhang D, Sun L, Dai Y (2009) Stress verification of a TLP under extreme wave environment. *J Mar Sci Appl* 8:132–136
- Yoneya T, Yoshida K (1982) The dynamics of tension leg platforms in waves. *J Energy Res Technol* 104:20–28
- Yoshida K, Ozaki M, Oka N (1984) Structural response analysis of tension leg platforms. *J Energy Res* 106:10–17
- Young AG, Kraft LM, Focht JA (1975) Geotechnical considerations in foundation design of offshore gravity structures. In: *Proceeding Offshore Tech Conference*, Paper No. 2371
- Younis BA, Teigenand P, Przulj VP (2001) Estimating the hydrodynamic forces on a mini TLP with computational fluid dynamics and design-code techniques. *Ocean Eng* 28:585–602
- Zdravkovich MM (1981) Review classification of various aerodynamic and hydrodynamic means for suppressing vortex shedding. *J Wind Eng Ind Aerodyn* 7:145–189
- Zeng X, Shen X, Wu Y (2007) Governing equations and numerical solutions of tension leg platform with finite amplitude motion. *J Appl Math Mech* 28(1):37–49
- Zhang F, Yang J, Li R, Gang C (2007) Numerical investigation on the hydrodynamic performances of a new spar concept. *Sci Direct J Hydrodyn* 19(4):473–481